University of Alberta

Sedimentology and diagenesis of the Scollard and Coalspur sandstones
in west-central Alberta

by

Ahmed Khalaf Khidir ©

A thesis submitted to the Faculty of Graduate Studies and Research in Partial fulfillment of the
Requirements for the degree of Master of Science

Department of Earth and Atmospheric Sciences

Edmonton, Alberta

Fall 2002

National Library
of Canada

Bibliothèque nationale
du Canada

Acquisitions and
Bibliographic Services

Acquisitions et
services bibliographiques

395 Wellington Street
Ottawa ON K1A 0N4
Canada

395, rue Wellington
Ottawa ON K1A 0N4
Canada

The author has granted a non-exclusive licence allowing the National Library of Canada to reproduce, loan, distribute or sell copies of this thesis in microform, paper or electronic formats.

The author retains ownership of the copyright in this thesis. Neither the thesis nor substantial extracts from it may be printed or otherwise reproduced without the author's permission.

L'auteur a accordé une licence non exclusive permettant à la Bibliothèque nationale du Canada de reproduire, prêter, distribuer ou vendre des copies de cette thèse sous la forme de microfiche/film, de reproduction sur papier ou sur format électronique.

L'auteur conserve la propriété du droit d'auteur qui protège cette thèse. Ni la thèse ni des extraits substantiels de celle-ci ne doivent être imprimés ou autrement reproduits sans son autorisation.

0-612-81419-X

Canada

University of Alberta

Library Release Form

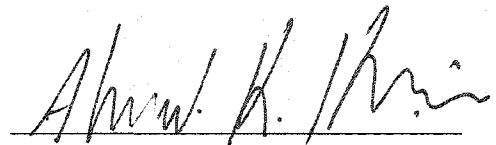**Name of Author:** Ahmed Khalaf Khidir

Title of thesis: Sedimentology and diagenesis of the Scollard and Coalspur sandstones in west-central Alberta

Degree: Master of Science

Year this Degree Granted: 2002

#201 13107- 83 St NW
Edmonton, Alberta, Canada
T5E 2W5

Submitted 30-09-2003

University of Alberta
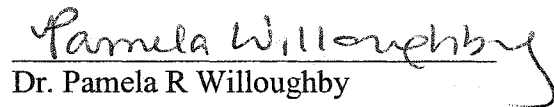
Faculty of Graduate Studies and Research

The undersigned certify that they have read, and recommend to the Faculty of Graduate Studies and Research for acceptance, a thesis entitled **Sedimentology and diagenesis of the Scollard and Coalspur sandstones in west-central Alberta**. Submitted by Ahmed Khalaf Khidir in partial fulfillment of the requirements for the degree of Master of Science.

Dr. Octavian Catuneanu (Supervisor)

Dr. John England

Dr. Pamela R Willoughby

Date: Sept. 24, 2002

Abstract

The petrography of the uppermost Cretaceous-Paleocene Scollard and Coalspur sandstones in west central Alberta is defined by litharenites and sublitharenites, which accumulated in a variety of fluvio-lacustrine environments. The textural types of volcanic, metamorphic, and sedimentary rock fragments indicate volcanic arc, metamorphic and sedimentary provenances.

This study presents the effects of diagenetic processes on the preservation of primary porosity, as well as on the development of several types of secondary porosity. Additionally, the distribution of authigenic minerals in the Scollard and Coalspur formations is presented.

The reconstruction of the paleo-climatic conditions during the accumulation of the Scollard and Coalspur formations is based on the detailed study of the framework grains and authigenic minerals. Wetter climatic conditions are interpreted for the arenites with higher amounts of mono- and/or polycrystalline quartz, kaolinite and quartz overgrowth. Drier climatic conditions are inferred for the arenites with lesser percentages of quartz but higher amounts of authigenic smectite.

To my parents:
Hadla and Khalaf

You are gone from me now,
but one they can't take away,
your memory resides inside my heart,
and lights up my darkest days...

ACKNOWLEDGEMENTS

Table of Contents

List of Tables

List of Figures

Appendix A

Appendix B

Appendix C

Chapter 1

Introduction

The Scollard and Coalspur formations are part of a fully nonmarine depositional sequence, which accumulated during the Late Maastrichtian-Early Paleocene interval in the foredeep of the Western Canada foreland system, and which is bounded by regional subaerial unconformities. The Scollard and the Coalspur accumulated in isolation from marine influences, on a dynamic topography controlled by tectonic mechanisms (Catuneanu and Sweet, 1999).

Gibson (1977) defined the Scollard Formation in the Scollard Canyon of the Red Deer Valley. Within the study area (Fig. 1-1), the Scollard Formation consists of thick grey to buff sandstone and siltstone units interbedded with thin olive-green mudstone beds and coal. The Scollard sequence is thinner towards the east. The thickness of the Scollard-age deposits in south-central Alberta along the Red Deer Valley is around 100 m, which increases to about 300 m in the Foothills of Alberta (Dawson, et al., 1994). The Foothills strata are referred to as "the Coalspur Formation." It was formalized on the basis of its lithologic succession consisting of interbedded mudstone, siltstone and fine-grained sandstone, with subordinate coarser grained sandstone layers and channel lag deposits.

The Coalspur and Scollard formations have well-defined boundaries (Fig. 1-2). The upper contact is overlain by the Paskapoo Formation, which is defined as a major unconformity associated with a stratigraphic gap for up to 4 million years (Lerbekmo et al., 1990). The lower contact of the Scollard Formation is overlies the lacustrine

1

mudstones of the Battle Formation, while the Coalspur Formation overlies the Brazeau Formation.

The paleo-depositional environment was dominated by fluvial and fluvial-lacustrine systems originated from the adjacent Cordilleran belt. The paleocurrent data of the cross-bedded sandstone units suggest a SE-ward paleoflow (lower Scollard) to S-SE-ward paleoflow (upper Scollard). The changes in paleoflow directions indicate a change in syn-depositional tilt was changed, resulting in different paleocurrent trends for each member.

The examination of the Scollard sequence throughout the field areas confirms that gradual shifting from braided to higher sinuosity paleochannels occurred during the Scollard-age. This interpretation is based largely on the observation of thick sandy channel storeys with minor mudstone at the top of the succession, which is pass upward into point bars dominated by lateral accretion within thick floodplain fines, characteristic of meandering rivers. These results imply that regionally-mappable changes in the proportion of channel belt sandstones versus floodplain mudstones may reflect changes in paleoslope gradients, rather than a major change in fluvial discharge.

This fluvial succession of the Scollard sequence has been the subject of various stratigraphic and coal geology studies, but the work presented in this thesis focuses on aspects that have not previously been addressed. This thesis presents a petrographic study of sandstone compositions, reservoir properties, paleoclimate, and diagenetic history. In addition, this thesis studies the pore systems of sandstone rocks in regards to morphology, size, and pore-linings. Composite information has been obtained from thin-

section petrography, scanning electronic microscopy, x-ray diffraction, and carbon and oxygen stable isotopes.

The research is presented in two chapters, in a journal publication format. Chapter 2 deals with the sedimentology and diagenesis of the Scollard Formation in the plain regions. Chapter 3 characterizes the sedimentology and diagenesis of the Coalspur Formation in the Foothill regions. Chapters 2 and 3 are independent studies, related to one another by their similar focus. Their similarity stresses the genetic relationship between the Scollard and Coalspur formations, which are the product of deposition within the same Scollard-age drainage systems.

Chapters 2 and 3 also present a petrographic study of thin sections. Thin-section petrology provides the means of evaluating the mineralogy and pore system of sandstone samples. This study indicates that the Scollard and Coalspur sandstones are composed mostly of lithic fragments, quartz, and feldspar grains classified as litharenite to sublitharenite based on Pettijohn's classification (Pettijohn et al., 1987). The variety in the lithics texture of the sandstone rocks indicated a diversity of parent rocks within the Cordilleran belt.

The distributions of authigenic minerals in the Scollard sandstones are discussed in Chapter 2. The Scollard sandstones are characterized by relative variability in the distribution of authigenic minerals. The Scollard Formation is dominated by grain–coating and pore-lining, and pore-filing clay minerals, such as kaolinite and smectite and less amount of illite. Grain-replacing calcite, authigenic quartz, and iron oxides are also present. Authigenic mineral distributions within the Coalspur sandstones are discussed in Chapter 3. The Coalspur strata are characterized by various authegenic minerals such as

3

chlorite, smectite/chlorite, smectite, illite, kaolinite and dickite. The main controls on these distributions were the paleo-environment, burial depth, and the chemistry of meteoric water.

The diagenetic history of the Scollard sequence is also stressed in Chapters 2 and 3 of this thesis. This study indicates that the diagenetic history of the Scollard sandstones is less complicated than that of the Coalspur sandstones, as was determined from thin-section slides and SEM examination. In plain regions, the limited conversion of smectite into illite, as well as the weak albitization of K-feldspar, implies relatively low maximum burial temperatures of less than 120° C (Hower et al., 1976). This limited conversion indicates a low burial depth. Chapter 3 discusses the burial history of the Coalspur Formation. In the Foothills regions the Coalspur Formation experienced a complex diagentic history due to increases in burial depth. Increases in burial depth are indicated by the presence of authigenic minerals such as smectite/chlorite, illite, chlorite and dickite.

The primary porosity and development of secondary porosity are also discussed in the thesis. The present porosity of the Scollard and Coalspur sandstones is both primary and secondary in origin. Secondary porosity was caused by the partial dissolution of soluble constituents and feldspar grains, and the leaching of intergranular carbonate cement. Initial compaction and authigenic clay minerals have a major reduction effect on primary porosity.

Finally, Chapters 2 and 3 also discuss pleoclimate reconstructions based on petrographic studies of detrital components correlated with electronic microscopic investigations of authigenic minerals and isotopic analyses of early calcite cement. As

neither the petrographic (framework grains) nor the SEM-XRD (authigenic clay mineralogy) data sets can be used to address the issue of paleoclimate in a definitive manner, the key for such interpretations is the correlation between the detrital and authigenic mineral constituents. The close correlation found between the two constituent types suggests that the precipitation of authigenic clay minerals took place relatively soon after burial. This correlation is in agreement with the meteoric origin of the diagenetic fluids indicated by the ^{18}O stable isotope data. Several cycles of climate fluctuations between wetter and dryer conditions controlled the composition of sandstones during the deposition of the Scollard Formation. During the formation of the Coalspur sandstones, the climate changed gradually from arid to semi-arid in the lower Coalspur to more humid during the upper Coalspur time.

In conclusion, this study demonstrates the value of petrographic and SEM analyses in the assessment of porosity in fluvial reservoirs. Such an outcrop study may be used as an analogue for the assessment of other fluvial reservoirs in the subsurface of the Western Canada Sedimentary Basin.
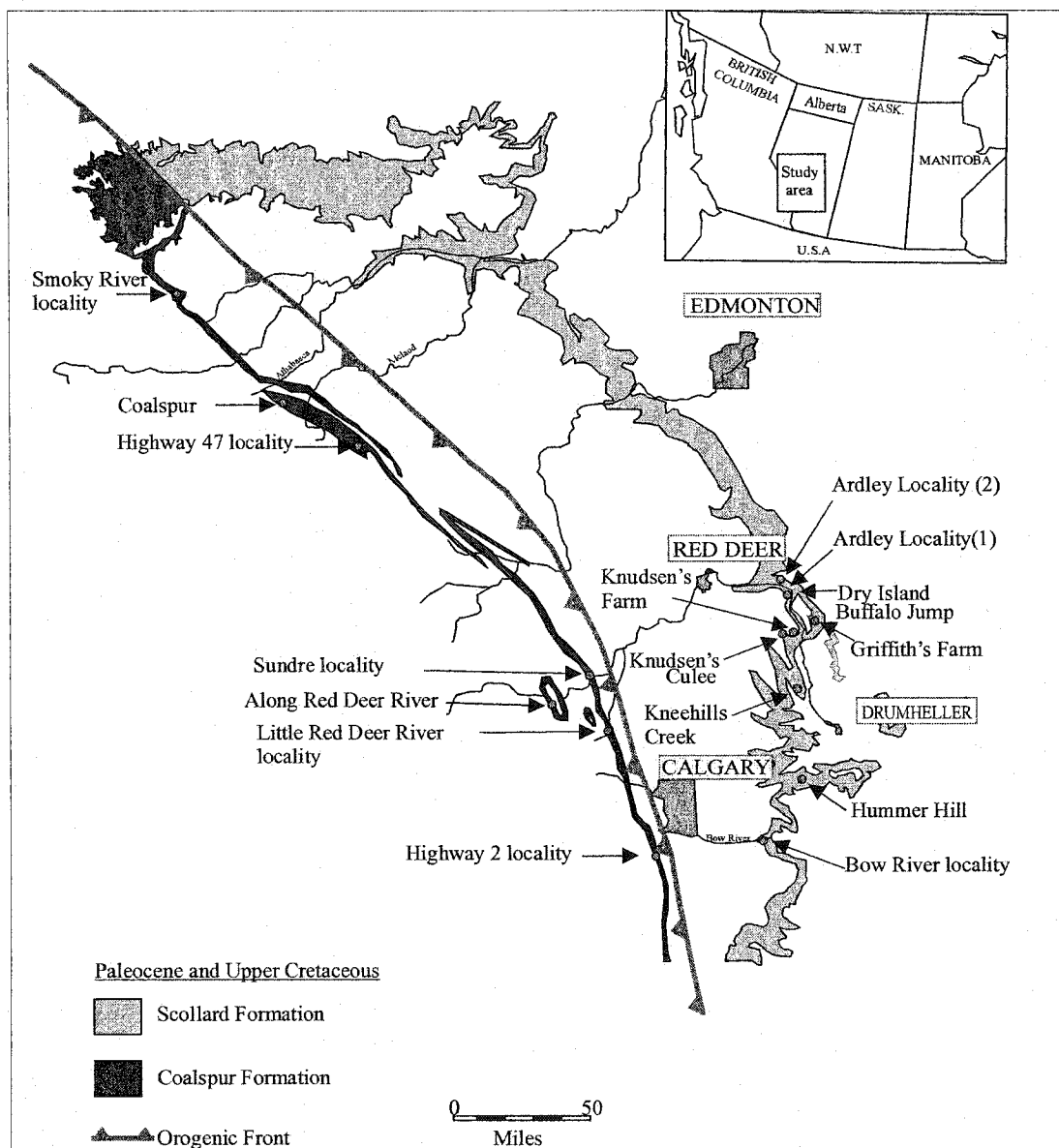
Figure 1-1. Outcrop distribution of the Scollard and Coalspur formations in Alberta, and the location of the studied outcrop sections.

AGE		Foothills				Plains		
		Stratigraphic Units						
Paleocene		Paskapoo Formation				Paskapoo Formation		
	Coalspur Formation	upper Coalspur	Val d'Or		Scollard Formation	upper Scollard	Ardley	
Maastrichtian		lower Coalspur	Mynheer			lower Scollard	Nevis	
			Entrance Member				Battle Formation	
							Whitemud Formation	
		Brazeau Formation					Horseshoe Canyon Formation	

Figure 1-2. Generalized chart of the late Maastrichtian-Paleocene stratigraphy of central Alberta, showing the position of the Scollard and Coalspur formations.

REFERENCES

Catuneanu, O. and Sweet, A.R. 1999. Maastrichtian-Paleocene foreland basin stratigraphies, Western Canada: A reciprocal sequence architecture. Canadian Journal of Earth Sciences, v. 36, p. 685-703.

Dawson, F.M., Evan, C. G., Marsh R., and Richardson, R. 1994. Uppermost Cretaceous and Tertiary of the Western Canada Sedimentary Basin. *In:* Geological Atlas of the Western Canada Sedimentary Basin. G.D. Mossop and I. Shetsen (comps.), Calgary. Canadian Society of Petroleum Geologists and Alberta Research Council, p. 387-406.

Hower, J., Eslinger, E. V., Hower, M. E., and Perry, E. A. 1976. Mechanism of burial metamorphism of argillaceous sediment: 1. Mineralogical and chemical evidence. Geological Society of America Bulletin, v. 87, p. 725-737.

Chapter 2

Sedimentology and diagenesis of the Scollard sandstones
in the Red Deer Valley area, central Alberta

INTRODUCTION

The Scollard Fm represents a fully nonmarine succession, which accumulated during the Late Maastrichtian-Early Paleocene interval in the foredeep of the Western Canada foreland system (Catuneanu and Sweet, 1999). The timing of the Scollard fluvial aggradation corresponds to a stage of loading in the thrust-fold belt that resulted in foredeep subsidence and forebulge uplift. As a result, the correlative forebulge stratigraphy is mostly reduced to an unconformity that marks a maximum regression of the Interior Seaway, i.e., the turnaround between the Bearpaw regression and the Cannonball transgression. The Scollard therefore accumulated in isolation from marine influences, on a dynamic topography controlled by tectonic mechanisms. Differential subsidence across the foredeep, with higher rates towards the thrust-fold belt, generated a gradual shallowing of the topographic gradient during orogenic loading, which resulted in a shift in fluvial styles from braided (lower Scollard) to meandering (upper Scollard) (Gibson, 1977; Eberth and O'Connell, 1995; Catuneanu and Sweet, 1999).

The Scollard Fm is well exposed in a number of locations in central Alberta (Fig. 2-1). The Formation includes commercially important coal seams, and is best known for containing within its sequence the Cretaceous-Tertiary boundary. This fluvial succession has been the subject of various stratigraphic and coal geology studies, but its diagenetic history has received little attention. Some of the diagenetic processes may be related to

paleoclimatic fluctuations that may have controlled the pore-water chemistry during the early post-depositional stages. Original detrital mineralogy also controlled the diagentic route of the Scollard sandstones. The purpose of this paper is to characterize the diagenesis and porosity evolution of the Upper Cretaceous-Lower Tertiary fluvial sandstones of the Scollard Formation, and to estimate the paleo-climatic shifts that took place during its sedimentation. This study may provide an outcrop analogue for the characterization of other subsurface reservoirs constituted of fluvial sandstones.

GEOLOGICAL BACKGROUND

Gibson (1977) defined the Scollard in the Scollard Canyon of the Red Deer Valley. Within the study area, the Scollard overlies the lacustrine mudstones of the Battle Formation and is overlain by the Paskapoo Formation (Fig. 2-2). The Scollard Formation consists of thick gray-to-buff sandstone and siltstone units interbedded with thin olive green mudstone beds and coal. Two informal members, separated by the K-T boundary, are recognized based on the abundance of coal (Dawson et al., 1994). The upper member (Early Paleocene) contains thick coal beds (Ardley coal zone), which are of economic importance. This coal zone includes 12 coal seams with a cumulative thickness of up to 20 m (Dawson et al., 1994). The lower member (Late Maastrichtian) is generally barren of coal. Both the upper and lower members of the Scollard thicken from east to west. The thickness of the Scollard-age deposits in south-central Alberta, along the Red Deer Valley, is around 100 m, but increases to about 300 m in the Foothills of Alberta (Dawson et al., 1994). The Foothills strata of Scollard age are referred to as the "Coalspur Formation".

The contact of the Scollard with the underlying Battle Formation has been interpreted as corresponding to a time of non-deposition, with or without erosion (Russell, 1983). In the outcrop, the distinctive mauve shales of the Battle are in sharp contrast to the buff to olive-green sediments of the Scollard Formation. The upper contact between the Scollard and the Paskapoo Formation is defined as a major unconformity associated with a stratigraphic gap of up to 4 million years (Lerbekmo et al., 1990). This contact is taken at the base of the first major sandstone above the Ardley coal zone (Gibson, 1977).

DATA BASE AND METHODOLOGY

Fieldwork was carried out in central Alberta along the Red Deer Valley and the Kneehills Creek. Standard logging techniques were applied to each outcrop section, including thickness measurements, facies analysis, paleoflow measurements, and sampling for laboratory work. Figure 2-3 illustrates the facies codes used for the description of all outcrop sections (Figs. 2-4 to 2-8). The localities studied along the Red Deer Valley include Knudsen's Farm and Knudsen's Coulee (Fig. 2-4), Buffalo Jump Provincial Park (Fig. 2-5), the Ardley locality (Fig. 2-6), Griffith's Farm (Fig. 2-7), and the Kneehills Creek locality (Fig. 2-8). Based on lithofacies and petrographic attributes, the correlation of the studied outcrop sections is illustrated in Figure 2-9. A total of 30 sandstone beds, 6 coal seams, and 9 shale and siltstone intervals were sampled and described within the studied area. All sandstone samples were impregnated with blue epoxy resin to highlight porosity before preparing the thin section slides. Representative

thin sections were point counted to calculate the relative amounts of detrital framework grains, interstitial minerals, and porosity.

To identify authigenic minerals and porosity, and to determine paragenesis, selected samples were examined by using a scanning electron microscope (SEM, JEOL JSM 6400) equipped with an energy-dispersive x-ray analyzer. To identify clay minerals, x-ray diffraction (XRD) analysis was preformed on bulk samples and separates of less than 2 μm.

Sandstone samples containing an early generation of calcite cement were selected for isotopic analyses (Table 2-1). The powdered rock samples were reacted with anhydrous phosphoric acid at 25°C. An oxygen-isotope CO_2-H_2O fractionation factor of 1.0412 at 25°C was used to calibrate the mass spectrometer reference gas. Oxygen isotopic compositions were calculated by using a phosphoric acid-CO_2 fractionation factor of 1.011025 at 25°C for calcite. The oxygen and carbon isotope data are reported in the normal δ notation relative to the Standard Mean Ocean Water (SMOW) for oxygen and the PeeDee Belemnite (PDB) standard for carbon. The reproducibility of duplicate analyses is generally better than ± 0.18‰ for each oxygen and carbon isotope measurement.

THIN SECTION PETROGRAPHY

The coarse framework of the Scollard Formation sandstones is composed mostly of lithic fragments, quartz, and feldspar grains, with varying percentages from one bed to another (Figs. 2-4 to 2-8). The sandstones are also characterized by a general lack of terrigenous matrix, with an average percentage of 2.5% (range 0-5%). Based on the

classification of clastic rocks (Pettijohn et al. 1987), the Scollard sandstones are considered to be litharenites to sublitharenites (Fig. 2-10). The texture of the arenites ranges from fine- to medium-grained and display moderate sorting.

The medium-grained sandstone dominates the lower member of the Scollard, whereas fine-grained sandstone dominates the upper member. Quartz and feldspar grains are mostly subangular, and lithic fragments range in roundness from subangular to subrounded, with the latter dominating.

ROCK FRAGMENTS

The most striking feature of the Scollard sandstones is the variety of types of rock fragments, ranging from sedimentary to metamorphic and igneous origins. The majority of lithoclasts range in size from 0.09 to 0.4 mm in diameter, with an average size of 0.15 mm, and are subangular in shape. Rock fragments make up 30% (on average, with a range of 20-55%) of the coarse framework of the rock. Lithoclasts of sedimentary origin are mostly represented by chert fragments and dominate the chief framework components of the lower Scollard sandstones (Fig. 2-11 A). Chert detritals are characterized by uniform microcrystalline quartz with no visible relict texture, which were derived from a sedimentary provenance. Additionally, there are detrital chert fragments with a combination of microquartz and megaquartz textures. Metamorphic rock fragments are also relatively abundant make up to 30% of the lithics. The detritals from metamorphic sources include polycrystalline quartzite characterized by sutured crystal boundaries (Fig. 2-11 B). Some of the metamorphic clasts show schistose textures, likely derived from high-grade metamorphic source rocks. Other identified

metamorphic features include numerous elongated and crenulated quartz crystals welded together. Igneous rocks are less abundant than the other lithoclast types, because of volcanic rock fragments are chemically less stable compared to other lithologies. When present, volcanic rocks occur as large grains with lath plagioclase set in a very fine crystalline matrix (Fig. 2-11 C). Various igneous textures such as microlitic, lathwork, felstic, vetric, and cryptocrystalline types were also recognized (Fig. 2-11 C, and D).

QUARTZ

Monocrystalline quartz grains average 30% (range of 25-45%) of the framework. Fifteen percent of the quartz-grain population displays undulatory extinction, requiring $>5^0$ stage rotation for complete extinction, a feature which may be attributed to plutonic sources. Some of the detrital quartz shows zones of inclusions near its outer margins (Fig. 2-11 E), similar in appearance to abraded authigenic quartz overgrowth, which is a common feature in grains of volcanic origin (Scholle, 1979). These are probably inclusions of the fluids present at the time of crystallization (Fig. 2-11 F). It can also infer a significant proportion of quartz grains of metamorphic origin because of the presence of associated quartzite lithoclasts. Other quartz grains are corroded and replaced by calcite cement. The grain shape ranges from subrounded to subangular.

FELDSPAR

Plagioclase is the dominant feldspar type in the Scollard sandstones (Fig. 2-12 A). Potassium feldspars (usually less than 4% of the feldspar grains) are also observed in both the lower and the upper Scollard sandstones. Although mostly albitized, the original

composition of the plagioclase was predominately andesine, as determined by measuring the maximum extension angles. Feldspar is relatively low, usually less than 15% of the framework, probably because of chemical alteration and dissolution. The microcline displays grid twinning and makes up only about 1% of the total feldspar components. Some of the plagioclase feldspars are of volcanic origin, as the presence of euhedral crystals indicates. Growth composition and albite twinning also indicate a predominately volcanic plagioclase (Scholle, 1979). Fresh detrital feldspars also occur, suggesting nearby source areas or/and high topographic relief. Plagioclase detritals show considerable alteration, mainly vacuolization and sericization (Fig. 2-12 B). Calcite replacement is also a very common form of diagenetic alteration in the Scollard Formation (Fig. 2-12 C).

MINOR CONSTITUENTS

In addition to the main framework components (quartz, feldspars and rock fragments), accessory minerals such as biotite, muscovite (Fig. 2-12 D), hornblende and pyroxene have also been identified within both lower and upper Scollard Formation.

DRAINAGE PATTERNS

The detrital composition of the sandstones and the texture of the rock fragments indicate a variety of parent rocks within the Cordilleran belt. As indicated by cross-bedding structures, the paleoflow directions gradually changed from dominantly SE (lower Scollard) to S-SE (upper Scollard) (Figs. 2-13, 2-14). The dominant subangular shape of the detrital grains, as well as the relatively high percentage of unstable

15

minerals, indicate relatively short transportation from the source areas to the depositional areas, and/or high relief. The variation with time in the petrographic composition of the Scollard sandstones is illustrated in Figure 2-15.

AUTHIGENIC MINERALS

The sandstones of the Scollard Formation in central Alberta contain a variety of authigenic minerals, including grain–coating and pore-lining clay minerals, pore-filing and grain-replacing calcite, authigenic quartz, and iron oxides.

CALCITE

Calcite is one of the major cement types in both the upper and lower members of the Scollard Formation, ranging in abundance from trace amounts to 40% of the rock. Diagenetic cementation of the Scollard sandstones occurred preferentially in zones of high primary permeability. The early calcite cements can be recognized based on distribution and textural attributes, as they display drusy and poikilotopic features (Fig. 2-12 C) (Jacka, 1970; Flock, 1974; Burns and Matter, 1995). Poikilotopic and blocky spar cements (Fig. 2-10 C) are most often related to precipitation in the phreatic zone (Jacka, 1970; Folk, 1974), which is probably the environment where the early diagenetic alteration of sandstone and the early calcite cementation took place. The element composition of the early calcite cement shows a significant iron content (Fig. 2-16 A), based on XRD analysis. This ferroan calcite is characteristic of meteoric water-phreatic environments (Richard and Fuchtbauer, 1978).

The calcite cement often fills the space between closely packed quartz grains (Fig. 2-16 B). The precipitation of calcite is often accompanied by the corrosion of the quartz grain boundaries (Fig. 2-16 B). Such areas of calcite precipitation form a crystal bond that appears to have enlarged the space between the grains through crystal growth. In these cases, the space between grains was thoroughly filled, and therefore the primary porosity of the sandstone was lost (Fig. 2-16 C). Figure 2-12 C illustrates small-scale expansion resulting from precipitation of calcite into intergranular pore space. Precipitation of calcite cement into originally grain-supported frameworks resulted in the detrital grains becoming surrounded by cement. This implies slow precipitation from dilute solution rather than rapid crystallization around many nucleuses.

In some cases, the calcite cement has invaded the clay-filled pore space and more or less engulfed the clay (Fig. 2-16 D). Extensive replacement of detrital feldspars by early calcite is observed as well (Fig. 2-16 E). The calcite cement typically pre-dates the quartz overgrowth, as the lack of quartz cementation within calcite-cemented zones indicates. Where the calcite post-dates the precipitation of authigenic silica, corrosion of the quartz grains and quartz overgrowths may be observed (Fig. 2-16 F).

Sources of calcite cement

Calcite cementation in the Scollard Formation may be attributed to a combination of internal and external sources. Internal sources include biogenic carbonate, carbonate rock fragments and plagioclase, which could be redistributed as cement by diffusion over short distances (millimeters to meters). Previous work by Walderhaug and Bjorkum (1998) indicates that if the source of Ca^{2+} in the calcite cement was provided by the

dissolution of Ca-rich feldspars (anorthite), which are present in the Scollard sandstones, then equilibrium problems are to be expected. Firstly, the dissolution of one volume of plagioclase would produce only Ca^{2+} for a fraction of the volume of calcite. Secondly, if Ca^{2+} was primarily produced via the dissolution of Ca-rich feldspars, this process would release other components such as silica and aluminum. The volume of diagenetic silica would then exceed the volume of diagenetic calcite, but this result was not observed in the samples of either upper or lower members of the Scollard Formation. As a result, it is unlikely that the dissolution of Ca-rich feldspars represented the primary source of calcite cement in the Scollard Formation, although a minor amount of calcite may probably form during albitization of Ca-rich plagioclase (Walderhaug and Bjorkum, 1992).

Samples from each bed were examined by SEM. Rod-shape particles of possible nanobacteria were observed entombed in the calcite cement in the lower Scollard (Fig. 2-17 A, and B). The role played by microbes is uncertain, but the possibility of microbially arbitrated precipitation of calcite must be considered.

Carbonate rock fragments, probably derived from the sedimentary strata in the Rocky Mountain Front Ranges, are another possible internal source for calcite cementation in the Scollard Formation. A likely external source is the dissolved carbonate brought into solution from the thrust-fold belt by fluvial systems.

CLAY MINERALS

The clay mineral content of the sandstones ranges from 0 to 15% and includes smectite, kaolinite, and illite. The analysis of clay minerals was performed by

X-ray diffractometry and SEM. The difference between the distributions of authigenic clay minerals in the Scollard sandstones may be attributed partly to the physico-chemical conditions to which the rocks were subjected during diagenesis.

An authigenic origin has been attributed to the clay rims that form coats around detrital sand grains (Wilson and Pittman, 1977). Supposing that the clay minerals are not replaced or pushed aside by the force of crystallization, clay covering other authigenic components must then be authigenic in origin as well (Wilson and Pittman, 1977). In our study, SEM and petrographic observations showed that the clay coatings are generally homogenous in thickness and that clay mineral growth is perpendicular to the grain surface (Fig. 2-18 A), a finding which supports an authigenic origin.

Smectite

Smectite is the most widely distributed clay mineral in the Scollard sandstones and occurs as coating rims (Fig. 2-18 A), altered detrital fragments, and pore-filling interstitial fibrous cement. Smectite is commonly of authigenic origin in the Scollard Formation and characterized by highly crenulated, honeycombed, and interlocking crystal shape, with an irregular, wavy plate or sheet-like architecture (Fig. 2-18 B, and C). Moreover, smectite rims commonly show preferred orientation perpendicular to the grain surface (Fig. 2-18 A), indicating authigenic growth (Wilson and Pittman, 1977). The high degree of crystallinity of the smectites in the Scollard sandstones is also a strong indicator of authigenic origin. Authigenic smectite has been observed in sandstones dominated by calcite cement, where the smectite is surrounded by calcite to some extent (Fig. 2-16 D). This finding suggests that the calcite cement precipitated

earlier relative to the smectite. Diagenesis of smectite comprises an initial phase of precipitation and growth, followed by, with increased depth of burial, regeneration and subsequent transformation into more stable clay minerals like illite (Hower, 1981; Eslinger and Pevear, 1988).

The alteration of Ca-feldspar is a possible source for authigenic smectite in the Scollard sandstones (Fig. 2-18 D). In addition, the abundance of smectite in some of the Scollard sandstones may be related to a pore-water chemistry controlled by an arid to semi-arid climate (Velde, 1985) and/or alteration of volcanic rock fragments.

Kaolinite

Kaolinite in the Scollard Fm occurs commonly as fragile aggregates of crystals (Fig. 2-19 A). The authigenic origin of the kaolinite is documented by using petrographic and SEM techniques. Booklet- and vermiform-shaped kaolinite occurs predominantly as pore fills (Fig. 2-19 A, and B) and only rarely as pore linings. The pore-lining kaolinite precipitated relatively early in the diagenesis, whereas the loosely packed pore-filling kaolinite formed later, after the precipitation of grain coating or pore-lining clay and authigenic quartz. The morphology of authigenic kaolinite in this Formation is dominantly of booklet type (Fig. 2-19 A) with relatively large crystals. Individual crystals, as seen under the SEM, have a characteristic pseudohexagonal form, with a well-defined crystalline shape. Kaolinite is unusually abundant where there is active drainage and no marked dry seasons (e.g., Sieffermann et al., 1968; Chamely, 1968; Quatin et al., 1975).

Illite

Illite is a less abundant authigenic mineral in the Scollard Formation, occurring mostly as flame-like structures that greatly reduce permeability (Fig. 2-19 C). Illite may form via direct precipitation from pore fluids during early diagenesis, but most often is a late diagenetic product of the alteration of smectite (Fig. 2-19 D), kaolinite, or K-feldspar. Moreover, XRD data from outcrop samples also indicate the presence of mixed layers of illite and smectite that represent a relatively minor constituent of the clay-mineral fraction in the Scollard Formation.

QUARTZ

Precipitation of authigenic quartz led to euhedral overgrowth on detrital grains (Fig. 20 A) during the early and middle stages in the diagenetic history of the Scollard Formation. Silica cementation formed discrete euhedral and subhedral crystals (Fig. 2-20 B) during early quartz overgrowth, which pre-dates the chemical compaction. Silica overgrowths generally postdate grain–coating, pore-lining and pore-filing clay minerals (Fig. 2-20 B), with the exception of some cases where an intimate intergrowth of authigenic silica with early clay minerals is observed. The boundaries between the hematite and silica cements indicate that the silica cementation predates the precipitation of hematite (Fig. 2-20 B). Relative to the timing of calcite cementation, the precipitation of authigenic silica may be earlier (where corrosion of silica is observed at the contact with calcite), or later.

Generally, the formation of siliceous overgrowth cement is less common in the Scollard Formation, probably because of the more efficient precipitation of calcite and clay mineral coatings.

Influence of grain coating on quartz cementation

The process of grain coating, via the precipitation of authigenic calcite, hematite or clay minerals, is an important diagenetic mechanism controlling the quartz cementation and the porosity evolution in sandstones (Heald and Larese, 1974). The coating of quartz grains is considered to be important in inhibiting the cementation in a significant number of sandstone reservoirs (Pittman and Lumsden, 1968). Other factors like the availability of silica sources, as well as burial temperatures, may also inhibit silica cementation as well.

In the Scollard Formation, the main factor that reduced silica cementation is the authigenic precipitation of calcite and clay minerals (Fig. 2-20 C). Although the clay cement is present in such small amounts in the Scollard Formation as to be a negligible factor, it appears to have prevented the quartz from forming strong bonds with the neighboring grains and resulted in the inhibition of quartz overgrowth.

Hematite coatings are relatively ineffective in preventing quartz cementation in this Formation, as the presence of quartz overgrowths in relatively high hematite-cemented beds indicates (Fig. 2-20 D). In addition, the absence of abnormally uneven growth of authigenic quartz in most of the beds, which would have been a consequence of coating, indicates that hematite cement did not considerably obstruct the secondary quartz growths.

Calcite coating of the detrital grains interferes with the normal enlargement of quartz grains via authigenic silica precipitation and is considered a major factor that inhibited quartz overgrowth in the Scollard Formation. The specks of calcite cement covering the detrital quartz grains are relatively abundant and caused the secondary silica to form only small isolated overgrowths in the early stages of enlargement with authigenic quartz (Fig. 2-20 E).

Quartz is a major porosity-destroying cement in many sandstone beds because the overgrowth of authigenic quartz reduces the pore space between the grains. Although coatings inhibit silica cementation, they also result in a major permeability reduction in the sandstone beds because of the obstruction of pore throats between the grains.

Sources of quartz cement

One possible source of quartz cement is the process of feldspar alteration or dissolution, where the feldspars have higher Si/Al ratios than the resulting secondary minerals. Clay minerals like smectite are also considered as additional internal sources of silica in sandstone by releasing silica during the process of illitization (Hower et al., 1976; Boles and Frank, 1979):

Smectite + Al + K = Illite + Si + Mg + Fe

However, smectite illitization was observed in only a few sandstone beds of the Scollard Formation, so it is not considered an important source of silica in this case study. Pressure dissolution of quartz grain contacts, dissolution of biogenic silica, and dissolution of volcanic fragments represent additional internal sources of quartz cementation. Overall, the internal sources of silica are most likely more important than

23

the external sources in the case of the Scollard Formation. Feldspar grains in the Scollard sandstones are mainly of igneous and metamorphic origin; therefore they are out of stability with the diagenetic conditions of pressure, temperature, and pore fluid chemistry. Hence, feldspars are subject to a diversity of diagenetic processes in order to reach the stability state, as the relatively abundant alteration and dissolution of feldspars in the Formation indicates (Fig. 2-20 F). Feldspar alteration may therefore be considered as an essential source of silica cementation in the Scollard Formation.

IRON OXIDES

Iron oxides represent a major cement in the red beds of both the upper and lower members of the Scollard Formation. The iron oxide occurs as radiating, or needlelike, hematite (Fig. 2-20 D) and may be closely associated with clay coatings around the framework grains (Figs. 2-11 E, 2-18 C). The red coatings are films of iron oxide developed by the dissolution of unstable iron-rich silicates such as hornblende.

The hematite cement occurs as a late diagenetic product in the history of the Scollard Formation, in oxidizing environments, possibly related to post-Scollard tectonic uplift. Alternating wet and dry conditions led to the introduction of iron in solution, followed by its oxidation. Iron-rich minerals such as pyroxene and hornblende may, under oxidizing conditions, yield up their iron to form hematite cement (Walker, 1967).

STABLE ISOTOPES

The isotopic composition of authigenic minerals in nonmarine environments is controlled mainly by the isotopic composition of meteoric water (Suttner and Dutta,

1986). Similarly, the isotopic composition of the early authigenic minerals (e.g., early calcite cement) is related to the meteoric water that was involved in the cementation of the unconsolidated sediment. This provides an independent criterion for interpreting the paleoclimate during the Scollard time and needs to be used in conjunction with the results of petrographic, SEM and XRD analyses. For a given region, a decrease in surrounding air temperatures or an increase in relative humidity over time should result in decreased $\delta^{18}O$ values for the local meteoric water. Depletion in ^{18}O occurs because of decreased evaporation during a cold or humid climate, whereas high $\delta^{18}O$ values indicate more evaporation of meteoric water under arid to semi-arid conditions (Anderson and Arthur, 1983; Lawrence and White, 1991).

The isotopic composition of the early calcite cement in the Scollard Formation ranges for ($\delta^{13}C$) from –4.844 to +4.79‰ PDB, whereas oxygen isotope values ($\delta^{18}O$) range from –19.667 to –11.875‰ PDB (Table 2-1). The negative isotopic composition of the oxygen in the Scollard Formation signifies that the calcite cement did not precipitate from the more saline compaction water in the deeper parts of the basin. The $\delta^{18}O$ values are consistent with the precipitation of early calcite cement from meteoric waters in phreatic and vadose cementation zones at relatively low temperatures (Fig. 2-21). The higher $\delta^{13}C$ values may be attributed to a significant involvement of carbon from soil-derived bicarbonate or oxidation of organic matter and isotopically heavier C_4 plant biomass (Mora et al., 1993). These higher $\delta^{13}C$ values are probably related to the large amounts of organic-rich coaly beds and coal measures in the upper Scollard Formation (Fig. 2-2).

Relatively wetter climatic conditions (increased humidity) result in isotopically more negative precipitation, as is seen in the samples measured from the Scollard Formation. These low $\delta^{18}O$ values have two probable causes: *(i)* the main mechanism for the precipitation of calcite was transpiration, and not evaporation; *(ii)* the aquifer has been recharged by mixing oxygen values from meteoric waters with those derived from the dissolution of detrital constituents, predominantly volcanic rock fragments and feldspar, which are ^{18}O-rich minerals. The dissolution of volcanic rock fragments and feldspars is common in the Scollard Formation sandstones (Fig. 2-20 F).

The variability in the isotopic compositions of the Scollard Formation (Fig. 2-21) might reflect fluctuations in the precipitation rates, abundance of vegetation, and seasonal temperatures (Wange et al., 1993).

DISCUSSION

DISTRIBUTION OF AUTHIGENIC MINERALS

The distribution of authigenic minerals in the Scollard sandstones is relatively variable (Figs. 2-4. 2-8). The lower member is characterized by two types of cements: clear calcite, and hematite. This member is also characterized by pore-filling and pore-lining kaolinite, and grain-coating smectite, with minor occurrences of illite and authigenic quartz.

The upper Scollard Formation displays two main types of cement: late diagenetic hematite (Fig. 20 B) and primary poikilotopic calcite (Fig. 2-12 C). The upper Scollard sandstones are also cemented by grain-coating and pore-filling clay minerals, mainly smectite (Figs. 2-16 D, 2-18 A), kaolinite (Fig. 2-19 A) and illite. The relative

abundance of smectite throughout the Scollard sandstones suggests that the conversion of smectite to illite was limited. This finding indicates relatively low maximum burial temperatures, considerably less than 120 °C (Hower et al., 1976). The alteration of smectite to illite also requires a supply of K^+ (Longstaffe and Ayalon, 1991). Thus, the clay mineral assemblages in the Scollard sandstones may possibly render a limited supply of potassium arising from detrital K-feldspar and low mica content in the original sediments. The variability in the distribution of these cements among the sandstone beds is likely controlled by changes in the chemistry of meteoric waters, which may be related to paleoclimatic fluctuations. Silica cementation is also noted in rare instances. Calcite and clay coatings controlled the distribution of authigenic quartz by preventing quartz overgrowths.

DIAGENETIC SEQUENCE

The sequence of diagenetic events, as determined from thin section slides and SEM examination, is summarized in Figure 2-22. Early diagenesis includes (1) initial mechanical compaction after deposition; (2) calcite cementation; (3) dissolution of detrital feldspars and volcanic fragments; (4) early authigenic quartz overgrowth; and (5) formation of clay coatings, rimes, pore-linings, and early clay pore fills. Ground water chemistry at this stage of shallow depths has great influence on early authigenesis and, in turn, controls later diagenetic episodes and reservoir quality.

Burial diagenesis is a stage characterized by the dissolution/replacement/alteration of minerals, generation of secondary porosity, and precipitation of neoformed minerals. Therefore, the burial diagenesis in the Scollard

Formation consists of precipitation of authigenic quartz and pore-filling kaolinite; dissolution of feldspar grains; corrosion and dissolution of quartz grains and authigenic silica; alteration of mica, biotite and other iron-bearing minerals; precipitation of hematite cement; and dissolution of calcite cement (Fig. 2-23 A). Albitization of detrital plagioclase was rare in the Scollard sandstones. Detrital K-feldspar grains in the sandstones were barely albitized where partial dissolution of detrital K-feldspar was observed. The weak albitization of K-feldspar implies that the maximum burial temperatures did not exceed 125°C (Ben et al., 1993). The conditions that set off dissolution/alteration reactions during burial diagenesis of the Scollard Formation are possibly related to factors like pore fluid chemistry, velocity of pore fluid, chemical stability of minerals and depth/temperature relationships.

POROSITY AND PERMEABLITY IN THE SCOLLARD SANDSTONES

The reduction of primary intergranular porosity in the Scollard sandstones began soon after deposition and initial burial, as the abundance of deformed ductile grains indicates. This suggests that most of the porosity may have been lost rapidly via mechanical compaction before any significant cementation occurred. In contrast, some samples of Scollard sandstones show that cementation by calcite was so rapid that only slight mechanical compaction occurred because of early calcite cementation.

Initial clast composition is one factor that affected the reduction of primary porosity in this Formation (Fig. 2-23 B). Subsequent reduction of primary porosity was rapid because of the abundance of unstable grains like biotite, feldspars, and some rock fragments (Fig. 2-11 A), which are more affected by mechanical compaction than the

stable minerals like quartz. Mechanical compaction also involved processes of grain rotation and rearrangement, grain fracturing, and deformation of ductile grains (Fig. 2-23 B). Rapid precipitation of calcite cement involved grain rotation and grain fracturing as well (Fig. 2-23 C).

The present porosity of the Scollard sandstones is both primary (2-23 D) and secondary in origin. Early calcite cementation affected the sandstone beds, completely occluding their porosity and forming a "tight sandstone". The early calcite cement interrupted mechanical compaction and prevented the precipitation of other cement types. Precipitation of authigenic clay minerals seemed to be less effective than calcite cementation in reducing the primary porosity of the Scollard sandstones.

Secondary porosity may be recognized by using criteria based on petrographic and scanning electronic microscope studies (Schmidt and McDonald, 1979). The Scollard sandstones are characterized by several types of secondary porosity, including (1) partial dissolution of soluble constituents (Fig. 2-23 E); (2) grain moldic porosity produced by partial dissolution of feldspar that occurs along cleavage and twin boundaries of feldspar grains (Figs. 2-20 F, 2-23 F); (3) corrosion of grains adjacent to pores (Fig. 2-16 F); (4) intra-constituent pores, which are generally the result of leaching of carbonates and incomplete replacement of feldspars grains; and (5) dissolution of intergranular carbonate cement. Fracturing porosity in the Scollard sandstones is volumetrically insignificant, but can be very effective in increasing the permeability of "tight" sandstones (Fig. 2-23 C). The porosity determined from thin sections ranges from 1% to 20% and averages 11%. Most of the secondary porosity in the Scollard Formation is intergranular and was formed by the dissolution of pore-filling and replacement

cements. Molds porosity demonstrates the dissolution of former framework grains and is observed in the Scollard sandstones (Fig. 2-20 F).

The distribution of authigenic clay minerals also has affected the primary porosity in the Scollard sandstones. For instance, the various individual kaolinite booklets, which have no preferred orientation relative to one another, consumed a large part of the original pore space, hence affecting the primary porosity. On the other hand, kaolinite contains a large number of small channels through which the fluids can still move (Fig. 2-19 A), and thus the rock still retains a reservoir-quality permeability (Neasham, 1977). This finding suggests that the permeability-reduction mechanism is an actual physical control and constriction in the pore throats rather than drag and increased turbulence of laminar flow created by a roughed surface (Howard, 1992). A reduction in permeability with a corresponding increase in the degree of illitization, as noted by Guven et al. (1980), is observed in the Scollard sandstones. Pore-filling interstitial fibrous smectite cements also reduce the porosity and permeability in sandstones because of their particular structure that causes the pore systems to have a very high surface-area-to-volume ratio (Almon, 1979).

Both clay rims and the solid grain overgrowths result in a permeability decline, although the former tend to preserve a higher porosity in the sandstone because of the microporous nature of the clays. A correlation between the degree of illitization and a corresponding reduction in permeability (Guven et al., 1980) is also observed within the Scollard sandstones.

The timing of secondary porosity generation is uncertain. The dissolution of unstable detrital grains (Fig. 2-24 A) was most likely a continuous process throughout

burial, which led to an increase in secondary porosity. It is possible that the processes of dissolution and consequent formation of secondary porosity started relatively early in diagenesis, shortly after compaction and the formation of clay coatings and rims.

The observed diagenetic features render the Scollard sandstones as semi-mature in the diagenesis maturity classification of Schmidt and McDonald (1979).

CLIMATIC FLUCTUATIONS DURING THE SCOLLARD TIME

The fluctuations in climatic conditions during the c. 3 My Scollard interval may be inferred from the results of our petrographic, SEM, XRD, and isotopic analyses. The cyclic changes in the relative abundance of rock fragments, quartz, and feldspars may be attributed to climatic variability in the study area (Basu, 1976), although the effects of sediment transport and source-rock variability must also be considered. The results of thin section petrography become more reliable climatic indicators when correlated with the shifts in the composition of authigenic minerals, as well as with the isotopic analyses of early diagenetic cements. The $\delta^{13}C$ values are possibly strongly influenced by the presence of organic matter and coal in the Formation. The $\delta^{18}O$ values, on the other hand, come from early calcite cements and can be more reliably related to paleoclimatic conditions. An important outcome of our isotopic analyses is the indication that the precipitation of early authigenic minerals took place in equilibrium with fluids of meteoric origin (Fig. 2-21), at relatively shallow depths and low diagenetic temperatures. This allows for the authigenic clay minerals to be used as paleoclimate indicators in conjunction with the results from thin section petrography.

Paleoclimate inferences from petrography

Numerous studies have investigated the effect of climate on the petrography of sandstones (Mann and Cavaroc, 1973; Young et al., 1975; Basu, 1976, 1985; Mack and Suttner 1977; Suttner and Dutta, 1986; Jermy and Michael, 1988). These studies have shown that a distinction between semi-arid and humid climates may be possible through the comparison of the plots of variation in relative amounts of detrital grains in sandstones. Younge et al. (1975) observed the effects of climate overprinting in recent fluvial sediments derived from low-rank metamorphic, high-rank metamorphic, and plutonic source rocks. They found that petrographic distinctions exist in the sediments derived from the same source area under humid (southeastern U.S.) and arid (northwest U.S.) conditions. Minerals more resistant to chemical weathering, such as quartz, are more abundant in a humid climate, whereas the percentage of rock fragments is significantly higher under an arid climate because of the less efficient chemical weathering.

The possible effect of climatic differentiation on the Scollard fluvial sandstones is best seen in the modal percentages of rock fragments and quartz (mono- and polycrystalline) in both the lower and the upper members of the Formation (Fig. 2-15). The percentage of feldspar does not vary significantly through time, which may imply proximity to the source areas and/or relatively steep topographic gradients. Climatic fluctuations may be inferred from the composite petrographic profile, which correlates well with the variability observed in the authigenic mineral composition (Fig. 2-15).

Paleoclimate inferences from authigenic clay minerals

Climate may play a significant role in determining the nature of early cements (Walker et al., 1978). In order for climate to exert a control on the authigenic clay minerals in sandstones, the clay must form relatively early and at shallow depths where interstitial waters are largely of meteoric nature (Suttner and Dutta, 1986). Cation-rich clays such as smectite form when rainfall is low and the resultant ionic concentration in the groundwater is high (Velde, 1985). Authigenic kaolinite and quartz cements are abundant in areas with high rainfall and warm climate (high humidity, relatively wetter conditions), where the groundwater has a low ionic concentration (Dutta, 1992). Therefore, the nature of the silicate cement is a function of the groundwater chemistry, which in turn may be controlled by climate (Suttner and Dutta, 1986).

The Scollard sandstones include a variety of authigenic minerals, as was mentioned earlier in the paper (Figs. 2-4 to 2-8). The dominant types of authigenic clay minerals are the smectite and the kaolinite, whose relative amounts vary significantly from one bed to another. These shifts in the relative proportions are not random, but correlate with the observed changes in lithosomes, as determined from thin section petrography. The arenites with a higher quartz percentage (Q_2 in Fig. 2-15) contain high amounts of kaolinite coupled with frequent occurrences of quartz overgrowth, a finding that points towards wetter climatic conditions and more efficient weathering (intervals 1, 3, 5, 7 and 8 in Fig. 2-15). The arenites with a higher lithoclast percentage (L_2 in Fig. 2-15) are, rather, dominated by the presence of smectite, suggesting less efficient chemical weathering and more arid conditions (intervals 2, 4, 9 and 10 in Fig. 2-15). The

correlation between the framework mineralogy and the authigenic clay content supports the possibility of a climatic control on the mineralogical composition of the Scollard sandstones for the stratigraphic intervals cited above (1-5 and 7-10 in Fig. 2-15). A lack of correlation between the framework mineralogy and the associated authigenic clays is noted for the intervals 6 and 11-13, where the high quartz percentages are not accompanied by any significant amounts of kaolinite. These exceptions may be explained by fluctuations in the chemical conditions of the diagenetic environment.

The formation of kaolinite within intervals 11-13 (Fig. 2-15) was likely inhibited by an alkaline chemistry of the pore water. At low pH values, with little silica in solution, kaolinite is in a stable state, whereas at higher pH values with much silica in solution, the clay minerals with higher proportions of silica such as smectite and illite are likely to be the stable form (Correns et al., 1939). Also, the presence of Ca^{++} tends to block the formation of kaolinite, favoring the precipitation of smectite and illite instead (Millot, 1942). Consequently, the abundance of calcite cement within intervals 11-13 (Fig. 2-15) is probably the main reason why kaolinite is absent or poorly represented. The climate during the accumulation of the beds within the intervals 11-13 might have been humid, in spite of the lack of kaolinite, as the abundance of quartz grains and the presence of coal seams within these intervals suggest. For similar reasons, wetter climatic conditions may also be inferred for interval 6, which is dominated by illite (Fig. 2-15). The formation of authigenic illite is often associated with the dissolution of unstable aluminous mineral phases such as kaolinite, smectite or K-feldspar in late diagenetic stages (Bjørlykke et al., 1995). In the case of this interval 6, SEM evidence

indicates kaolinite as the source for illite (Fig. 2-24 B), which supports the interpretation of a wetter syndepositional regime.

CONCLUSIONS

1. The petrography of the Scollard sandstones in the Red Deer Valley region is defined by sublitharenites and lithic arenites, which accumulated in braided (lower Scollard) and meandering (upper Scollard) fluvial systems. The sandstone composition, reservoir properties, paleoclimate, and diagenetic history have been studied by using the composite information obtained from thin section petrography, scanning electronic microscopy, x-ray diffraction, and carbon and oxygen stable isotopes.

2. Isotopic analyses indicate that the precipitation of early authigenic minerals took place in equilibrium with fluids of meteoric origin, at relatively shallow depths and low diagenetic temperatures. This suggests a relatively small lag time between the deposition of the sandstone detrital grains and the precipitation of early authigenic minerals, and allows for such authigenic minerals to be used as paleoclimate indicators in conjunction with the results of thin section petrography.

3. The correlation between the framework grain petrography and the authigenic clay mineralogy supports a climatic interpretation based on the composition of the Scollard sandstones. Wetter climatic conditions are interpreted for the arenites with higher amounts of mono- and/or polycrystalline quartz, as well as abundant kaolinite and quartz

overgrowth. Drier climatic conditions are inferred for the arenites with lesser percentages of quartz but higher amounts of authigenic smectite.

4. The diagenetic sequence was established based on the relationships observed between the framework grains and the various types of authigenic minerals. The early diagenesis of the Scollard sandstones is characterized by initial mechanical compaction; early calcite cementation; early dissolution of detrital feldspars along with the dissolution of volcanic fragments; early authigenic quartz overgrowth; and the formation of authigenic clay minerals as coatings, rimes, pore-linings and early pore-fills. Burial diagenesis is dominated by precipitation of authigenic quartz and pore-filling kaolinite; dissolution of feldspar grains; corrosion and dissolution of quartz grains and authigenic silica; alteration of mica, biotite and iron-bearing minerals; dissolution of calcite cement; and precipitation of hematite cement.

5. The limited conversion of smectite into illite, as well as the weak albitization of K-feldspar, imply relatively low maximum burial temperatures of less than 120° C.

6. Initial mechanical compaction, pore-filling clay minerals, and calcite cement substantially reduced porosity in the Scollard sandstones. However, in certain facies, a relatively high percentage of the primary porosity was preserved by the early formation of clay rims and coats that inhibited further cementation. These latter facies present moderate to good reservoir properties. Several types of secondary porosity have also been observed in the Scollard sandstones. This study may provide an outcrop analogue

for the reservoir characterization of other fluvial sandstones in the subsurface of the

Western Canada Sedimentary Basin.
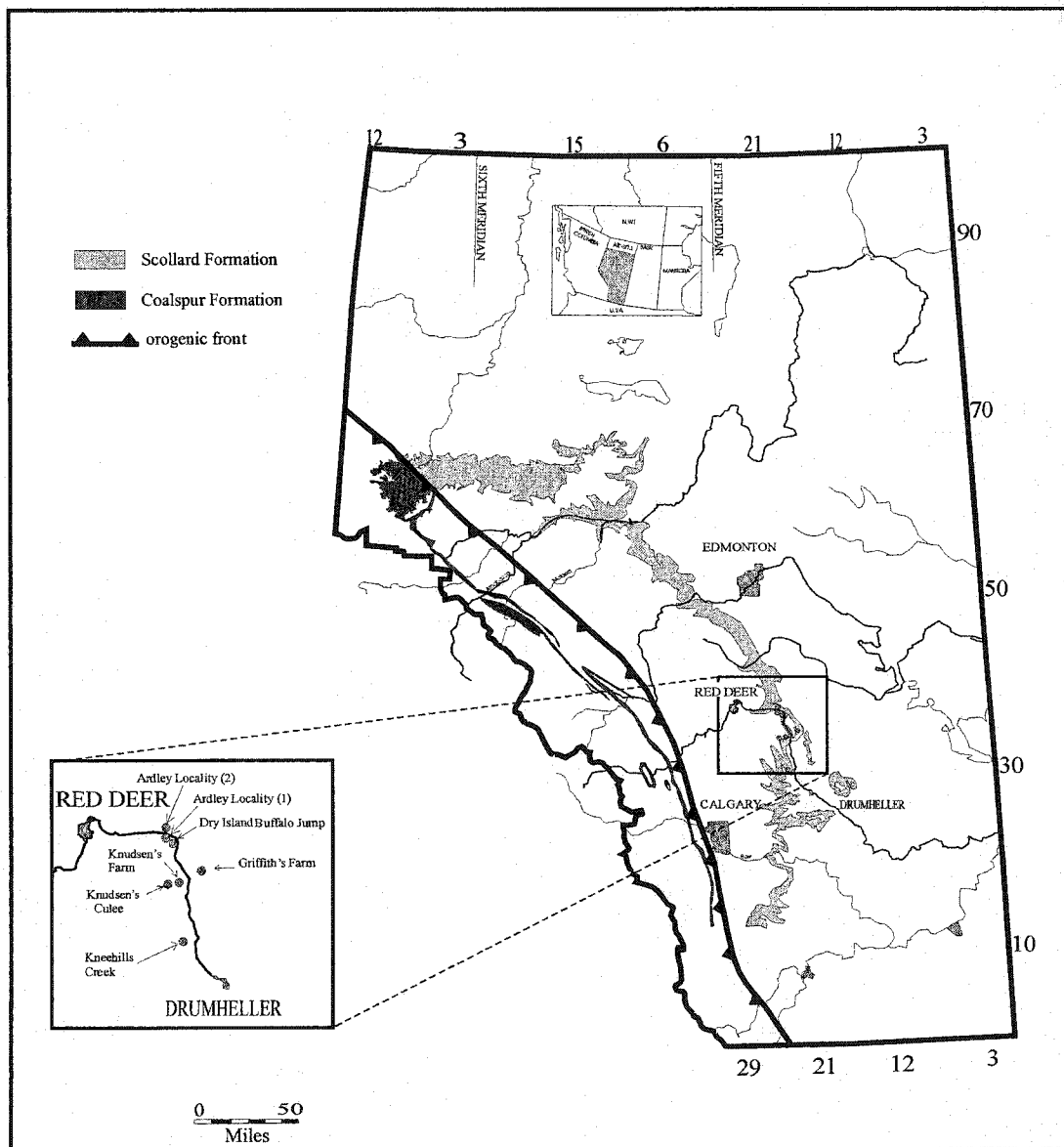
Figure 2-1. Outcrop distribution of the Scollard and Coalspur formations in Alberta, and the location of the studied outcrop sections.

AGE	Stratigraphic units
Paleocene	Paskapoo Formation
	Scollard Formation — upper Scollard / lower Scollard — Ardley / Nevis
Maastrichtian	Battle Formation
	Whitemud Formation
	Horseshoe Canyon Formation

Figure 2-2. Generalized chart of the late Maastrichtian-Paleocene stratigraphy of central Alberta, showing the position of the Scollard Formation and its two major coal seams (Nevis and Ardley).
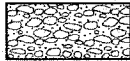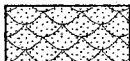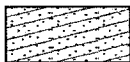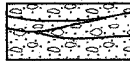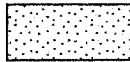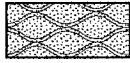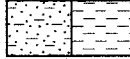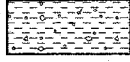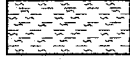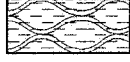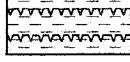
Facies	Facies code and symbol		Sedimentary structures
Gh		Clast-supported, crudely bedded gravel	Horizontal bedding, imbrication
St		Sand, fine to very coarse, may be pebbly	Solitary or grouped trough cross-beds
Sp		Sand, fine to very coarse, may be pebbly	Solitary or grouped planar cross-beds
Sr		Sand, very fine to coarse	Ripple cross-lamination
Sh		Sand, very fine to coarse, may be pebbly	Horizontal lamination, parting or streaming lineation
Sl		Sand, very fine to coarse, may be pebbly	Low-angle ($<15°$) cross-beds
Ss		Sand, fine to very coarse, may be pebbly	Broad, shallow scours
Sm		Sand, fine to coarse	Massive or faint lamination
Sb		Sand, fine to very coarse, may be pebbly	Ball-and-pillow structure, may show internal lamination
Sf		Sand, fine to coarse with mud	Massive, may be laminated
Fl		Sand, silt, mud	Fine lamination, very small ripples
Fsm		Silt, mud	Massive
Fp		Mud with pebbles	Vague laminated mud with floating, isolated clasts
Fs		Mud with sand, fine to coarse	Massive, may be laminated
Fb		Mud, silt	Ball-and-pillow structure, may show internal lamination
Fm		Mud, silt	Massive, desiccation cracks
C		Coal, carbonaceous mud	Plant, mud films

Figure 2-3. Facies types used to describe the sedimentological characteristics of the studied outcrop sections (Figs. 4-8).

Sample Number	Quartz %	Feldspar%	Lithics%	Calcite	Hematite	Smectite	Kaolinite	Illite	Quartz overgrowth	Biotite	Muscovite	Pyroxene
K-9	60	10	30	very abundant	x	very abundant	less abundant	x	x	x	x	very abundant
K-8	65	8	27	very abundant	less abundant	very abundant	?	less abundant	x	x	x	very abundant
K-7	50	10	40	very abundant	less abundant	very abundant	?	less abundant	x	x	very abundant	x
K-6	35	15	50	less abundant	very abundant	very abundant	less abundant	x	very abundant	x	very abundant	x
K-5	25	10	65	less abundant	very abundant	very abundant	x	x	less abundant	less abundant	less abundant	x
K-4	30	8	62	less abundant	very abundant	less abundant		x	very abundant	x	very abundant	x

CLAY | SILT | Vf | F | M | C | Vc |

← SAND →

Explanation

━━━━━━ very abundant
- - - - - less abundant
x absent

NE ... SW

38 m

117 m

Figure 2-4. Outcrop sketch and vertical profile for the Knudsen's Farm locality. The table shows the sandstone composition in terms of detrital constituents and authigenic minerals. The relative percentages of the three main framework constituents (quartz, feldspars, lithoclasts), out of 100%, is used to classify the sandstones (Fig. 10). The polycrystalline quartz is counted under lithoclasts. See Figure 3 for facies codes.

41
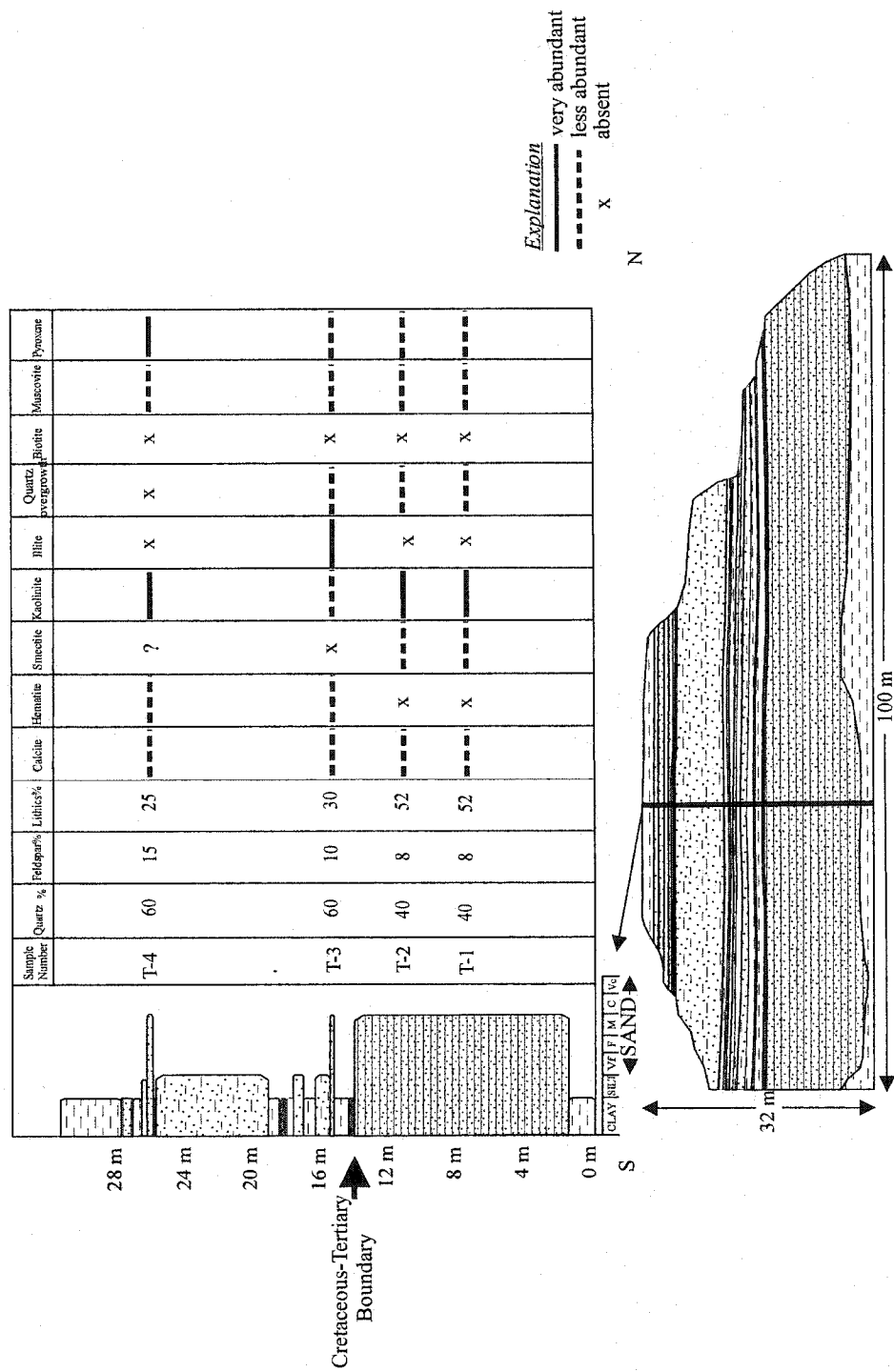
Figure 2-5. Outcrop sketch and vertical profile for the Buffalo Jump Park locality. The table shows the sandstone composition in terms of detrital constituents and authigenic minerals. The relative percentages of the three main framework constituents (quartz, feldspars, lithoclasts), out of 100%, is used to classify the sandstones (Fig. 10). The polycrystalline quartz is counted under lithoclasts. See Figure 3 for lithofacies codes.

Explanation
——— very abundant
- - - - less abundant
x   absent

Sample Number	Quartz %	Feldspar %	Litbits %	Calcite	Hematite	Smectite	Kaolinite	Illite	Quartz overgrowth	Biotite	Muscovite	Pyroxene
T-4	60	15	25	dashed	dashed	?	very abundant	x	x	x	dashed	very abundant
T-3	60	10	30	dashed	dashed	x	dashed	very abundant	dashed	x	dashed	dashed
T-2	40	8	52	dashed	x	dashed	very abundant	x	dashed	x	dashed	dashed
T-1	40	8	52	dashed	x	dashed	very abundant	x	dashed	x	dashed	dashed

Cretaceous-Tertiary Boundary

28 m, 24 m, 20 m, 16 m, 12 m, 8 m, 4 m, 0 m
S

CLAY | SILT | vf | f | m | c | vc
◀ SAND ▶

100 m
32 m
N

42

Figure 2-6. Outcrop sketch and vertical profile for the Ardley locality. The table shows the sandstone composition in terms of detrital constituents and authigenic minerals. The relative percentages of the three main framework constituents (quartz, feldspars, lithoclasts), out of 100%, is used to classify the sandstones (Fig. 10). The polycrystalline quartz is counted under lithoclasts. See Figure 3 for facies codes.

43

Sample Number	Quartz %	Feldspar%	Lithics%	Calcite	Hematite	Smectite	Kaolinite	Illite	Quartz overgrowth	Biotite	Muscovite	Pyroxene
G-11	40	15	45	very abundant	X	less abundant	less abundant	?	X	X	less abundant	less abundant
G-10	63	8	29	very abundant	less abundant	less abundant	less abundant	less abundant	X	X	less abundant	less abundant
G-9	55	10	35	very abundant	less abundant	very abundant	less abundant	less abundant	less abundant	X	less abundant	less abundant
G-4	40	7	53	very abundant	very abundant	less abundant	less abundant	X	very abundant	very abundant	very abundant	X
G-2	45	15	40	less abundant	very abundant	very abundant	?	less abundant	very abundant	X	X	X
G-5	35	10	55	less abundant	very abundant	less abundant	less abundant	very abundant	less abundant	less abundant	less abundant	X

CLAY | SILT | Vf | F | M | C
◄ SAND ►

Explanation
———— very abundant
- - - - - - less abundant
x   absent

NW   SE

12 m

◄———————————————— 29 m ————————————————►

Figure 2-7. Outcrop sketch and vertical profile for the Griffith's Farm locality. The table shows the sandstone composition in terms of detrital constituents and authigenic minerals. The relative percentages of the three main framework constituents (quartz, feldspars, lithoclasts), out of 100%, is used to classify the sandstones (Fig. 10). The polycrystalline quartz is counted under lithoclasts. See Figure 3 for facies codes.

44

Sample Number	Quartz %	Feldspar%	Lithics%	Calcite	Hematite	Smectite	Kaolinite	Illite	Quartz overgrowth	Biotite	Muscovite	Pyroxene
Kn-5	35	10	55	less	X	very	X	X	less	less	less	less
Kn-6	35	15	50	less	X	very	X	X	very	less	less	less
Kn-4B	35	10	55	very	X	very	X	X	X	less	less	X
Kn-4A	35	10	55	very	X	very	X	X	X	very	less	X
Kn-3	55	10	35	less	X	less	very	X	very	X	less	X
Kn-2	35	15	50	less	X	very	X	less	less	X	less	less
Kn-1	30	10	60	less	X	less	X	less	X	X	less	less

Explanation
▬▬▬ very abundant
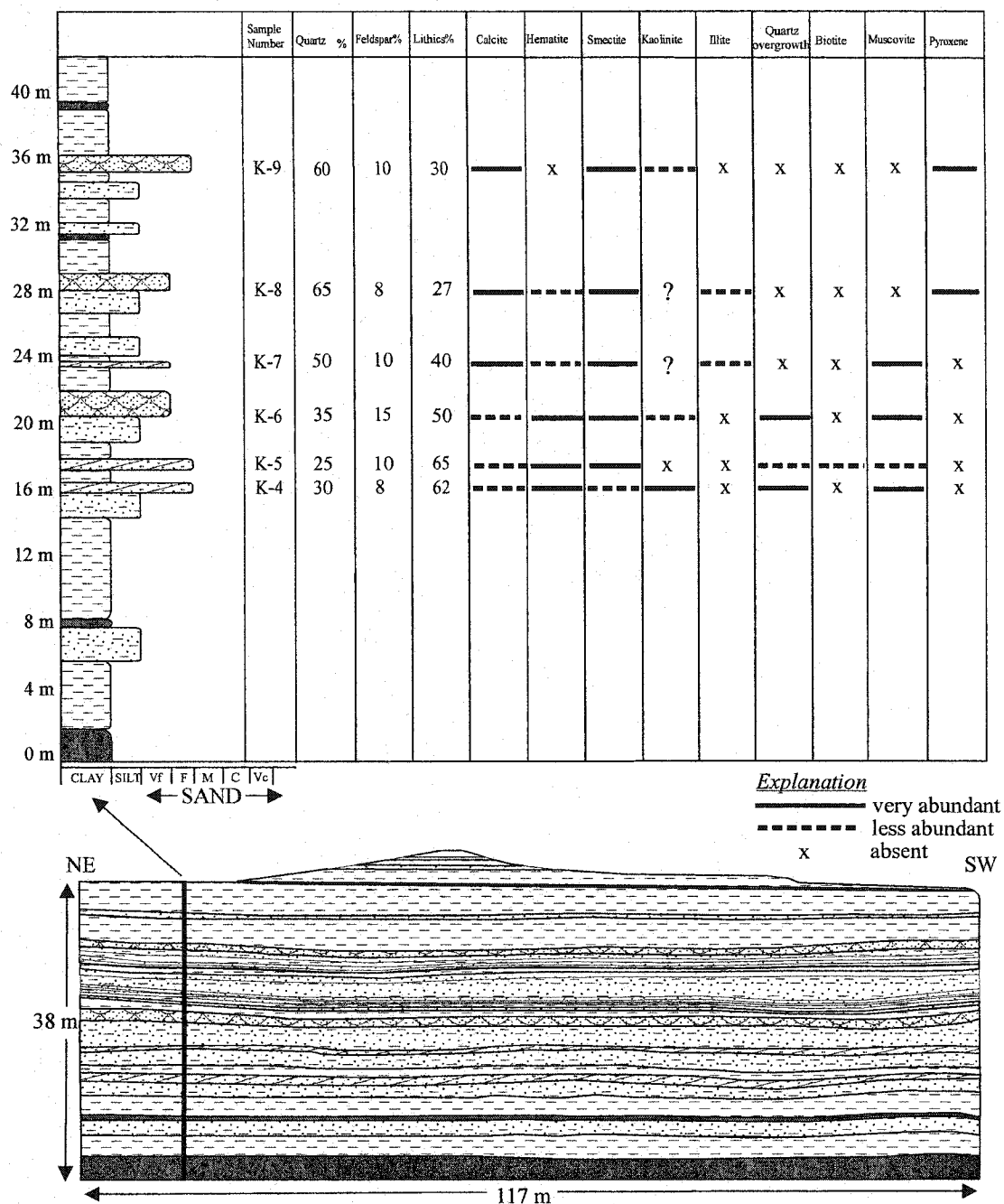- - - - less abundant
X absent
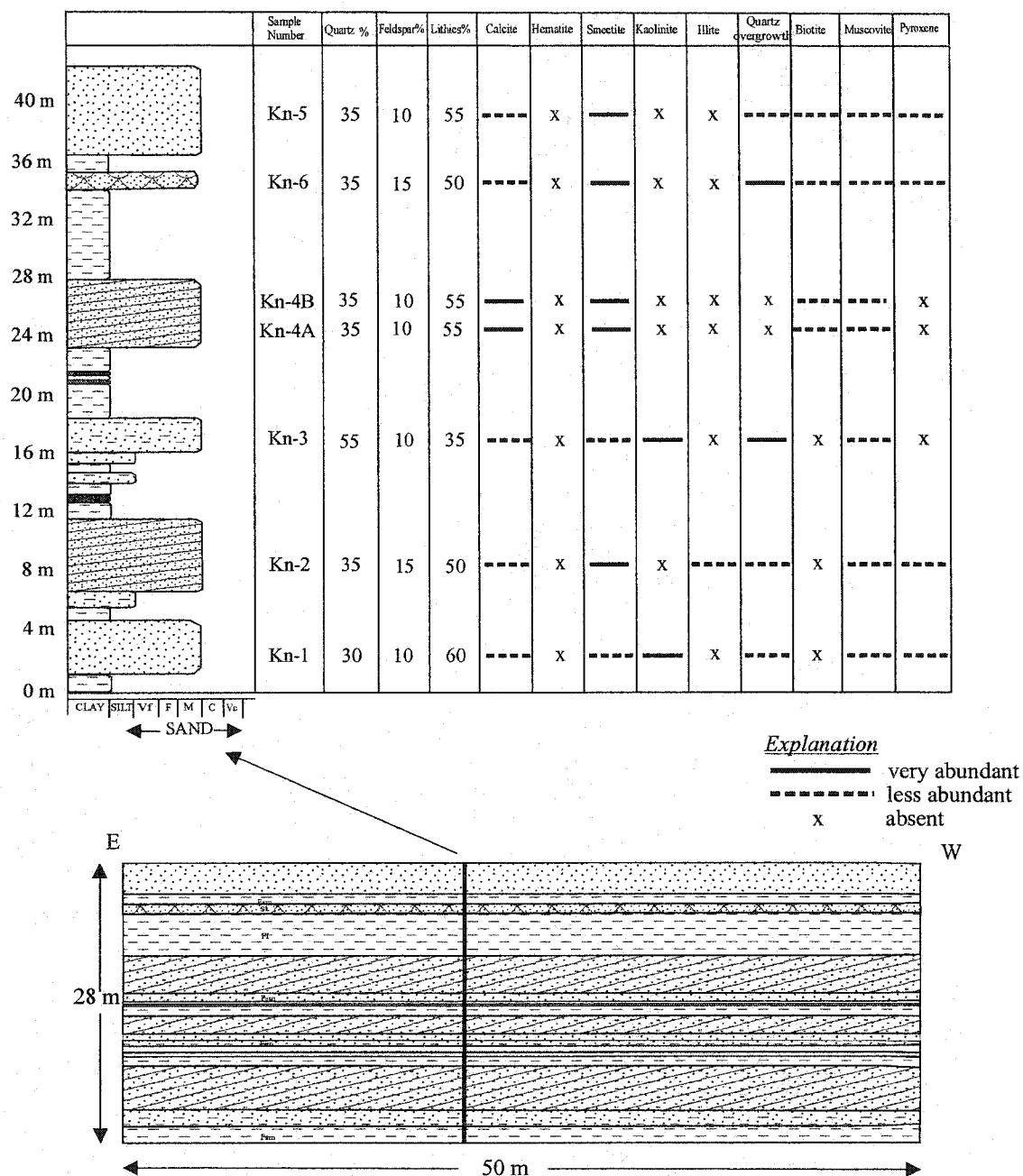
Figure 2-8. Outcrop sketch and vertical profile for the Kneehills Creek locality. The table shows the sandstone composition in terms of detrital constituents and authigenic minerals. The relative percentages of the three main framework constituents (quartz, feldspars, lithoclasts), out of 100%, is used to classify the sandstones (Fig. 10). The polycrystalline quartz is counted under lithoclasts. See Figure 3 for facies codes.
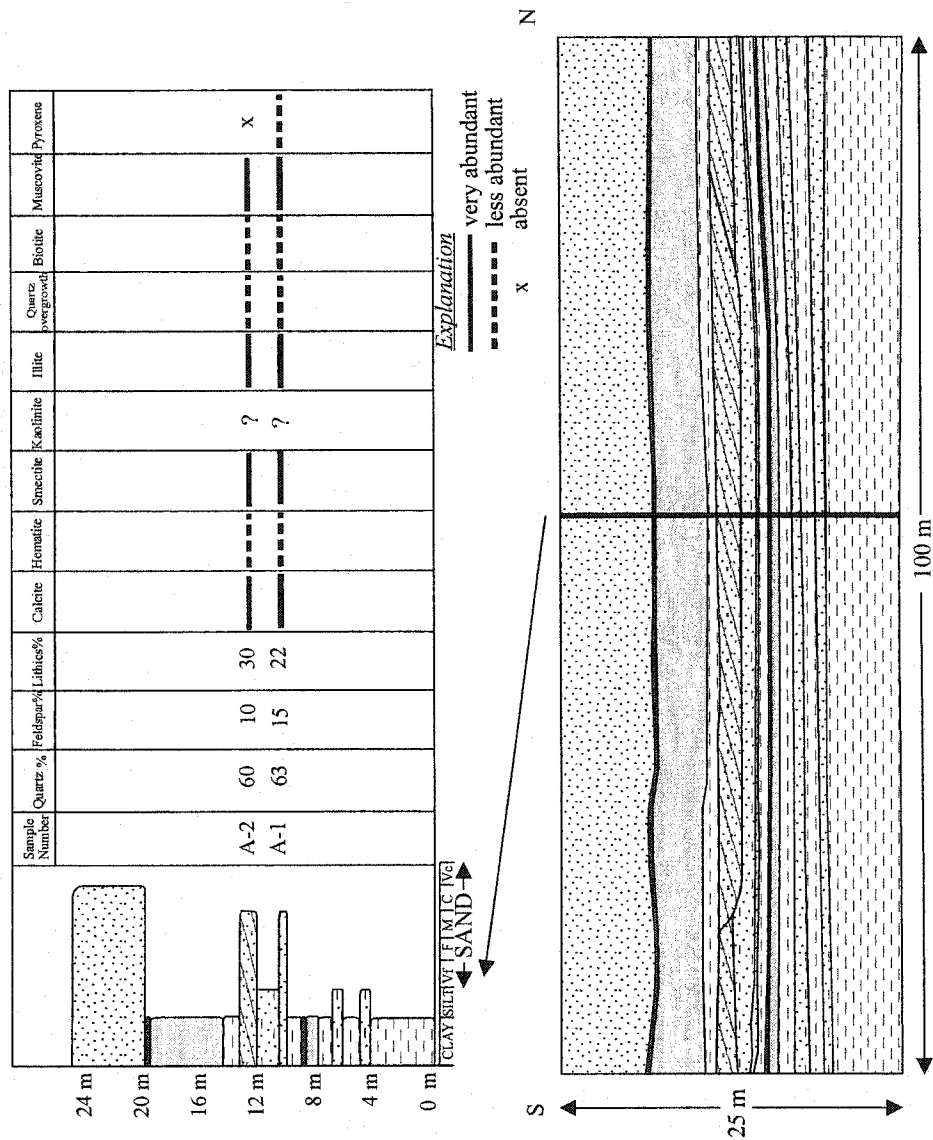
45
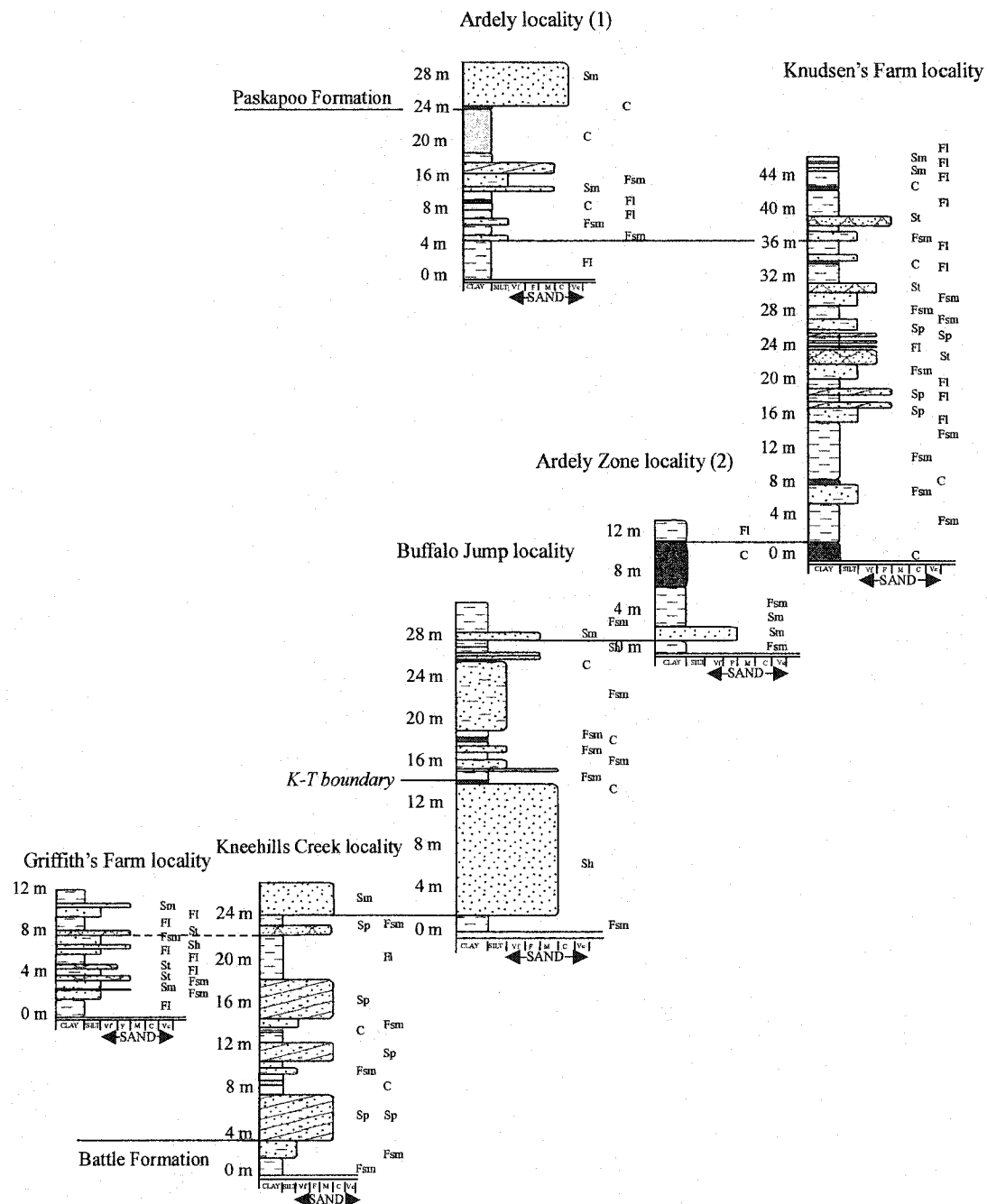
Figure 2-9. Correlation of the outcrop sections in the Red Deer Valley , based on petrofacies attributes.
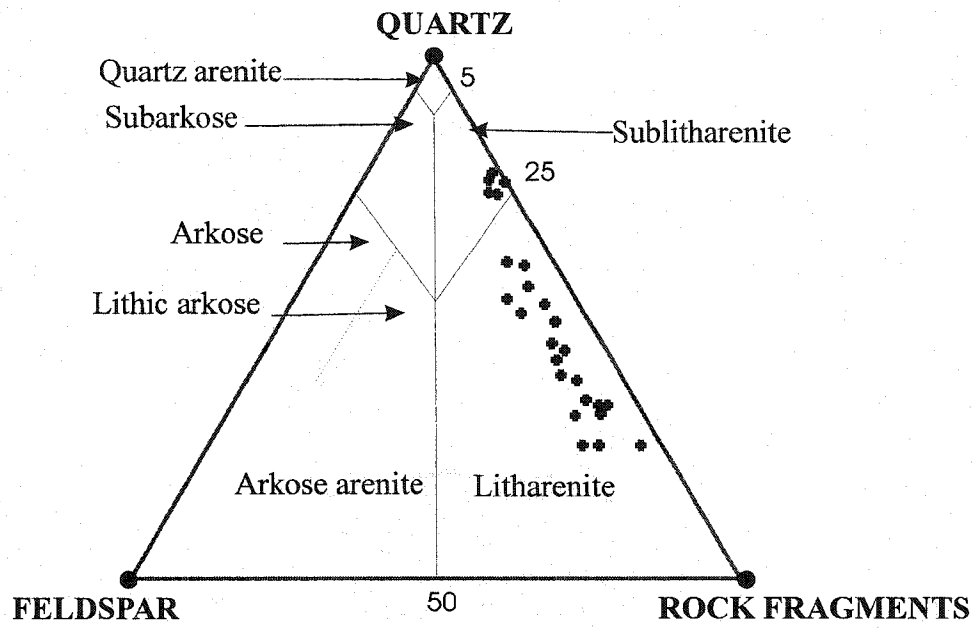
Figure 2-10. Classification of the Scollard Formation sandstones (after Pettijohn et al., 1987).
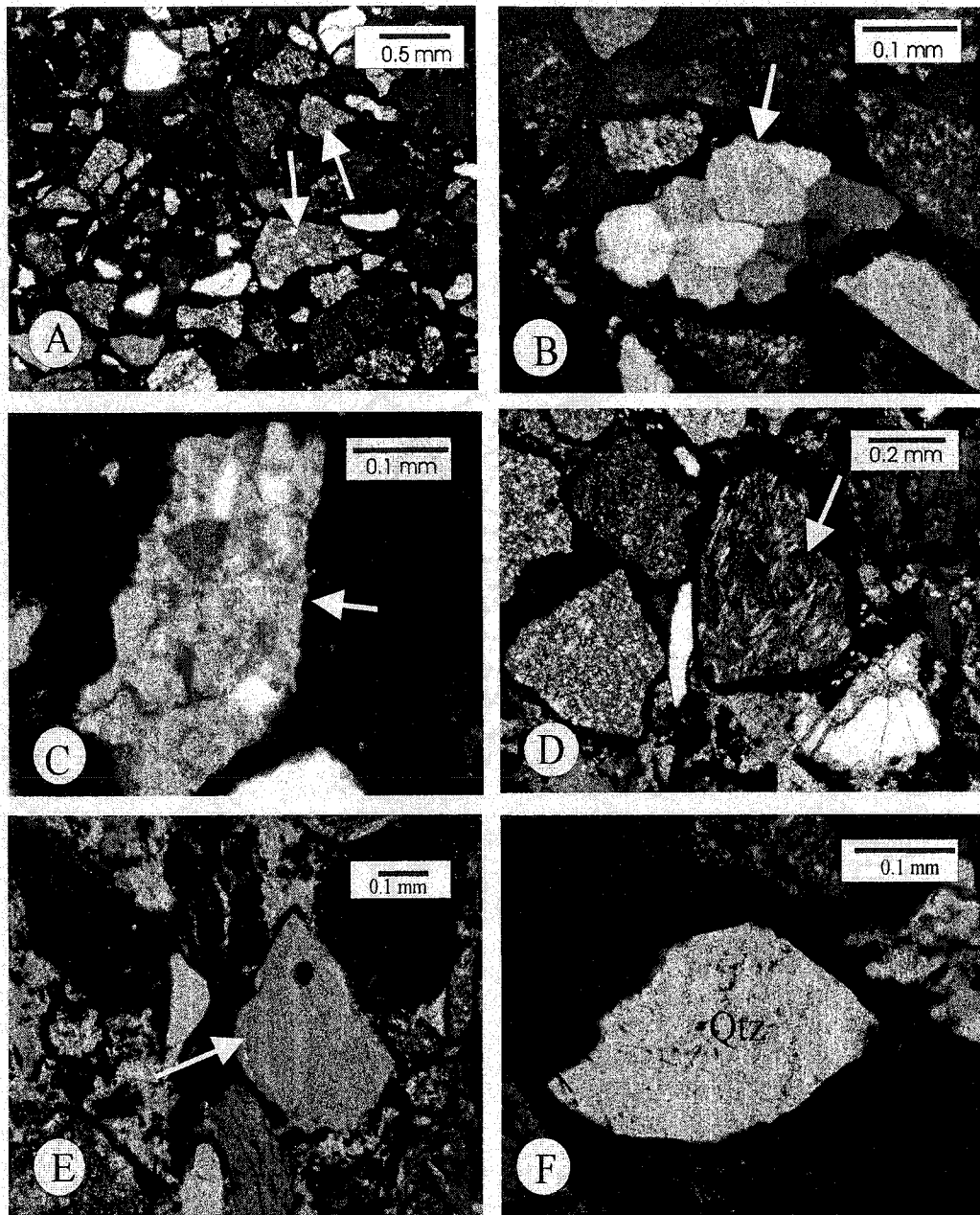
Figure 2-11. Thin-section photomicrographs: (A) litharenite from the Griffith's Farm locality, with chert lithoclasts (arrows). Note the uniform microcrystalline quartz with no visible relict texture, as well as detrital chert fragments showing a combination of micro- and megaquartz textures (sample G-1, lower Scollard Formation, Griffith's Farm locality); (B) detrital grain of polycrystalline quartz of metamorphic origin (arrow) (sample K-4, upper Scollard Formation, Knudsen's Farm locality); (C) and (D) detrital grains of igneous origin (arrows) (sample K-5, upper Scollard Formation, Knudsen's Farm locality); (E)and (F) fluid inclusions associated with quartz grains (sample G-6, lower Scollard Formation, Griffith's Farm locality).
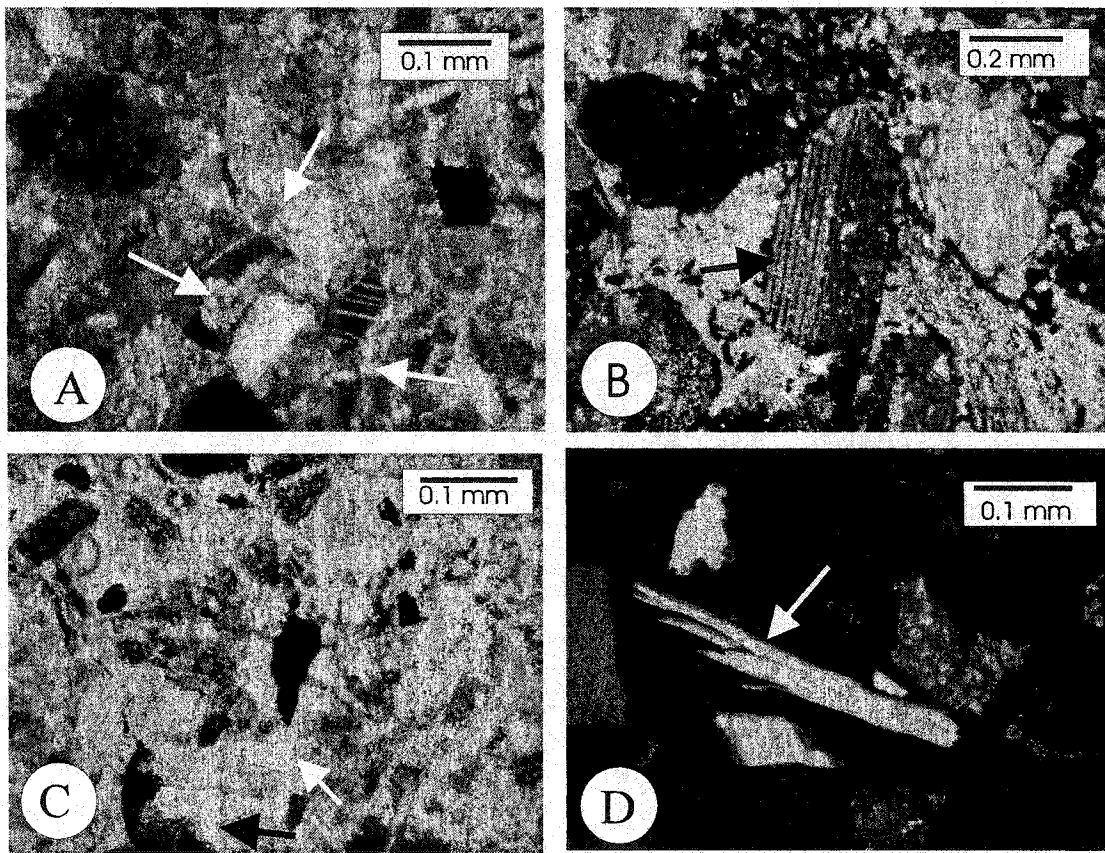
Figure 2-12. Thin-section photomicrographs: (A) poikilotopic calcite cement (arrows) (sample G-9, lower Scollard Formation, Griffith's Farm locality); (B) detrital plagioclase showing alteration, vacuolization and sericitization (arrow). Note the early calcite cement and the late hematite cement around the detrital feldspar (sample G-1, lower Scollard Formation, Griffith's Farm locality); (C) early poikilotopic calcite cement (black arrow). The plagioclase shows signs of dissolution and diagenetic replacement with calcite. A small-scale expansion of the rock is noted from the precipitation of the calcite in the intergranular pore space (white arrow) (sample G-9, lower Scollard Formation, Griffith's Farm locality); (D) detrital muscovite (arrow), more chemically stable and abundant than biotite (sample Kn-2, lower Scollard Formation, Kneehills Creek Locality).
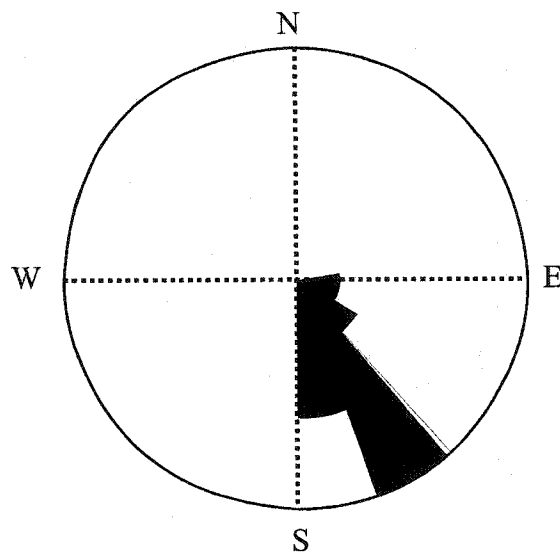
Number of Points: 23
Class Size: 20
Maximum Percent: 43
Vector Mean: 141.13
Vector Magnitude: 22.27
Consistency Ratio: 0.9249

Figure 2-13. Rose diagram showing the paleoflow directions for the lower Scollard Formation.
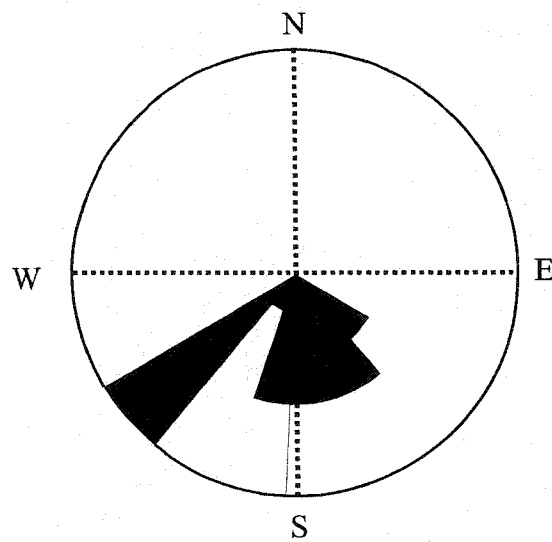
Number of Points: 17
Class Size: 20
Maximum Percent: 29
Vector Mean: 183
Vector Magnitude: 143
Consistency Ratio: 0.84

Figure 2-14. Rose diagram showing the paleoflow directions for the upper Scollard Formation.
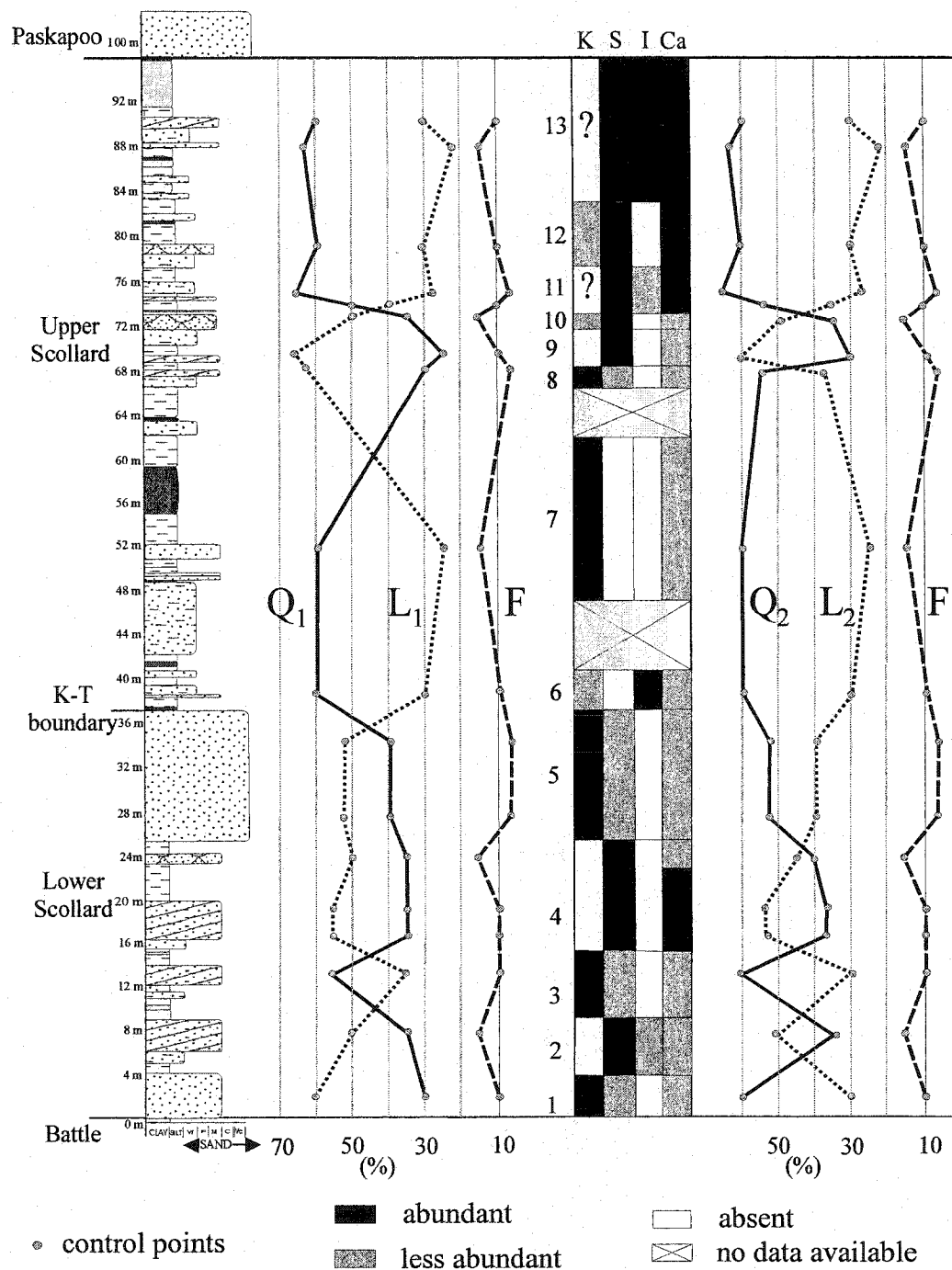
Figure 2-15. Composite vertical profiles of the Scollard Formation in the Red Deer Valley region, showing the variability in lithofacies (see Fig. 3 for symbols), framework constituents, and main authigenic mineral composition. Abbreviations: Q1 monocrystalline quartz; L1 lithoclasts (including polycrystalline quartz); F feldspar; Q2 quartz (mono- and polycrystalline); L2 lithoclasts (excluding polycrystalline quartz); K kaolinite; S smectite; I illite; Ca calcite cement. The framework component curves to the left (Q1, L1, F) describe the sandstone petrography (see also Figs. 4-8, 10). The framework component curves to the right (Q2, L2, F) are used for paleoclimate interpretations.

52
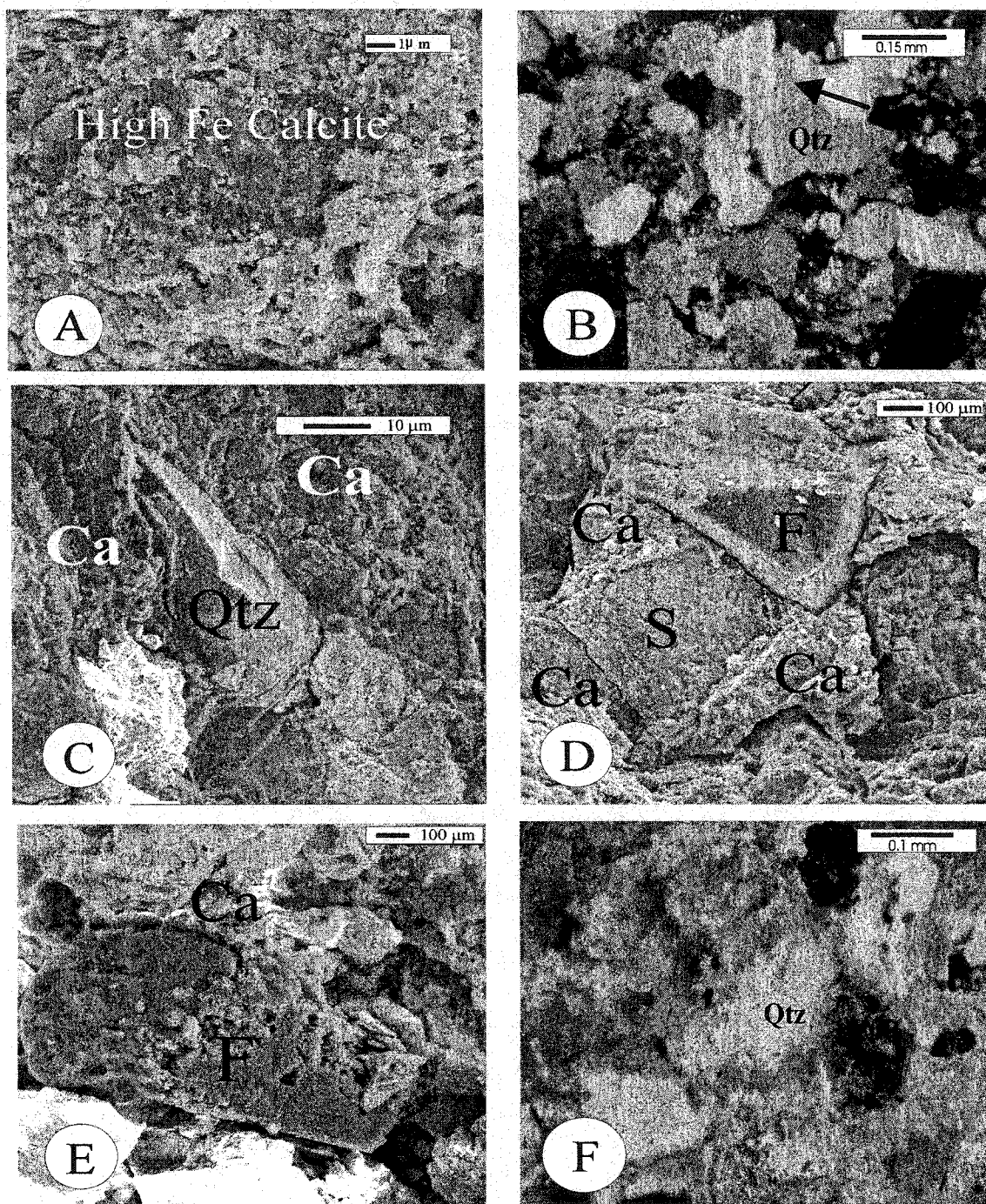
Figure 2-16. Scanning electronic photomicrographs: (A) Fe-rich calcite cement, as determined by XRD analysis (sample K-8, upper Scollard Formation, Knudsen's Farm locality); (B) local "island" of calcite (arrow) surrounded by closely packed quartz grains; corrosion may be observed at the grain margins (sample T-2, upper Scollard Formation, Buffalo Jump locality); (C) calcite cement that completely destroyed the primary porosity (sample G-11, lower Scollard Formation, Griffith's Farm locality); (D) calcite cement that invaded the clay-filled pore space and engulfedthe smectite (sample K-9, upper Scollard Formation, Knudsen's Farm locality); (E) feldspar subject to dissolution and calcite replacement (sample K-5, upper Scollard Formation, Knudsen's Farm locality); (F) quartz grain corroded by early poikilotopic calcite cement (sample K-9, upper Scollard Formation, Knudsen's Farm locality). Abbreviations: Ca calcite; Qtz quartz; S smectite; F feldspar.

53
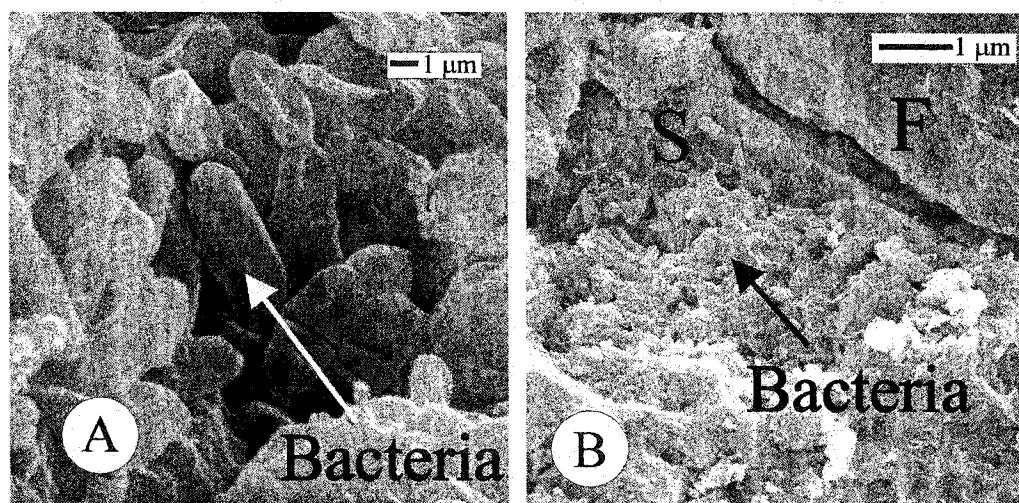
Figure 2-17. Scanning electronic photomicrographs, (A) and (B): rod-shaped bacteria (arrows) entombed in calcite cement (sample G-11, lower Scollard Formation, Griffith's Farm locality). Abbreviations: S smectite; F feldspar.
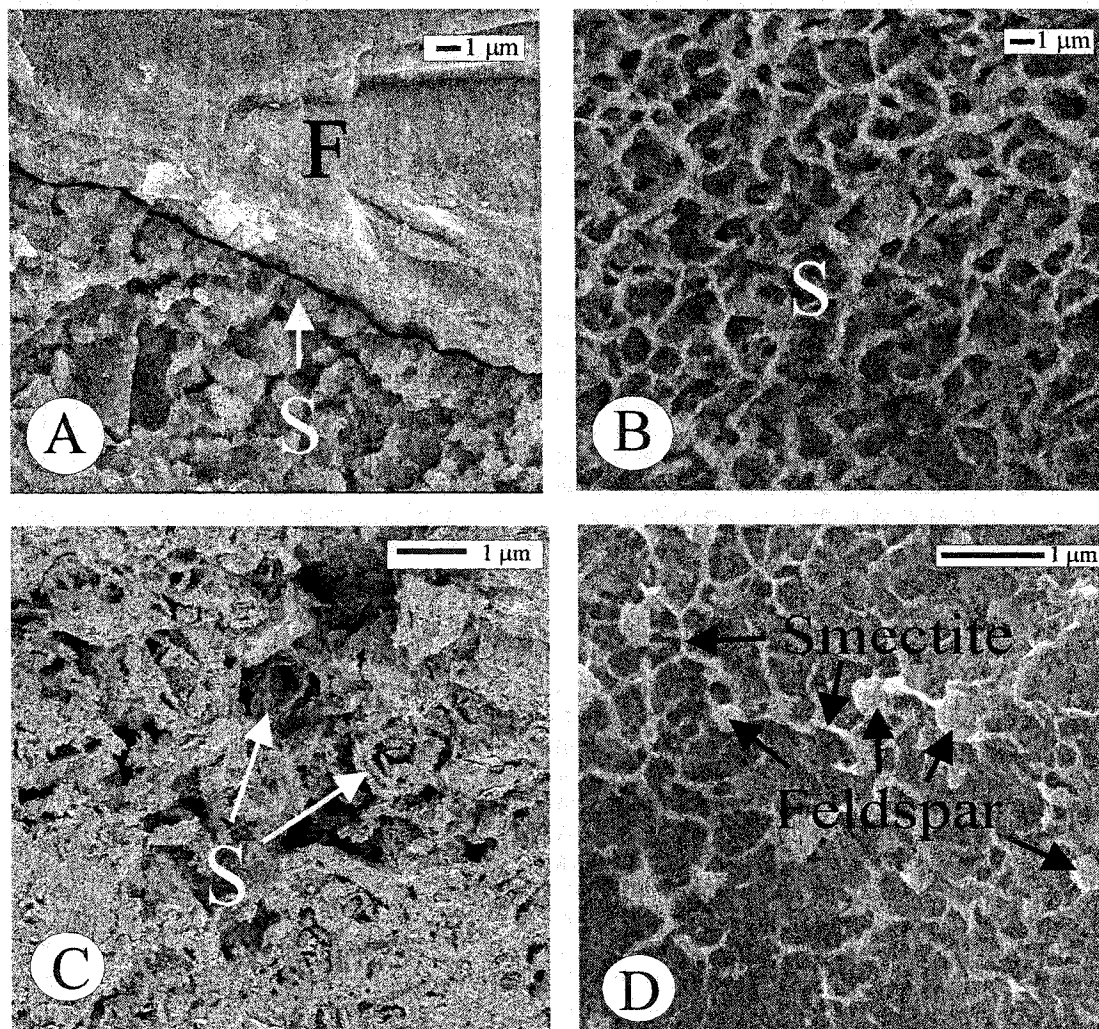
Figure 2-18. Scanning electronic photomicrographs: (A) coating rim of authigenic smectite .Note the smectite growth perpendicular to the surface of the feldspar grain (sample Kn-2, lower Scollard Formation, Kneehills Creek locality); (B) authigenic smectite showing highlycrenulated, honeycombed, and interlocking crystal shapes (sample Kn-5, lower Scollard Formation, Kneehills Creek locality). Abbreviations: S smectite; F feldspar; (C) highly crenulated authigenic smectite, with trace amounts of hematite (sample K-4, upper Scollard Formation, Knudsen's Farm locality); (D) - feldspar alteration into smectite (sample G-2, lower Scollard Formation, Griffith's Farm locality.
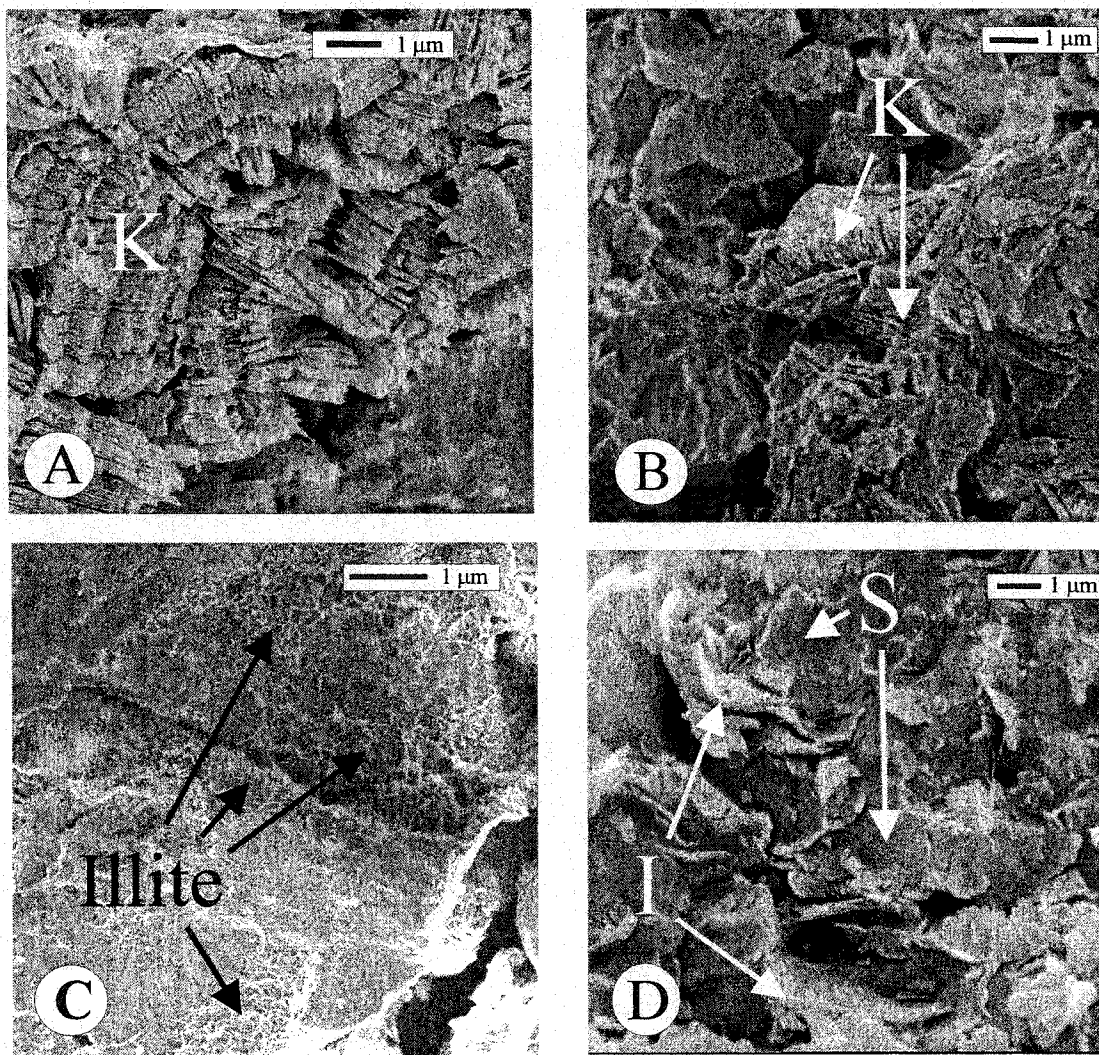
Figure 2-19. Scanning electronic photomicrographs: (A) and (B) vermicular aggregates of euhedral crystals of authigenic kaolinite. The kaolinite booklets have no preferred orientation, and consume much of the primary porosity. Note the numerous small channels between the kaolinite crystals that still allow fluids to flow, which is why the rock retains a good permeability (sample Kn-1, lower Scollard Formation, Kneehills Creek locality); (C) thick illite coating quartz grains, which considerably reduces the porosity and permeability of the rock (sample T-3, upper Scollard Formation, Buffalo Jump Park locality); (D) alteration of smectite into illite (sample Kn-3, lower Scollard Formation, Kneehills Creek locality); Abbreviations: K kaolinite; S smectite; I illite.
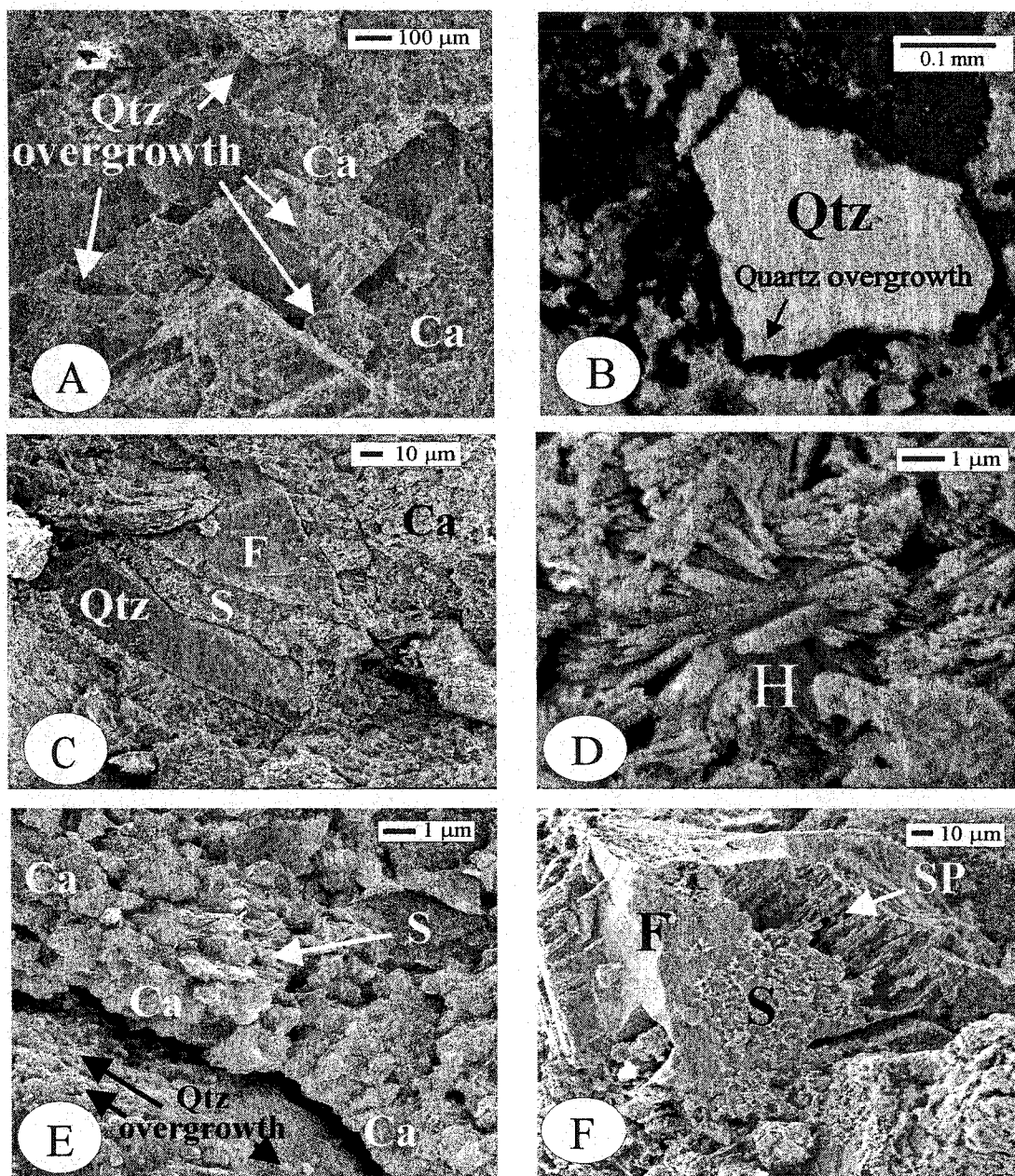
Figure 2-20. Scanning electronic photomicrographs: (A) - individual small quartz overgrowths joining together into single euhedral crystals. The precipitation of the authigenic quartz post-dates the calcite cement (sample G-2, lower Scollard Formation, Griffith's Farm locality); (B) late stage of quartz overgrowth, post-dating the precipitation of the calcite cement (sample K-7, upper Scollard Formation, Knudsen's Farm locality); (C) smectite pore filling cement (sample K-9, upper Scollard Formation, Knudsen's Farm locality); (D) late diagenetic needle like hematite (sample K-5, upper Scollard Formation, Knudsen's Farm locality); (E) calcite coating of detrital grains inhibiting the process of quartz overgrowth in the early diagenetic stages (sample Kn-3, lower Scollard Formation, Kneehills Creek locality); (F) alteration of feldspar grains, and the formation of authigenic smectite; note the formation of secondary porosity due to the chemical alteration of feldspar (sample G-4, lower Scollard Formation, Griffith's Farm locality).Abbreviations: Qtz quartz; S smectite; H hematite; Ca calcite; F feldspar; SP secondary porosity.
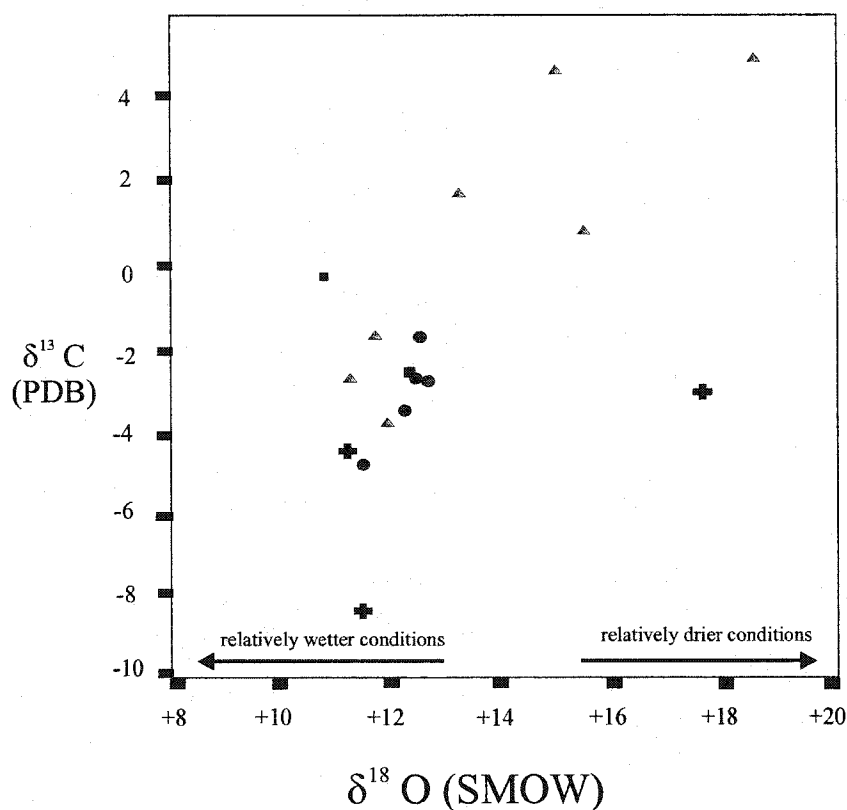
57

Figure 2-21. Carbon-isotope versus oxygen-isotope composition of the calcite cements in the Scollard sandstones. The isotopic values indicate that the calcite precipitated in equilibrium with fresh water of meteoric origin (Keith and Weber, 1964; Longstaffe, 1994). The relatively low 18O values suggest that calcite precipitation took place at low temperatures and shallow burial depths, possibly during early diagenesis (Longstaffe, 1994; Tang et al., 1997). The 13C values are higher for the upper Scollard due to the more abundant coal seams above the K-T boundary. The 18O values suggest overall drier climatic conditions during the accumulation of the upper Scollard deposits, relative to the lower Scollard time.

Diagenesis sequence	Early ──────────────────────── Late
Compaction	Mechanical ──── Chemical ────
Calcite cementation	──────────────────- - - - - - - - - -?
Dissolution of feldspar and volcanic fragments	───────────────────
Quartz overgrowth	────────- - - - - - - - - - -?
Smectite pore fill	────────
Kaolinite pore fill	───────────- - - - - - - -?
Quartz dissolution	───────
Calcite dissolution	───────
Formation of illite	───────
Hematite cementation	- - -?────────

Figure 2-22. Generalized diagenetic sequence for the Scollard Formation in the Red Deer Valley region.

59
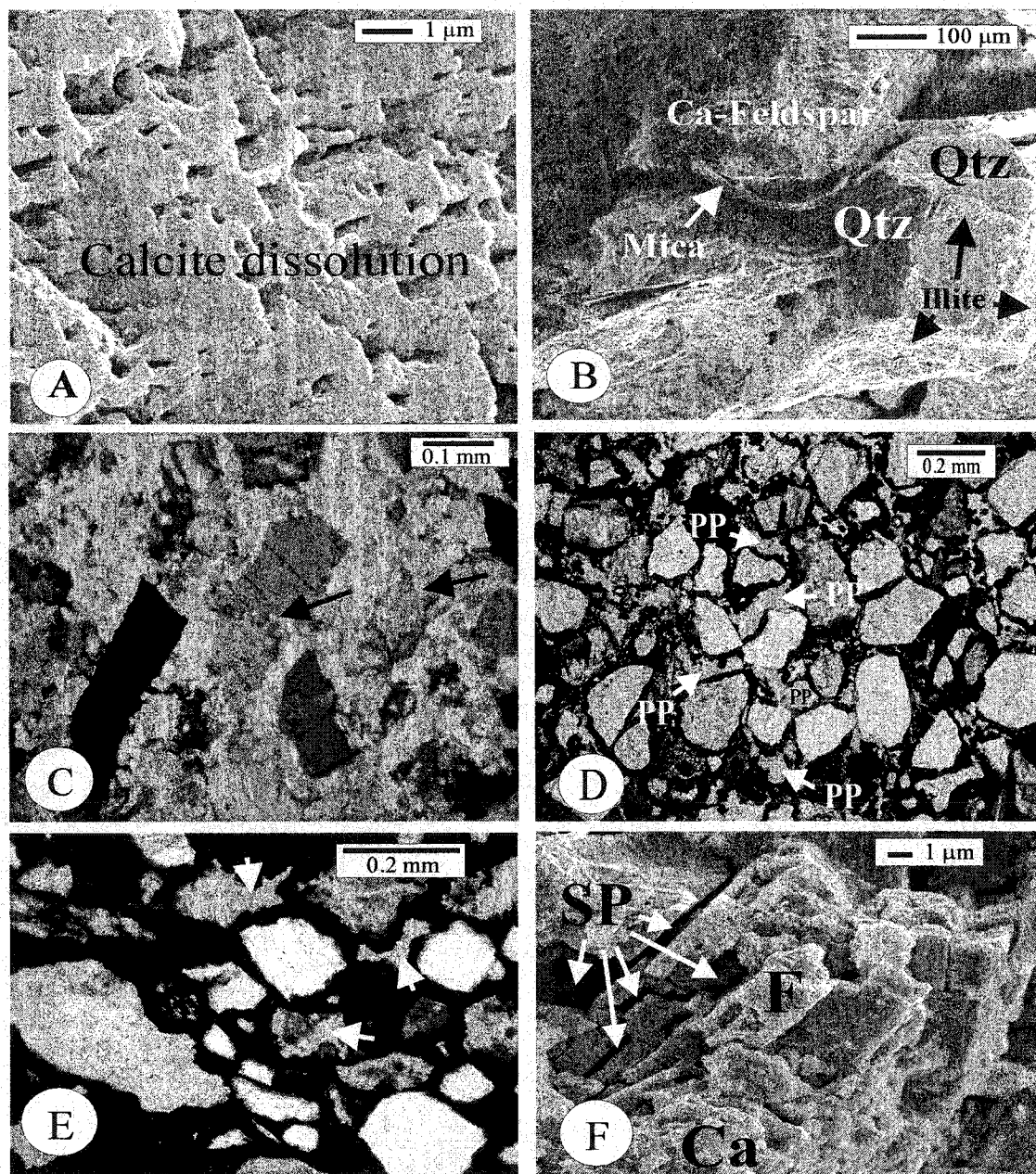
Figure 2-23. Scanning electronic and thin section photomicrographs: (A) - late diagenetic calcite dissolution (sample K-8, upper Scollard Formation, Knudsen's Farm locality); (B) mineral deformation (mica) during the early stage of sediment compaction; this results in a decrease in primary porosity. The illite coats the quartz grains as a late diagenetic product of alteration of earlier clay minerals (kaolinite or smectite) (sample T-4, upper Scollard Formation, Buffalo Jump Park locality); (C) dissolution of feldspar grains followed by partial replacement with calcite (arrows). Note the fracturing and reorientation of the feldspar grains caused by the precipitation of the calcite cement (sample G-10, lower Scollard Formation, Griffith's Farm locality); (D) primary porosity preserved in the sandstones (sample G-5, lower Scollard Formation, Griffith's Farm locality); (E) secondary porosity (arrows) resulting from the dissolution of authigenic cements, as seen under the petrographic microscope (sample G-4, lower Scollard Formation, Griffith's Farm locality); (F) secondary (dissolution) porosity (SP), as seen under the SEM. Note the secondary leaching of the feldspar and the dissolution along the cleavage planes (sample T-1, upper Scollard Formation, Buffalo Jump Park locality). Abbreviations: Qtz quartz; F feldspar; Ca clacite; PP primary porosity; SP secondary porosity.

60
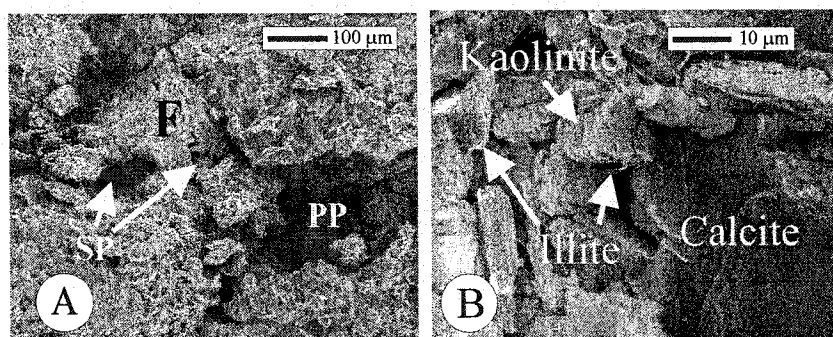
Figure 2-24. Scanning electronic photomicrographs: (A) - secondary (partial dissolution of feldspar grains) and residual primary porosity (sample T-1, upper Scollard Formation, Buffalo Jump locality);(B) late diagenetic illite formed via the alteration of kaolinite (sample T-3, upper Scollard Formation, Buffalo Jump locality).

Sample Number	Carbon PDB	Oxygen PDB	SMOW Oxygen	Locality	
K-4	-2.57	-17.56	12.81	Knudsen's Farm locality	Upper Scollard Formation
K-5	4.79	-11.875	18.667		
K-6	0.844	-14.984	15.463		
K-7	-1.942	-18.515	11.828		
K-8	1.84	-17.03	13.35		
K-9	-3.87	-18.34	12		
K-11	4.648	-15.458	14.974		
T-1	-2.532	-18.131	12.219	Buffalo Jump locality	Lower Scollard Formation
T-2	0.151	-19.668	10.634		
G-2	-2.65	-17.84	12.51	Griffith's Farm Locality	
G-4	-2.58	-18.02	12.33		
G-9	-4.844	-18.780	11.549		
G-10	-3.41	-18.17	12.118		
G-11	-1.8	-17.72	12.456		
Kn-5	-2.907	-12.645	17.874	Kneehills Creek locality	
Kn-4 A	-4.325	-18.974	11.350		
Kn-2	-8.673	-18.763	11.567		

Table 1. Oxygen and carbon isotopic compositions from the upper Scollard (Knudsen's Farm) and lower Scollard (Buffalo Jump, Griffith's Farm, and Kneehills Creek localities) Formation. The samples position is shown in Figures 4, 5, 7 and 8.

REFERENCES

Almon, W. R. 1979. Sandstone diagenesis as a factor in stimulation design. Preceeding of the 24th Annual Southwest Petroleum Short Course, Lubbock, Texas.

Anderson, T.F., and Arthur, M.A. 1983. Stable isotopes of oxygen and carbon and their application to sedimentologic and paleoenvironmental problems. *In:* Stables in Sedimentary Geology, SEMP Short Course No. 10, (eds.) Anderson, and Arthur, p. 1-1 to 1-151.

Basu, A. 1976. Petrology of Holocene sands derived from plutonic source rocks; implications to the paleoclimatic interpretation. Journal of Sedimentary Petrology, v. 46, p. 694- 709.

Ben, M., Friz, B., and Made, B. 1993. Diagentic albitization of K-feldspar and plagioclase in sandstone reservoir: thermodynamic and kinetic modeling. Journal of Sedimentary Research, v.63, p. 1100-1109.

Bjørkum, P.A. 1995. How important is pressure in causing dissolution of quartz in sandstones? Journal of Sedimentary Research, v. 66, p.147-154.

Boles, J.R. and Franks, S.G. 1979. Clay diagenesis in Wilcox sandstones of southwest Texas: Implication of smectite diagenesis on sandstone cementation. Journal of Sedimentary Petrology, v. 49, p. 55-70.

Burns, S.J. and Matter, A. 1995. Geochemistry of carbonate cement in surficial alluvial conglomerates and their paleoclimatic implications, Sultanate of Oman. Journal of Sedimentary Research, A65 (1), p. 170-177.

Catuneanu, O. and Sweet, A.R. 1999. Maastrichtian-Paleocene foreland basin stratigraphies, Western Canada: A reciprocal sequence architecture. Canadian Journal of Earth Sciences, v. 36, p. 685-703.

Chamley, H. 1968. La sedimentation argileuse actuelle en Mediterranée nord-occidentale. Bulletin Societé G éologique du France, v. 10, p. 75-88.

Chang, H. K., Mackenzie, F. T., and Schoonmarker, J. 1986. Comparison between the diagenesis of decahedral and trioctahedral smectite, Brazilian offshore basins: Clays and Clay Minerals, v. 34, p. 407-423.

Correns, C. W., T. F. Barth, and P. Eskola. 1939. Die Enstehung der Gesteine. Julius Springer, Berlin.

Dawson, F.M., Evan, C. G., Marsh R., and Richardson, R. 1994. Uppermost Cretaceous and Tertiary of the Western Canada Sedimentary Basin. *In:* Geological Atlas of the

Western Canada Sedimentary Basin. G.D. Mossop and I. Shetsen (comps.), Calgary. Canadian Society of Petroleum Geologists and Alberta Research Council, p. 387-406.

Dutta, P. 1992. Climatic influence on diagenesis fluvial sandstones, *In:* Diagenesis, III. Devlopments in sedimentology, 47, Wolf, K. and Chillingrain, G. (eds.), 674p.

Eberth, D., A. and O'Connell, 1995. Note on changing paleoenvironments across the Cretaceous- Tertiary boundary (Scollard Formation) in the Red Deer River valley of southern Alberta. Bulletin of Canadian Petroleum Geology, v. 43. no. 1, p. 44-53.

Eslinger, E., and Pevear, D. 1988. Clay minerals for petroleum geologist and engineers. Society of Economic Paleontologists and mineralogists Short Course Note, No.22, p 413.

Folk, R. L. 1974. The nature history of crystalline calcium carbonate: effect of magnesium contact and salinity. Journal of Sedimentary Petrology, v. 44, p. 40-53.

Folk, R. L. 1993. SEM imaging of bacteria and nannobacteria in carbonate sediments and rocks. Journal of Sedimentary Petrology, v. 63, p. 990-999.

Gibson, D. W. 1977. Upper Cretaceous and Tertiary coal bearing strata in the Drumheller – Ardley region, Red Deer River valley, Alberta. Geological Survey of Canada, Paper 76-35, p. 1-41.

Guven, N., Hower, W.F. and Davies, D. K. 1980. Nature of authigenic illites is sandstone reservoirs. Journal of Sedimentary Petrology v. 50, p 761- 766.

Heald, M. and Larese R. 1974. Influence of coatings on quartz cementation. Journal of Sedimentary Petrology, v. 44, no. 4, p. 1269-1274.

Hower, J., Eslinger, E. V., Hower, M. E., and Perry, E. A. 1976. Mechanism of burial metamorphism of argillaceous sediment: 1. Mineralogical and chemical evidence. Geological Society of America Bulletin, v. 87, p. 725-737.

Hower, J. 1981. Shale diagenesis, clays and resource geologist. *In:* Longstaffe, F. J., ed., Short course Handbook 7. Mineralogical Association of Canada, p. 60-80.

Jacka, A.D. 1970. Principles of cementation and porosity-occlusion in Upper Cretaceous sandstone, Rocky Mountain Region. *In:* Wyoming Geological Association Guidebook, Twenty-second Annual Field Conference, p. 265-258.

Jermy, G. and Michael, A. 1988. The influence of climate and topography on rock-fragment abundance in modern fluvial sands of the Southern Blue Ridge Mountains, North Carolina. Journal of Sedimentary Petrology, v. 58. no. 2, p. 219-227.

Keith, M.L. and Weber, J.N. 1964. Carbon and oxygen isotopic composition of selected limestones and fossils. Geochim. Cosmochim. Acta 28, p. 1787-1816.

Lerbekmo, J.F., Evans, M.E., and Hoye, G.S. 1990. Magnetostratigraphic evidence bearing on the magnitude of the subPaskapoo disconformity in the Scollard Canyon-Ardley area of the Red Deer Valley, Alberta. Bulletin of Canadian Petroleum Geology, v.23, p. 120-124.

Longstaffe, F.J. 1994. Stable isotopic constraints on sandstone diagenesis in the Western Canada sedimentary basin. In: A. Parker and B.W. Sellwood, eds. Quantitative diagenesis: recent developments and applications to reservoir geology. Dordrecht, Kluwer Academic Publishers, p. 223-274.

Longstaffe, F.J. and Ayalon, A. 1991. Mineralogical and O-isotope studies of diagenesis and porewater evolution in continental sandstones, Cretaceous Belly River Group. Alberta, Canada. Applied Geochemistry, v. 6. p. 291-303.

Lowrnce, J.R., and White, J. W. C. 1991. The elusive climate signal in the isotopic composition of precipitation, In: Stable Isotope Geochemistry , A tribute to Sam Epstein. (eds.) Tyler, J., and Kaplan, The Geochemical Society, Special Publication, v. 3, p. 169-185.

Mack and, H., and Suttner. L. 1977. Paleoclimatic interpretation from petrographic composition of Holocene Sandss and the Fountain Formation (Pennsylvanian) in the Colorado Front Range, Journal of Sedimentary Petrology, v. 47, NO. 1, p. 89-100.

Mann, W. R., and Cavaroc, V. 1973. Composition of sands released from three source areas under humid, low relief weathering in the North Carolina piedmont. Journal of Sedimentary Petrology, v. 43, p. 870- 881.

Millot, G. 1942. Relations entre la constitution et la genese des roches sedimentaires argileuses. Geolgical Appliq. Et Prosp. Min., v.II.

Mora, C.I., Fastovsky, D.E. and Driese, S.G. 1993. Geochemistry and stable Isotopes of paleosols. University of Tennessee Department of Geology Sciences. Studies in Geology, 65p.

Neasham J.W., 1977. The morphology of dispersed clay in sandstone reservoirs and its effect on sandstone shaliness, pore space and fluid flow properties. Society of Petroleum Engineers of AIME, Denver, SPE 6858, 7p.

Pettijohn, F. J., Potter, P.E. and Siever, R. 1987, Sand and sandstone, 2nd (ed.). Springer-Verlag, New York, 553 p.

Pittman, E., and Lumsden, D. N. 1968. Relationship between chlorite coating on quartz grain and porosity, Spiro Sand, Oklahoma: Journal Sedimentary Petrology, v. 38, p. 668-670.

Quatin, P., Badaut-Trauth, D., Weber, F. 1975. Mise en evidence de mineraux secondaires, argils et hydroxides, dans les andolosols des Nouvelles-Hebrides, après la deferrification par la method de Endrey. Bulletin du Groupe d'Argiles du France, v. 27, p.51-67.

Richard, D.k. and Fuuchtbauer, H., 1978. Ferraon calcite replacement indicates former magnesian calcite skeleton. Sedimentology, v. 25, p. 843-860.

Russell, I. 1983. Evidence for unconformity at the Scollard-Battle contact, Upper Cretaceous strata, Alberta. Canadian Journal of Earth Sciences, v. 20, p. 1231-1245.

Sunttenr J, and Dutta, K. 1986. Alluvial sandstone composition and paleoclimate, II. Authigenic Mineralogy. Journal of Sedimentary Petrology, v. 56, no. 3, p. 346- 358.

Schmidt V. and McDonald, A. 1979. Secondary Reservoir porosity in the course of sandstone diagenesis, Short Course AAPG, 50 p.

Scholle, A. (ed.) 1979. A color illustrated guide to constituents, textures, cements, of sandstone and Associated Rocks, American Association of Petroleum Geologist, 201p.

Sieffermann, G., Jehl, G., Millot, G. 1968. Allophanes et mineraux argileux des alterations recentes des basalts du mount cameroun. Bulletin du Groupe d' Argiles du France, v. 20, p.109-129.

Tang, Z., Parnell, J. and Longstaffe, F.J. 1997. Diagenesis and reservoir potential of Permian-Triassic fluvial/lacustrine sandstones in the southern Junggar Basin, northwestern China. American Association of Petroleum Geologists Bulletin, v. 81, No. 11, p. 1843-1865.

Velde, B. 1985. Clay minerals, a physico-chemical explanation of their occurrence: Developments in Sedimentology, v. 4, New York, Elsevier, 427 p.

Walderhaug, O. and Bjorkum, P. A. 1992. Effect of meteoric water flow on calcite cementation in the Middle Jurassic Oseberg Formation, well 30/3-2, Veslefrikk Field, Norwegian North Sea. Marin Petroleum Geology, v. 9, p. 308-318.

Walderhaug, O., Bjorkum, P.A. 1998. Calcite cement in shallow marine sandstone: Growth mechanism and geometry. Special publication of the International Association of Sedimentologists, v. 26, p. 179-192.

Walker, T.R. 1967. Formation of red beds in modern and ancient deserts. Bulletin of Geological Society of America, v. 78, p. 353-368.

Walker, T.R., Waugh, B., and Crone, A. 1978. Diagenesis in first cycle desert alluvium of Cenozoic age, southern U. S. and northwest Mexico, Geological Society of America Bulletin, v.89, p. 19-32.

Wange, Y., Cerling, Erling, T.E., Quade, J. and Bowman, J.R. 1993. Stable isotopes of paleosols and fossil teeth as paleoecology and paleoclimate indicator: an example from the St David Formation, Arizona. *In:* Climate Change in Continental Isotopic records. Swart, P., Lohman, K.C. and Mackenzie, J.A. (ed.). Geophysics Monographer, American. Geophysics Union, v. 78, p. 241-248.

Wilson, M. D., and Pittman, E.D. 1977. Authigenic clays in sandstones: recognition and influence on reservoir properties and paleoenvironmental analysis. Journal of Sedimentary Petrology, v. 47, p. 3-31.

Wolf, H. and Chiliingarian, G. (eds.) 1988. Developments in Sedimentology 47, Diagenesis III, Elsevier, Amsterdam, 360p.

Young, S., Basu, A., Suttner, j., Mack, G., and Darnell, N. 1975. Use of size composition trends in Holocene soil and fluvial sand derived from paleoclimate interpretation. Proceedings IX International Sedimentary Congress, Nice, France, Theme 1, p. 201-209.

Chapter 3

Sedimentology and diagenesis of the Coalspur sandstones in the Foothills region of west-central Alberta

INTRODUCTION

The Coalspur Formation is a nonmarine succession, which accumulated during most upper Cretaceous- lower Tertiary time in the foredeep of the Western Canada foreland system (Catuneanu and Sweet, 1999). The Coalspur Formation accumulated in isolation from marine influences, on a dynamic topography controlled by tectonic mechanisms (Catuneanu and Sweet, 1999).

The Coalspur Formation is well exposed in a number of locations in western Alberta, including Sundre, the Red Deer River, Coalspur, along Highway 22, Smoky River Valley, and near Entrance (Fig. 3-1). The Formation includes an economically significant amount of high-quality thermal coal occurring within the upper Paleocene part of the Formation named "the Coalspur coal zone". The Coalspur Formation is noted for containing within its sequence the Cretaceous-Tertiary boundary as well.

The Coalspur Formation and its coal zone have been described and studied from numerous drillholes, test pits, and other outcrop sections in western Alberta, but its diagenetic history has received little attention. In turn, diagenetic processes may be related to depositional environments, burial depth, temperature, pore fluid migration, original mineralogy, and paleoclimatic variability that controlled the pore-water chemistry during the various diagenetic stages. This paper characterizes the diagenesis and porosity of the Upper Cretaceous-Lower Tertiary fluvio-lacustrine sandstones of the

Coalspur Formation, via detailed outcrop and laboratory work. This study may provide an outcrop analogue for the characterization of other subsurface reservoirs consisting of fluvial-lacustrine sandstones.

GEOLOGICAL BACKGROUND

Mackay (1949) named the Coalspur Fm as "the Coalspur beds". This Fm is a non-marine succession of interbedded mudstone, siltstone and fine-grained sandstones with minor coarser-grained sandstone layers and channel lags. Within the study area the Coalspur overlies the upper massive sand of the Brazeau Formation and is overlain by the Paskapoo Formation (Fig. 3-2). The Coalspur Formation consists of two informal successions with well-defined boundaries. The upper boundary is placed at the lowest sandstone layer above the highest thick coal seam (Val d 'Or) of the Coalspur coal zone. The upper part of the Formation is characterized by extensive development of numerous coal zones. The upper Coalspur Formation, which consists of fine-to-medium-grained buff-colored sandstones, lies conformably above the coal-barren sediments of the lower Coalspur Formation. This stratigraphic interval ranges from more than 175 m thick in the west to less than 120 m thick in the east. To the south, in the Foothills near Sundre, the correlative upper Coalspur Formation increases in thickness to greater than 250 m, while on the plain the correlative upper Scollard Fm thins to less than 50 m in the outcrop along the Red Deer valley. The lower succession consists primarily of thin fining-upward cycles of fine-to-medium-grained sandstones interbedded with green-to-grey colored siltstones and mudstones. The thicknesses of these cycles vary from 4 m to 16 m. The contact between the lower Coalspur Formation and the underlying Brazeau

Formation is commonly abrupt. This contact occurs at the base of the Entrance Conglomerate, which has an average thickness of about 6 m, but occasionally reach 15 m. The Entrance Conglomerate consists of closely packed pebbles of quartzite and chert averaging 2.54 to 6.35 cm in diameter, with a sandy matrix. The conglomerate is occasionally interbedded with sandstone beds. Jerzykiewicz's and Mclean's (1980) detailed analyses indicate that the Entrance Member in the north of the Alberta Foothills is equivalent to the Entrance conglomerate defined in the southern Alberta Foothills. As well, the Entrance Member is correlative with the resistant lower most sandstone bed of the Scollard Formation (Dawson et. al., 1994).

DATA BASE AND METHODOLOGY

Fieldwork was completed in Foothills of central Alberta. Each outcrop section has studied in detail, including thickness measurements, facies analysis, paleoflow measurements, and sampling for laboratory work. Figure 3-3 illustrates the facies codes used for the description of all outcrop sections (Figs. 3-4 to 3-9). Several localities studied in the Foothills of central Alberta include the Sundre (Fig. 3-4), the outcrop along the Red Deer River (Fig. 3-5), Coal Valley (Fig. 3-6), the roadcut near the Red Deer River (Fig. 3-7), the Smoky River locality (Fig. 3-8), and the roadcut near Highway 22 (Fig. 3-9). Based on the observed lithofacies and petrographic attributes in this study, plus the information from Smith et al. (1977), the composite profile of the studied outcrop sections is illustrated in Figure 10. A total of 35 sandstone beds, and 13 shale and siltstone intervals were sampled and described within the studied area. To study the porosity, sandstone samples were soaked with blue epoxy resin before preparing the thin

section slides. Representative thin sections were point counted to calculate the relative amounts of detrital framework grains, interstitial minerals, and porosity.

To distinguish authigenic minerals, and to verify paragenesis of Coalspur sandstones, samples were studied by using a scanning electron microscope JEOL JSM 6400. X-ray diffraction (XRD) analysis was carried out on bulk samples and separates of less than 2 μm.

Isotopic analysis of calcite cement was preformed (Table 3-1). The powdered rock samples were reacted with anhydrous phosphoric acid at 25°C. An oxygen-isotope CO_2-H_2O fractionation factor of 1.0412 at 25°C was used to calibrate the mass spectrometer reference gas. Oxygen isotopic compositions were calculated by using a phosphoric acid-CO_2 fractionation factor of 1.011025 at 25°C for calcite. The oxygen and carbon-isotope data are reported in the normal δ notation relative to the Standard Mean Ocean Water (SMOW) for oxygen and the PeeDee Belemnite (PDB) standard for carbon. The reproducibility of duplicate analyses was generally better than $\pm$ 0.16‰ for each oxygen and carbon isotope measurement.

THIN SECTION PETROGRAPHY

The Coalspur Formation is composed mostly of sandstones, while the Entrance Member consists of conglomerate up to 16 m thick with clasts usually 2 to 5 cm in diameter, but which can be up to 15 cm. Pebbles are usually well rounded and sorted with spheroidal or discoidal shape, and often show good imbrications. The conglomerate is massive to crudely horizontally bedded and contains irregular lenses of sandstone, up to 0.5 m thick. Extraformational pebble types include quartz, chert, siliceous phylite,

metaquartzite, quartz-muscovite schist, and some volcanic rock fragments. The sandstone consists mainly of quartz, rock fragments, and feldspar grains, with percentages varying from one bed to another (Figs 3-4 to 3-9). The sandstones are also characterized by a general lack of terrigenous matrix, with an average percentage of 2% (range 0-4%). Based on the classification of Pettijohn et al.'s (1987), the Coalspur sandstones are classified as litharenites to sublitharenites (Fig. 3-11). These sandstones range in size from fine- to medium-grained and display good sorting, in contrast Entrance sandstones ranged from medium-to-coarse-grained in size. Quartz and feldspar grains are mostly subangular, and lithic fragments range in roundness from subangular to subrounded, with the latter dominating.

ROCK FRAGMENTS (INCLUDE POLYCRYSTALLINE QUARTZ)

The predominant rock fragments in the Coalspur sandstones are the silica group of quartz and chert; the argillaceous group including shale, slate, phylite and schist; and lithics of igneous origin. The majority of rock fragments ranges in size from 0.09 to 0.2 mm in diameter, with an average size of 0.1 mm, and are subrounded in most of the lower and upper Coalspur Formation. Rock fragments make up 35% (on average, with a range of 30-60%) of the coarse framework. The dominate lithoclasts is chert fragments (Fig. 3-12 A). Chert detritals are characterized by uniform microcrystalline quartz with no visible texture. Detrital chert fragments with a combination of microquartz and megaquartz are also observed in the Coalspur sandstones. Detritals from metamorphic sources include polycrystalline quartz characterized by sutured crystal boundaries (Fig. 3-12 B) and are a relatively abundant component. Some of the metamorphic clasts show

schistose textures, likely derived from high-grade metamorphic sources. Other identified metamorphic features include elongated and crenulated quartz crystals welded together. Igneous rocks are mainly of felsic to intermediate intrusive origin and are less abundant than other lithoclasts, because of the early alteration of volcanic rock fragments, which are responsible for chlorite formation in many of the Coalspur sandstones. When present, volcanic rocks occur as large grains with lath plagioclase set in a fine crystalline matrix (Fig. 3-12 C). Various igneous textures such as lathwork, vetric, and cryptocrystalline types were also recognized (Fig. 3-12 D).

QUARTZ

The detrital mineralogy of the sandstones is dominated by quartz (un-strained, strained), which constitutes more than 45% of the framework components. Monocrystalline quartz averages 50% (range 75-25%) of the framework grains. The original shape of the quartz grains is difficult to define with a petrographic microscope in some of the upper Coalspur sandstones (near Sundre) because of the precipitation of overgrowths (Fig. 3-12 E). Generally, quartz grain shapes range from subangular to subrounded. Some of the detrital quartz shows well-rounded nucleus quartz grains outlined by a thin envelope of clay and iron oxides on the surface (Fig. 3-12 F). Zones of inclusions of either vacuole or microlite types are also observed.

FELDSPAR

Feldspar is less abundant than quartz grains, averaging 15% (range 5-30%) of the framework. The feldspar abundance is related to the source rocks, composition, chemical

weathering in the source area, abrasion and dissolution during transportation, and dissolution during diagenesis (Pittman, 1963). Feldspar, which exhibits a size range similar to that of quartz, is less common in the finer fraction and is a major part of the course fraction only. Much but not all feldspar shows multiple twinning (Fig. 3-13 A), some of it crossed. The feldspars within the Entrance Member sandstones are generally fresh and have a few highly weathered grains. Observations of fresh detrital feldspars suggest close source areas or/and high topographic relief. Potassium feldspars are also observed in both the lower and the upper Coalspur sandstones (usually less than 3%). Microcline displays grid twinning and makes up only about 1% of the total feldspar components. Parts of the plagioclase feldspars are of volcanic origin, as indicated by the presence of euhedral crystals and albite twining (Scholle, 1979). Plagioclase detritals show considerable alteration, mainly vacuolization and sericization (Fig. 3-13 B).

In addition to the main framework components (quartz, feldspars and rock fragments), accessory minerals such as muscovite, hornblende, and pyroxene (Fig. 3-13 D) have also been identified within both the lower and upper Coalspur Formation.

DRAINAGE PATTERNS

Variety lithics texture of the sandstone rocks indicated a diversity of parent rocks within the Cordilleran belt. The directions of paleoflow changed from NE (upper Coalspur) to S-SE (lower Coalspur) (Figs. 3-14, 3-15, and 3-16), as indicated by measuring cross-bedding structures

AUTHIGENIC MINERALS

Different authigenic minerals observed within the Coalspur sandstones in central Alberta including authigenic quartz, calcite, grain–coating, pore-lining clay minerals, and pore-filing.

CALCITE

A relatively small amount of calcite cement is observed in the Coalspur sandstones. With the exception of the Sundre locality, where calcite cement is the major cement type, this calcite ranges in abundance from trace amounts to 20% of the rock. The early calcite cements can be recognized based on distribution and textural attributes, as they display drusy and poikilotopic features (Fig. 3-17 A) (Jacka, 1970; Folk, 1974; Burns and Matter, 1995). Poikilotopic and blocky spar cements (Fig. 3-17 B) are most often related to precipitation in the phreatic zone (Jacka, 1970; Folk, 1974), which is probably the environment where the early diagenetic alteration of sandstone constituents and the early calcite cementation took place. Where the rock is strongly dominated by quartz grains, the presence of carbonate cement is evident by its position in the pore spaces between the quartz grain frameworks, which are observed in the upper Coalspur sandstones (Sundre locality) (Fig. 3-17 C). The time of introduction of this cement is uncertain and may be an early crystallization event. An early stage of carbonate precipitation can be recognized by crystals of carbonate that are embedded by closely packed quartz grains (Fig. 3-17 D). In these cases, the space between grains was thoroughly filled, and therefore the primary porosity of the sandstone was lost.

Introduction of carbonate does not involve a volumetric expansion but, rather, corrodes and replaces quartz grains. Replacement of detrital feldspars by early calcite is observed as well (Fig. 3-17 E). The calcite cement typically post-dates the quartz overgrowth as is indicated by the corroded boundaries between overgrowths and carbonate (Fig. 3-17 F).

Sources of calcite cement

The dissolution of Ca-rich feldspars probably represented the primary source of calcite cement in the Coalspur Formation because the volume of diagenetic silica exceeded the volume of diagenetic calcite, as was observed in the samples from the upper Coalspur Formation in the Sandre locality (Fig. 3-17 D). Carbonate rock fragments are another possible source of calcite cement in the Coalspur Formation and were probably derived from sedimentary strata in the Rocky Mountain Front Ranges. Biogenic carbonate, carbonate rock fragments, and plagioclase were possible internal sources of calcite cement by flow over short distances.

CLAY MINERALS

The clay mineral content of the sandstones ranges from 5 to 20% and includes chlorite, smectite, chlorite-smectite, kaolinite, dickite, and minor illite. Recognition of clay minerals was preformed by using X-ray diffractometry and SEM.

Chlorite

Chlorite is the most common diagenetic mineral in the Coalspur sandstones. "Chlorite appears as pore linings (rims) composite of crystals perpendicularly oriented to grain surfaces (Fig. 3-18 A)" and locally evolves into complete pore fillings. In a thin

section, chlorite is recognized by its homogeneous-green to brownish-green color. Under the SEM, authigenically formed chlorite commonly appears as rosettes of pseudohexagonal crystals or honeycombed (Fig. 3-18 B). The latter growth consists of plates arranged in a cellular pattern analogous to a honeycomb (Fig. 3-18 C). The crystals are attached to the edges of the detrital sand grains and commonly curve and intersect to form the distinctive cellular pattern. XRD analysis indicates the presence of both magnesium and iron-rich type of chlorite.

Generally the precipitation of chlorite requires a source of Fe and Mg. Possible sources of Fe and Mg are clastic biotite, basic rock fragments or early diagenetic Fe minerals. With the Coalspur sandstones the probable source of chlorite is the late diagenetic chloritization of smectite, which requires an elevated $Fe^{+2}/(OH^+)^2$ ratio in the pore water (Chang et al., 1986). It is thus likely the chlorite tends to occur in the sedimentary layers enriched in detrital Fe-silicates and Fe-oxide. The presence of mixed layers of chlorite-smectite coatings supports this hypothesis. The chemical composition of authigenic chlorite exhibits a definite temperature dependence (Jahren and Aagaard, 1989), at temperatures ranging between >100-130° C (Velde, 1975). According to the synthetic work of Nelson and Roy (1958), septechlorite appears to form at lower temperature, while the normal chlorite needs considerably higher temperatures to be synthesized, a process which might occur during late diagenesis.

Chlorite crystals become coarser grained with increasing burial depth (Fig. 3-18 D) as a result of crystal growth (Jahren and Aagaard, 1989). Detailed study of these crystals provides insight into the dynamic nature of chlorite growth during burial diagenesis. Relatively, the amount of authigenic chlorite in the Coalspur sandstones is

higher in coarse-grained sandstones. Spötl et al. (1994) have described the same correlation between the occurrence of chlorite and coarsening sandstones in the Arkoma foreland basin, USA. These data suggest that chlorite formation within the Coalspur sandstones is controlled mainly by initial mineralogical composition, burial depth and the grain size of framework constituents.

Chlorite/Smectite (C-S)

Chlorite-smectite clay minerals have been identified in the Coalspur sandstones (Fig. 3-19 A) and are clearly authigenic, occurring in individual crystals oriented perpendicular to grain surfaces (Fig. 3-19 B). Chlorite/smectite is commonly associated with hypersaline evaporites and/or lacustrine environments (Fisher, 1988). Therefore, the abundance of chlorite/smectite in the Coalspur sandstones is a good indicator for the recognition of lacustrine environments or hypersaline evaporite environments. In Coalspur sandstones, chlorite/smectite occurs as a pore lining and pore-filling clay. The parent material for chlorite/smectite may have been detrital clay or partially degraded mica or chlorite (Plamer, 1987; Fisher, 1988). The writers did not observe transitions from detrital mica to chlorite/smectite, nor chlorite/smectite occurring in individual laminae. Such occurrences would suggest that C-S formed from a pre-existing detrital mica, while the morphology and chemistry of chlorite/smectite in this Formation, which observed from SEM and XRD study, suggest that it formed from detrital smectite enriched in Mg and Fe by the dissolution of detrital ferromagnesian minerals which observed in the Coalspur sandstone and possibly by saline water derived from lacustrine sediments during deposition or early burial.

Smectite

Smectite, which forms at lower temperatures, either in dry continental environments or in sandstones with a relatively high content of volcanoclastics, is a widely distributed clay mineral in the Coalspur sandstones and occurs as coating rims (Fig. 3-20 A), altered detrital fragments, and pore filling interstitial fibrous cement. Smectite is commonly of authigenic origin in the Coalspur sandstones and is characterized by a highly crenulated, honeycombed, and interlocking crystal shape, with an irregular, wavy plate or sheet-like architecture (Fig. 3-20 B). Moreover, smectite rims commonly show preferred orientation perpendicular to the grain surface (Fig. 3-20 C) (Wilson and Pittman, 1977). The occurrence of the clay minerals as oriented perpendicular to the grain surface in the sandstone indicates authigenic growth. As well, the high degree of crystallinity of the smectites in the Coalspur sandstones is a strong indicator of authigenic origin.

Ca-feldspar and alteration of volcanic rock fragments are a possible source of smectite formation in the Coalspur sandstones (Fig. 3-20 D). A pore-water chemistry controlled by an arid to semi-arid climate is another source of smectite development as well (Velde, 1985).

Kaolinite

Kaolinite abundance in the Coalspur sandstones is highly variable, with most kaolinite occurring close to the coal zone within the upper Coalspur Formation. Kaolinite occurs as fine-grained crystals of booklet- or vermiform-shape, or as lath-

shaped pseudohexagonal crystals (Fig. 3-21 A). It is abundant as pore filling cement and replaces feldspar and micas. Texturally, dickite can be distinguished from kaolinite by its more blocky habit (Fig. 3-21 B, and C) (Ehrenberg et al., 1993) which was observed in the upper Coalspur sandstones. Kaolinite's authigenic origin is documented by using petrographic and SEM techniques (Fig. 3-21 D). Kaolinitization occurred early in the diagenetic history, and may be related to climate and feldspar alteration according to the following reaction (Bjørlykke, 1989):

$$2KaAlSi_3O_8 + 2H^+ + 9H_2O \longrightarrow Al_2Si_2O_5(OH)_4 + H_4SiO_4 + 2K^+$$

Besides the transformation of K-feldspar, vermiform aggregates of kaolinite plates are also associated with the replacement of muscovite grains (Bjørlykke, 1989):

$$2KaAl_3Si_4O_{10} + 2H^+ + 3H_2O \longrightarrow 3Al_2Si_2O_5(OH)_4 + 2K^+$$

Both processes are reported as taking place under acidic conditions. They require the removal of silica and/or potassium so that the K^+/H^+ ratio and the silica concentration remain inside the kaolinite stability field (Garrels and Christ, 1965). Moreover the release of organic acid from organic matter may decrease the K^+/H^+ ratio. According to Bjørlykke (1994), important kaolinite formation during the early stage of diagenesis, consequential from alteration of K-feldspar and muscovite, is a function of meteoric water flux through the sediment. Because of the fluvio-lacustrine nature of the Coalspur sandstone units, the presence of meteoric water during early diagenesis is most likely. Meteoric water may be directly responsible for feldspar dissolution because the dissolution is faster in acidic pore-water, and meteoric water is often slightly acidic due to dissolved CO_2 and organic acids produced in the soil profile (Giles and deBoer, 1990).

Besides the influx of meteoric water, acidic fluids, which formed during the coalification of organic matter, could also cause a decrease in pH. Therefore, at low pH values, little silica would be in solution, and kaolinite is likely to be the stable form (Grim, 1953). This kind of environment could explain the increase of kaolinite concentration near the sandstone-coal contacts, while the rapid decrease in the related amount of kaolinite away from the coal seam could suggest that the organic acids become rapidly dispersed by pore fluid advection (Mullis, 1992).

Two types of kaolin morphologies are observed in the Coalspur sandstones: vermiform kaolinite (Fig. 3-21 A) and blocky kaolinite (Fig 3-21 B, and C). Blocky kaolinite is habitually dickite. Osborne et al. (1994), suggested that kaolinite morphologies are related to the depth of burial; precipitation of vermiform kaolinite occurs at shallow depth while at great depths, blocky kaolinite precipitates. The blocky morphology has been reported in deeply buried sandstone reservoirs (Hurst and Irwin, 1982; Osborne et al., 1994). We suggest that diagenetic vermiform kaolinite (Fig. 3-21 A) precipitated during shallower burial at low temperature under conditions of low supersaturation within the upper Coalspur sandstones. During deeper (higher temperature) burial, increased rates of feldspar dissolution resulted in higher degrees of supersaturation, and more blocky kaolinite (Figs. 3-21 B and D) precipitated into the open pore-space. The abundance of kaolinite might also relate to meteoric water chemistry which is controlled by climate. Kaolinite is usually abundant where there is active drainage and no marked dry season (e.g., Sieffermann et al. 1968; Chamley 1968; Quatin et al. 1975).

Illite

Illite is a less abundant authigenic mineral in the Coalspur Formation. Illite can be observed to replace kaolinite in the upper Coalspur sandstones if the K-feldspar is available as a source of potassium. An additional possible source of illite within the Coalspur Formation is smectite (Fig. 3-22), which tends to transform to illite with deeper burial.

An authigenic origin is attributed to the clay rims that form coats around detrital sand grains (Wilson and Pittman, 1977). If the clay minerals are not replaced or pushed aside by the force of crystallization, the clay covering other authigenic components must then be authigenic in origin as well (Wilson and Pittman, 1977). In our study, SEM and petrographic observations showed that the clay coatings are generally homogenous in thickness and that clay mineral growth is perpendicular to the grain surface (Fig. 3-19 B), a finding that supports an authigenic origin.

QUARTZ

Authigenic quartz cementation is observed within the Coalspur sandstones. Precipitation of authigenic quartz led to euhedral overgrowth on detrital grains during the early and middle stages of the diagenesis history of the Coalspur sandstones (Fig. 3-23 A). Euhedral growth boundaries also can be seen in many partially cemented zones, which are pre-dated by the mechanical compaction. Moreover, silica overgrowths are generally postdated by grain–coating, pore-lining and pore-filing clay minerals (Fig. 3-23 B). Generally, the formation of siliceous cement is abundant in the Coalspur sandstones, with of the exception where sandstone samples are dominated by authigenic

clay minerals and/or chert, probably because of the influence of grain coatings, which possibly played a role in inhabiting further silica cementation.

Influence of grain coating on quartz cementation

Grain-coating in clastic quartz-rich sandstones has long been recognized as an important porosity-preserving constituent in medium-to-deep-burial diagenesis. Normally the process of grain coatings, via the precipitation of chert or authigenic clay minerals such as chlorite and smectite, is an important diagenetic mechanism that controls the quartz cementation and the porosity evolution in sandstones (Pittman and Lumsden; 1968; Heald and Larese, 1974). Other factors like the availability of silica sources, as well as burial temperatures, may have been important as well. Increasing temperature by increasing burial depth enhances kaolinite and/or smectite-to-illite transformation. These chemical alterations, which release Si, are considered important sources of authigenic quartz formation, where the limited quantity of available silica resulted in small quartz overgrowths in relation to the pore space.

Well-developed clay coats, particularly chlorite, are commonly effective physical barriers that prevent silica from nucleating on detrital quartz grains under medium- to deep-burial conditions (Fig. 3-23 C). This mechanism is effective for preserving primary intergranular porosity in sublitharenite sandstones, while clay coatings are not an effective porosity-preservation mechanism in lithic arenites with 45% or more lithic material because of the low-quartz content. The continuous chlorite coatings on some quartz grains may have prevented secondary growth. When the coating was discontinuous and thin, authigenic quartz was able to connect with the lattice of the

detrital grains (Fig. 3-23 D). Therefore, the continuity and the thickness of the coating are important factors in inhabiting quartz cementation in the Coalspur sandstones. The nature of the quartz overgrowth is a good indicator of the relative effectiveness of different kinds of coatings in restricting cementation (Heald and Larese, 1974). Although the clay cement appeared in a relatively small quantity in the Coalspur Formation, it apparently prevented further silica cementation (Fig. 3-23 E).

The uneven growth of authigenic quartz in most of the beds and the irregular distribution of quartz in the Coalspur sandstones resulted from local variation in the thickness of the grain coatings. The uneven enlargement of the cement areas indicates that although coating had interfered with silica growth, it was not able to prevent the filing of some pores.

The calcite coating of the detrital grains is relatively ineffective in inhibiting quartz cementation in the Coalspur sandstones because of the minor abundance of calcite cement, which is observed as isolated patches. The specks of calcite cement covering the detrital quartz grains are not abundant enough to stop quartz cementation.

Quartz is porosity-destroying cement in many sandstone beds because the overgrowth of authigenic quartz reduces the pore space between the grains. Although coatings inhibit silica cementation, they also result in a major permeability reduction in sandstone beds because of the obstruction of pore throats between the grains.

Sources of quartz cement

The precipitation of quartz cements is generally related to (1) a release of silica during the kaolinitization of feldspar (Bjørlykke, 1983); (2) pressure solution (Pettijohn

et al., 1972); or (3) release of silica during smectite illitization (Hower et al., 1976; Boles and Frank, 1979).

Smectite illitization was observed in only a few sandstone beds of the Coalspur Formation, so it is not considered an important source of silica in this particular case study. In contract, meteoric kaolinitization of feldspars may have played a more important role in the Coalspur Formation. Dissolutions are probably associated with grain-to-grain contact and silica would be internally derived by diffusion from pressure dissolution along intergranular contact (Bjølykke and Egeberg, 1993). As well, the dissolution of volcanic fragments represents an additional internal source of quartz cementation. Overall, the internal sources of silica are most likely more important than the external sources in the case of the Coalspur Formation.

STABLE ISOTOPES

The carbon isotopic composition ($\delta^{13}C$) of the early calcite cement in the Coalspur Formation ranges for from -0.417 to $-5.616\%_o$ PDB, whereas oxygen isotope values ($\delta^{18}O$) range from -17.507 to $-10.383\%_o$ PDB (Table 3-1). The oxygen isotopic composition of the calcite cement is in equilibrium with meteoric water origin at relatively low temperatures (Fig. 3-24). The negative isotopic composition of the oxygen in the Coalspur Formation signifies that the calcite cement precipitate from fresh water. Carbon and oxygen values have effected directly by the environment of precipitation in the Coalspur Formation.

The variability in the isotopic compositions of the Coalspur sandstones (Fig. 3-24) might reflect changes in the precipitation rates, abundance of vegetation, and seasonal temperatures (Wange et al., 1993).

DISCUSSION

DISTRIBUTION OF AUTHIGENIC MINERALS

The formation of authigenic clay minerals in sandstones involves nucleation and growth from a supersaturated aqueous solution and, consequently, occurrences have thermodynamic and kinetic constraints. Kinetic constraints may stop precipitation from a supersaturated solution. The saturation state of a mineral, at a specified pressure and temperature, is determined by the chemical composition of co-exiting porewater composition. The nucleation of authigenic minerals and growth rates also depend on the degree of supersaturation as well as temperature (Mclean, 1965; Ridley and Thompson, 1986). In addition, the porewater composition will influence the mineral-water interface properties, which are important for growth and nucleation. Consequently, the degree of supersaturation, the temperature and the porewater composition directs the distribution of authigenic clay minerals.

This distribution of authigenic minerals in the Coalspur sandstones is relatively variable (Figs. 3-4 to 3-9). The Entrance Member and the lower Coalspur sandstones are mainly characterized by pore-filling and pore-lining chlorite, and authigenic quartz. The upper Coalspur Formation displays two main types of cement: poikilotopic calcite cements (Fig. 3-17 A) and chert cement. The upper Coalspur sandstones are also cemented by grain-coating and pore-filling clay minerals, mainly smectite (Figs. 3-20

A), kaolinite (Fig. 3-21 A), dickite, chlorite-smectite, chlorite, and lesser amounts of illite.

Smectites and chlorites

Chlorite–smectite and magnesian chlorite, which are present in both the lower and upper Coalspur sandstones, are commonly formed in lacustrine and/or a hypersaline environments. Lacustrine and hypersaline environments are supply magensian which considers essential chemical element of magnesian chlorite and chlorite-smectite composition (Bodine and Madsen, 1987; Morrison and Parry, 1986; Hillier, 1993, 1994). Hillier et al. (1996) noted that pore-lining magnesian and ferroan chlorite are most abundant in sandstones that interfinger with lacustrine shales. Therefore, the relative abundance of chlorite-smectite (Fig. 3-19 A) and magnesian chlorite throughout the Coalspur sandstones suggests that the Coalspur sandstones are associated with high water table fluvial-lacustrine environments.

A mechanism invoking the chloritization of detrital smectite, variably enriched in Mg and Fe, during daigenesis of the Coalspur sandstones appear to most acceptably clarification for the early texture of the clays, their morphological similarities and the distribution of the clays within this formation. Thus, the depositional facies, the influence of saline groundwaters produced from the lacustrine environments, and the detrital compositions of the sediment appear to be important factors controlling the abundance of clays in sediment of the Coalspur sandstones.

Kaolinite-to-dickite reaction in Coalspur sandstones

The transition of kaolinite (Fig. 3-21 A) to dickite (Fig. 3-21 B) is poorly understood. It is unknown whether there are factors other than temperature and burial pressure influence this transition, and to what extent it involves the total dissolution of kaolinite and precipitation of dickite.

Authigenic kaolin is the most common clay mineral of the upper Coalspur sandstones. The term "kaolin" refers to the different minerals of the kaolin group, i.e., kaolinite (Fig. 3-21 A), dickite (Fig. 3-21 B) and nacrite. Several researchers pointed out that what was previously named "blocky kaolinite" is often dickite (Ehrenberg et al., 1993; McAulay et al., 1994) and indicated that diagenetic kaolinite and dickite show different morphologies and habits depending on burial depth. Based on morphology and habit observation, two types of kaolin are identified in the upper Coalspur sandstones: booklet kaolinite (Fig. 3-21 A) and dickite (Fig. 3-21 B). Beaufort et al. (1998) pointed out that dickite progressively replaces kaolinite within a range of burial depths between 2500 m and 5000 m. Beaufort et al. (1998) also noted that kaolinite-to-dickite reaction is accompanied by gradual structural changes related to crystal coarsening and change from the booklet to blocky morphology. Also Beaufort et al. (1998) suggested that dickite progressively replaces kaolinite through a continuous growth mechanism which consists of the dissolution of smaller and more disordered crystals of kaolinite which tend to transfer to more stable form via better stacking order. As burial depth increases the stacking order in dickite increases in closes relations to disappearance of the vermiform habit. At 5000 m depth the dickite transform toward more isometric blocky

crystals (Fig. 3-21 C). Kaolinite within the Coalspur sandstones tends to obtain an increase in the degree of stacking order with increasing degree of burial from the delicate, fragile shapes of kaolinite booklets (Fig. 21 A) to more blocky kaolinite (Fig. 3-21 C). This finding suggests that mineralogical reactions could proceed from the dissolution of unstable smaller crystals of kaolinite to the coarsening of the more stable blocky crystals of dickite as burial depth increases. The transformation of kaolinite into dickite suggests that dickite and not illite may be the stable phase during the continuous fluid-rock interaction at deep burial depth that leads to the complete dissolution of detrital feldspars. We suggest that the shift from kaolinite-to-dickite in the Coalspur sandstones indicates a burial depth in between 2500 m and 4500 m (Fig. 3-25).

DIAGENETIC SEQUENCE

The Coalspur sandstones exhibit a complex diagenetic history that strongly influenced their porosity and permeability, including, loss, and enhancement. The sequence of diagenetic events, as determined from thin section slides and SEM examination, is summarized in Figure 3-26.

Very early diagenetic stages

The earliest diagenetic event is compaction. This is significant for sediments with a high clay content and abundance of unstable grains like biotite, feldspars, and some rock fragments. The rate of compaction of sediments decreases through time; later diagenetic cementation of sandstones by quartz, calcite, chert and clay minerals stabilizes the grain framework, decreasing porosity and permeability loss through the

rearrangement of grains. Early diagenesis after initial mechanical compaction includes (1) silica precipitation; (2) calcite cementation; (3) formation of 'septechlorite' and Fe-chlorite; (4) dissolution of volcanic fragments together with early dissolution of detrital feldspars; and (5) formation of clay coatings, rime, pore-linings of early kaolinite and smectite. The ground water chemistry at this stage of shallow depths has great influence on early authigenesis.

Early-to-middle diagenetic stages

In these diagenetic stages, rime chlorite grows perpendicular to quartz grain surfaces and appears to be intergrown with the quartz cements (Fig. 3-23 B). The early-to-middle diagenetic events are; (1) formation of smectite-chlorite pore fills; (2) formation of rims of chlorite perpendicular to grain surfaces, and contemporaneous silica overgrowth; (3) continuous dissolution of detrital feldspars along with dissolution of volcanic fragments; and (4) continued formation of clay coatings, rime, pore-linings, and pore fills of kaolinite and smectite.

Middle-to-late diagenetic stages

Burial diagenesis is a stage characterized by the dissolution/replacement/alteration of minerals, generation of secondary porosity, and precipitation of neoformed minerals. Therefore, the middle-to-late diagenetic stages in the Coalspur Formation consist of the; (1) authigenic quartz precipitation; (2) dissolution of feldspar grains, (3) dissolution of kaolinite and smectite; (4) formation of illite; (5) corrosion and dissolution of quartz grains and authigenic silica; (6) formation of dickite

pore filling; (7) alteration of mica, biotite and other iron-bearing minerals; and (8) continued precipitation of chlorite. Albitization of detrital plagioclase was rare in the Coalspur sandstones. Detrital K-feldspar grains in the sandstones were barely albetizied, where partial dissolution of detrital K-feldspar was observed. The conditions setting off dissolution/alteration reactions during burial diagenesis of the Coalspur Formation are possibly related to factors like pore fluid chemistry, velocity of pore fluid, chemical stability of minerals, depth/temperature relationships, and paleoenvironments.

POROSITY AND PERMEABILITY IN THE COALSPUR SANDSTONES

Sediment compaction, mineral cementation, and dissolution are the primary processes affecting porosity evolution in the Coalspur sandstones. Separating porosity change caused by compaction from those caused by cementation and dissolution is difficult. The reduction of primary intergranular porosity in the Coalspur sandstones began soon after deposition and initial burial, as is indicated by the abundance of deformed soft and ductile grains (Fig. 3-27 A). This finding suggests that a fraction of the porosity may have been lost rapidly via mechanical compaction before any significant cementation occurred. The primary porosity of Coalspur sandstones also decreased through the internal slipping of sand grains during initial compaction, pressure solution, and precipitation of cement. Additionally, the form and composition of sand grains, diagenesis, pore solutions, and changes in pressure and temperature had a significant role in reducing the porosity of the Coalspur sandstones.

Subsequent reduction of primary porosity was rapid because of the abundance of unstable grains like biotite, feldspars, and some rock fragments (Fig. 3-12 C), which are

more affected by mechanical compaction than the stable minerals like quartz. Mechanical compaction also involved grain rotation and rearrangement, grain fracturing, and deformation of ductile grains (Fig. 3-27 A).

Part of the silica cement of the Coalspur sandstones is derived from pressure solution at the points of contact along which the grains slipped into denser packing style (Fig. 3-17 D). More silica dissolved where the smaller and steeper contact faces of the grains are. The amount of quartz increases with compaction as the contact faces become larger. As well, more horizontal contacts form. This finding indicates that mechanical slipping (rearrangement) of the Coalspur sandstone grains occurred before cementation during initial compaction, whereas the chemical compaction (pressure solution) predominated during later stages. Decreased silica cementation in some sandstone beds results from the influence of chlorite coating in deep burial (Fig. 3-23 C), which inhibited further cementation. The grain size and sorting are also important factor that controlled the amount of porosity. The higher porosity of the fine-grained upper Coalspur sandstones was caused by the large number of grain contacts per unit of volume, causing higher resistance against compaction. The porosity of the Coalspur sandstones also decreased with increasing calcite content (Fig. 3-17 A). The present porosity of the Coalspur sandstones is both primary (Fig. 3-27 B) and secondary in origin (Fig. 3-27 C, D and E). Early calcite cementation has a less important effect on primary porosity relative to the role played by clay minerals, distribution of ductile grains and silica cements (Fig. 3-27 A).

Secondary porosity may be recognized by using criteria based on petrographic and scanning electronic microscope studies (Schmidt and McDonald, 1979). Dissolution

of feldspar leads to a significant increase in porosity in some beds in the Coalspur sandstones (Fig. 3-27 E). Even where primary porosity has been nearly eliminated because of the effect of mechanical and chemical compactions, significant secondary porosity resulting from the dissolution of feldspars may still form (Fig. 3-27 E). This formation is characterized by several types of secondary porosity, including (1) partial dissolution of soluble constituents (Fig. 3-27 C); (2) grain moldic porosity produced by the partial dissolution of feldspar along cleavage planes and twin boundaries (Fig. 27 E); (3) corrosion of grains adjacent to pores (Fig. 3-27 D); (4) intra-constituent pores which are generally the result of incomplete replacement of feldspars grains. Fracturing porosity in the Coalspur sandstones is volumetrically insignificant.

The porosity determined from thin sections ranges from 3% to 18% and averages 10%. Most of the secondary porosity in the Coalspur Formation is intergranular and was formed by the dissolution of pore filling and replacive cements. Molds porosity demonstrates the dissolution of former framework grains and is observed in the Coalspur sandstones (Fig. 3-27 F).

The presence of authigenic clays in the pores of the Coalspur sandstones reduces permeability, due to the constriction of pore throats (Fig. 3-27 F) and increased turbulence by roughening the pore wall surface (Ives, 1987). The distribution of authigenic clay minerals also affected the primary porosity in the Coalspur sandstones. For instance, progressive cementation by smectite or chlorite produces a decline in permeability because of the blocking of pore throats (Fig. 3-27 C). The various individual kaolinite booklets, which have no preferred orientation relative to one another, consumed a large part of the original pore space, hence affecting the primary

porosity, but more importantly, authigenic kaolinite-filled pores would have the least effect on transport properties. This suggests that the permeability-reduction mechanism is an actual physical control and constriction of the pore throats rather than drag and increased turbulence of laminar flow created by a roughed surface (Howard, 1992).

Grain-rimming clays such as illite also result in a more significant permeability decline than overgrowth cementation. This reduction in permeability is caused by the microporous grain rims, which behave like solid overgrowths as far as the fluid flow is concerned. At the same time, the Coalspur sandstones with clay grain rims have higher porosity than those with solid grain overgrowths. A dramatic reduction in permeability, with corresponding increase in the degree of illitization (Guven et al., 1980), is observed within the Coalspur sandstones. Pore filling interstitial fibrous smectite also result in a porosity and permeability reduction because of their very high surface area to volume ratio (Almon, 1979). Microscopic recovery efficiency (microporosity) in chlorite-rich sandstones tends to be higher than in mixed-layer rich sandstones because the chlorite rims commonly cause no increase in the pore system heterogeneity.

The timing of secondary porosity generation is uncertain. The deformation of relict clay coatings or rims may suggest early primary porosity reduction, possibly shortly after compaction. The dissolution of unstable detrital grains (Fig. 3-27 E) most likely was a continuous process throughout burial, which also caused a slight increase in secondary porosity.

The observed diagenetic features render the Coalspur sandstones as semi-mature in the diagenesis maturity classification of Schmidt and McDonald (1979).

CLIMATE DURING THE COALSPUR TIME

The climatic conditions during the Coalspur time may be inferred from the results of our petrographic and SEM studies. Variations in the relative abundance of detrital constituents among sandstone rocks may be attributed to climatic changeability in the study area (Basu, 1976). Topographic relief and climate in a source area also control the effect of chemical weathering (Basu, 1985), although the effects of distance transportation and provenance variability must be considered.

Paleoclimate inferences from thin section petrography

Chemical weathering influences the detrital composition of sand size sediment derived from source areas. For the purpose of paleoclimatic interpretations, the polycrystalline quartz aggregates are counted as a type of quartz rather than rock fragments. Of the grain types studied, rock fragments are most sensitive to chemical degradation. Therefore, their abundance is a good indicator of cumulative weathering effects (Grantham and Velbel, 1988; Mack and Suttner 1977). The effect of climate on the petrography of sandstones has been studied by many scientists (Mann and Cavaroc, 1973; Young et al., 1975; Basu, 1976, 1985; Mack and Suttner 1977; Suttner and Dutta, 1986; Jermy and Michael, 1988). These investigations have shown that under arid to semi arid climatic conditions the percentage of rock fragments is significantly higher because of the less extensive chemical weathering under these conditions. These studies also indicated that minerals, such as quartz (mono-and polycrystalline), are more abundant in a humid climate because quartz is more resistant to chemical weathering.

The climatic effect on the detrital frameworks of the Coalspur sandstones is best observed in the modal percentages of rock fragments and quartz (Figs. 3-4 to 3-9, 3-28 A and B). The percentage of feldspar remained consistent through time, with the exception of the Entrance Member, where the relatively higher percentage of feldspar may indicate closer source areas and/or relatively high topographic gradients. Gradual climatic changes may be inferred from the composite petrographic profile, which correlates well with the variability observed in the authigenic mineral composition (Fig. 3-28 A and B). In the Foothills region of west-central Alberta, the climate seems to have shifted from arid/semi-arid (lower Coalspur) to more humid conditions (upper Coalspur).

Paleoclimate inferences from authigenic clay minerals

Climate variability may control the nature of early cement (Walker et al., 1978). The climate has significant control over authigenic clay minerals in sandstones from meteoric origin (Suttner and Dutta, 1986). When rainfall is low and the consequential ionic concentration in the groundwater is high, Cation-rich clays such as smectite and chlorite form (Velde, 1985). In a region with a high rainfall and warm climate, authigenic kaolinite and quartz cements are abundant because the groundwater has a low ionic concentration (Dutta, 1992). Therefore, the character of clay cement is a function of the groundwater chemistry, which the climate may control (Suttner and Dutta, 1986).

The Coalspur sandstones include a diversity of authigenic minerals (Figs. 3-4 to 3-9). Their major types are the chlorite, chlorite-smectite, smectite, quartz and the kaolin minerals, such as kaolinite and dickite, whose relative amounts vary significantly from one bed to another. These shifts in the distribution of authigenic clays correlate with the

changes in detrital components. The sublitharenites (which contains a higher quartz percentage) have high amounts of kaolinite, dickite, and quartz overgrowth, indicating wetter climatic conditions within the upper Coalspur Formation (Fig. 3-28 B). The litharenites (which contain a higher lithoclast percentage) are dominated by smectite, chlorite and chlorite-smectite, suggesting semi-arid to arid climatic conditions and less effect of chemical weathering within the lower Coalspur sandstones in the center and south of the Foothills. A climatic control on the mineralogical composition is supported by a good correlation between the framework mineralogy and the authigenic clay content of the Coalspur sandstones.

A lack of correlation between the framework mineralogy and the associated authigenic clays is noted for intervals "A" of the upper Coalspur Formation (Fig. 3-28 B), where high quartz percentages are not accompanied by any significant amounts of kaolinite. These exceptions may be explained by fluctuations in the chemical conditions of the diagenetic environment. The formation of kaolinite within these intervals "A" was likely inhibited by an alkaline chemistry of the pore water. At low pH values, with little silica in solution, kaolinite is in a stable state, whereas at higher pH values with much silica in solution, the clay minerals such as smectite and illite, with higher proportios of silica, are likely to be the stable form (Correns et al., 1939). As well, the presence of Ca^{++} tends to block the formation of kaolinite, favoring the precipitation of smectite and illite instead (Millot, 1942). Consequently, the abundance of calcite cement is probably the main reason why kaolinite is absent or poorly represented in intervals "A." Intervals "B" (Fig. 3-28 B) are characterized by the presence of both kaolinite and smectite, which are associated with high quartz percentages. We interpret this presence to reflect wetter

climatic conditions, with the high amounts of smectite being explained by the abundance of calcite cement, which favors smectite precipitation. Like intervals A and B, intervals "C" also correlates with relatively wet climatic conditions, as the high amounts of detrital quartz and authigenic kaolinite, and the low amounts of authigenic smectite indicate.

CONCLUSIONS

1. The Coalspur sandstones in the Foothills region of west-central Alberta are classified by sublitharenites and lithic arenites.

2. The shifts from kaolinite to dickite in the Coalspur sandstones indicate a maximum burial depth between 2500 m and 4500 m.

3. The deposition environments of the Coalspur sandstones are fluvio-lacustrine environments as the early authigenic clay minerals indicate.

4. Climatic shifts between drier in the lower Coalspur Formation to wetter climate conditions within the Foothills are inferred from the composite information derived from thin-section petrography, scanning electronic microscopy, and x-ray diffraction.

5. The sublitharenites with higher amounts of quartz combined with abundant kaolinite, decikite and quartz overgrowth indicated wetter climatic conditions.

6. The lithic arenites rich in lithoclasts, authigenic chlorite, and smectite indicated drier climatic conditions.

7. The diagenetic sequence was established based on the relationships observed between the framework grains and the various types of authigenic minerals. The early diagenesis of the Coalspur sandstones is characterized by (1) initial mechanical compaction, (2) silica precipitation, (3) calcite cementation, (4) formation of 'septechlorite' and Fe-chlorite, (5) early dissolution of detrital feldspars along with dissolution of volcanic fragments, and (6)- formation of clay coatings, rime, pore-linings, early kaolinite and smectite pore fills. Burial diagenesis is dominated by (1) precipitation of authigenic quartz, (2) dissolution of feldspar grains, dissolution of kaolinite, and smectite, (3) formation of illite, (4) corrosion and dissolution of quartz grains and authigenic silica, (5) formation of dickite pore filling, (6) alteration of mica, biotite and other iron-bearing minerals, and (7) precipitation of chlorite.

8. This study demonstrates the value of petrographic and SEM analyses in the assessment of porosity in fluvial reservoirs. Both primary, and several types of secondary porosity have been observed in the Coalspur sandstones. Such an outcrop study may be used as an analogue for the assessment of other fluvial-lacustrine reservoirs in the subsurface of the Western Canada Sedimentary Basin.

99

Figure 3-1. Outcrop distribution of the Scollard and Coalspur formations in Alberta, and the location of the studied outcrop sections.
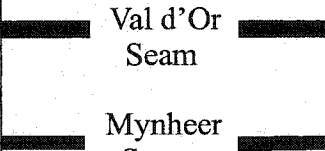
AGE	Stratigraphic Units		
Paleocene	Paskapoo Formation		
Paleocene	Coalspur Formation	upper Coalspur	Val d'Or Seam
Maastrichtian	Coalspur Formation		Mynheer Seam
Maastrichtian	Coalspur Formation	lower Coalspur	
Maastrichtian			Entrance Member
Maastrichtian	Brazeau Formation		

Figure 3-2. Generalized chart of the late Maastrichtian-Paleocene stratigraphy of west-central Alberta, showing the position of the Coalspur Formation and its two major coal seams (Val d'Or and Mynheer).

101

Facies	Facies code and symbol		Sedimentary structures
Gh		Clast-supported, crudely bedded gravel	Horizontal bedding, imbrication
St		Sand, fine to very coarse, may be pebbly	Solitary or grouped trough cross-beds
Sp		Sand, fine to very coarse, may be pebbly	Solitary or grouped planar cross-beds
Sr		Sand, very fine to coarse	Ripple cross-lamination
Sh		Sand, very fine to coarse, may be pebbly	Horizontal lamination, parting or streaming lineation
Sl		Sand, very fine to coarse, may be pebbly	Low-angle ($<15°$) cross-beds
Ss		Sand, fine to very coarse, may be pebbly	Broad, shallow scours
Sm		Sand, fine to coarse	Massive or faint lamination
Sb		Sand, fine to very coarse, may be pebbly	Ball-and-pillow structure, may show internal lamination
Sf		Sand, fine to coarse with mud	Massive, may be laminated
Fl		Sand, silt, mud	Fine lamination, very small ripples
Fsm		Silt, mud	Massive
Fp		Mud with pebbles	Vague laminated mud with floating, isolated clasts
Fs		Mud with sand, fine to coarse	Massive, may be laminated
Fb		Mud, silt	Ball-and-pillow structure, may show internal lamination
Fm		Mud, silt	Massive, desiccation cracks
C		Coal, carbonaceous mud	Plant, mud films

Figure 3-3. Facies types used to describe the sedimentological characteristics of the studied outcrop sections (Figs. 4-8).

102
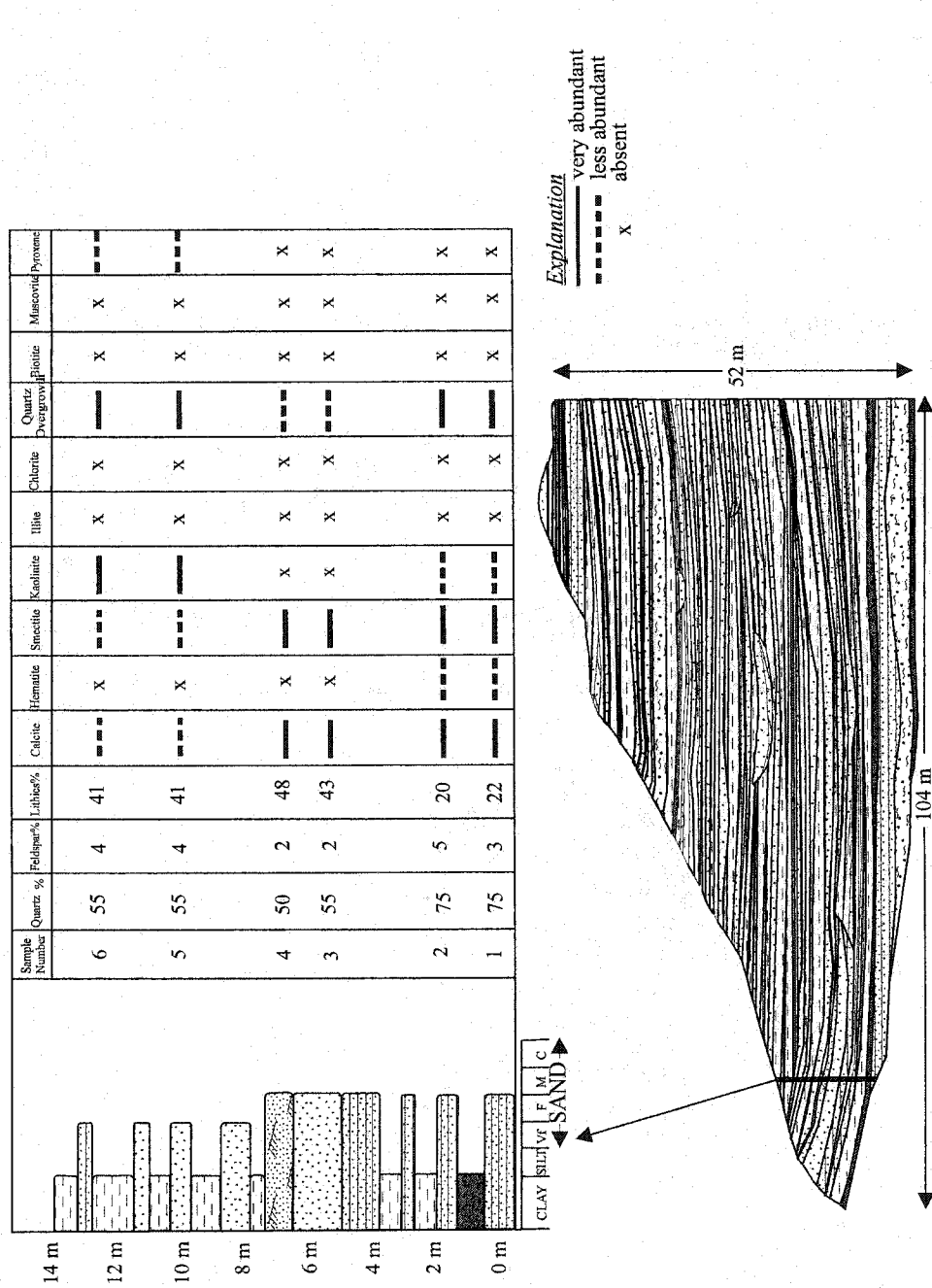
Figure 3-4. Outcrop sketch and vertical profile for the Sundre locality. The table shows the sandstone composition in terms of detrital constituents and authigenic minerals. The relative percentages of the three main framework constituents (quartz, feldspars, lithoclasts), out of 100%, is used to classify the sandstones (Fig. 10). See Figure 3 for facies codes.

Explanation
- ▬▬▬ very abundant
- - - - less abundant
- x absent

Sample Number	Quartz %	Feldspar%	Lithics%	Calcite	Hematite	Smectite	Kaolinite	Illite	Chlorite	Quartz Overgrowth	Biotite	Muscovite	Pyroxene
6	55	4	41	- - -	x	- - -	- - -	x	x	▬	x	x	- - -
5	55	4	41	- - -	x	- - -	- - -	x	x	▬	x	x	- - -
4	50	2	48	- - -	x	▬	x	x	x	- - -	x	x	x
3	55	2	43	▬	x	▬	x	x	x	- - -	x	x	x
2	75	5	20	- - -	- - -	- - -	- - -	x	x	▬	x	x	x
1	75	3	22	▬	x	▬	- - -	x	x	▬	x	x	x

52 m

104 m

103

Sample Number	Quartz %	Feldspars%	Lithics%	Calcite	Smectite	Kaolinite	Chlorite	Illite	Quartz overgrowth	Biotite	Muscovite	Pyroxene
9	45	15	40	x	▬	▪▪▪	▬	x	▪▪▪	▬	▬	▬
8	30	20	50	x	x	▪▪▪	▬	▬	▪▪▪	x	▪▪▪	▬
7	40	15	45	▪▪▪	▬	x	▬	▬	▪▪▪	x	▬	▬
6	40	20	40	▪▪▪	▬	x	x	x	▪▪▪	x	▪▪▪	▬
5	35	15	50	▪▪▪	▬	x	x	x	▪▪▪	x	▪▪▪	▬
4	35	15	50	▪▪▪	▬	x	▬	x	▪▪▪	x	▬	▪▪▪
3	35	20	45	x	▬	x		x	x	▪▪▪			
2	40	10	50	▪▪▪	x	x	▬		▬	x	▪▪▪	x
1	40	15	45	x	▪▪▪	▬	▬	x	▪▪▪	x	▪▪▪	x

Figure 3-5. Outcrop sketch and vertical profile for the Rude cut along Red Deer River locality. The table shows the sandstone composition in terms of detrital constituents and authigenic minerals. The relative percentages of the three main framework constituents (quartz, feldspars, lithoclasts), out of 100%, is used to classify the sandstones (Fig. 11). See Figure 3 for facies codes.

104

Figure 3-6 (rotated). Stratigraphic profile, composition table, and outcrop sketch for the Coal Valley locality.

Vertical profile scale (left axis):
Paskapoo Formation — 48 m, 42 m, 36 m, 30 m, 24 m
Coalspur Formation — 18 m, 12 m, 6 m, 0 m
Grain size axis: C VC L M C VF F M C N cl — Gravel ◄ SAND

Explanation
— very abundant
--- less abundant
x absent

Sample Number	Quartz %	Feldspar%	Lithics%	Calcite	Hematite	Smectite	Kaolinite	Illite	Chlorite	Quartz Overgrowth	Biotite	Muscovite	Pyroxene
6	70	5	25	—	---	---	—	x	x	—	x	—	x
5	75	5	20	—	---	—	—	x	x	—	x	—	x
4	50	10	40	—	---	---	—	x	x	---	x	---	x
3	55	5	40	---	---	—	---	x	x	---	x	—	x
2	50	5	45	x	x	—		x	x	---	x	—	x
1	55	10	35	x	x	—		x	x	—	x	—	x

Outcrop sketch: 70 m (horizontal) × 7 m (vertical).
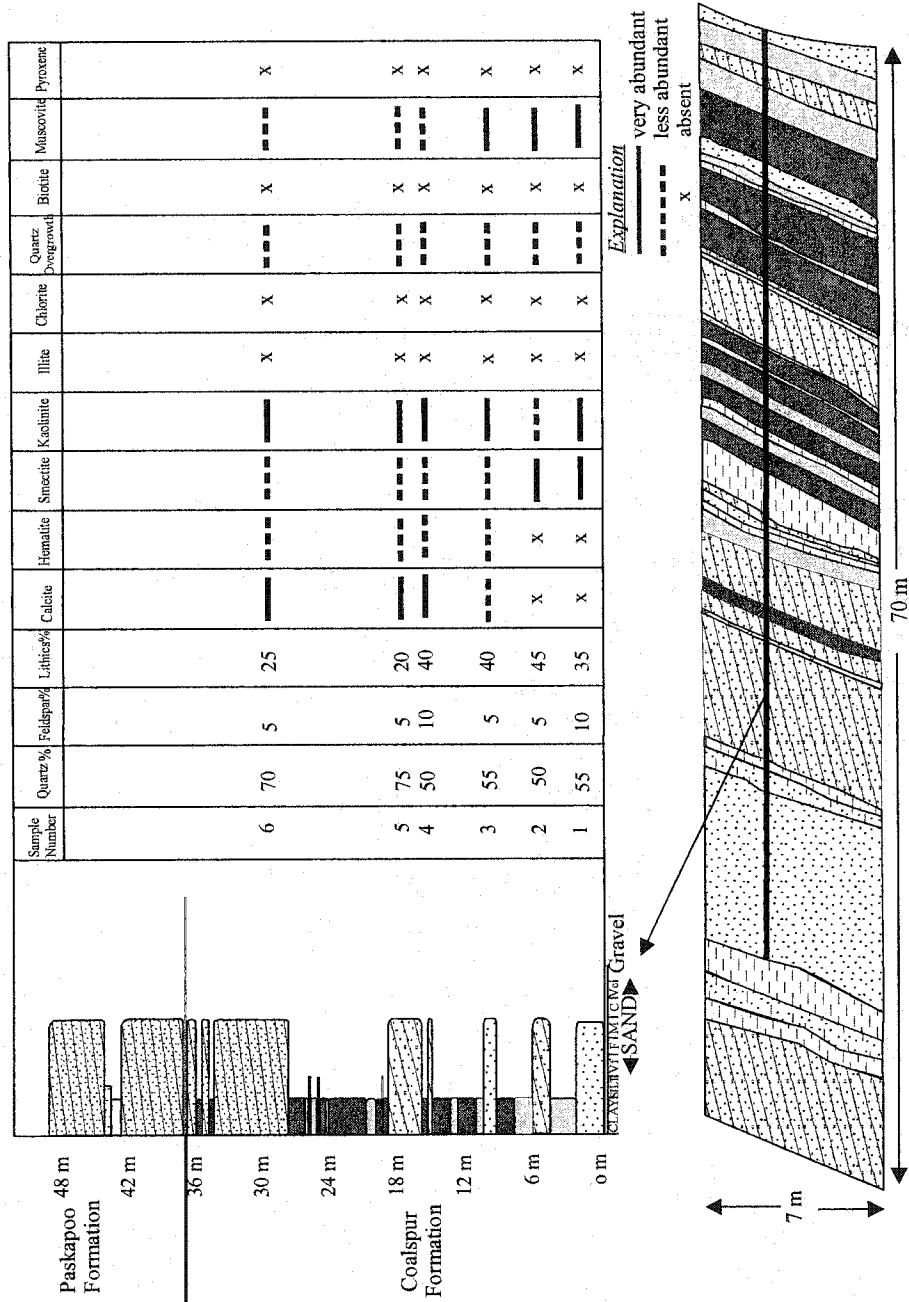
Figure 3-6. Outcrop sketch and vertical profile for the Coal Valley locality. The table shows the sandstone composition in terms of detrital constituents and authigenic minerals. The relative percentages of the three main framework constituents (quartz, feldspars, lithoclasts), out of 100%, is used to classify the sandstones (Fig. 11). See Figure 3 for facies codes.

105
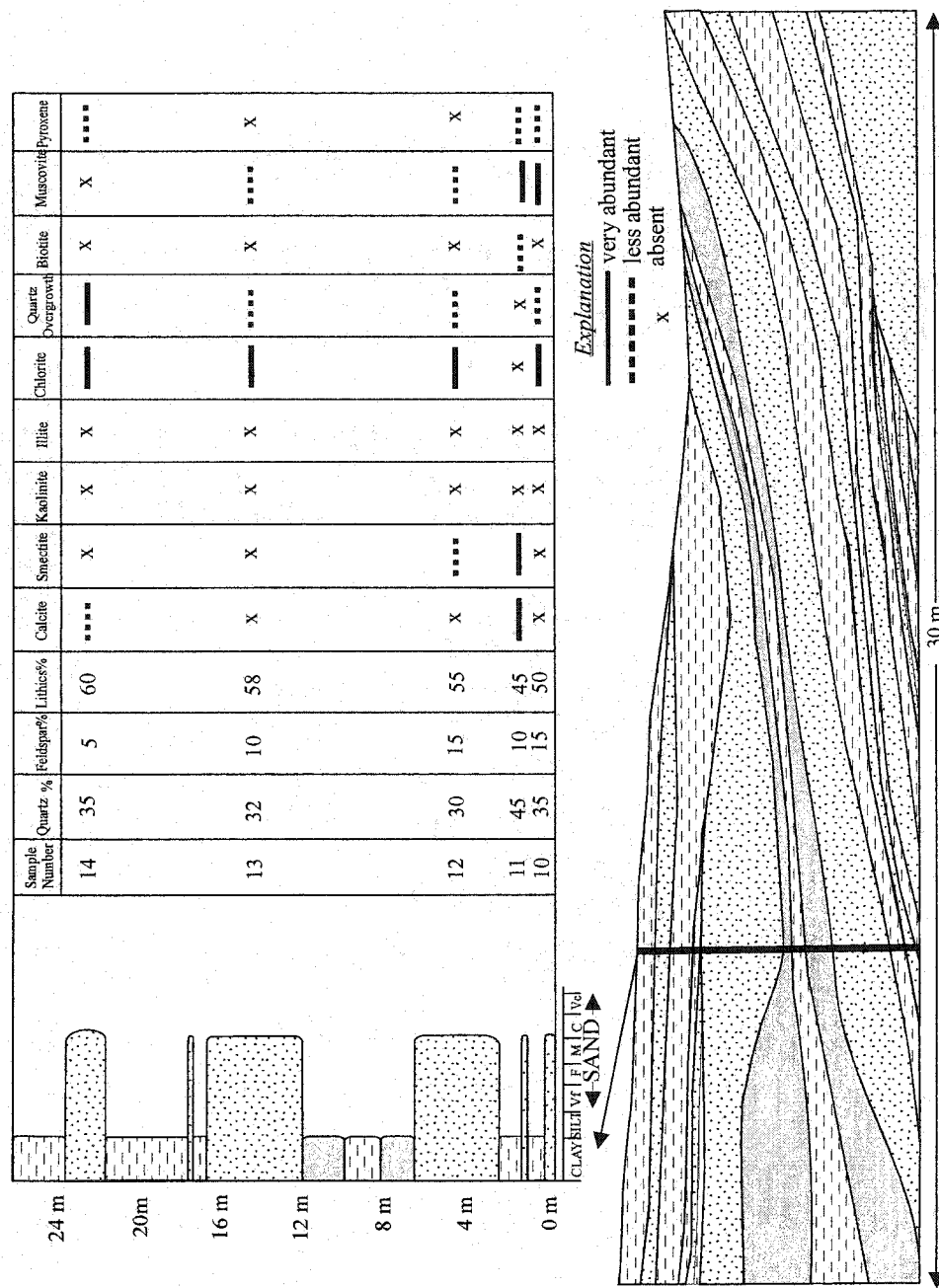
Figure 3-7. Outcrop sketch and vertical profile for the roadcut along Red Deer River locality. The table shows the sandstone composition in terms of detrital constituents and authigenic minerals. The relative percentages of the three main framework constituents (quartz, feldspars, lithoclasts), out of 100%, is used to classify the sandstones (Fig. 11). See Figure 3 for facies codes.

Table (from figure):

Explanation
▬▬▬ very abundant
▪▪▪▪ less abundant
x absent

Sample Number	Quartz %	Feldspar %	Lithics %	Calcite	Smectite	Kaolinite	Illite	Chlorite	Quartz Overgrowth	Biotite	Muscovite	Pyroxene
14	35	5	60	▪▪▪▪	x	x	x	▬▬	▬▬	x	x	▪▪▪▪
13	32	10	58	x	x	x	x	▬▬	▪▪▪▪	x	▪▪▪▪	x
12	30	15	55	x	▪▪▪▪	x	x	▬▬	▪▪▪▪	x	▪▪▪▪	x
11	45	10	45	▬▬	▬▬	x	x	x	x	▪▪▪▪	▬▬	▪▪▪▪
10	35	15	50	x	x	x	x	x	x	x	▪▪▪▪	▪▪▪▪

CLAY silt vf f m c vc
◄—— SAND ——►

24 m 20 m 16 m 12 m 8 m 4 m 0 m

30 m

106

Figure 3-8 (Smokey River locality)

Sample Number	Quartz %	Feldspar %	Lithics %	Calcite	Smectite	Kaolinite	Chlorite	Illite	Quartz Overgrowth	Biotite	Muscovite	Pyroxene
5	60	10	30	less abundant	less abundant	very abundant	X	X	less abundant	X	very abundant	less abundant
4	75	5	20	very abundant	less abundant	very abundant	X	X	less abundant	less abundant	less abundant	less abundant
3	65	10	25	very abundant	less abundant	very abundant	X	X	less abundant	X	less abundant	less abundant
2	60	10	30	less abundant	less abundant	very abundant	X	X	less abundant	X	less abundant	very abundant
1	65	10	25	less abundant	less abundant	very abundant	X	X	less abundant	X	less abundant	very abundant

CLAY | vf | F M C | vc
◄SAND►

48 m
40 m
32 m
24 m
16 m
8 m
0 m

70 m

50 m

Explanation
——— very abundant
------- less abundant
x absent

Figure 3-8. Outcrop sketch and vertical profile for the Smokey River locality. The table shows the sandstone composition in terms of detrital constituents and authigenic minerals. The relative percentages of the three main framework constituents (quartz, feldspars, lithoclasts), out of 100%, is used to classify the sandstones (Fig. 11). See Figure 3 for facies codes.

Sample Number	Quartz %	Feldspar%	Lithics%	Calcite	Hematite	Smectite	Kaolinite	Illite	Chlortie	Quartz Overgrowth	Biotite	Muscovite	Pyroxene
3	30	20	50	X	X	- - -	X	X	▬▬▬	- - -	X	- - -	X
2	25	15	60	X	X	- - -	X	X		- - -	X	- - -	X
1	22	15	63	X	X	- - -	X	X	- - -	- - -	X	- - -	- - -

Explanation

▬▬▬ very abundant
- - - less abundant
x absent

CLAY | slt | vf | f | M | c | vc | Gravel
◄─ SAND ▲

16 m — Entrance Member

12 m

8 m — Brazeau Formation

4 m

0 m

20 m
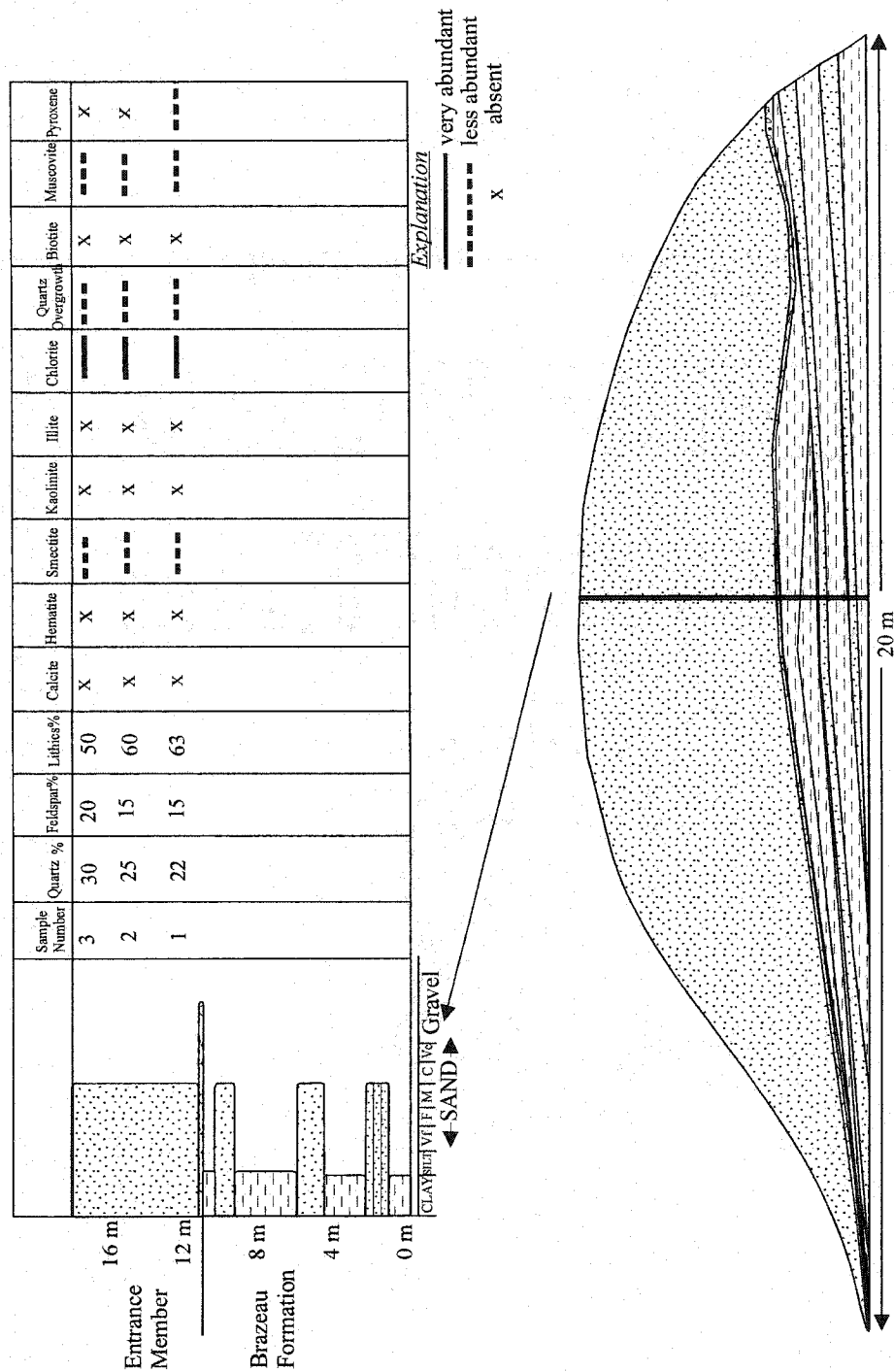
Figure 3-9. Outcrop sketch and vertical profile for the Highway 22 locality. The table shows the sandstone composition in terms of detritalconstituents and authigenic minerals. The relative percentages of the three main framework constituents (quartz, feldspars, lithoclasts), out of 100%, is used to classify the sandstones (Fig. 11). See Figure 3 for facies codes.
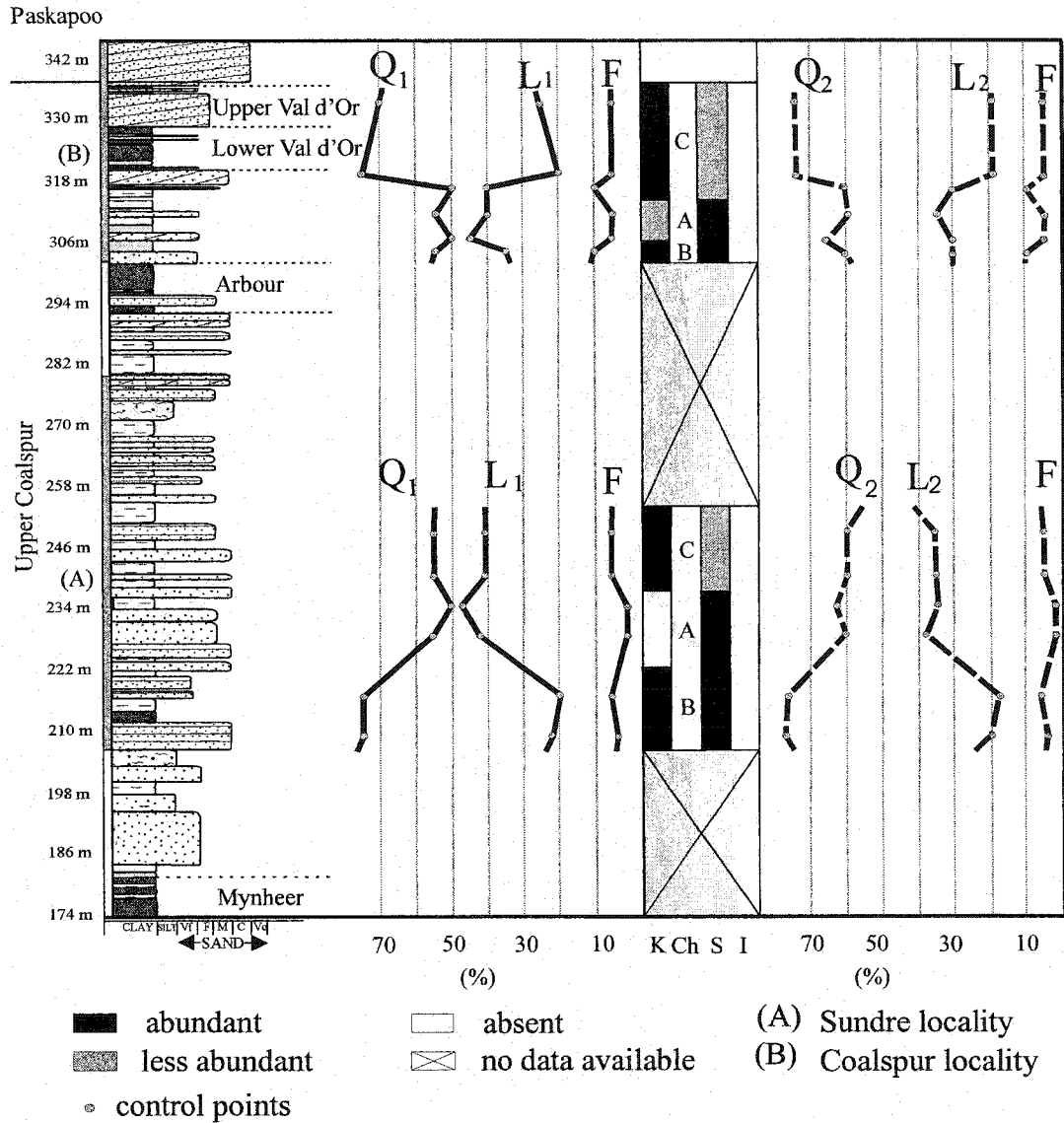
108
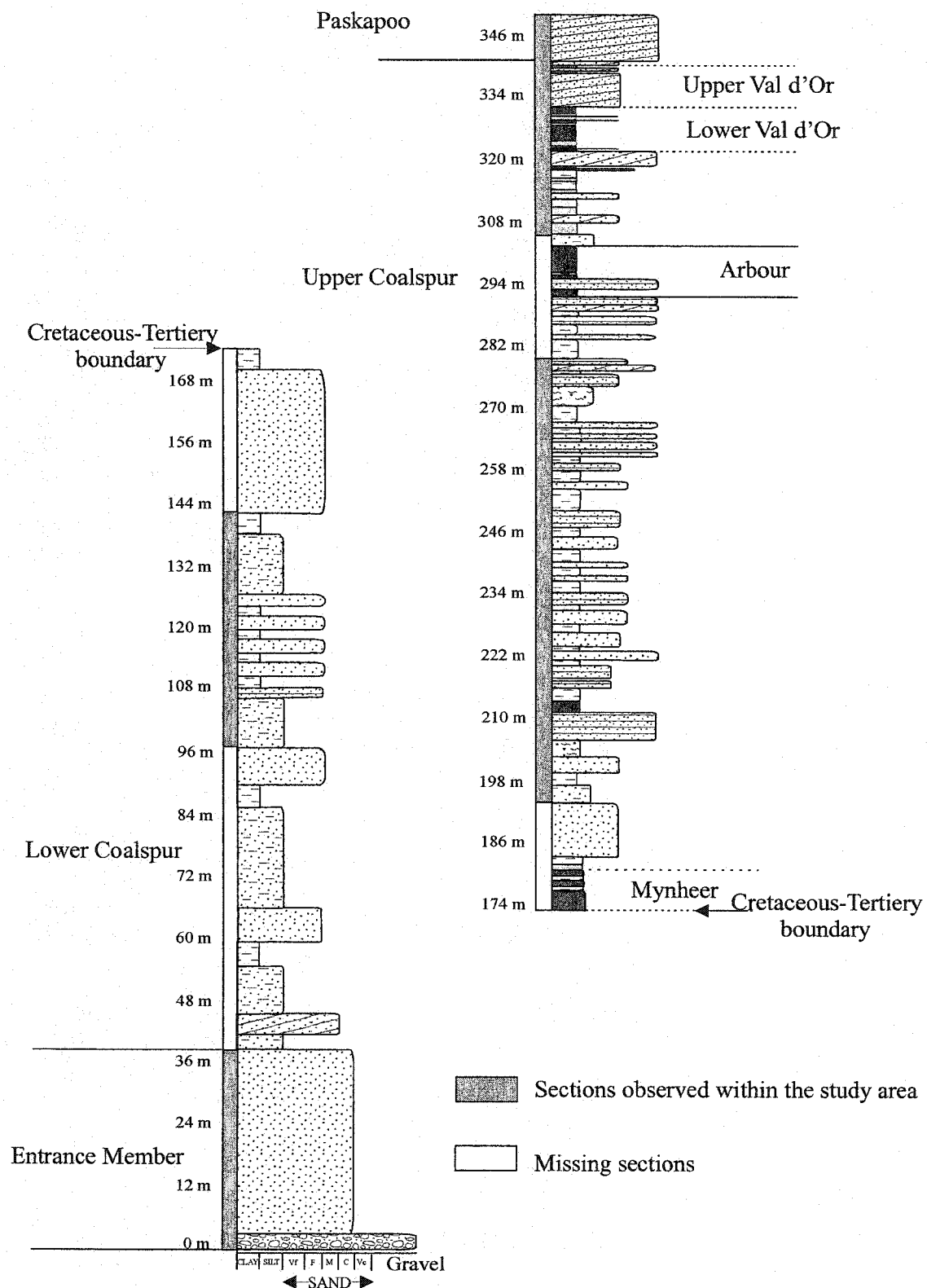
Figure 3-10. Composite vertical profiles of the Coalspur Formation in the in the Foothills region of west-central Alberta (Note missing sections modified after Smith et al., 1977 and geophysical log response).
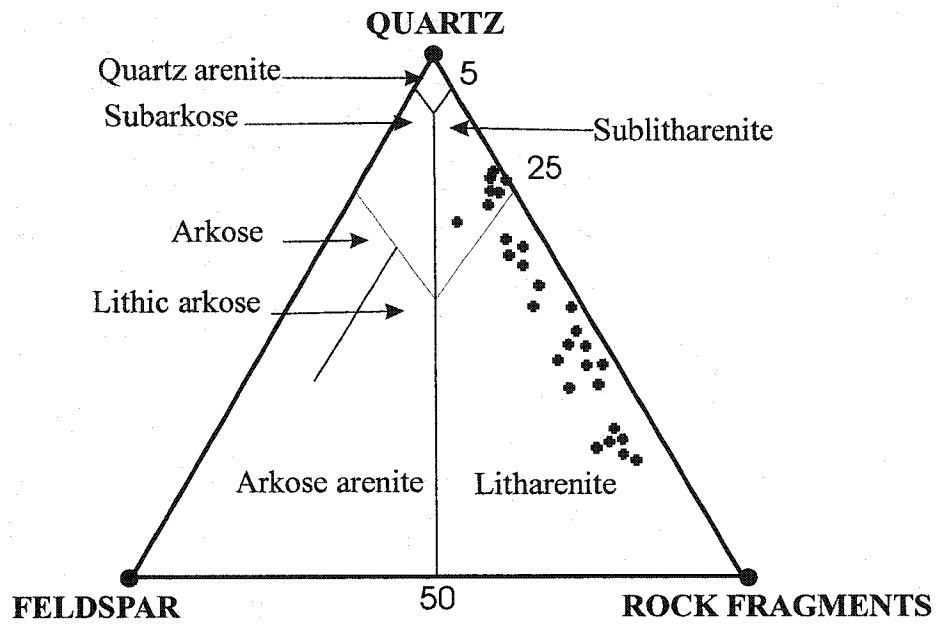
Figure 3-11. Classification of the Coalspur Formation sandstones

(after Pettijohn et al., 1987).
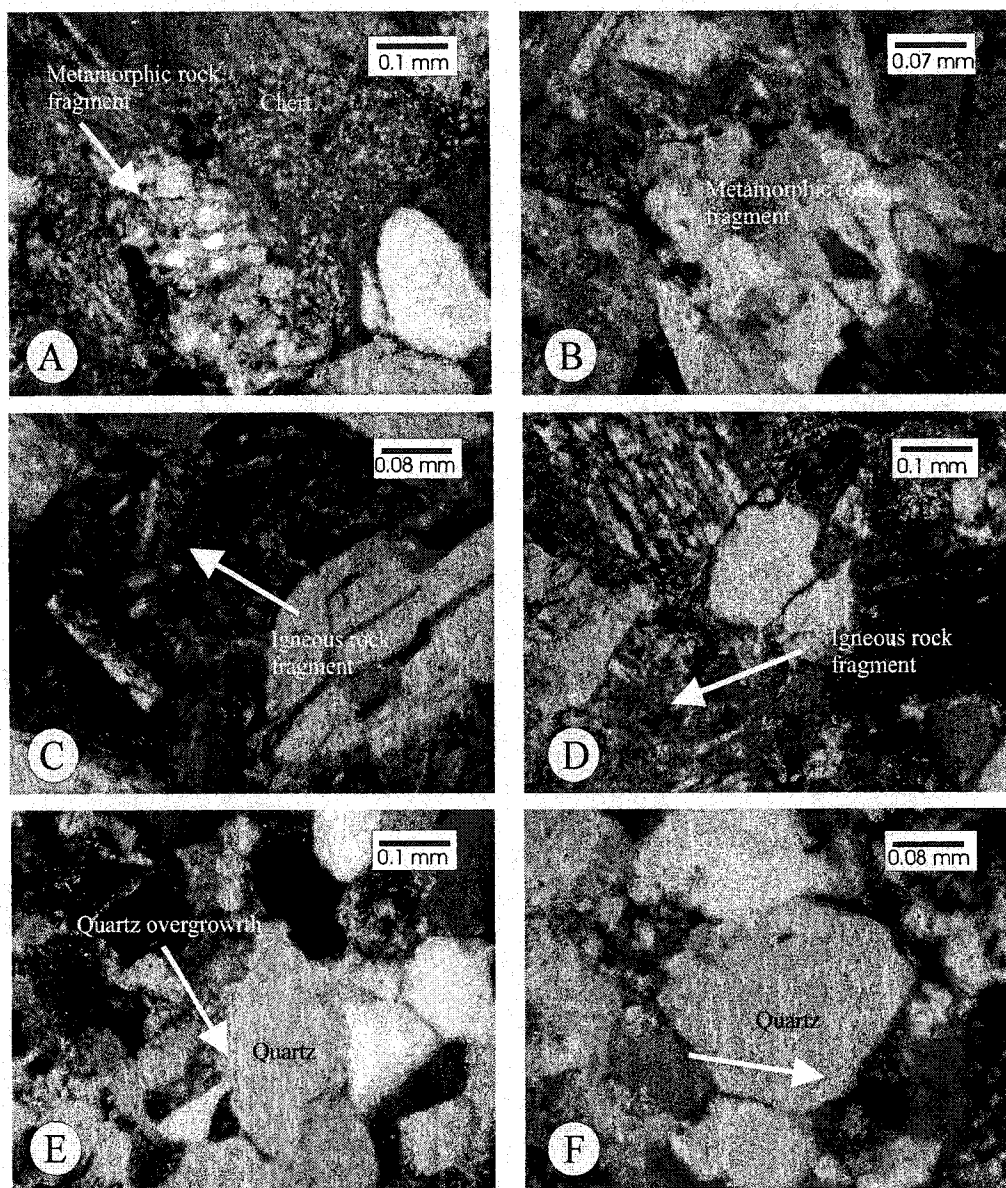
Figure 3-12. Thin-section photomicrographs: (A) litharenite from the Highway 22 locality, with metamorphic and chert lithoclasts. Note the uniform microcrystalline quartz with no visible relict texture, (sample -1, Entrance Member, Highway 22 locality); (B) detrital grain of polycrystalline quartz of metamorphic origin(sample 3, upper Coalspur Formation, Sundre locality); (C) and (D) detrital grains of igneous origin (sample2, Entrance Member Coalspur Formation, Highway 22 locality);(E) fluid inclusions (arrow) associated with quartz grains (sample 1, upper Coalspur Formation, Sundre locality); (F) fluid inclusions associated with quartz overgrowth (arrow) (sample 2, upper Coalspur Formation, Sundre locality).

111
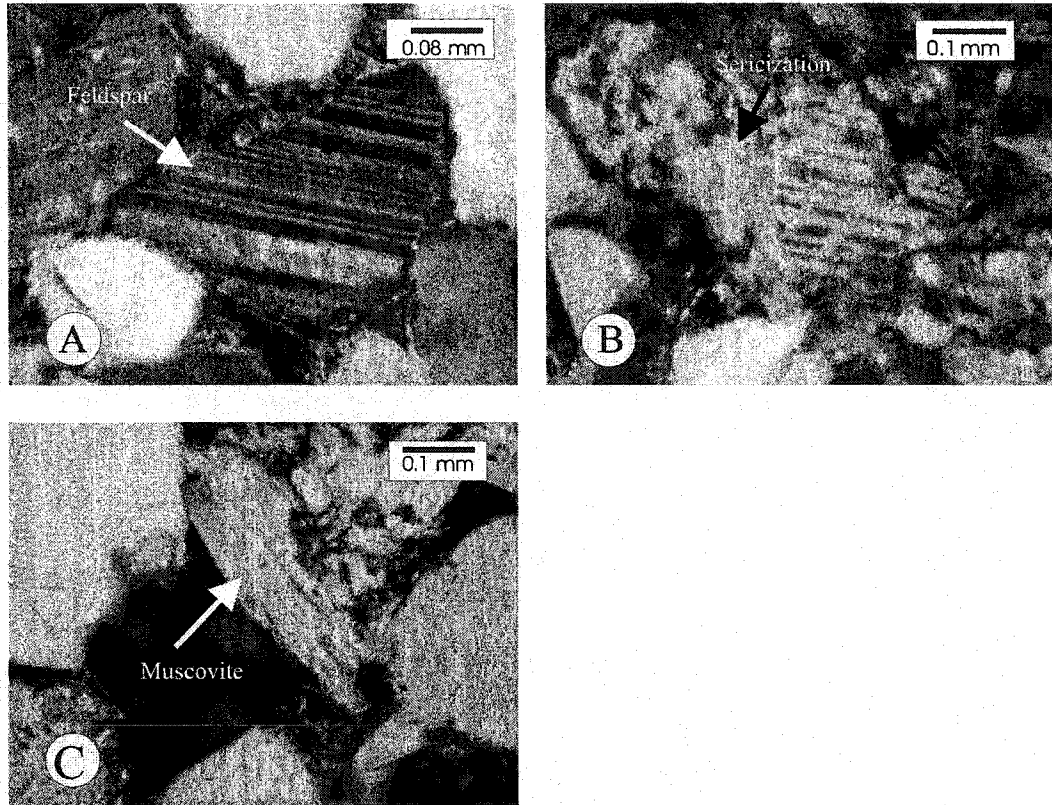
Figure 3-13. Thin-section photomicrographs: (A) feldspar shows multiple twinning, (sample -1, Entrance Member, Highway 22 locality); (B) - plagioclase detrital shows considerable alteration, mainly vacuolizationand sericization (sample 4, upper Coalspur Formation, Sundre locality); (C)- muscovite flank (arrow) (sample2, Coalspur Fraction, Coal Valley locality).
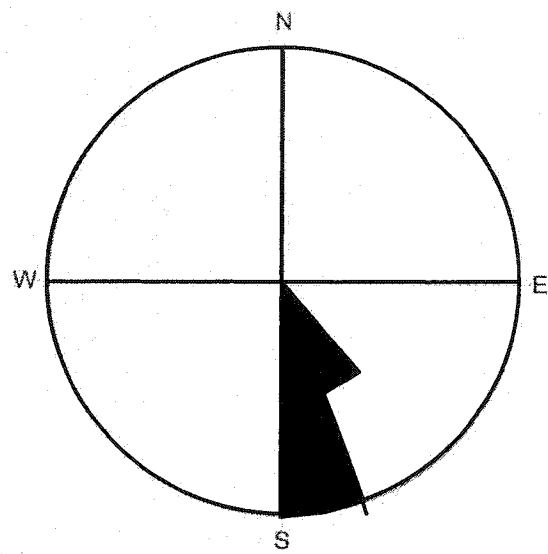
Arithmetic Plot
Number of Points: 6
Class Size: 20
Maximum Percent: 66
Vector Mean: 159.98
Vector Magnitude: 5.95
Consistency Ratio: 0.9912

Figure 3-14. Rose diagram showing the paleoflow directions for the Entrance

Member.

113
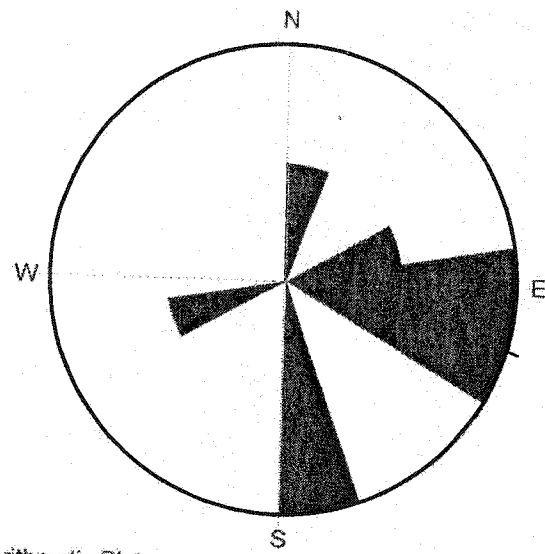
Arithmetic Plot
Number of Points: 9
Class Size: 20
Maximum Percent: 22
Vector Mean: 105.94
Vector Magnitude: 4.74
Consistency Ratio: 0.5269

Figure 3-15. Rose diagram showing the paleoflow directions for the lower

Coalspur Formation.
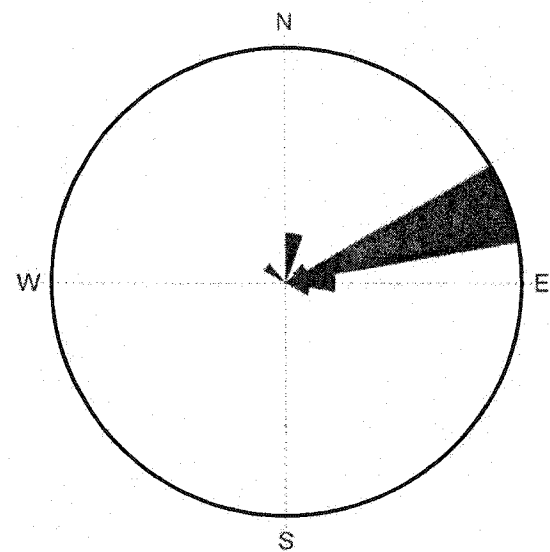
Arithmetic Plot
Number of Points: 16
Class Size: 20
Maximum Percent: 56
Vector Mean: 59.64
Vector Magnitude: 12.84
Consistency Ratio: 0.8025

Figure 3-16. Rose diagram showing the paleoflow directions for the upper
Coalspur Formation
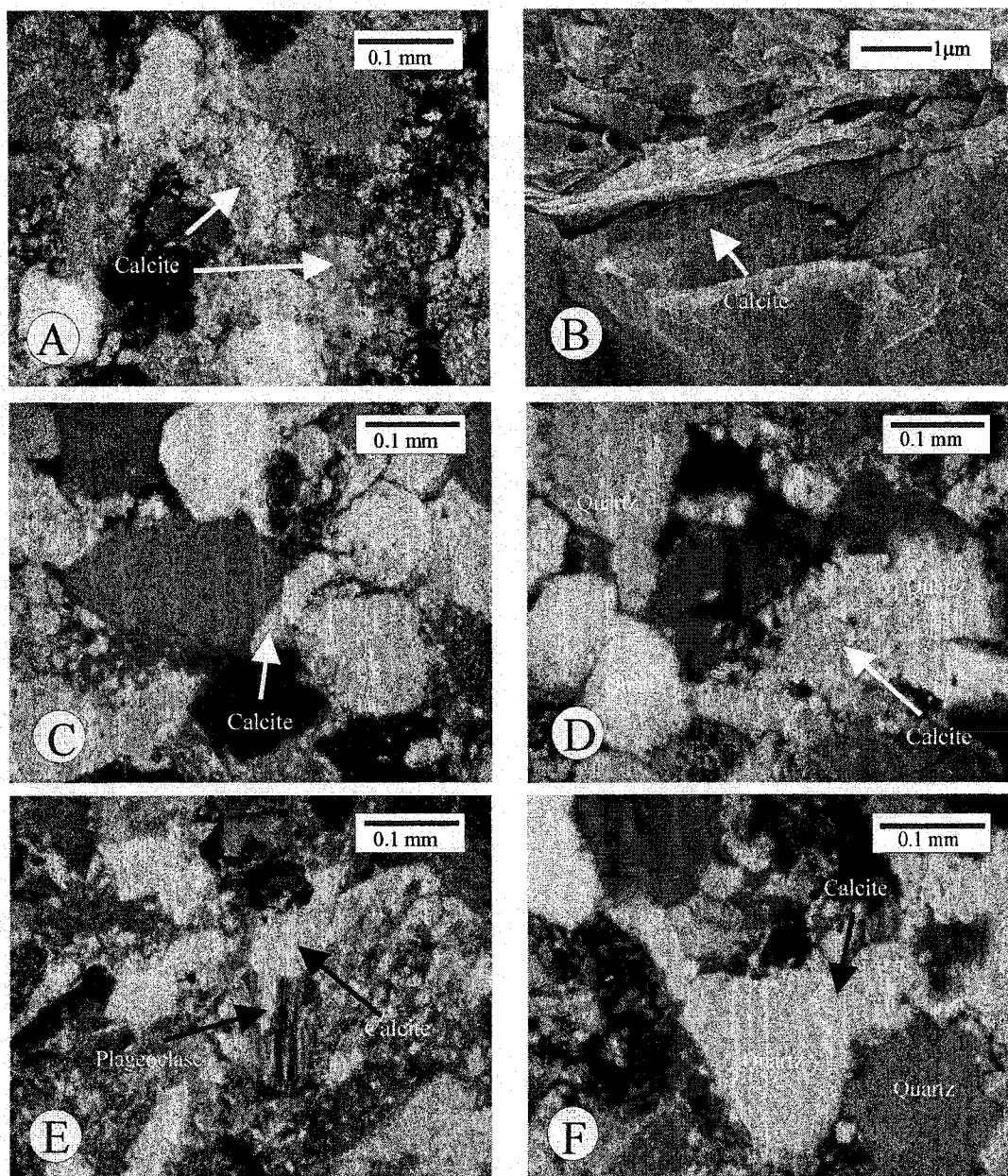
Figure 3-17. Thin-section photomicrographs and Scanning electronic photomicrograph: (A) poikilotopic calcite (arrow) cement (sample 3, Upper Coalspur Formation, Sundre locality); (B) early blocky calcite cement (sample 5, upper Coalspur Formation, Sundre locality); © An early stage of carbonate precipitation can be recognized by crystals of carbonate which are embedded by closely packed quartz grains (sample 1, upper Coalspur Formation, Sundre locality); (D) calcite cement precipitation between pore space (sample 2, upper Coalspur Formation, Sundre locality); (E) detrital plagioclase showing alteration, vacuolization and sericitization. Note the early calcite cement altered the detrital feldspar (sample 2, upper Coalspur Formation, Sundre locality); (F) quartz grain corroded by early poikilotopic calcite cement (sample 3, upper Coalspur Formation, Red Deer locality).

116
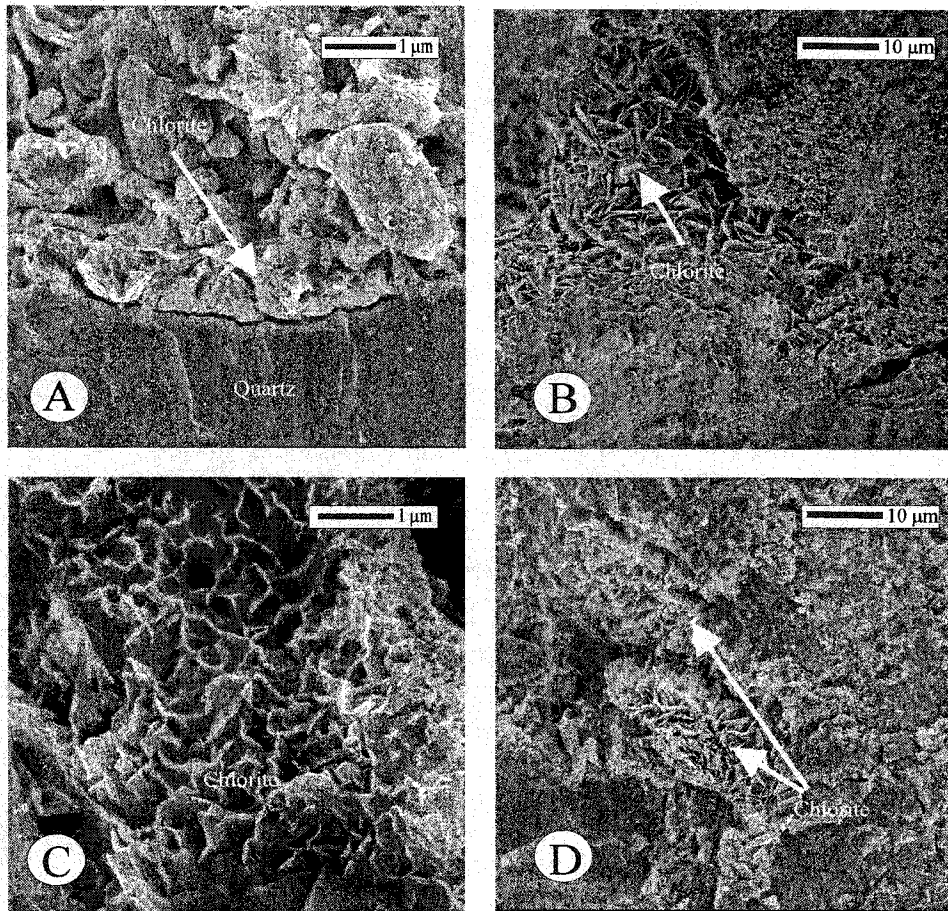
Figure 3-18. Scanning electronic photomicrographs: (A) chlorite appears as a pore linings (rims)composite of crystals perpendicularly oriented to grain surface (arrow) of quartz grain (sample 12, upper Coalspur Formation, the Red Deer River); (B) authigenically formed chlorite (arrow) appearsas rosettes of pseudohexagonal crystals (sample 3, Entrance Member Coalspur Formation, roadcut Highway 22); (C) pore filling chlorite arranged in a cellular pattern (sample 4, upper Coalspur Formation, the outcrop along the Red Deer River); (D) coarser chlorite crystals grained (arrows).Note the increase in crystals size with increasing burial depth (sample2, Entrance Member, roadcut, Highway 22).
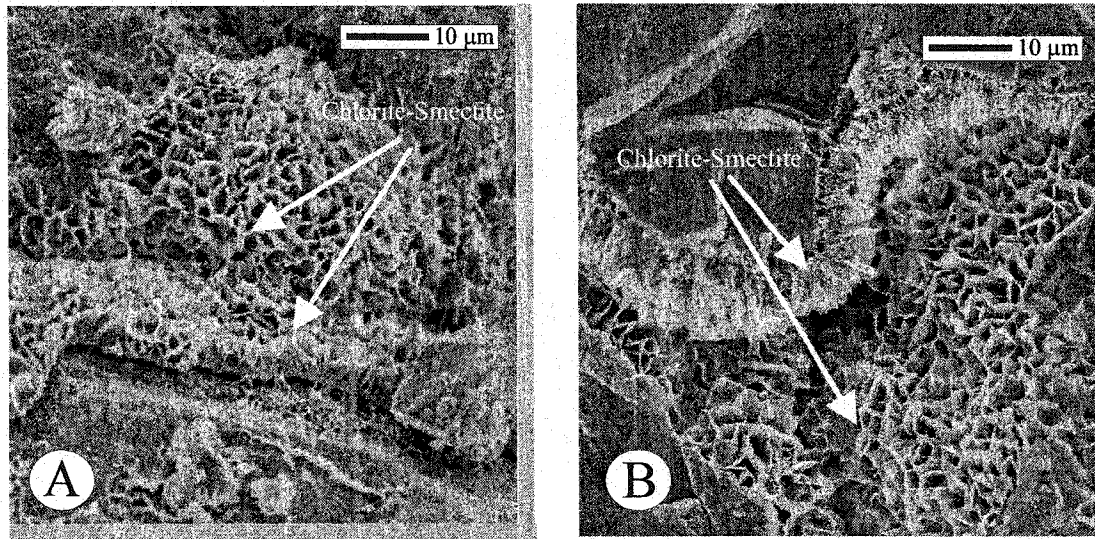
Figure 3-19. Scanning electronic photomicrographs: (A) chlorite-smectite (arrows) appears as a pore linings (rims) and a pore filling clay (sample 1, upper Coalspur Formation, the outcrop along the Red Deer River); (B) authigenically formed chlorite-smectite (arrows) appears as composite of crystals perpendicularly oriented to grain surface (sample 3, upper Coalspur Formation, the outcrop along the Red Deer River).

118
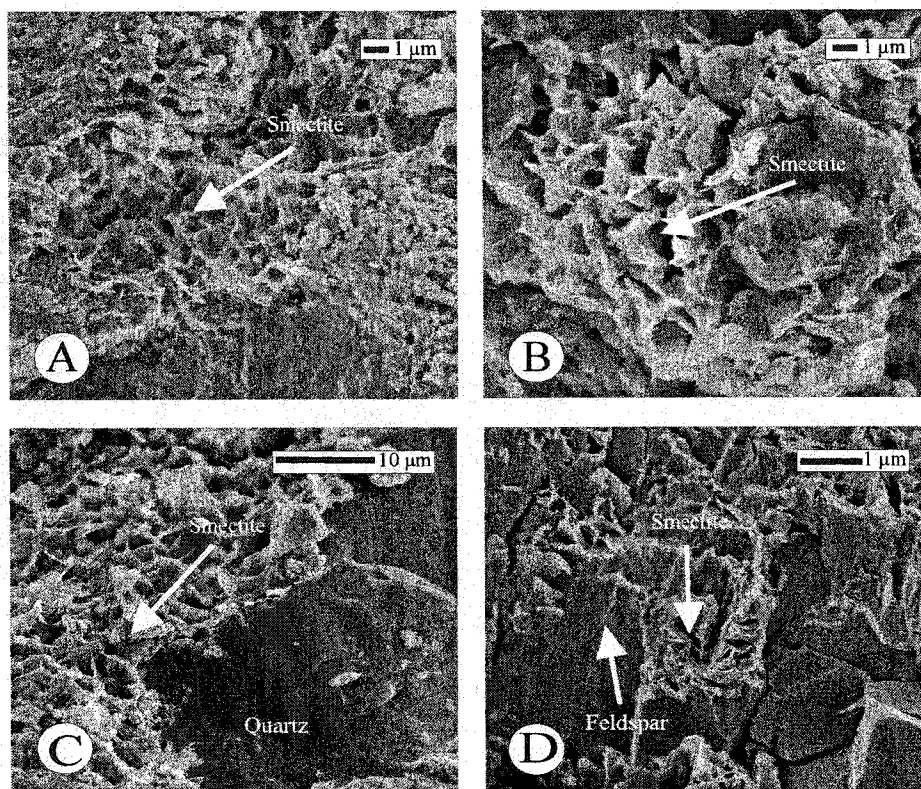
Figure 3-20. Scanning electronic photomicrographs: (A) coating rim of authigenic smectite. (sample 6, upper Coalspur Formation, road cut Red Deer River locality); (B) authigenic smectite showing highly crenulated, honeycombed, and interlocking crystal shapes (sample 4, upper Coalspur Formation, the outcrop along the Red Deer River). (C) pore filling smectite. Note the smectite growth perpendicular to the surface of the quartz grain (sample 7, upper Coalspur Formation, the outcrop along the Red Deer River); (D) feldspar alteration into smectite (sample 5, upper Coalspur Formation, Coal valley locality).

119
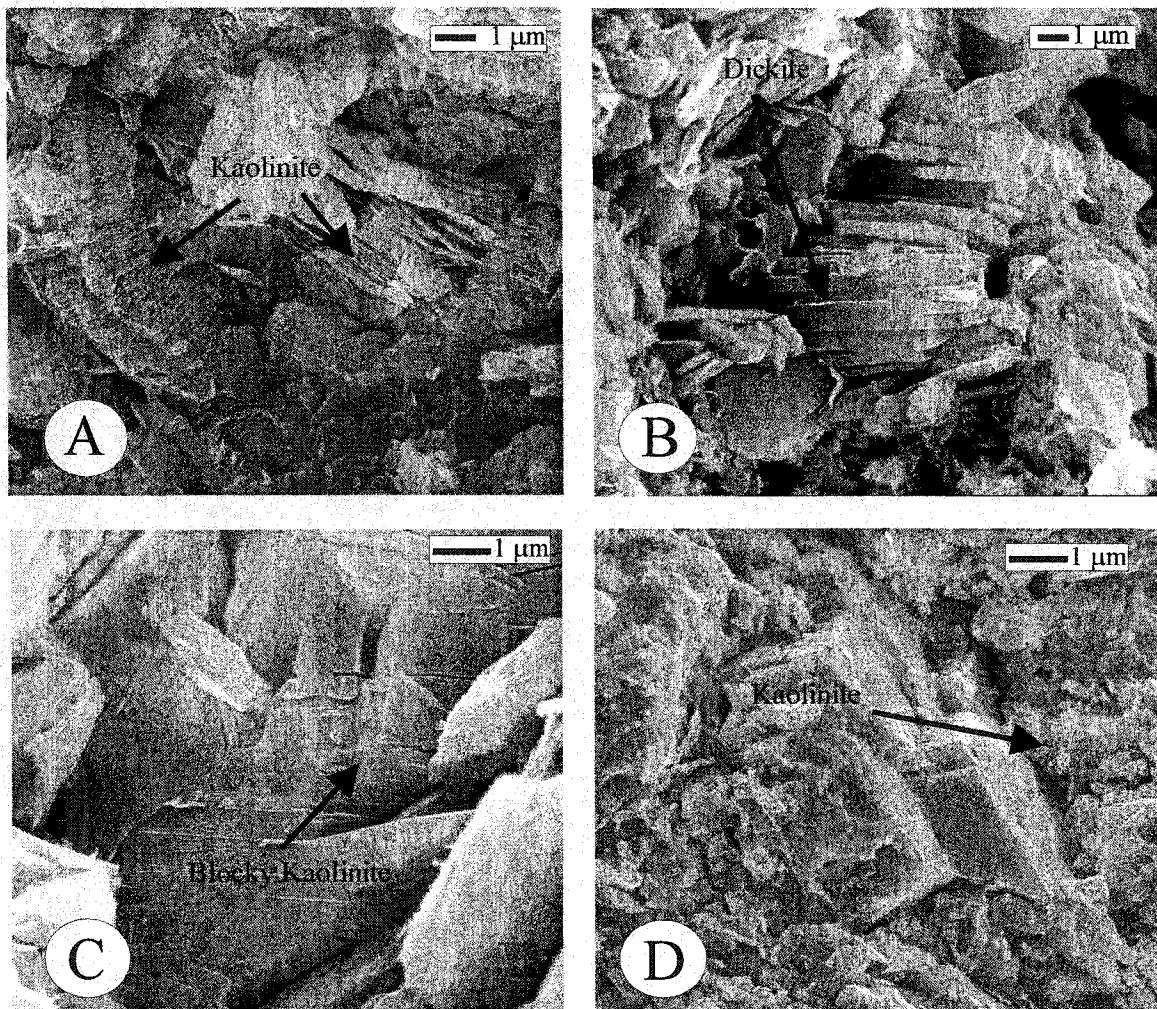
Figure 3- 21. Scanning electronic photomicrographs: (A) and vermicular aggregates of euhedral crystals of authigenic kaolinite (arrows). (sample 1, upper Coalspur Formation, Coalspur locality); (B) blocky kaolin (dickite). Note the thickness and blocky habit of the crystals(sample 3, upper Coalspur Formation, Coal Valley locality); (C) blocky kaolin (dickite). Note the thickness and blocky habit of the crystals indicated the dickite transform toward more isometric blocky crystals within 4000 to 5000 m depth (sample 3, upper Coalspur Formation, Coal Valley locality); (D) vermicular aggregates of euhedral crystals of authigenic kaolinite perpendicular to grain surface (arrow). (sample 1, upper Coalspur Formation, Coal Valley locality).
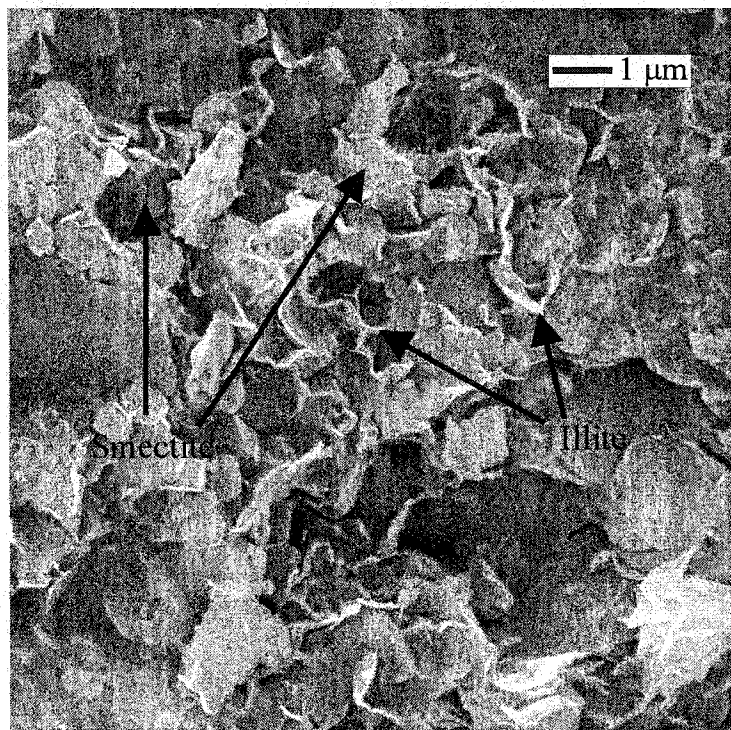
Figure 3-22. Scanning electronic photomicrographs shows alteration of smectite grain coating to illite (arrows) (sample 1, upper Coalspur Formation, along the Red Deer River).
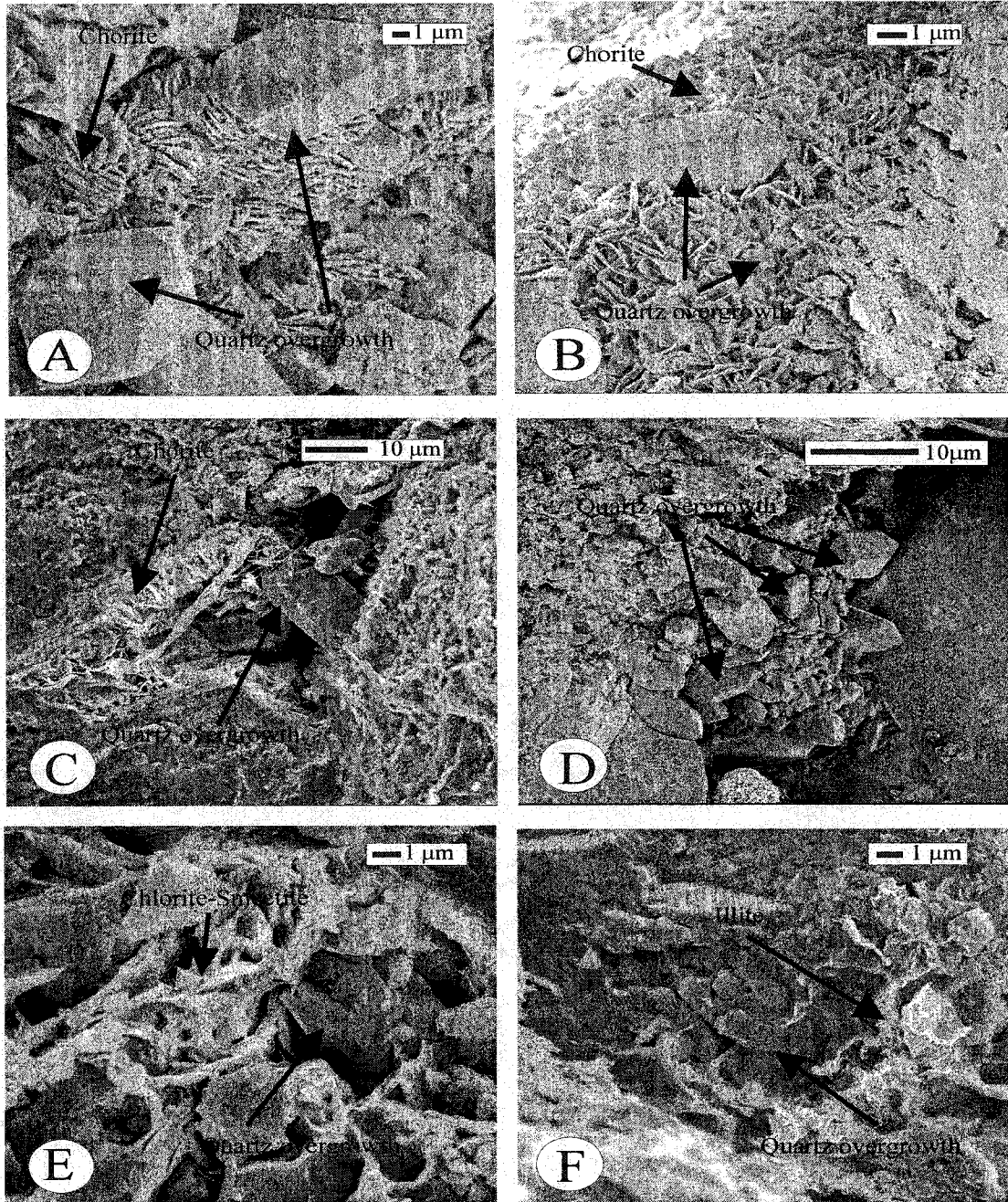
Figure 3-23. Scanning electronic photomicrographs: (A) - euhedral quartz overgrowth (sample 13, upper Coalspur Formation, the road cut near the Red Deer River); (B) silica overgrowths postdated by pore-filing chlorite (sample 10, upper Coalspur Formation, along the Red Deer River); (C) chlorite interfering with the process of quartz overgrowth. Note preservation of primary intergranular porosity by chlorite coating (sample 2, Entrance Member, Coalspur Formation, the road cut near Highway 22); (D) discontinuous and thin chlorite coating and quartz overgrowth. Note authigenic quartz was able to connect with the lattice of the detrital grains (sample 14, upper Coalspur Formation, the road cut near the Red Deer River); (E) smectite-chlorite coating interfering with quartz overgrowth (sample 12, upper Coalspur Formation, the road cut near the Red Deer River); (F) illite grain coating interfering with authigenic quartz overgrowth (sample 7, upper Coalspur Formation, along the Red Deer River).

122

+14   +16   +18   +20   +22   +23

δO^{18} SMOW
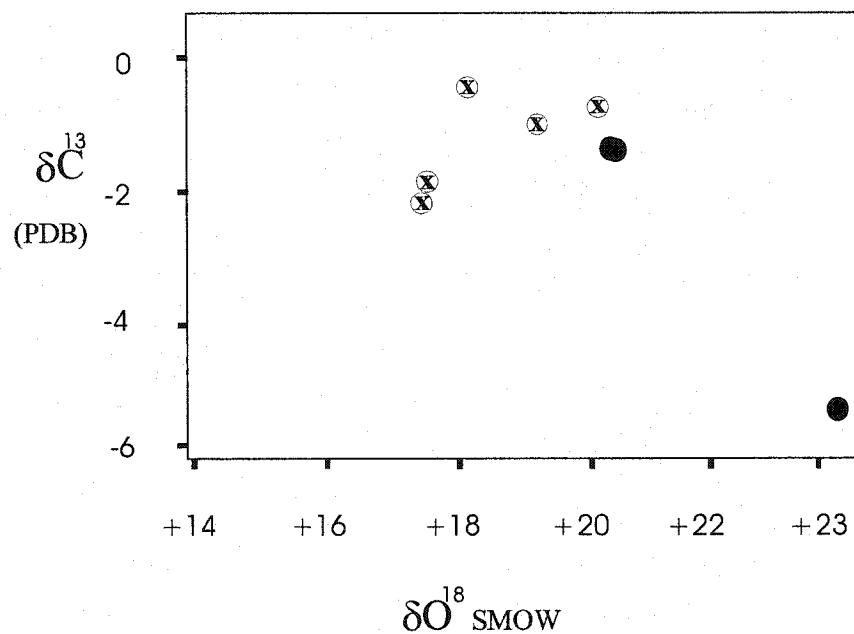
Ⓧ Upper Coalspur Formation the Sundre locality.

● Upper Coalspur Formation the Red Deer River locality.

Figure 3-24. Carbon-isotope versus oxygen-isotope composition of the calcite cements in the Coalspur sandstones. The isotopic values indicate that the calcite precipitated in equilibrium with fresh water of meteoric origin (Keith and Weber, 1964; Longstaffe, 1994). The relatively high 18O values suggest that calcite precipitation took place at low temperatures, during early diagenesis (Longstaffe, 1994; Tang et al., 997).

SEM photomicrographs	Kaolinite to dickite reaction	Burial depth
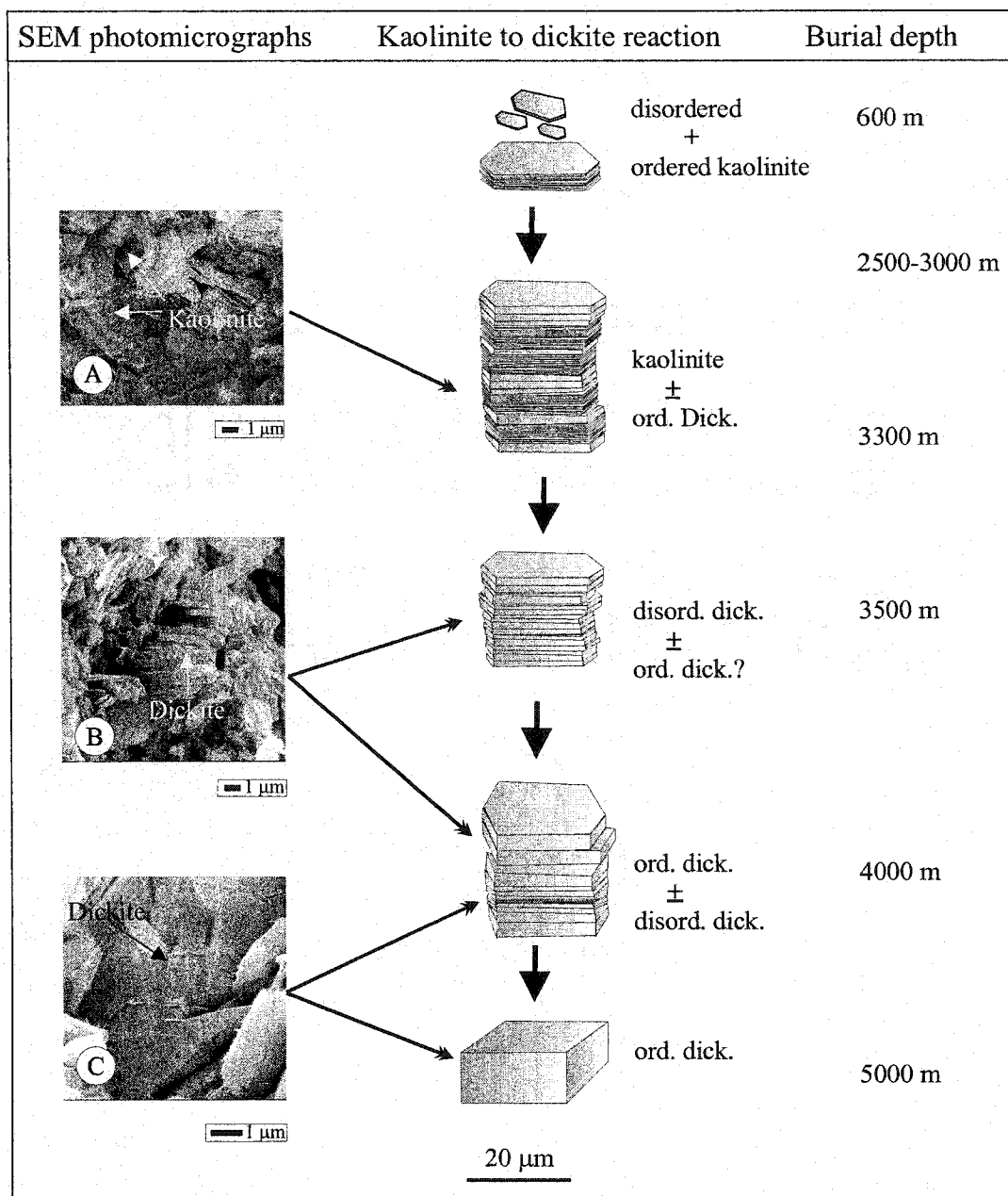
Figure 3-25. Schematic model of kaolinite-to-dickite reaction, showing SEM photomicrographs of kaolinte-to-dickite transformation and their relation to the maximum burial within the Coalspur Formation (modified from Beaufort et al., 1998).

Diagenesis sequence	Early ══════════════════════════ Late
Compaction	Mechanical ▬▬▬▬▬ Chemical ▬▬▬▬▬
Quartz overgrowth	▬▬▬▬▬▬▬▬▬▬▬▬▬
Calcite cementation	▬▬▬▬▬▬▬
Formation septechlorite and Fe-chlorite	▬▬▬
Dissolution of feldspar and volcanic fragments	▬▬▬▬▬▬▬▬▬▬▬
Smectite pore fill	▬▬▬▬▬▬▬▬
Kaolinite pore fill	▬▬▬▬▬▬▬▬
Formation of chlorite	▬▬▬▬▬▬
Formations of smectite-chlorite pore filling	▬▬▬▬▬
Formation of illite	▬▬▬
Quartz dissolution	▬▬▬
Formation of dickite	▬▬
Mica and biotite alteration	▬▬

Figure 3-26. Generalized diagenetic sequence for the Coalspur Formation in the Foothills region of west-central Alberta.
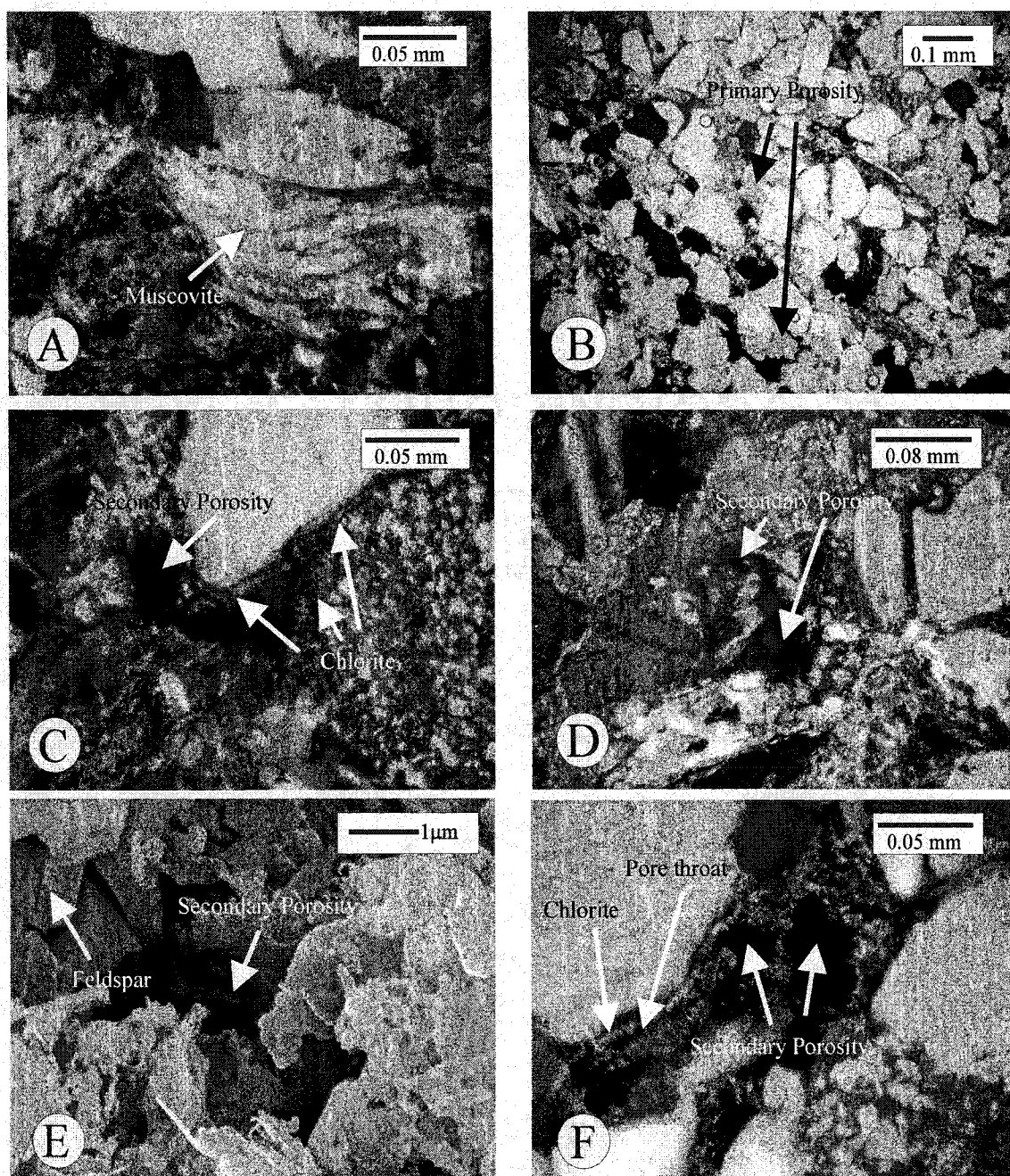
Figure 3-27. Scanning electronic and thin section photomicrographs: (A) deformation of muscovite grain during stage of sediment compaction (sample 2, upper Coalspur Formation, Coalspur locality); (B) primary porosity preserved in the sandstones (arrows) (sample 2, Entrance Member, roadcut Highway 22); (C) secondary porosity (arrow) resulting from the dissolution of authigenic cements, as seen under the petrographic microscope. Note effect of authigenic chlorite (arrows) on permeability and porosity of sandstones (sample 2, Entrance Member, Coalspur Formation, roadcut Highway 22); (D) secondary porosity (arrows) resulting from corrosion of chert grain adjacent to pore (sample 2, Entrance Member, roadcut Highway 22); (E) grain moldic porosity produced by partial dissolution of feldspar thatoccurs along cleavage and twin boundaries of feldspar grains, as seen under the petrographic microscope (sample 3, upper Coalspur Formation, Coalspur locality); (F) secondary (dissolution) porosity (Sp), as seen under the SEM .Note molds porosity (arrows) demonstrates the dissolution of former framework grains (sample 3, Entrance Member, roadcut Highway 22).

126

abundant   absent   (A) Highway 22 locality   o control points

less abundant   no data available   (B) Smokey River locality
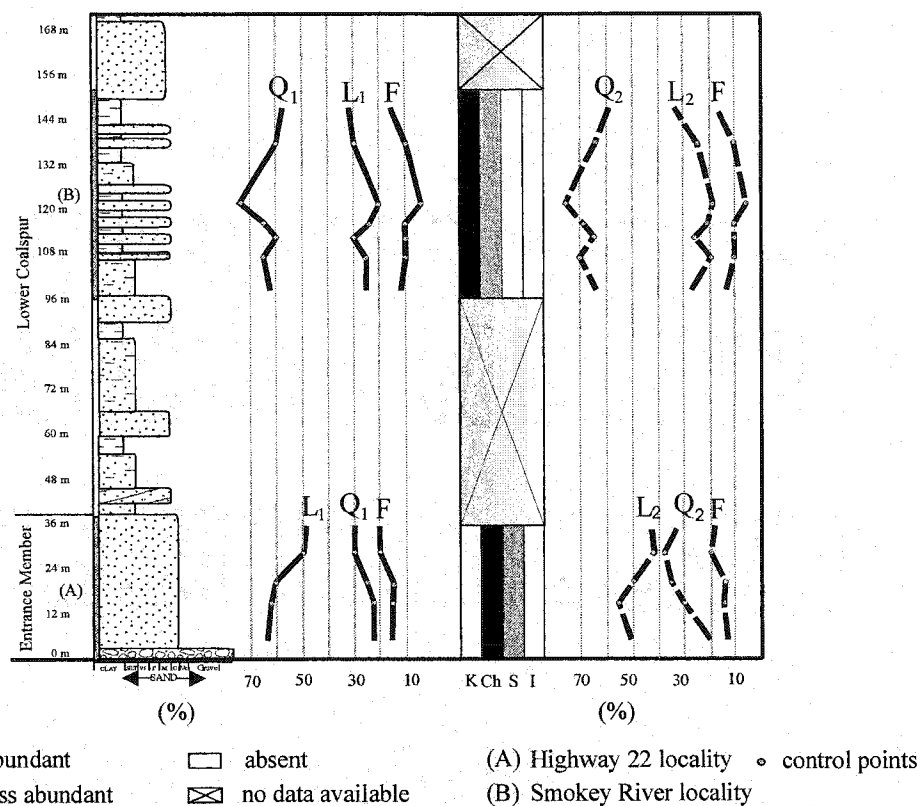
Figure 3-28 A. Composite vertical profiles of the lower Coalspur Formation in the in the Foothills region of west-central Alberta, showing the variability in lithofacies (see Fig. 3 for symbols), petrography, and main authigenic mineral composition Abbreviations: Q1 monocrystalline quartz; L1 lithoclasts (including polycrystalline quartz); F feldspar; Q2 quartz (mono- and polycrystalline); L2 lithoclasts (without polycrystalline quartz); K kaolinite; S smectite; I illite; Ch -chlorite.

127

Figure 3-28 B. Composite vertical profiles of the upper Coalspur Formation in the in the Foothills region of west-central Alberta, showing the variability in lithofacies (see Fig. 3 for symbols), petrography, and main authigenic mineral composition. Abbreviations: Q_1 monocrystalline quartz; L_1 lithoclasts (including polycrystalline quartz); F feldspar; Q_2 quartz (mono- and polycrystalline); L_2 lithoclasts (without polycrystalline quartz); K kaolinite; S smectite; I illite; Ch -chlorite.

Sample Number	Carbon PDB	Oxygen PDB	SMOW Oxygen	Locality	
S-1	-0.839	-10.481	20.105		
S-2	-0.417	-12.204	18.019		
S-3	-2.130	-13.039	17.468	Sundre locality	Upper Coalspur Formation
S-4	-1.165	-11.244	19.318		
S-5	-1.883	-13.098	17.407		
3	-1.377	-10.383	20.200		
4	-1.377	-10.383	20.200	Coal Valley locality	
5	-5.616	-17.507	23.244		

Table 3-1. Oxygen and carbon isotopic compositions from the upper Coalspur froamtion (Sundre locality and Coal Valley locality). The samples position is shown in Figure 3-4 , and 3-6.

REFERENCES

Almon, W. R. 1979. Sandstone diagenesis as a factor in stimulation design, Precedings of the 24th Annual Southwest Petroleum Short Course, Lubbock, Texas.

Basu, A. 1976. Petrology of Holocene sands derived from plutonic source rocks; implications to the paleoclimatic interpretation. Journal of Sedimentary Petrology, v. 46, p. 694- 709.

Basu, A. 1985. Influence of climate and relief on compositions of sands released at source areas, in Zuffa, G. G., ed., Provenance of Arenites: Holland, Reidel, p. 1-18.

Beaufort, D., A. Cassagnabere, S. Petit, B. Lanson, G. Berger, J. C. Lacharpagne, and H. Johansen, 1998. Kaolinite-to-dickite reaction in sandstone reservoirs, Clay Minerals, v. 33, p. 297-316.

Bjørlykke, K. 1983. Diagenesis reaction in sandstones. *In*: Sediment Daigenesis (A. Parker and B. W. Sellwood, eds.), D. Reidel Publishing Company, Holland, p. 169-213.

Bjørlykke, K. 1989. Sedimentology and Petroleum Geology. Springer-verlag, Berlin.

Bjørlykke, K. 1994. Fluid-flow processes and diagenesis in sedimentary basin. *In*: Geofluid: Origin, Migration and Evolution of fluid in sedimentary basins (J. Parnell, ed.), p. 127-140.

Bjørlykke, K., and Aagaard, P. 1992. Clay Minerals in North Sea sandstones. *In*: Origin, Diagenesis and Perophysics of Clay Minerals in Sandstones (D. W. Houseknecht and E. D. Pittman, eds.), SEMP special publication, v. 47, p. 65- 80.

Bodine, M. W., and Madsen, B. M. 1987. Mixed layer chlorite/smectites from a Pennsylvanian evaporite cycle, Grand County, Uth. Proc. International Clay Conference, Denver, p. 85-93.

Boles, J.R., and Franks, S.G. 1979. Clay diagenesis in Wilcox sandstones of southwest Texas; Implication of smectite diagenesis on sandstone cementation. Journal of Sedimentary Petrology, v. 49, p. 55-70.

Burns, S.J., and Matter, A. 1995. Geochemistry of carbonate cement in surficial alluvial conglomerates and their paleoclimatic implications, Sultanate of Oman. Journal of Sedimentary Research, A65 (1), p. 170-177.

Catuneanu, O., and Sweet, A.R. 1999. Maastrichtian-Paleocene foreland basin stratigraphies, Western Canada: A reciprocal sequence architecture. Canadian Journal of Earth Sciences, v. 36, p. 685-703.

Chamley, H. 1968. La sedimentation argileuse actuelle en Mediterranée nord-occidentale. Bulletin Societé Géologique du France, v. 10, p. 75-88.

Chang, H. K., Mackenzie, F. T., and Schoonmarker, J. 1986. Comparison between the diagenesis of decahedral and trioctahedral smectite, Brazilian offshore basins: Clays and Clay Minerals, v. 34, p. 407-423.

Correns, C. W., T. F. Barth, and P. Eskola. 1939. Die Enstehung der Gesteine. Julius Springer, Berlin.

Dawson, F.M., Kalkreuth, W.D., and Sweet, A.R. 1994. Stratigaphy and coal resource potential of the Upper Cretaceous to Tertiary strata of northwestern Alberta, Geological Survey of Canada Bulletin 466.

Dutta, P. 1992. Climatic influence on diagenesis o fluvial sandstones, In: Diagenesis, III. Developments in sedimentology, 47, Wolf, K. and Chillingrain, G. (eds.), 674p.

Dutta, P. K., and Suttner, L. J. 1984. Alluvial sandstone composition and paleoclimate, II. Authigenic mineralogy, Journal of Sedimentary Petrology, v. 56, p. 346-358.

Ehrenberg S. M., Aagaard P., Wilson M.J., Fraser A. R., and Duthie D.M.L. 1993. Depth-dependent transformation of kaolinite to dickite in sandstones of Norwegian continental shelf. Clay Minerals. v. 28, p. 325-352.

Ehrenberg S. N. 1993. Preservation of anomalously high porosity in deeply buried sandstones by grain coating chlorite: Examples from Norwegian Continental Shelf, American Association of Petroleum Geologists Bulletin, v. 77, p. 1260-1286.

Ehrenberg, S. N., and Nadeau, P. H. 1989. Formation of diagenetic illite in sandstones of the Garn Formation, Haltenbanken area, mid-Norwegian continental shelf, Clay Minerals, v. 24, p. 233-253.

Fisher, R. S. 1988. Clay minerals in evaporite host rocks, Palo Duro Basin, Texas Panhandle: Journal of Sedimentary Petrology, v. 58, p. 836-844.

Folk, R. L. 1974. The nature history of crystalline calcium carbonate: effect of magnesium contact and salinity, Journal of Sedimentary Petrology, v. 44, p. 40-53.

Garrels, R. M., and Christ, C. L. 1965. Solutions, Minerals and Equilibria, Harper and Row, New York.

Gibson, D. W. 1977. Upper Cretaceous and Tertiary coal bearing strata in the Drumheller – Ardley region, Red Deer River valley, Alberta. Geological Survey of Canada, Paper 76-35, p. 1-41.

Giles, M. R., and DeBoer, R. B., 1990. Origin and significance of redistributional secondary porosity, Mineral Petrology Geology, v. 7, p. 378-397.

Grantham, J. H., and Velbel, A. 1988. The influence of climatic and topographic on rock-fragments abundance in modern fluvial sands of the Southern Blue Ridge Mountain, North Carolina, Journal of Sedimentary Petrology, v. 2, p. 219-227.

Grim, R. E. 1953. Clay mineralogy, McGraw-Hill Series in Geology, 377p.

Guven, N., Hower, W.F. and Davies, D. K. 1980. Nature of authigenic illites in sandstone reservoirs. Journal of Sedimentary Petrology, v. 50, p 761- 766.

Heald, M. and Larese R. 1974. Influence of coatings on quartz cementation. Journal of Sedimentary Petrology, v. 44, no. 4, p. 1269-1274.

Helmold, K. P., and van de Kamp, P.C. 1984. Diagenetic mineralogy and control on albitization and laumontite formation in Paleogene arkoses. Santa Ynez Mountains, California. *In*: Clastic Diagenesis (D.A. McDonald and R. C. Surdam, eds), American Association of Petroleum Geologist, Memoir, v. 37, p. 239-276.

Hillier, S. J. 1993. Origin, diagenesis and mineralogy of chlorite minerals in Devonian lacustrine mudrocks. Orcadian Basin, Scotland, Clays Clay Minerology, v. 41, p. 240-259.

Hillier, S. J. 1994. Pore-lining chlorite in siliciclastic reservoir sandstones: electronic microprobe, SEM an XDR data, and implications for their origin, Clay Minerals, v. 26, p. 665-679.

Hillier, S. J., Fallick, A. E. and Matter, A. 1996. Origin of pore lining chlorite in the Aeolian Rotliegened of northern Germany, Clay Minerals, v. 31, p. 153-171.

Hower J., Eslinger W. V., Hower M. and Perry E. A. 1976. Mechanical of burial metamorphism of argillaceous sediments I. Mineralogical and chemical evidence, Geological Society of America Bulletin, v. 87, p. 725-737.

Howard, J. 1992. influence of authigenic clay minerals on permeability, Origin, Daigenesis, and Petrophysics of Clay minerals in Sandstones, SEPM, Special Publication No. 47, p. 257-263.

Hurst, A., and Irwin, H. 1982. Geological modeling of clay diagenesis in sandstones, Clay Minerals, v. 17, p. 5-22.

Ives, K. 1987, Filtration of clay suspensions though sand, Clay Minerals, v. 22, p. 49-61.

Jacka, A.D. 1970. Principles of cementation and porosity-occlusion in the Upper Cretaceous sandstone. Rocky Mountain Region, *In:* Wyoming Geological Association Guidebook, Twenty-second Annual Field Conference, p. 265-258.

Jahren, J. S. and Agaard, P. 1989. Compositional variations in diagenetic chlorites and illites, and relationships with formation water chemistry, Clay Minerals, v. 24, p. 157-170.

Janks, J. S., M. R. Yusas and C. M. Hall, 1992. Clay mineralogy of an interbedded sandstone, and anhydrite the Permian Yates Formation. Winkler county, texas, Diagenesis and Petrophysics of Clay Minerals in Sandstones, SEMP Special Publication No. 47.

Jerzykiewicz, T. and Mclean, J. R. 1980. Lithostratigraphical and sedimentological framework of coal-bearing Upper Cretaceous and Lower Tertiary strata. Coal Valley area, central Alberta Foothills, Geological Survey of Canada, Paper 79-12, 47 p.

Jermy, G. and Michael, A. 1988. The influence of climate and topography on rock-fragment abundance in modern fluvial sands of the Southern Blue Ridge Mountains. North Carolina, Journal of Sedimentary Petrology, v. 58. No. 2, p. 219-227.

Lang, A. H. 1945. Entrance map-area. Alberta, Geological Survey of Canada, p. 45-11.

Lerbekmo, J.F., Evans, M.E., and Hoye, G.S. 1990. Magnetostratigraphic evidence bearing on the magnitude of the subPaskapoo disconformity in the Scollard Canyon-Ardley area of the Red Deer Valley. Alberta, Bulletin of Canadian Petroleum Geology, v. 23, p. 120-124.

Lønøy, A., Akselsen, J., and Rønnings, 1986. Diagenesis of deeply buried sandstones from a deeply buried sandstones reservoir. Hild field, Northern North Sea, Clay Minerals, v. 21, p. 497- 511.

Mack and, H., and Suttner. L. 1977. Paleoclimatic interpretation from petrographic composition of Holocene Sands and the Fountain Formation (Pennsylvanian) in the Colorado Front Range, Journal of Sedimentary Petrology, v. 47, NO. 1, p. 89-100.

Mackay, B. R., 1949. Coal areas of Alberta, Geological Survey of Canada Atlas to accompany estimate of coal reserves prepared for Royal Commission on Coal.

Mann, W. R., and Cavaroc, V. 1973. Composition of sands released from three source areas under humid, low relief weathering in the North Carolina piedmont, Journal of Sedimentary Petrology, v. 43, p. 870- 881.

McAulay, G. E., Burley, S. D., Fallick, A. E., and Kusnir, N. J. 1994. Paleohydrodynamic fluid flow regimes during diagenesis in the Brent Group in Hutton-

NW Hutton reservoirs: constraints from oxygen isotope studies of authigenic kaolin and reverse flexural modeling, Clay Minerals, v. 29, p. 609-626.

Mclean J. R. and Jerzykiewicz, T. 1978. Cyclicity, tectonics and coal: some aspects of fluvial sedimentology in the Brazeau- Paskapoo Formations. Coal valley area, Alberta, Canada, In: fluvial Sedimentology, Miall (ed.). Canada Society of Petroleum Geologists Memoir 5, p. 441-468.

Mclean, D. D. 1965. The science of metamorphism. Edinburgh, Oliver and Boyd, p. 103-108.

Millot, G. 1942. Relations entre la constitution et la genese des roches sedimentaires argileuses. Geolgical Appliq. Et Prosp. Min., v.II.

Mora, C.I., Fastovsky, D.E. and Driese, S.G. 1993. Geochemistry and stable Isotopes of paleosols. University of Tennessee Department of Geology Sciences, Studies in Geology, 65p.

Morrison, S. J., and Parry, W. T. 1986. Dioctahhedral corrensite from Permian red beds. Lisbon Valley, Utah, Clays Clay minerals, v. 34, p. 613-624.

Mullis, A. M. 1992. A numerical model for porosity modification in a sandstone-mudstone boundary by quartz pressure dissolution and diffuse mass transfer, Sedimentology, v. 39, p. 99-107.

Nelson, B. W., and Roy, R. 1958. Synthesis of the chlorites and their structure and chemical constitution, American Mineralogy, v. 43, p. 707-725.

Nielsen, K. A. 1964. Kinetics of precipitation. New York, MacMilian, 151p.

Odin G. S., Debeney J. B. and Masse J. M. 1988. The verdine facies identified in 1988, p. 131- 148, In: Green Marine Clays (G. S. Odin, ed.), Devs. In: Sedimentology 45.

Osborne, M., Haszeldine, R. S., and A. E., Fallick, 1994. Variation in kaolinite morphology with growth temperature in isotopically mixed pore-fluids, Brent Group, UK North Sea, Clay Minerals, v. 29, p. 591-608.

Pettijohn, F. J., Potter P. E., and Siever R. 1972. Sand and Sandstones, Springer- Verlag, Berlin, 618 p.

Pittman, E. D. 1963. Uses of zoned plagioclase as an indicator of provenance, Journal of sedimentary petrology, v. 33, p. 380-386.

Pittman, E., and Lumsden, D. N. 1968. Relationship between chlorite coating on quartz grain and porosity, Spiro Sand. Oklahoma, Journal Sedimentary Petrology, v. 38, p. 668-670.

Plamer, D. P. 1987. A saponite and chlorite-rich clay assemblage in Permian evaporite and red bed strata. Palo Duro Basin, Texas Panhandle, University of Texas Bureau of Economic Geology Circular 87-3, 21p.

Quatin, P., Badaut-Trauth, D., Weber, F. 1975. Mise en evidence de mineraux secondaires, argiles et hydroxides, dans les andolosoles des Nouvelles-Hebrides, après la deferrification par la method de Endrey. Bulletin du Groupe d' Argiles du France, v. 27, p.51-67.

Ridley, J., and Thompson, A. B., 1986. The role of mineral kinetics in the development of metamorphic microtextures, In: Thompson, A. B., and Rubie, D. C. (eds.), Metamorphic reaction: Kinetics Texture and Deformation: Advances in Physical Chemistry, v. 4, p. 154-193.

Russell, I. 1983. Evidence for unconformity at the Scollard-Battle contact, Upper Cretaceous strata, Alberta. Canadian Journal of Earth Sciences, v. 20, p. 1231-1245.

Schmidt V. and McDonald, A. 1979. Secondary Reservoir porosity in the course of sandstone diagenesis, Short Course American Association of Petroleum Geologist, 50 p.

Scholle, A. (ed.) 1979. A color illustrated guide to constituents, textures, cements, of sandstone and Associated Rocks, American Association of Petroleum Geologist, 201p.

Sieffermann, G., Jehl, G., Millot, G. 1968. Allophanes et mineraux argileux des alterations recentes des basaltes du Mount Cameroun. Bulletin du Groupe d' Argiles du France, v. 20, p.109-129.

Smith, W. K., D. C. and Krueger, V.P., 1977. Geological procedures for a preproduction evaluation of the thermal coal deposit at Coal Valley. Alberta, Canadian Institute of Mining and Metallurgy, Journal, v. 70, p. 179-186.

Spötl C, Houseknecht D. W., and Longstaffe F. I. 1994. Authigenic chlorite in sandstones as indicators of high-temperature daigenesis. Arkoma Foreland Basin, USA, Journal Sedimentary Research, A64, v. 3, p. 553-566.

Suttner J, and Dutta, K. 1986. Alluvial sandstone composition and paleoclimate, II. Authigenic Mineralogy, Journal of Sedimentary Petrology, v. 56, no. 3, p. 346- 358.

Thomas, M. 1986, Diagenesis sequences and K/Ar dating in Jurassic sandstones. Central Viking Graben: effects on reservoir properties: Clay Minerals, v. 21, p. 695-710.

Velde B., Raoult, J. F., and Leikine M. 1975. Metamorphosed berthierine pellets in mid-Cretaceous rocks from northeast Algeria, Journal of Sedimentary Petrology, v. 39, p. 1249-1516.

Velde, B. 1985. Clay minerals, a physico-chemical explanation of their occurrence: Developments in Sedimentology, v. 4, New York, Elsevier, 427 p.

Walderhaug, O. and Bjorkum, P. A. 1992. Effect of meteoric water flow on calcite cementation in the Middle Jurassic Oseberg Formation. Well 30/3-2, Veslefrikk Field, Norwegian North Sea, Marin Petroleum Geology, v. 9, p. 308-318.

Walker, T.R., Waugh, B., and Crone, A. 1978. Diagenesis in first cycle desert alluvium of Cenozoic age, southern U. S. and northwest Mexico, Geological Society of America Bulletin, v. 89, p. 19-32.

Wange, Y., Cerling, Erling, T.E., Quade, J. and Bowman, J.R. 1993. Stable isotopes of paleosols and fossil teeth as paleoecology and paleoclimate indicator: an example from the St David Formation. Arizona, *In:* Climate Change in Continental Isotopic records, 374p.

Wilson, M. D., and Pittman, E.D. 1977. Authigenic clays in sandstones: recognition and influence on reservoir properties and paleoenvironmental analysis, Journal of Sedimentary Petrology, v. 47, p. 3-31.

Young, S., Basu, A., Suttner, Mack, G., and Darnell, N. 1975. Use of size composition trends in Holocene soil and fluvial sand derived from paleoclimate interpretation, Proceedings the IX International Sedimentary Congress, Nice, France, Theme 1, p. 201-209.

Chapter 4

Concluding Remarks

This dissertation presents two studies that examine the diagenesis, porosity and permeability of the Upper Cretaceous-Lower Tertiary fluvio-lacustrine sandstones of the Scollard and Coalspur formations, via detailed outcrops and laboratory work. As well, the intention of this thesis is to restructure paleoclimates during the Scollard time.

Chapter 2 presents the sedimentology and diagenesis of the Scollard sandstones in the Red Deer Valley area of central Alberta. The petrography of the Scollard sandstones in the Red Deer Valley region is defined by sublitharenites and lithic arenites, which accumulated in braided (lower Scollard) and meandering (upper Scollard) fluvial systems. The sandstone composition, reservoir properties, paleoclimate, and diagenetic history have been studied by using the composite information obtained from thin section petrography, scanning electronic microscopy, x-ray diffraction, and carbon and oxygen stable isotopes. Isotopic analyses indicate that the precipitation of early authigenic minerals took place in equilibrium with fluids of meteoric origin, at relatively shallow depths and low diagenetic temperatures. This suggests a relatively small lag time between the deposition of the sandstone detrital grains and the precipitation of early authigenic minerals, and allows for such authigenic minerals to be used as paleoclimate indicators in conjunction with the results of thin section petrography. The good correlation between the framework grain petrography and the authigenic clay mineralogy supports a climatic interpretation based on the composition of the Scollard sandstones. Wetter climatic conditions are interpreted for the arenites

with higher amounts of mono- and/or polycrystalline quartz, as well as abundant kaolinite and quartz overgrowth. Drier climatic conditions are inferred for the arenites with lesser percentages of quartz but higher amounts of authigenic smectite.

The diagenetic sequence was established based on the relationships observed between the framework grains and the various types of authigenic minerals. The early diagenesis of the Scollard sandstones is characterized by (1) initial mechanical compaction; (2) early calcite cementation; (3) early dissolution of detrital feldspars along with the dissolution of volcanic fragments; (4) early authigenic quartz overgrowth; and (5) formation of authigenic clay minerals as coatings, rimes, pore-linings and early pore-fills. Burial diagenesis is dominated by (1) precipitation of authigenic quartz and pore-filling kaolinite; (2) dissolution of feldspar grains; (3) corrosion and dissolution of quartz grains and authigenic silica; (4) alteration of mica, biotite and iron-bearing minerals; (5) dissolution of calcite cement; and (6) precipitation of hematite cement. The limited conversion of smectite into illite, as well as the weak albitization of K-feldspar, imply relatively low maximum burial temperatures of less than 120° C.

This dissertation indicates that initial mechanical compaction, pore-filling clay minerals, and calcite cement substantially reduced porosity in the Scollard sandstones. However, in certain facies, a relatively high percentage of the primary porosity was preserved by the early formation of clay rims and coats that inhibited further cementation. These latter facies present moderate to good reservoir properties. Several types of secondary porosity have also been observed in the Scollard sandstones.

Chapter 3 presents the sedimentology and diagenesis of the Coalspur sandstones in the Foothills region of west-central Alberta. The petrography of the Coalspur sandstones is defined by sublitharenites and lithic arenites, which accumulated in fluvio-lacustrine systems. The shifts from kaolinite to dickite in the Coalspur sandstones indicate a maximum burial depth between 2500 m and 4500 m.

Climatic shifts between drier and wetter climate conditions within the Foothills are inferred from the composite information derived from thin-section petrography, scanning electronic microscopy, and x-ray diffraction. Wetter climatic conditions are inferred for the sublitharenites, which have higher amounts of quartz (because of more efficient chemical weathering), abundant kaolinite and quartz overgrowth. Drier climatic conditions are inferred for the lithic arenites, which are rich in lithoclasts (because of less efficient chemical weathering), authigenic chlorite, and smectite.

This dissertation indicates that the early diagenesis of the Coalspur sandstones is characterized by (1) initial mechanical compaction; (2) silica precipitation; (3) calcite cementation; (4) formation of 'septechlorite' and Fe-chlorite; (5) early dissolution of detrital feldspars along with dissolution of volcanic fragments; and (6) formation of clay coatings, rimes, pore-linings, early kaolinite and smectite pore fills. Burial diagenesis is dominated by (1) precipitation of authigenic quartz; (2) dissolution of feldspar grains, dissolution of kaolinite, and smectite; (3) formation of illite; (4) corrosion and dissolution of quartz grains and authigenic silica; (5) formation of dickite pore filling; (6) alteration of mica, biotite and other iron-bearing minerals; and (7) precipitation of chlorite.

In conclusion, this study demonstrates the value of petrographic and SEM analyses in the assessment of porosity in fluvial reservoirs. Both primary, and several types of secondary porosity have been observed in the Coalspur sandstones. Such an outcrop study may be used as an analogue for the assessment of other fluvial reservoirs in the subsurface of the Western Canada Sedimentary Basin.

Appendix A: outcrop photographs, thin section photographs, scanning electronic photography, and x-ray diffraction pattern from the Scollard Formation sandstones.
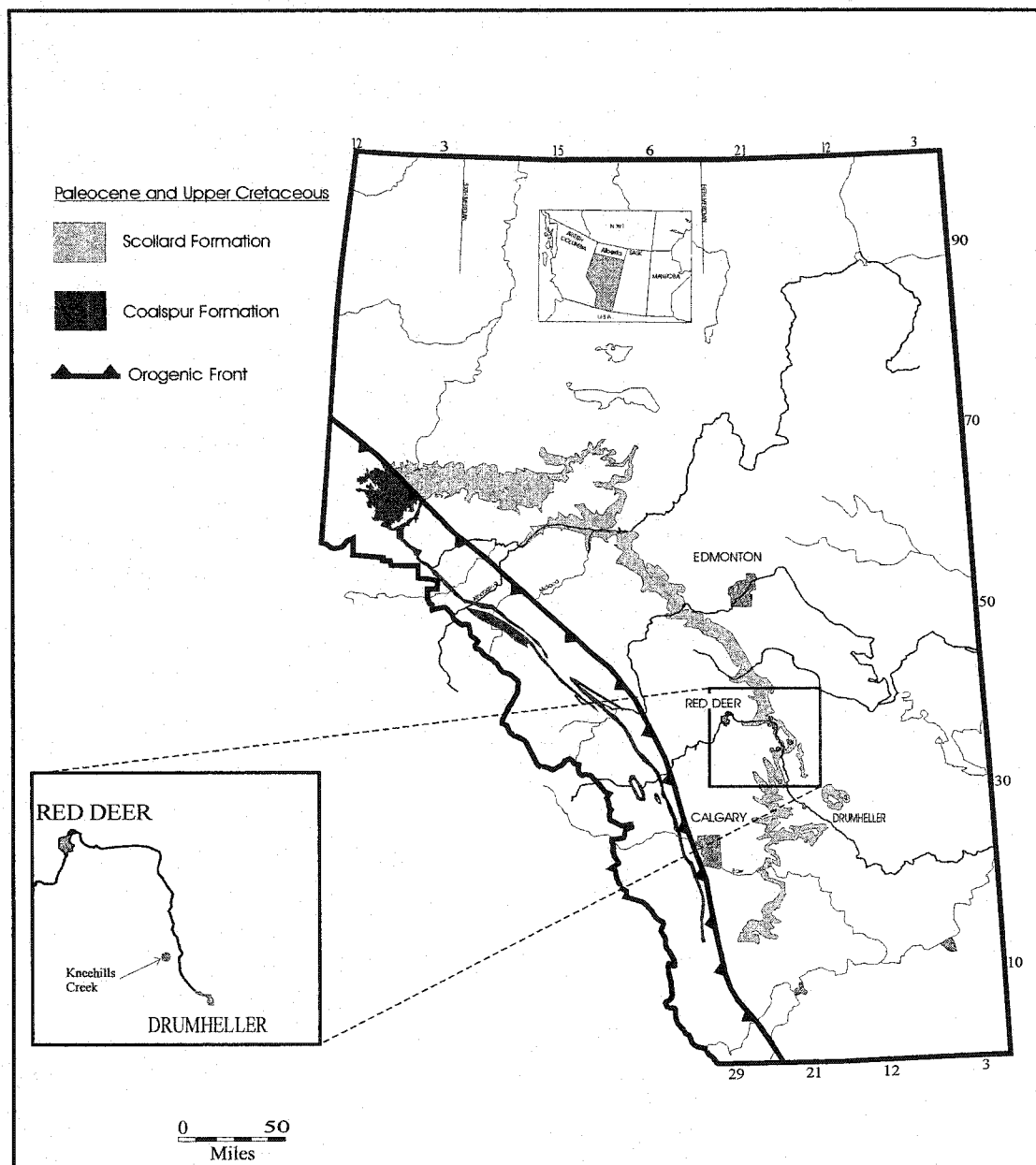
Figure A-1. Outcrop distribution of the Scollard and Coalspur formations in Alberta, and the location of the studied outcrop section.
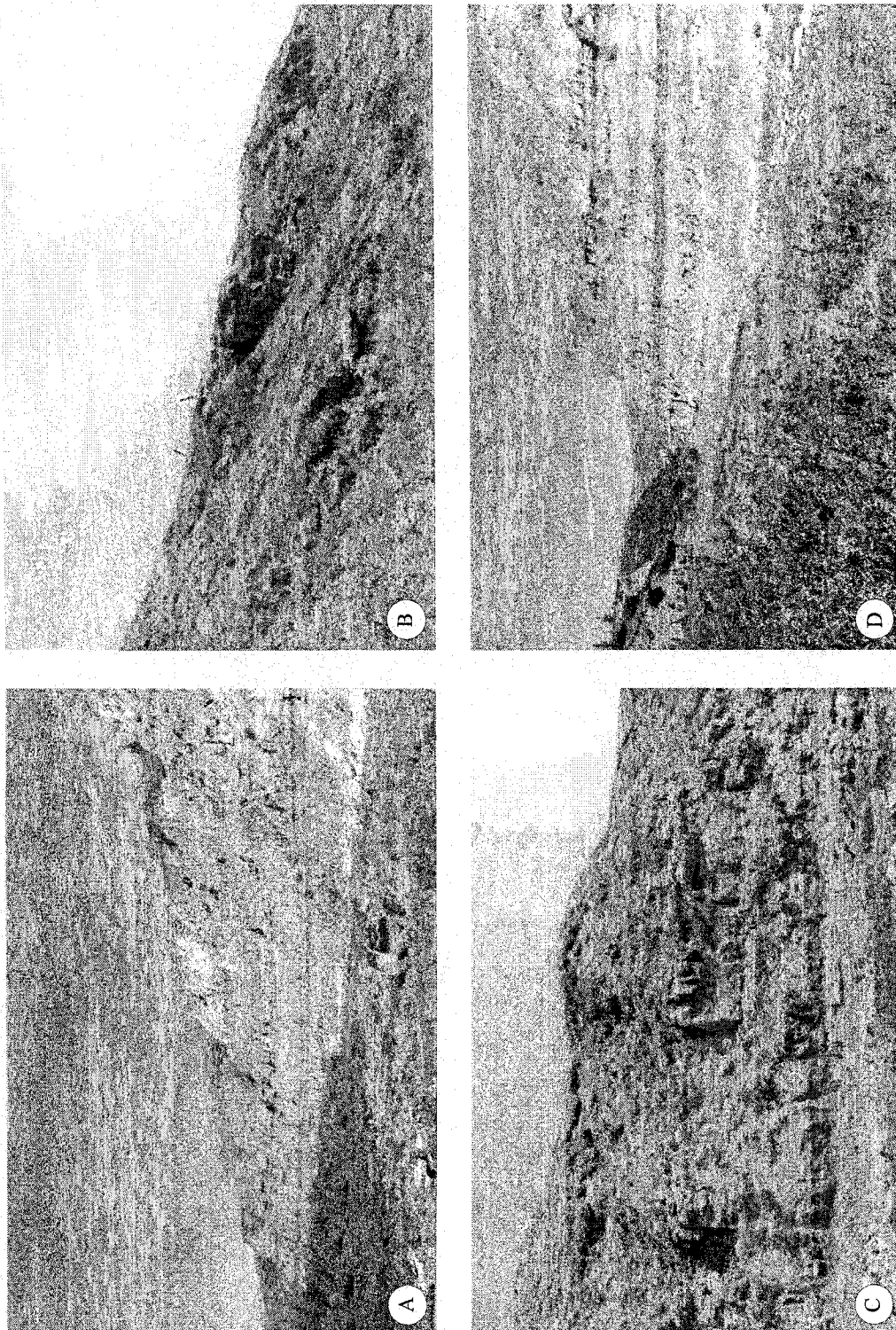
Figure A-2. Outcrop photographs of the lower Scollard Formation, Kneehills Creek locality: (A), (C), and (D) outcrop photographs showing crevasse splay and meander channel deposits (B) meander channels.
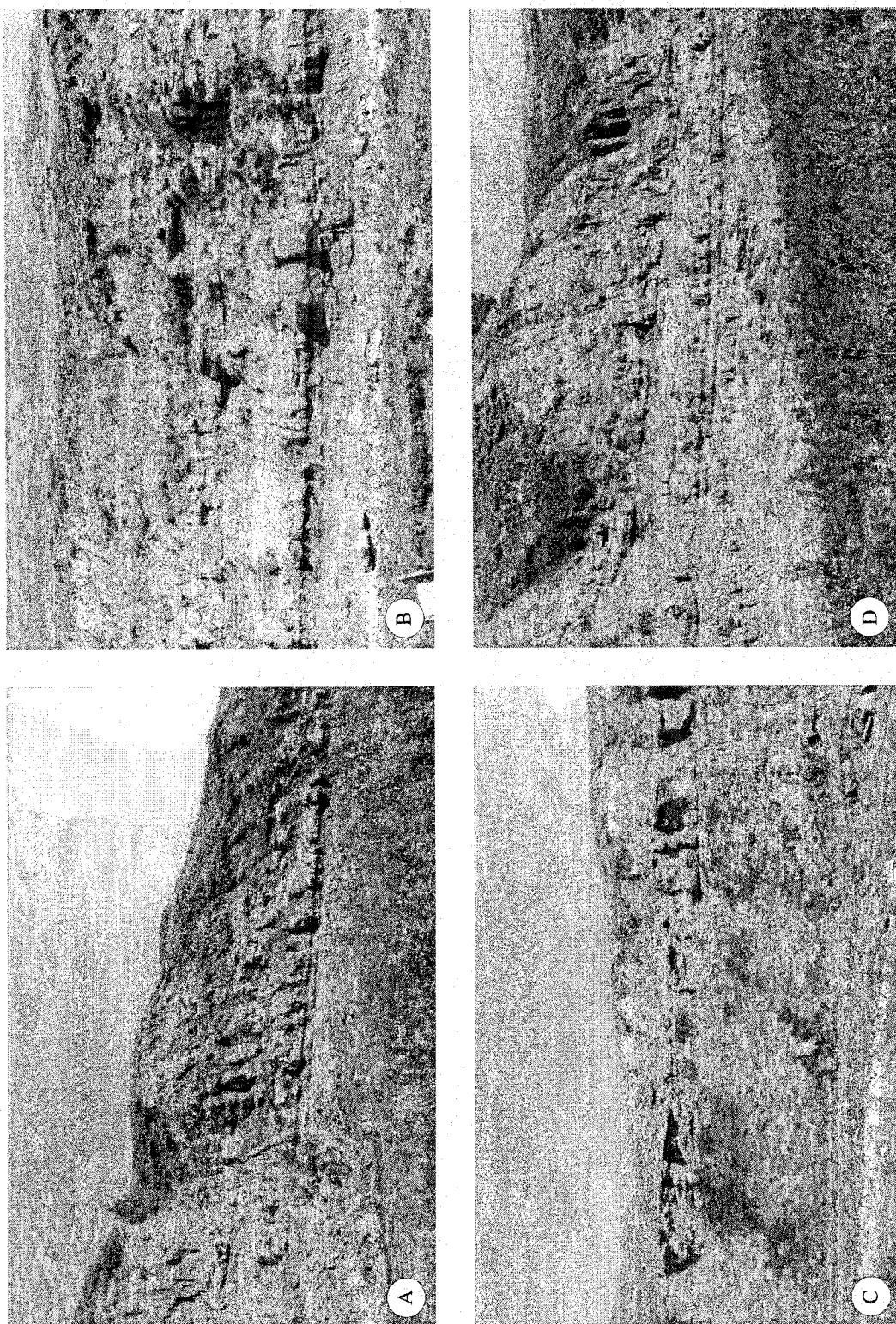
Figure A-3. Outcrop photographs of the lower Scollard Formation, Kneehills Creek locality: (A), (B), (C), and (D) outcrop photographs showing crevasse splay deposits.
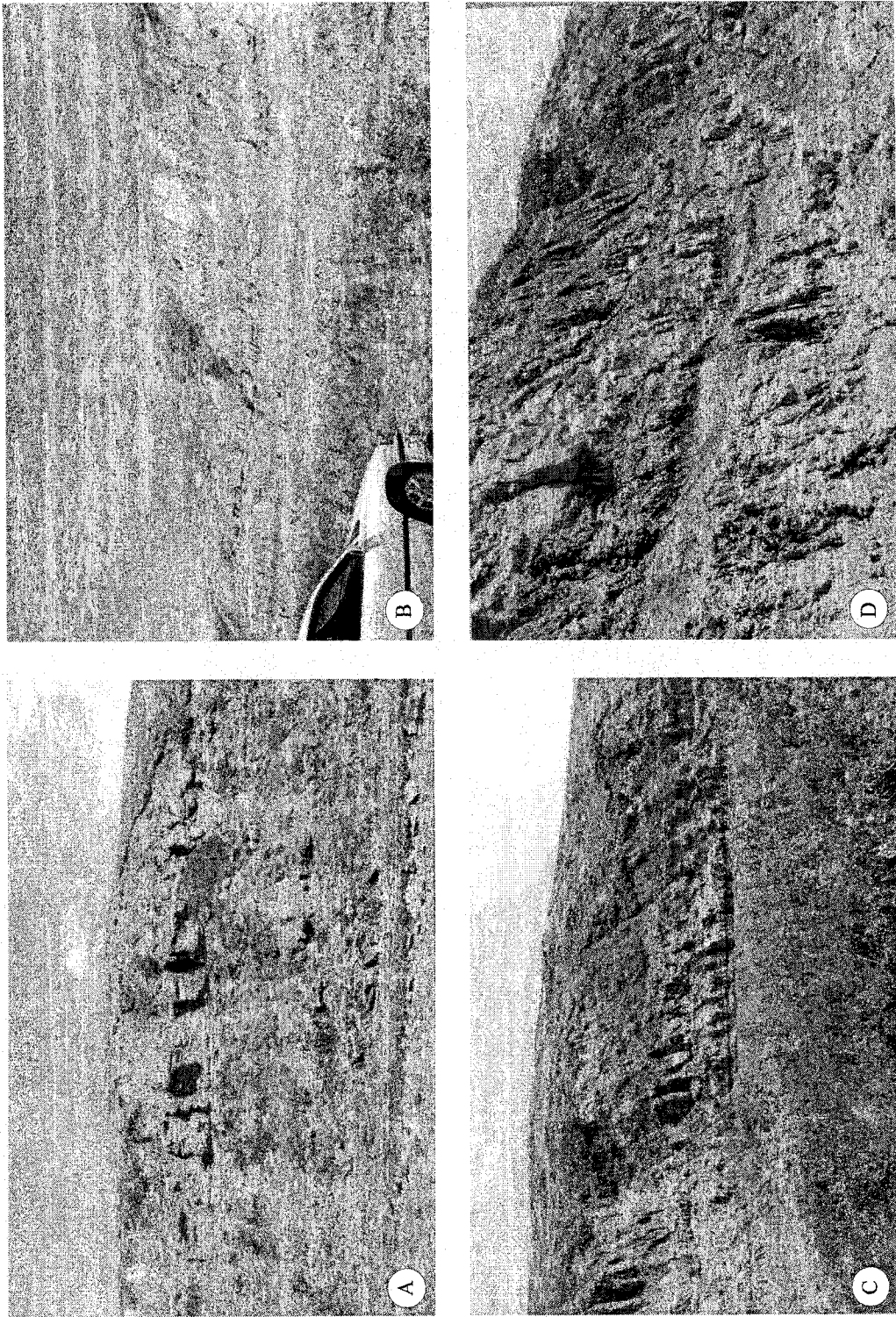
Figure A-4. Outcrop photographs of the lower Scollard Formation, Kneehills Creek locality: (A) and (D) interbedded sandstone-claystone beds formed in a meander system; (A), (C), and (D) outcrop photographs showing crevasse splay deposits.

145
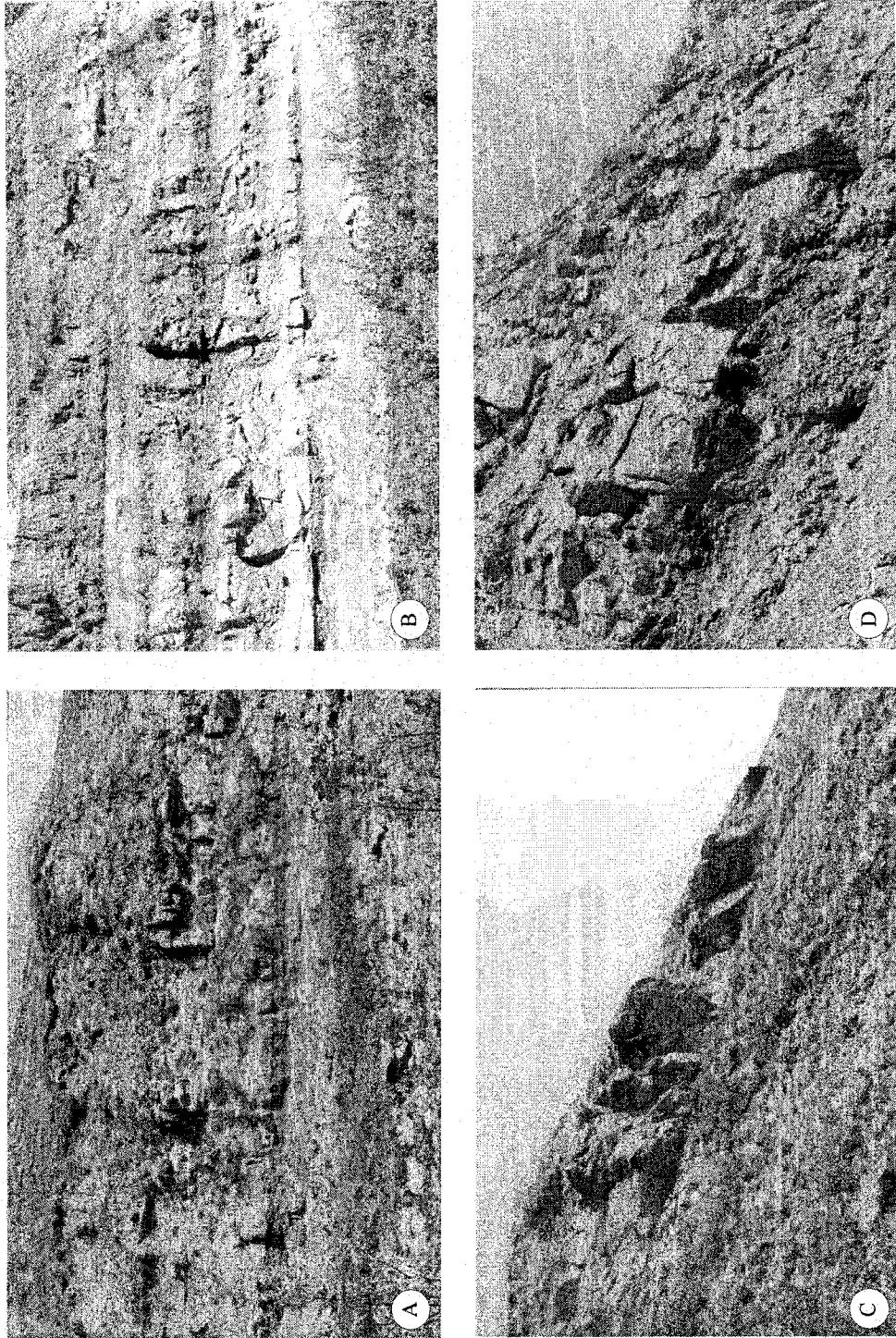
Figure A-5. Outcrop photographs of the lower Scollard Formation, Kneehills Creek locality: (A) and (B) crevasse splay deposits.; (C and D) of sandstone units of meander channel deposits.

146
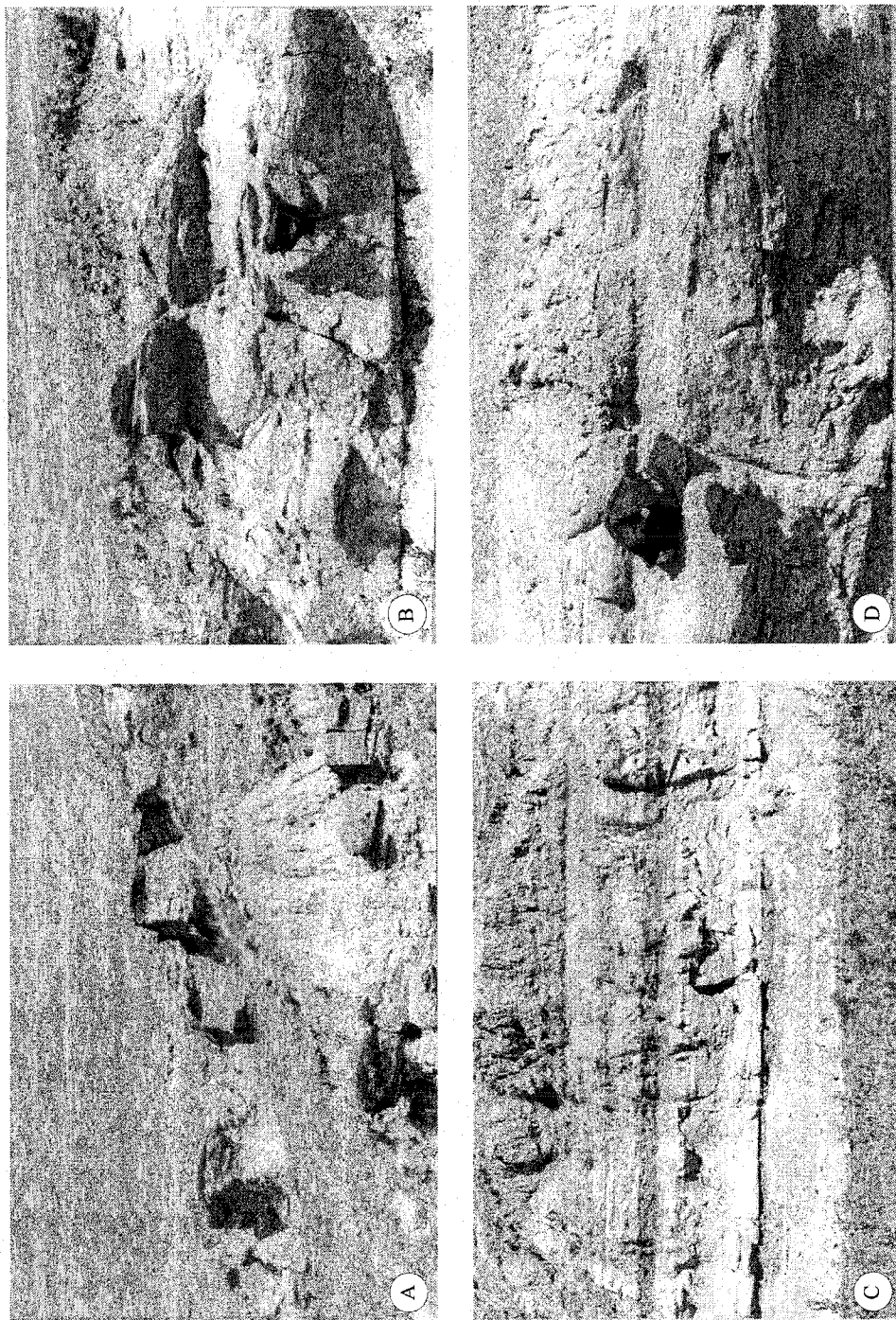
Figure A-6. Outcrop photographs of the lower Scollard Formation, Kneehills Creek locality: (A) (B)and (C) outcrop photograph showing crevasse splay deposits; (D) close-up outcrop photograph showing planer cross bedding (arrow) lithofacies (Sp).
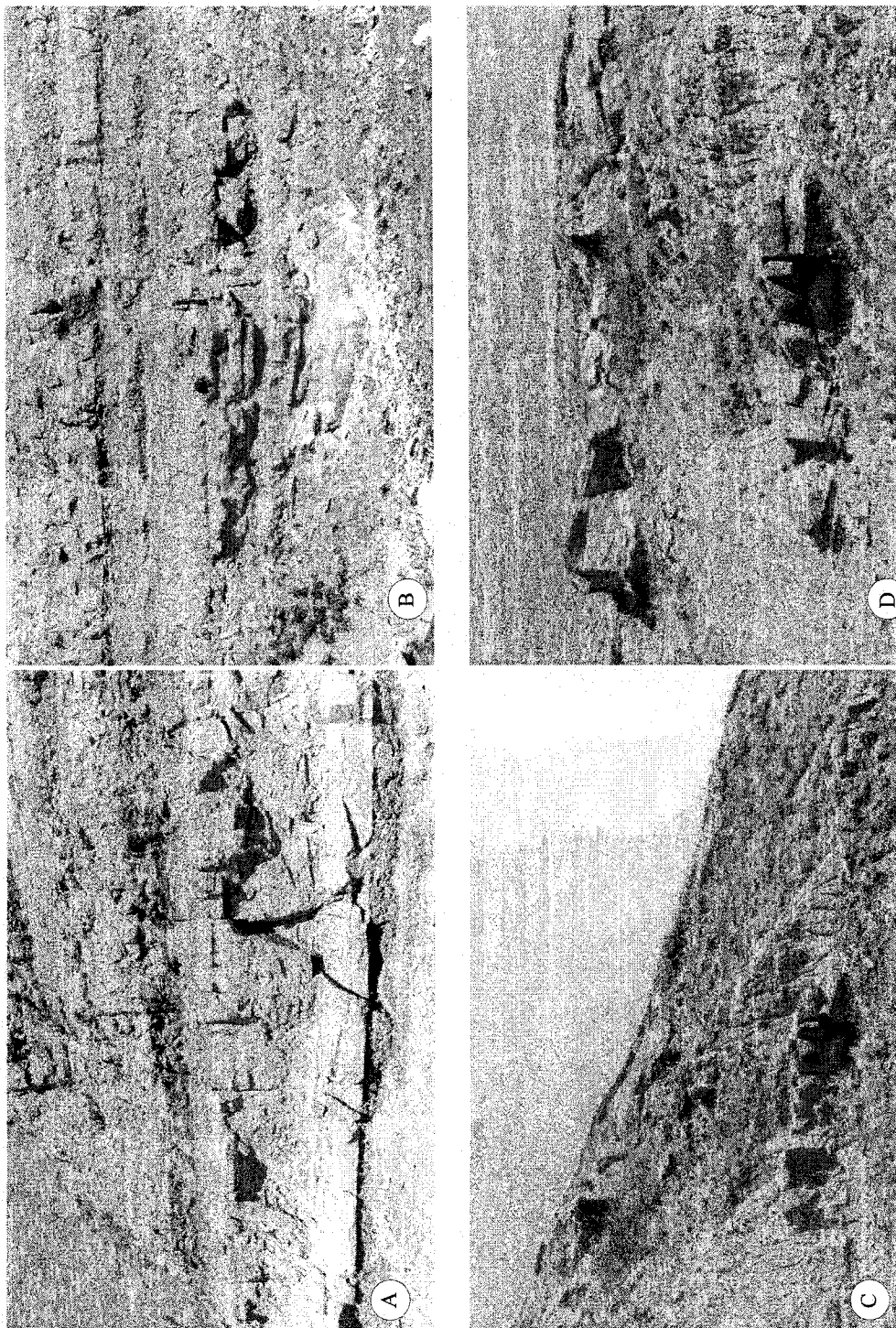
Figure A-7. Outcrop photographs of the lower Scollard Formation, Kneehills Creek locality: (A), (B), (C), and (D) crevasse splay deposits.
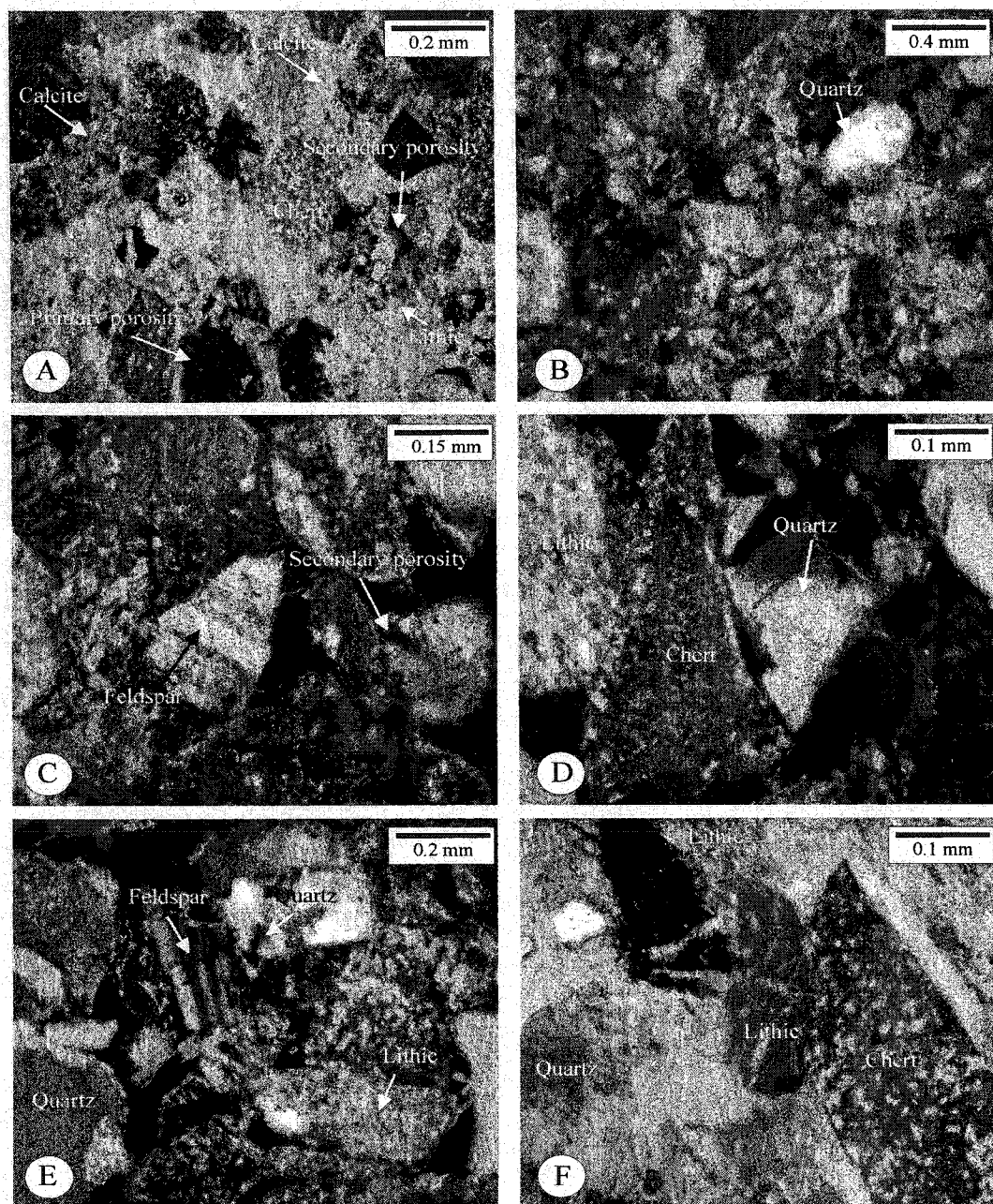
Figure A-8. Thin-section photomicrographs: (A)   poikilotopic calcite cement, chert and lithic grains (arrows). Note primary and secondary porosity (sample Kn-1 lower Scollard Formation, Kneehills Creek locality); (B) detrital quartz showing alteration (arrow) (sample Kn-2, lower Scollard Formation, Kneehills Creek locality); (C) plagioclase grain shows signs of dissolution (arrow) (sample Kn-3, lower Scollard Formation, Keehills Creek locality); (D), and (F) detritals chert and lithic, lithic less chemically stable and abundant than chert (sample Kn-2, lower Scollard Formation, Kneehills Creek locality); (E)   plagioclase shows signs of dissolution and diagenetic replacement with calcite. A small-scale expansion of the rock is noted from the precipitation of calcite. Note quartz grain alteration (sample Kn-3, lower Scollard Formation, Kneehills Creek locality).

149
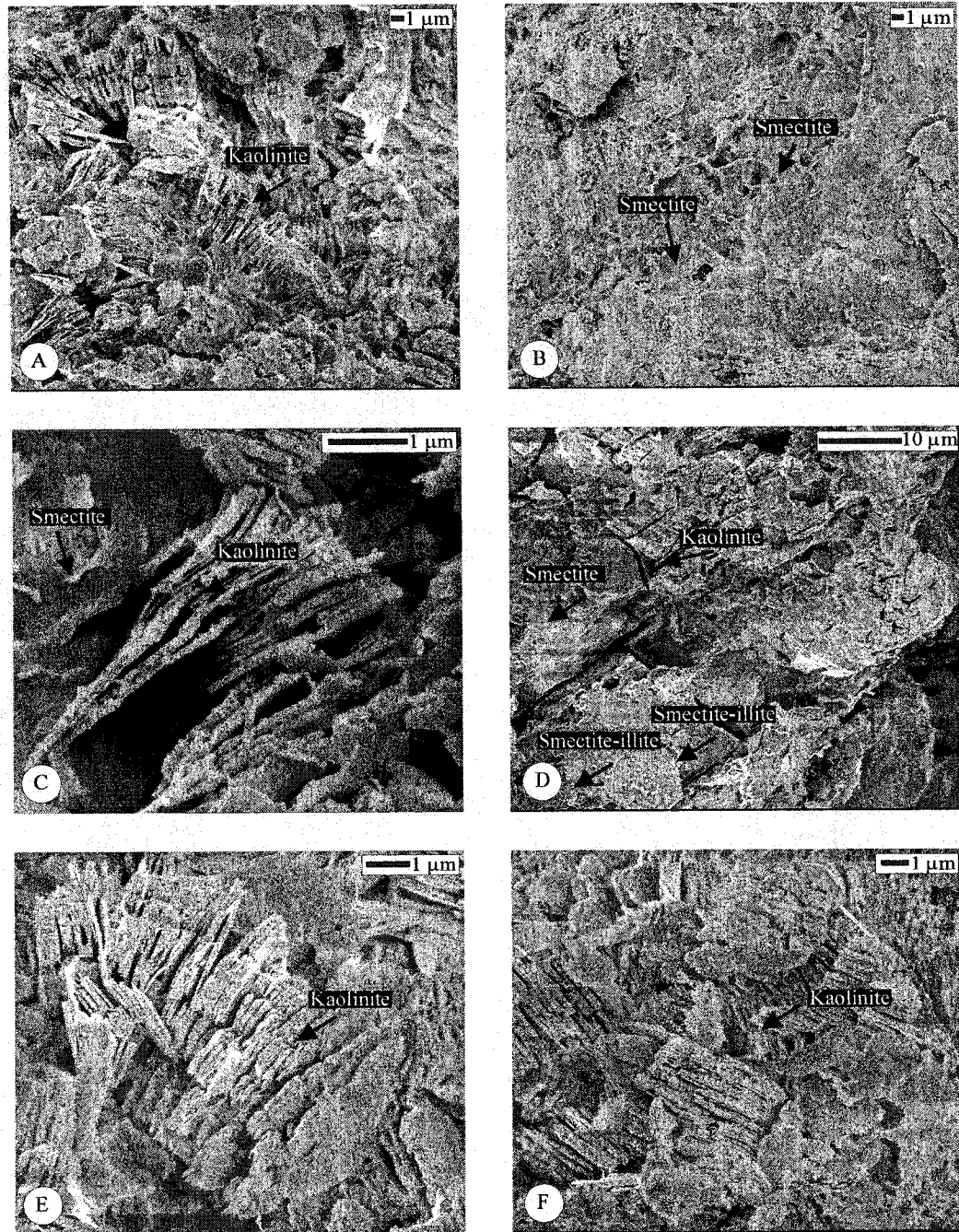
Figure A-9. Scanning electronic photomicrographs: (A), (C), (E), and (F) vermicular aggregates of euhedral crystals of authigenic kaolinite. The kaolinite booklets have no preferred orientation, and consume much of the primary porosity. Note the numerous small channels between the kaolinite crystals that still allow fluids to flow, which is why the rock retains a good permeability (sample Kn-1, lower Scollard Formation, Kneehills Creek locality; (B)non-authigenic smectite (sample Kn-2, lower Scollard Formation, Kneehills Creek locality); (D) mixed layers smectite-illite and kaolinite (Sample Kn-2, lower Scollard formation, Kneehills Creek locality).
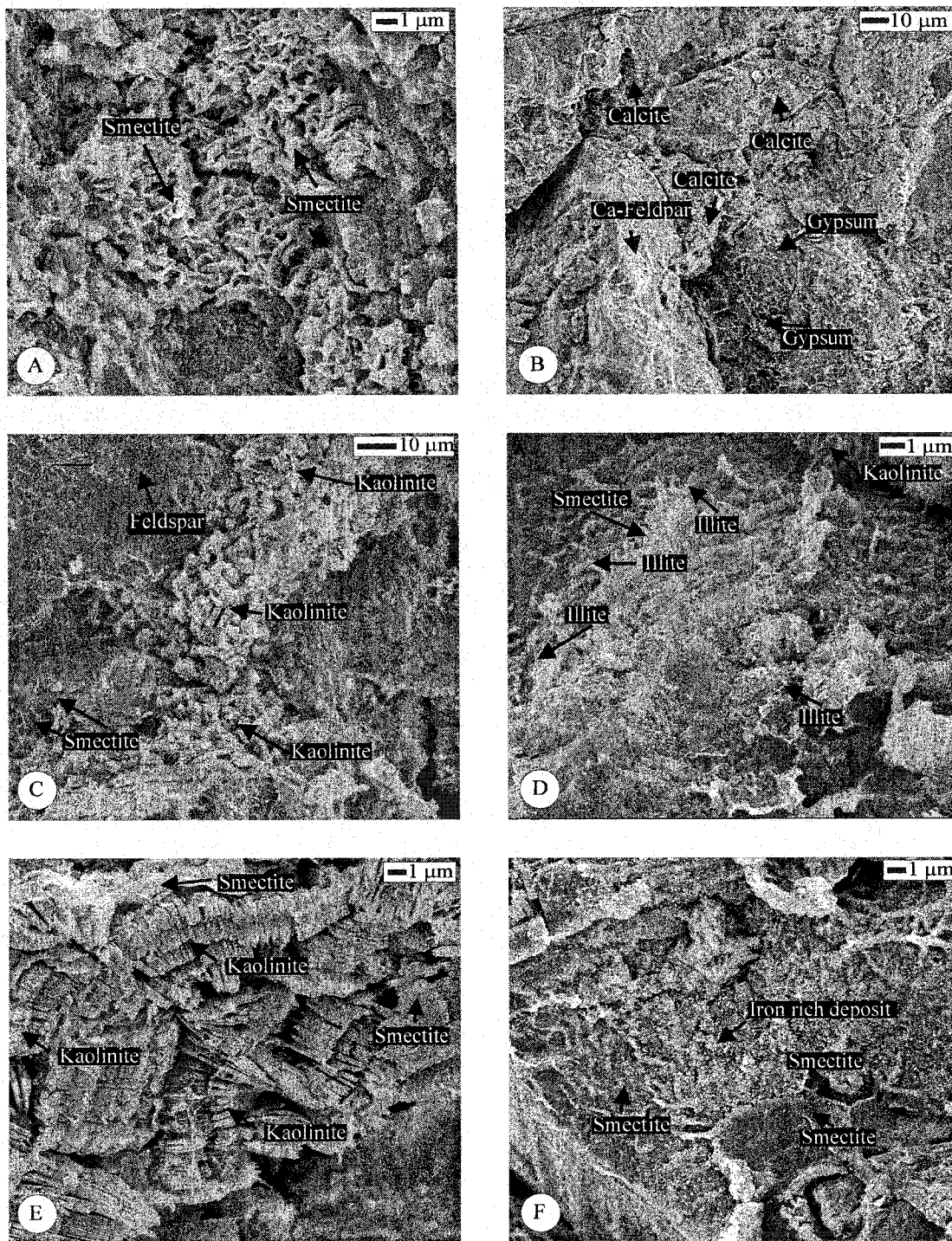
Figure A-10. Scanning electronic photomicrographs: (A) authigenic smectite showing highly crenulated, honeycombed, and interlocking crystal shapes (sample Kn-5, lower Scollard Formation, Kneehills Creek locality); (B) coating of calcite cement on Ca-feldspar grain (sample Kn-2, lower Scollard Formation, Kneehills Creek locality); (C and E) vermicular aggregates of euhedral crystals of authigenic kaolinite (sample K-1, upper Scollard Formation, Knudsen's Farm locality); (D) alteration of smectite into illite (sample Kn-3, lower Scollard Formation, Kneehills Creek locality); (F) smectite pore filling cement (sample Kn-2, lower Scollard Formation, Kneehills Creek locality).

151
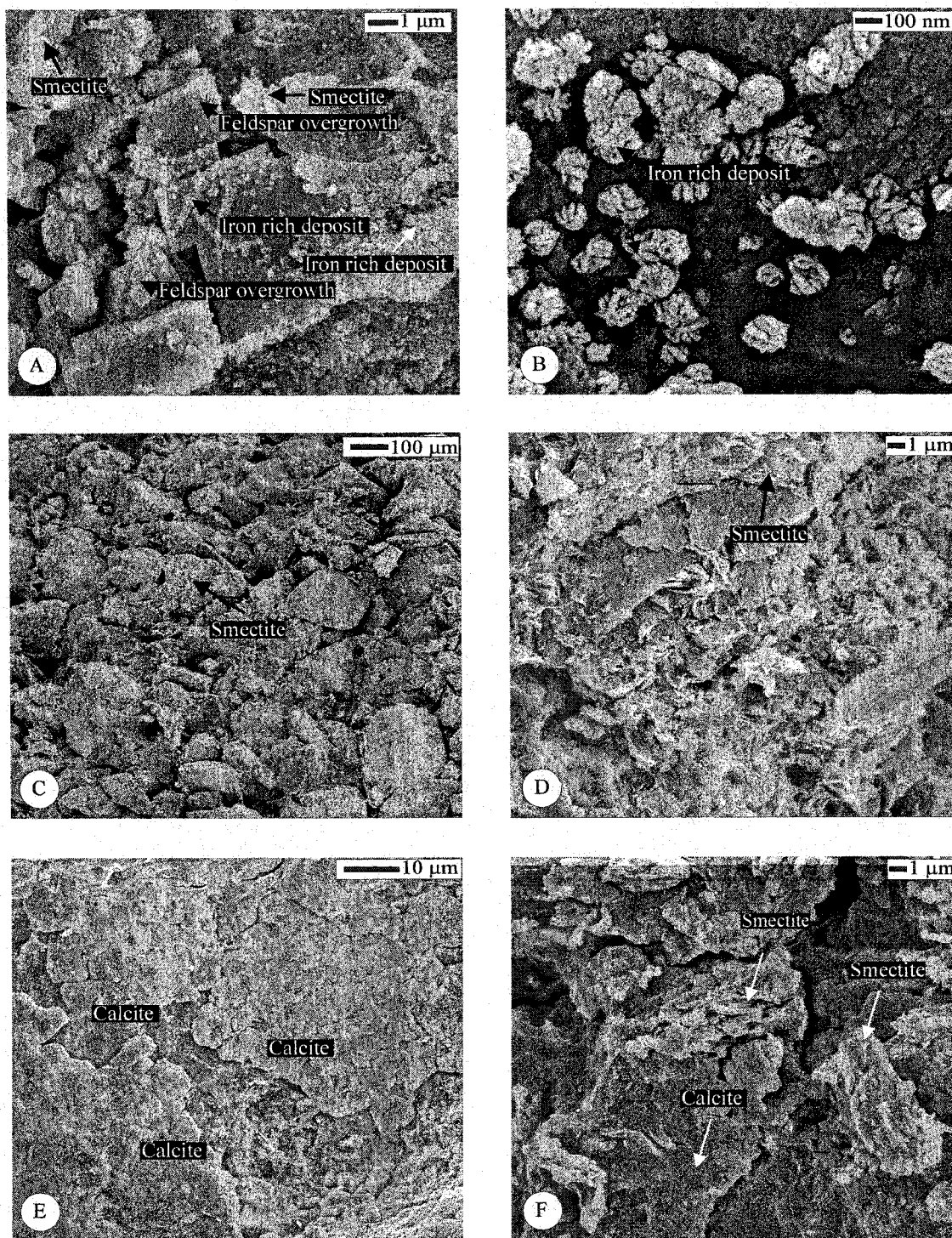
Figure A-11. Scanning electronic photomicrographs: (A) feldspar overgrowth covered by iron rich deposits (sample Kn-5, lower Scollard Formation, Kneehills Creek locality); (B) iron rich deposits on feldspar grain (sample Kn-5, lower Scollard Formation, Kneehills Creek locality); (C), (D) coating rim of authigenic smectite on Ca-feldspar grain (sample Kn-2, lower Scollard Formation, Kneehills Creek locality); (E) blocky calcite cement (sample Kn-2, lower Scollard Formation, Kneehills Creek locality); (E) blocky calcite cement and authigenic smectite (sample Kn-2, lower Scollard Formation, Kneehills Creek locality).

152
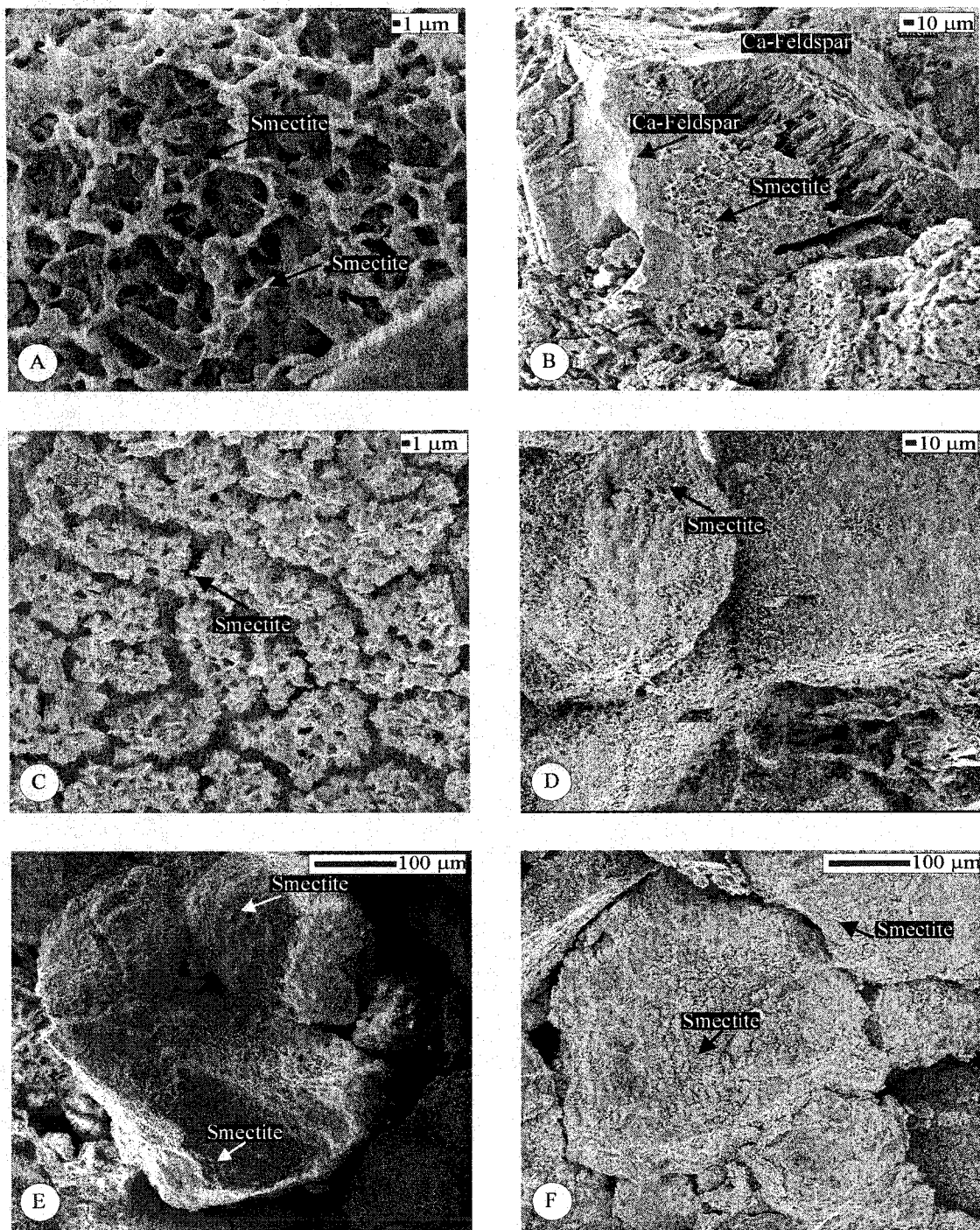
Figure A-12. Scanning electronic photomicrographs: (A) and (C) authigenic smectite showing highly crenulated, honeycombed, and interlocking crystal shapes (sample Kn-5, lower Scollard Formation, Kneehills Creek locality); (B) feldspar alteration into smectite (sample Kn-2, lower Scollard Formation, Kneehills Creek locality); (D), (E) and (F) coating rim of authigenic smectite on feldspar grains (Sample Kn-3, lower Scollard Formation, Kneehills Creek locality).

153
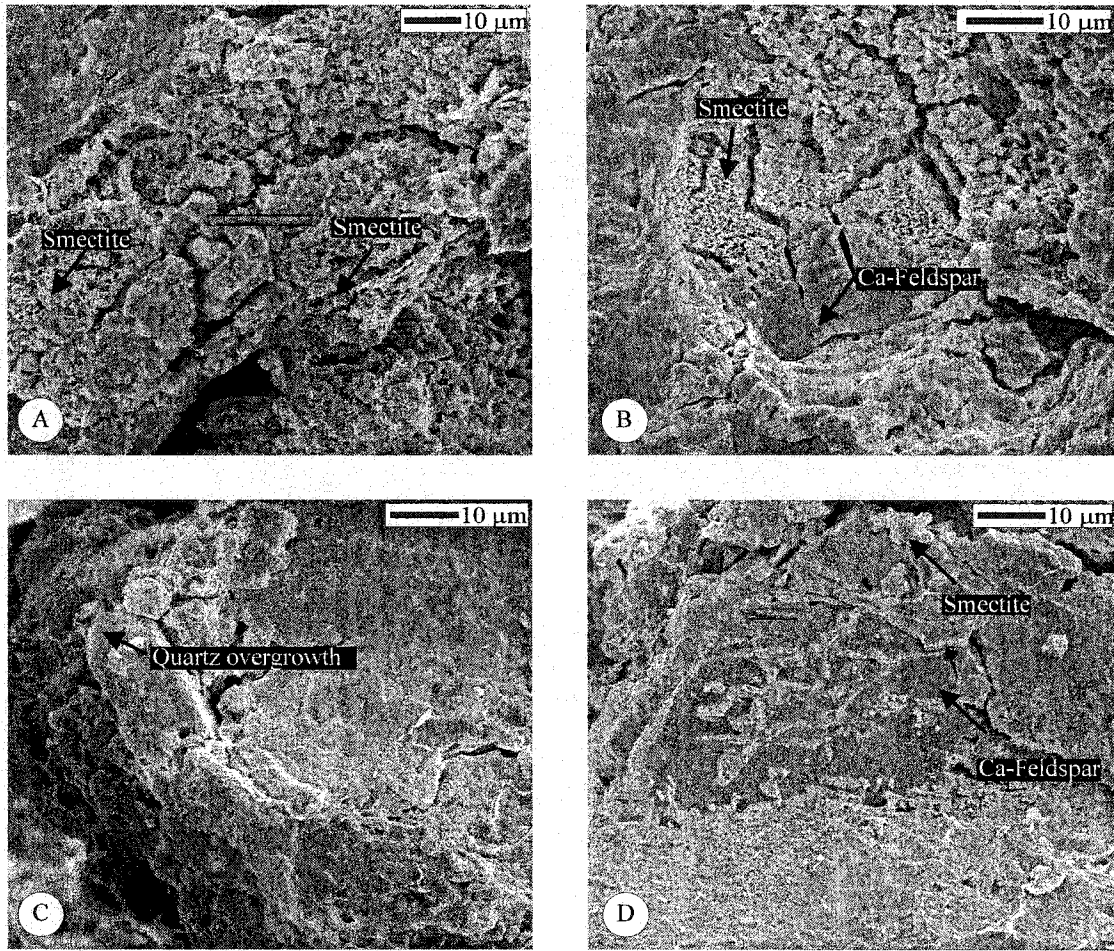
Figure A-13. Scanning electronic photomicrographs: (A) authigenic smectite showing highly crenulated, honeycombed, and interlocking crystal shapes (sample Kn-5, lower Scollard Formation, Kneehills Creek locality); (B) feldspar alteration into smectite (sample Kn-2, lower Scollard Formation, Kneehills Creek locality); (C) quartz overgrowth (sample Kn-5, lower Scollard Formation, Kneehills Creek locality); (D) coating rim of authigenic smectite on feldspar grain (sample Kn-3, lower Scollard Formation, Kneehills Creek locality).
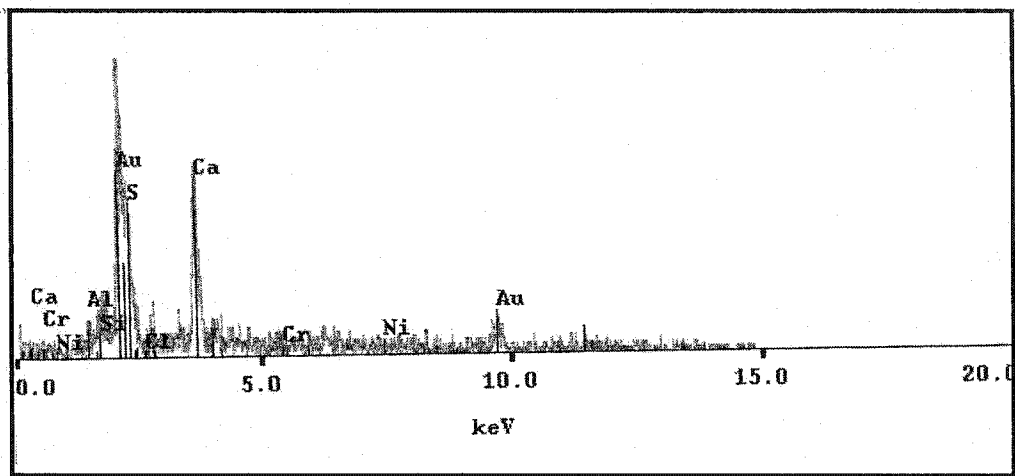
Figure A-14. X-ray diffraction pattern showing the presence of Ca-feldspar (sample 2 ,lower Scollard Formation, Kneehills Creek locality).
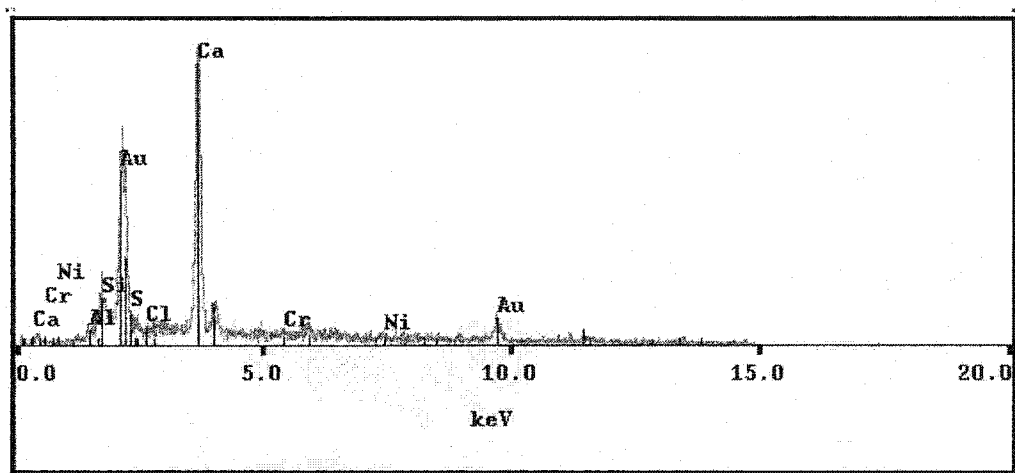
Figure A-15. X-ray diffraction pattern showing the presence of calcite (sample 3 , lower Scollard Formation, Kneehills Creek locality).
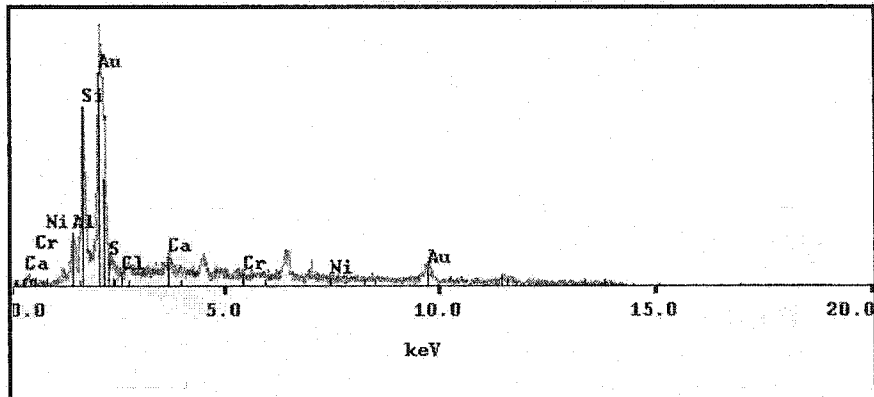
Figure A-16. X-ray diffraction pattern showing the presence of smectite (sample 2 , lower Scollard Formation, Kneehills Creek locality).
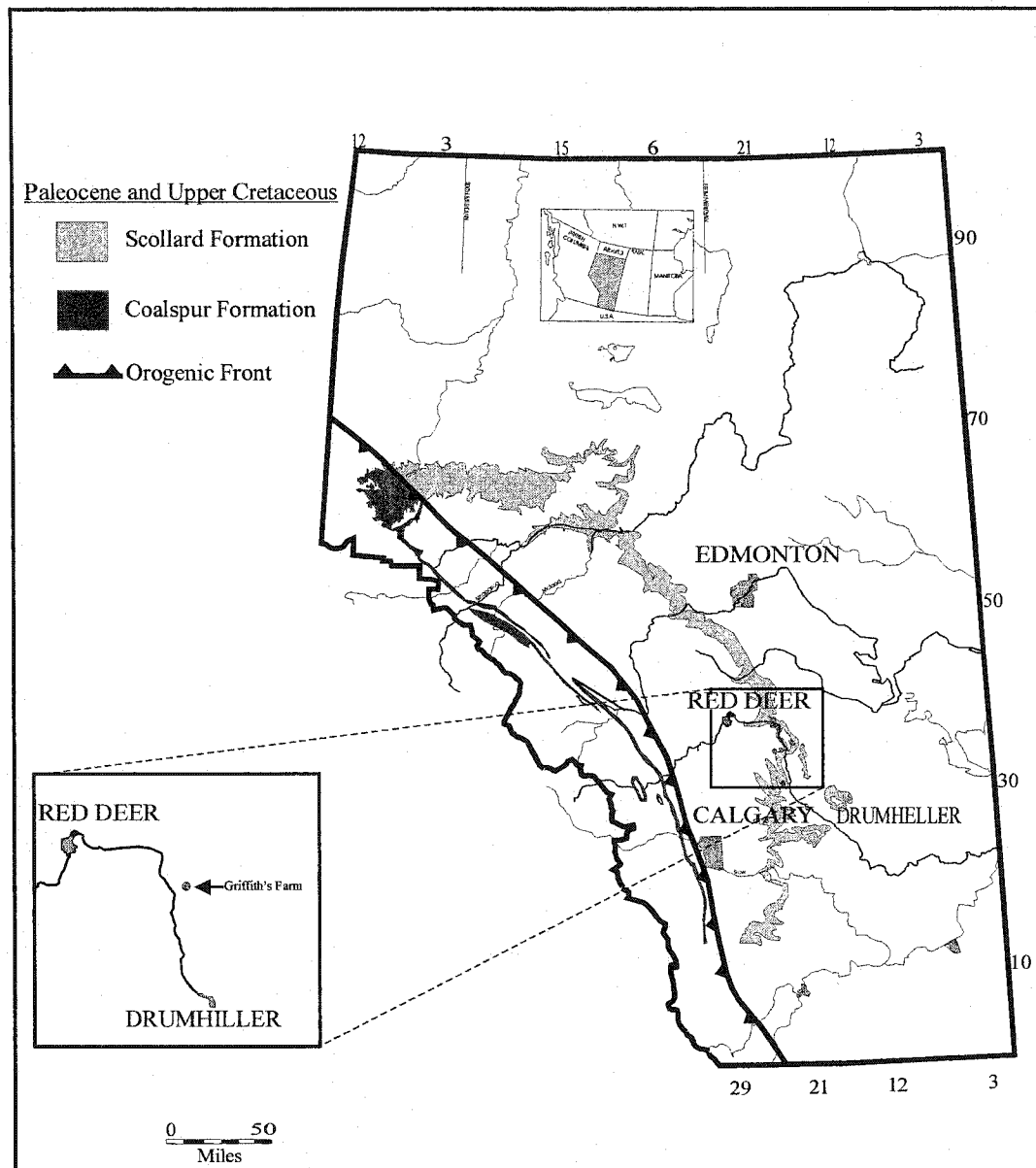
Figure 17. Outcrop distribution of the Scollard and Coalspur formations in Alberta, and the location of the studied outcrop section.
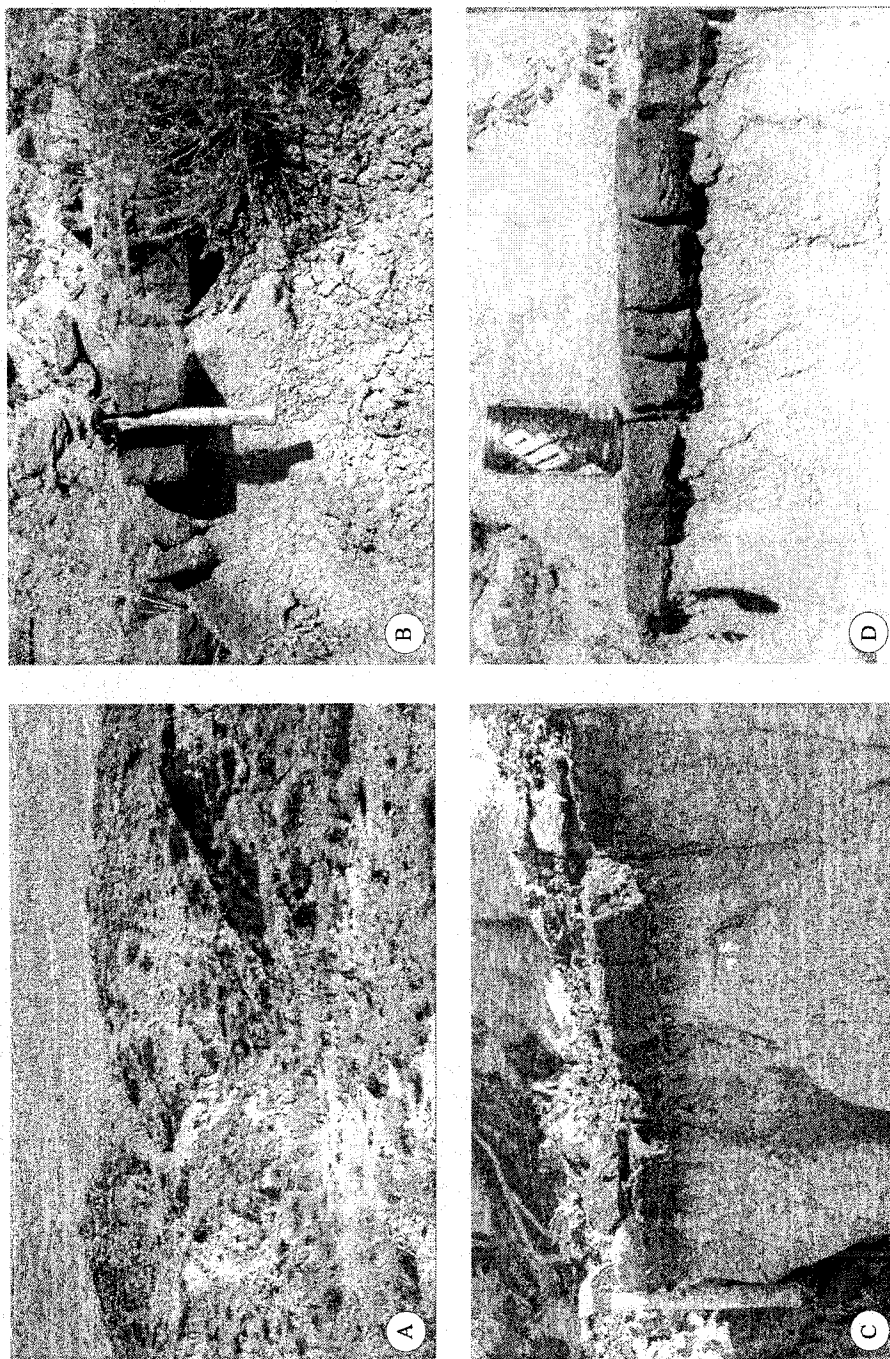
Figure A-18. Outcrop photographs of the lower Scollard Formation, Griffith's Farm locality: (A) outcrop view of the Griffith's Farm locality (B), (C), and (D) crevasse splay deposits.
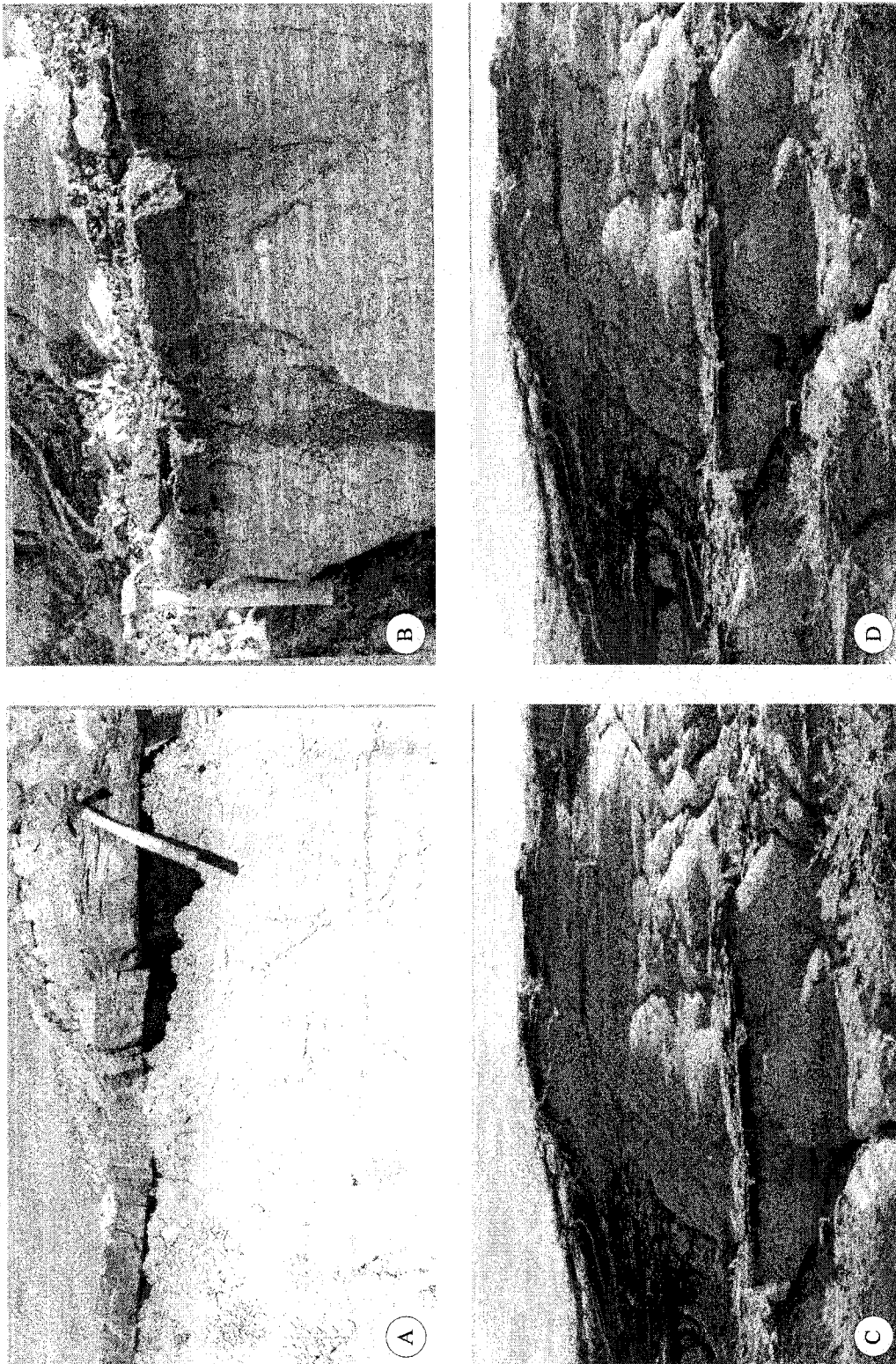
Figure A-19. Outcrop photographs of the lower Scollard Formation, Griffith's Farm locality: (A), (B), (C), and (D) crevasse splay deposits.

159
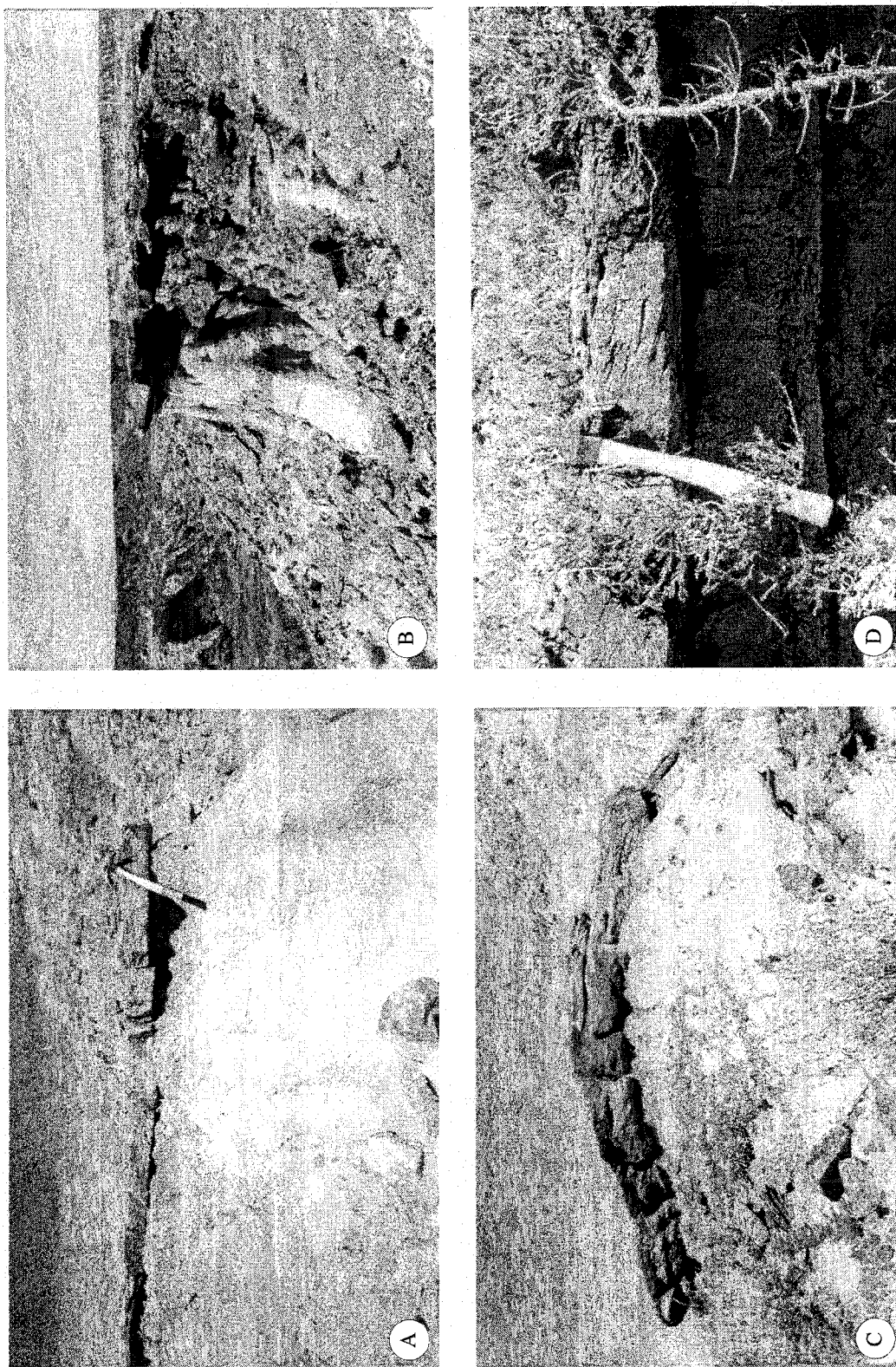
Figure A-20. Outcrop photographs of the lower Scollard Formation, Griffith's Farm locality: (A), (B), (C), (D) crevasse splay deposits.

160
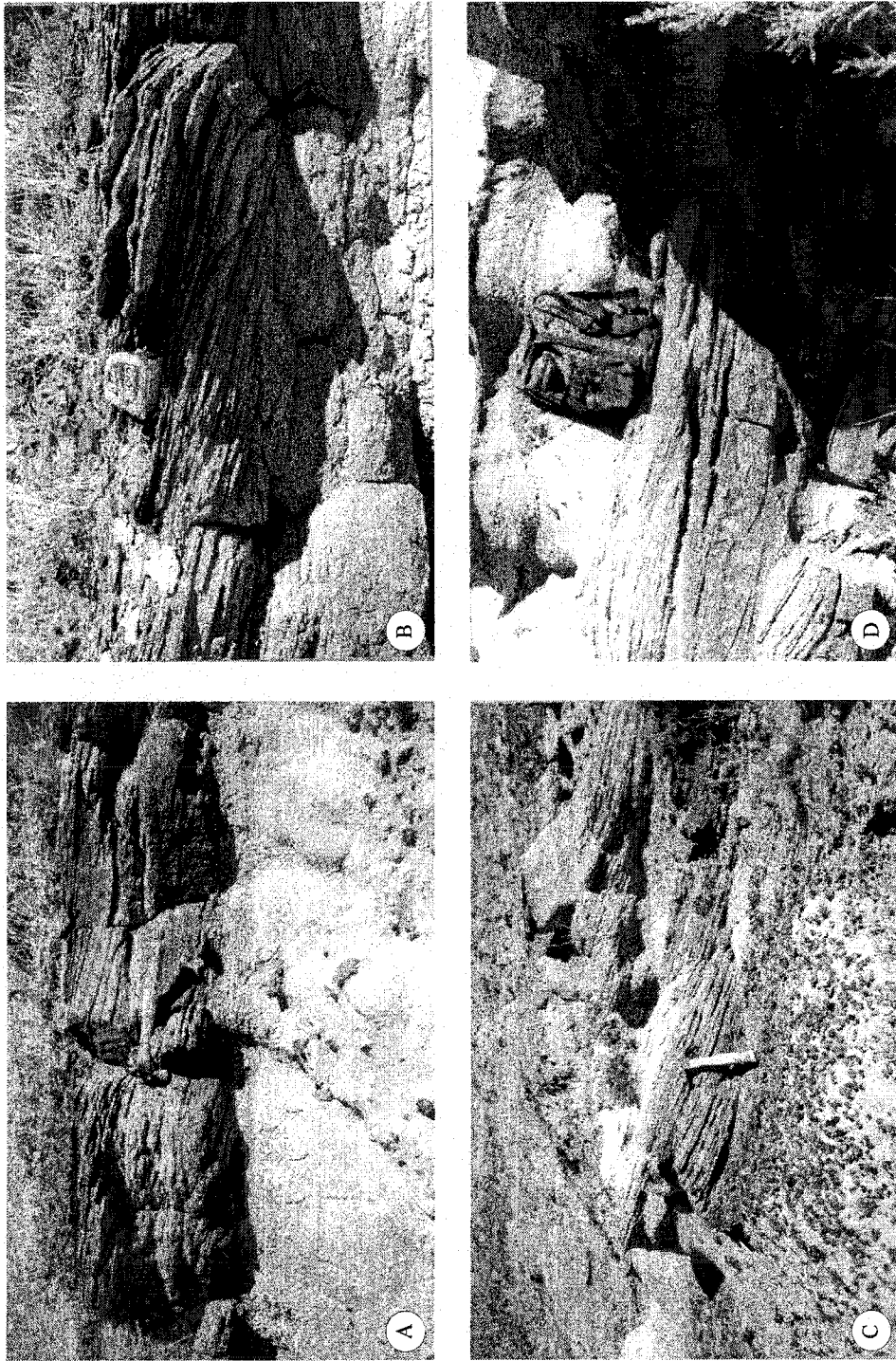
Figure A-21. Outcrop photographs of the lower Scollard Formation, Griffith's Farm locality: (A), (B), and (D) close-up views showing trough cross beds; (C) outcrop photograph showing trough cross beds.

161
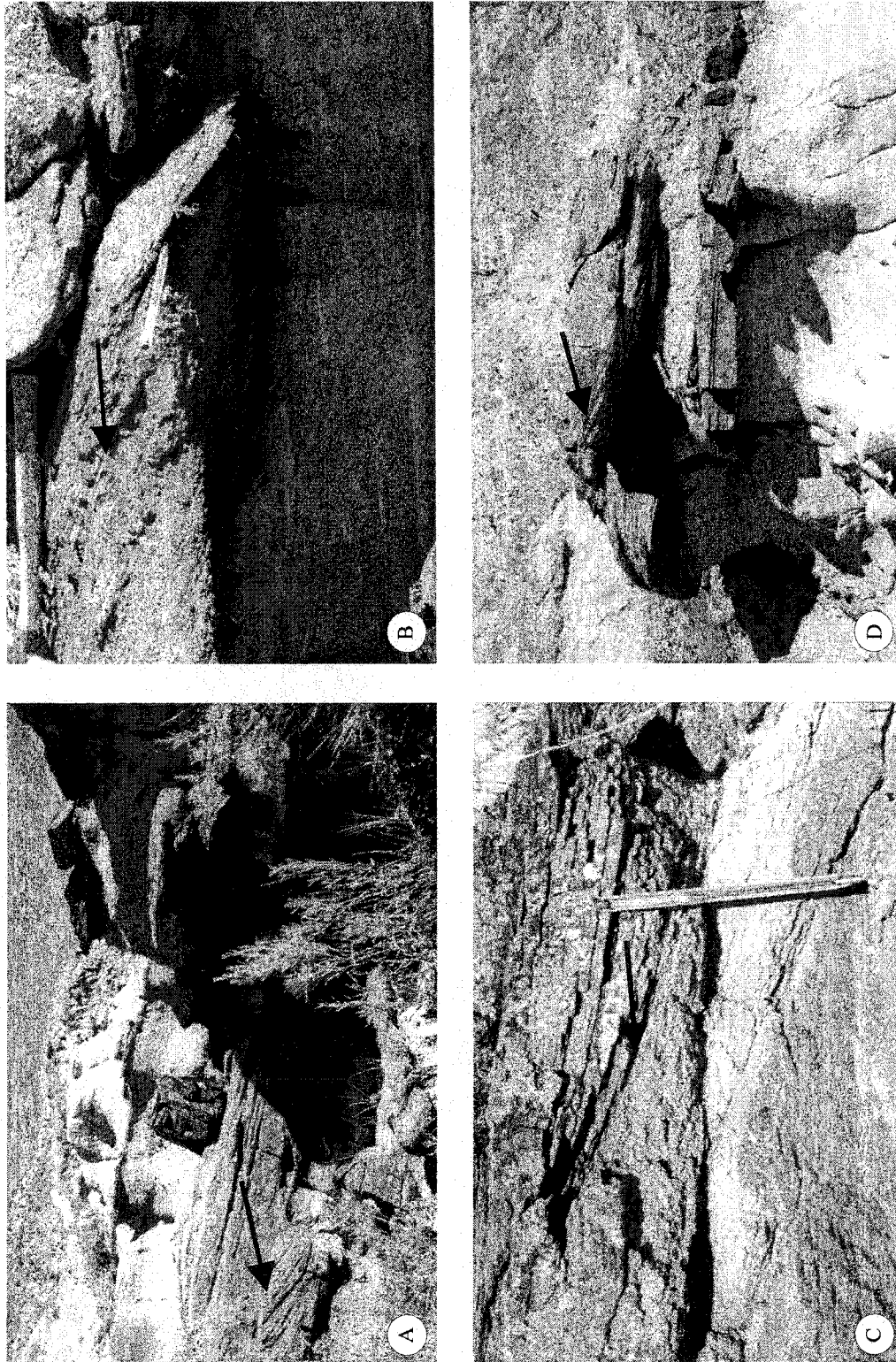
Figure A-22. Outcrop photographs of the lower Scollard Formation, Griffith's Farm locality showing trough cross beds indicated by arrows..

162
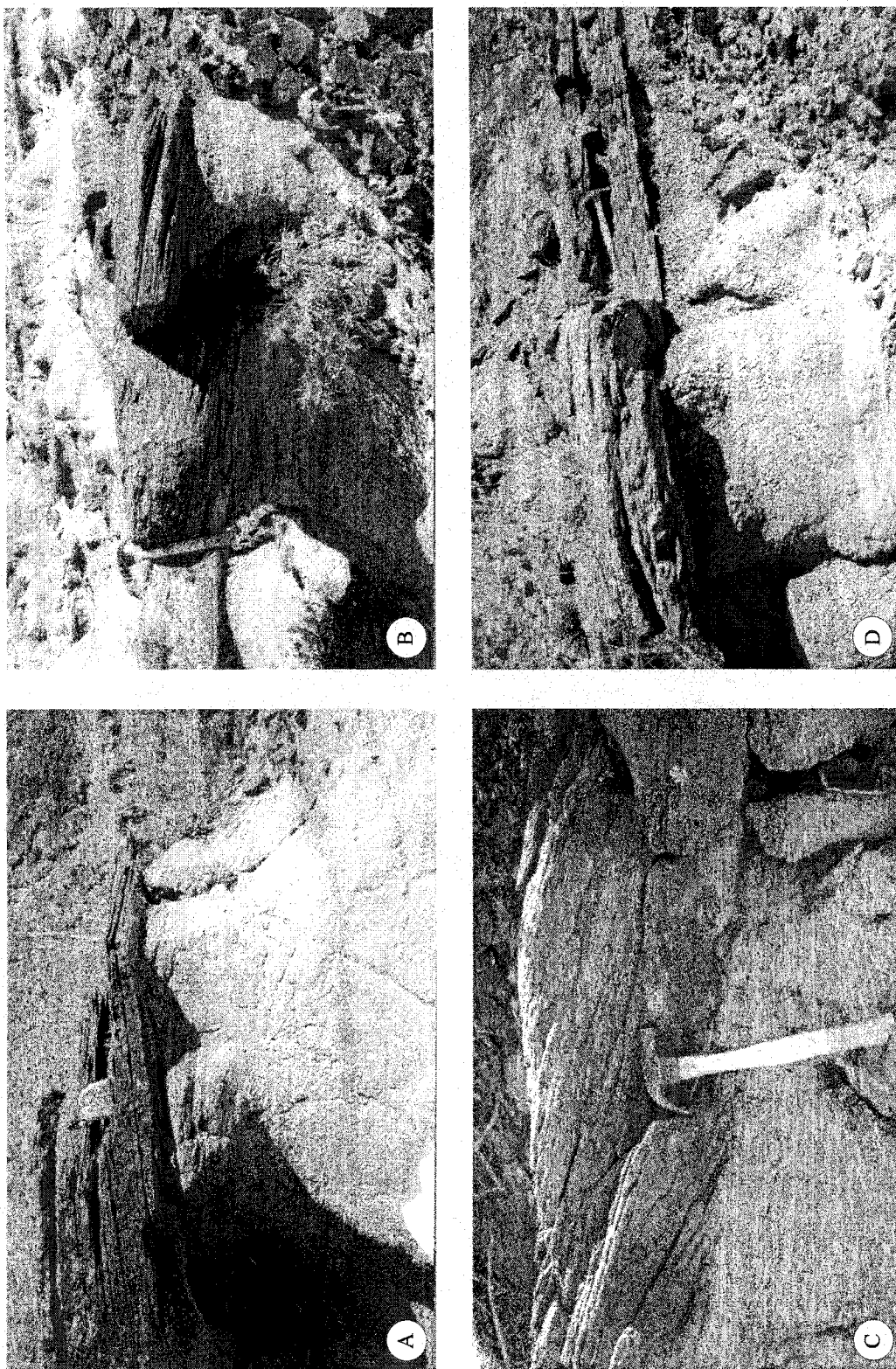
Figure A-23. Outcrop photographs of the lower Scollard Formation, Griffith's Farm locality: (A), (B) and (D) outcrop photograph showing crevasse splay deposits; (C) close-up views showing trough cross beds.
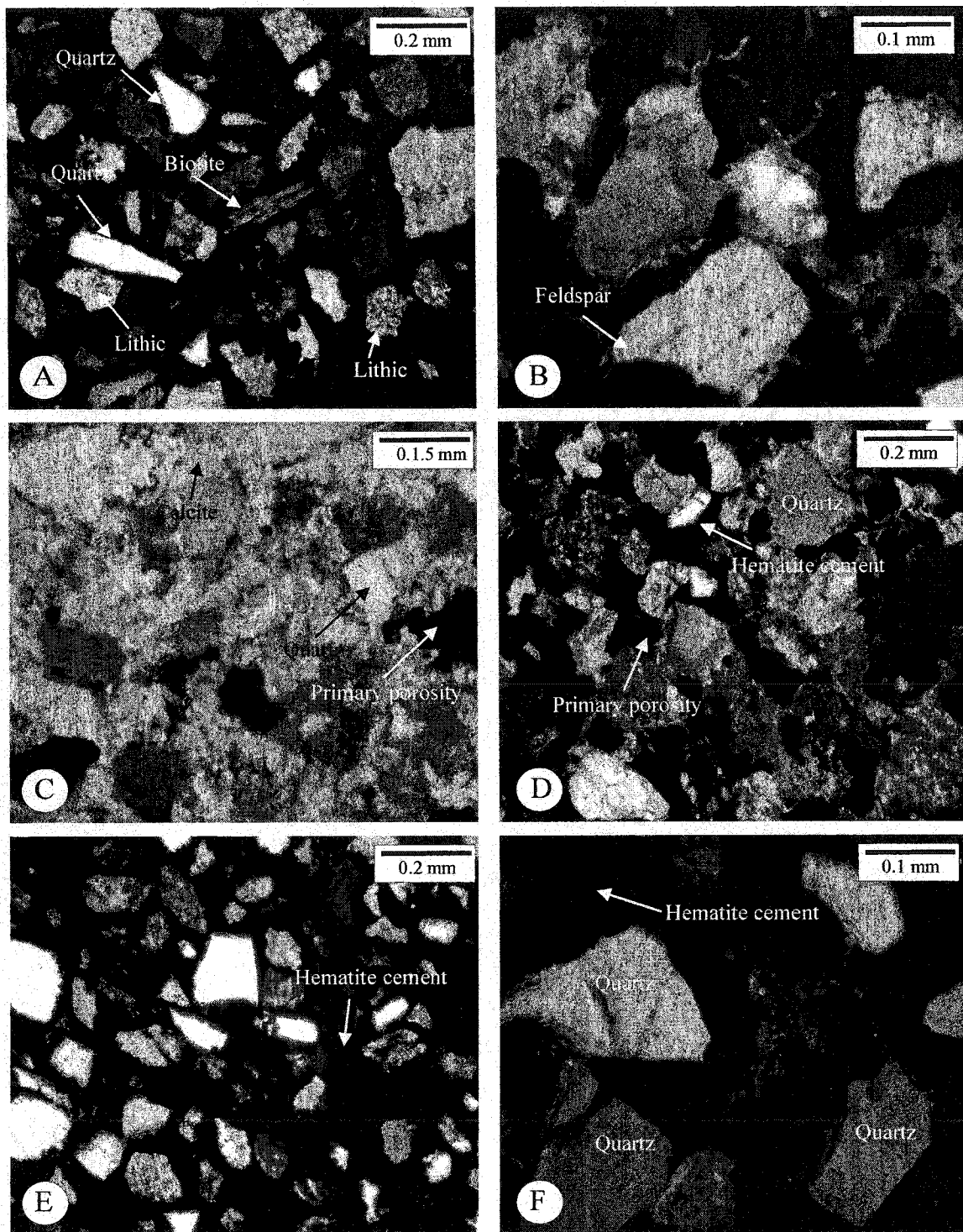
Figure A-24. Thin-section photomicrographs: (A) litharenite with igneous lithoclasts (arrows). Note the uniform microcrystalline quartz with no visible relict texture(sample G-1, lower Scollard Formation, Griffith's Farm locality); (B) detrital grain of feldspar (arrow) (sample K-4, lower Scollard Formation, Griffith's Farm locality); (C) poikilotopic calcite cement (arrows) (sample G-9, lower Scollard Formation, Griffith's Farm locality); (D), (E), and (F) late diaginetic hematite cement (sample G-2, lower Scollard Formation, Griffith's Farm locality).

164
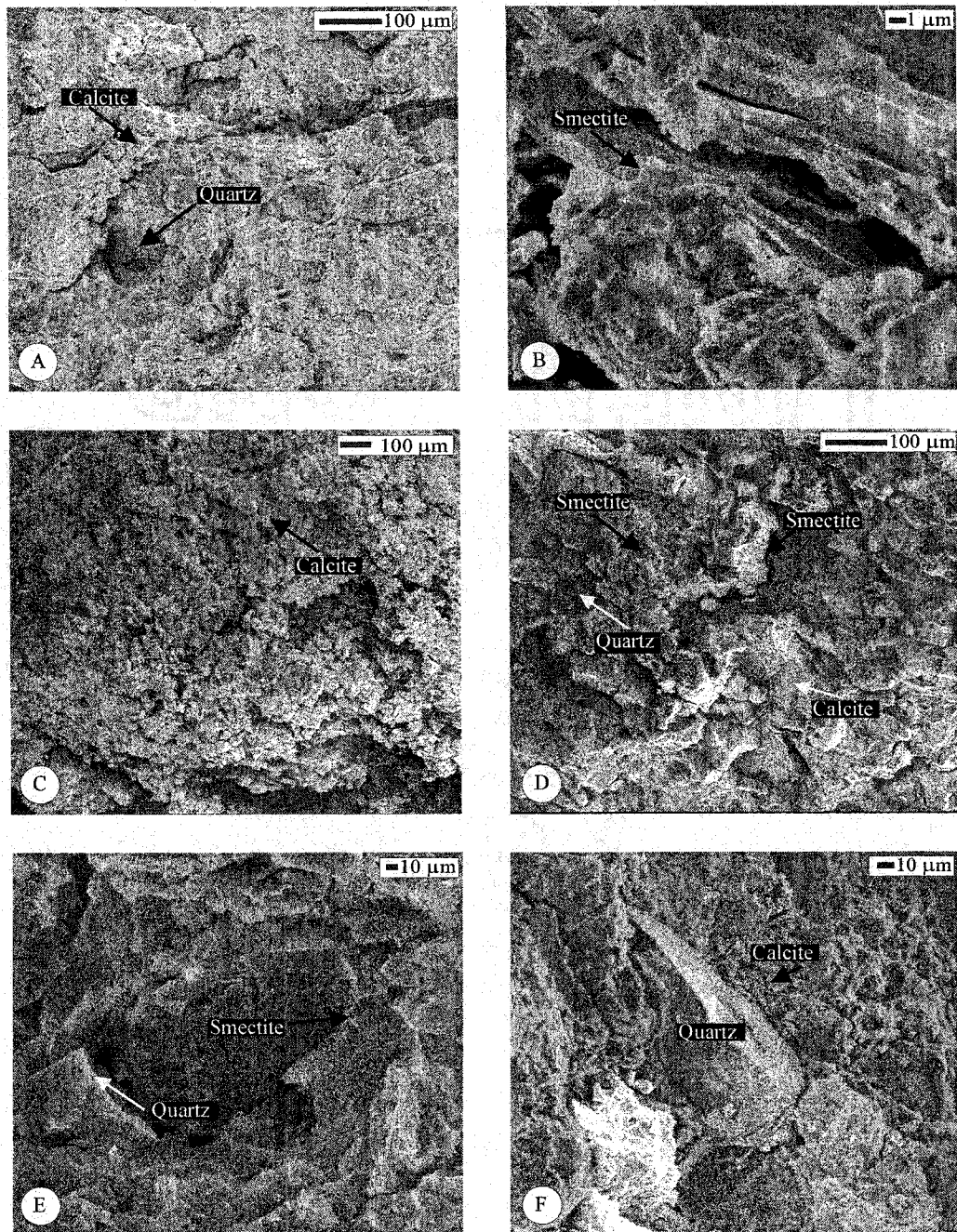
Figure A-25. Scanning electronic photomicrographs: (A), (C), and (F) calcite cement that completely destroyed the primary porosity (sample G-11, lower Scollard Formation, Griffith's Farm locality); (B) coating rim of authigenic smectite (sample G-9, lower Scollard Formation, Griffith's Farm locality); (D) and (E) quartz grain coated by rim of authigenic smectite (sample G-9, lower Scollard Formation, Griffith's Farm locality).

165
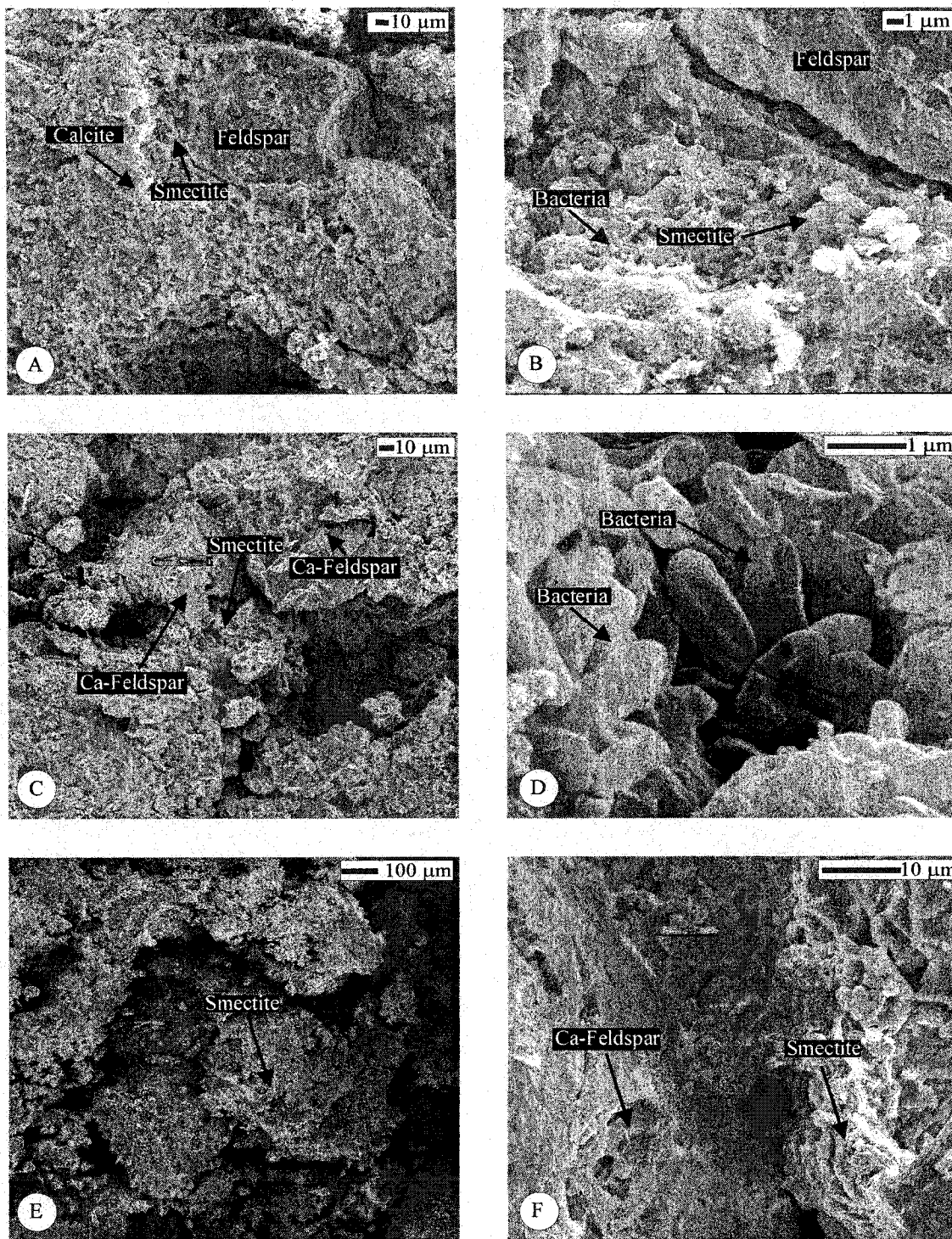
Figure A-26. Scanning electronic photomicrographs: (A) coating rim of authigenic smectite .Note the smectite growth perpendicular to the surface of the feldspar grain; (B) and (D) rod-shaped bacteria (arrows) entombed in calcite cement (sample G-11, lower Scollard Formation, Griffith's Farm locality); (C) feldspar alteration into smectite (sample G-2, lower Scollard Formation, Griffith's Farm locality); (E) coating rim of authigenic smectite; (F) authigenic smectite showing highly crenulated, honeycombed, and interlocking crystal shapes (sample G-9, lower Scollard Formation, Griffith's Farm locality).
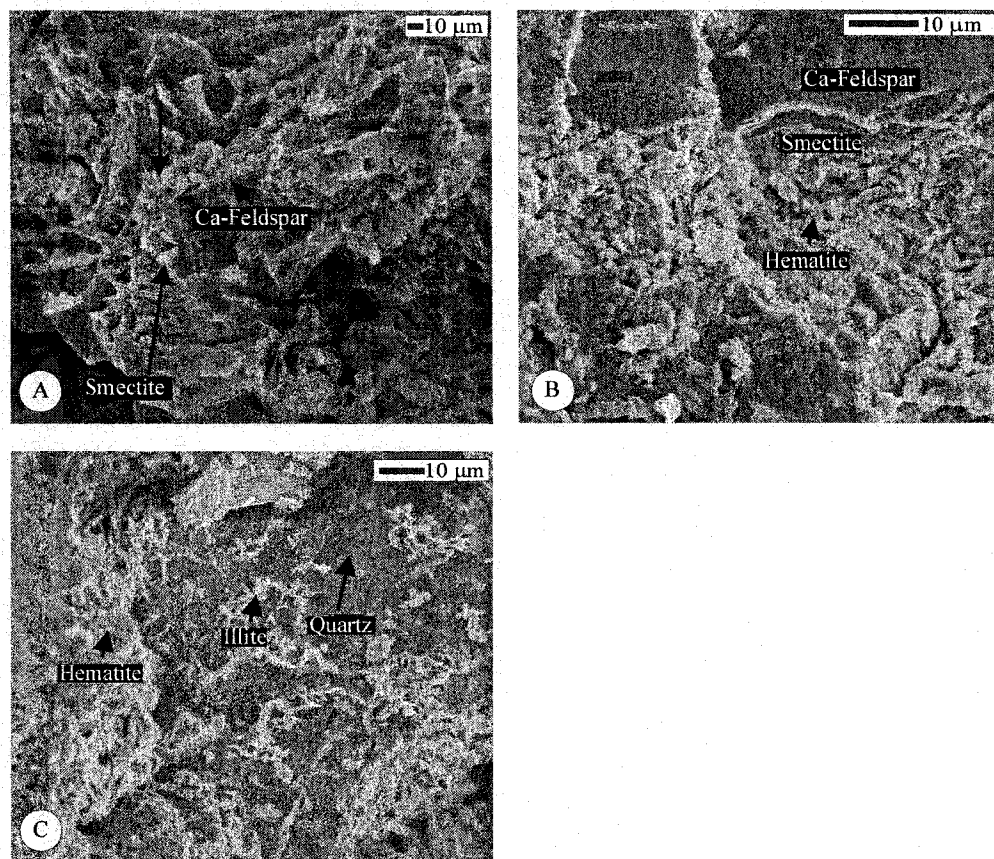
Figure A-27. Scanning electronic photomicrographs: (A) and (B) smectite coating Ca-feldspar grains; (C) illite coating quartz grains, which considerably reduces the porosity and permeability of the rock (sample G-7, lower Scollard Formation, Griffith's Farm locality).
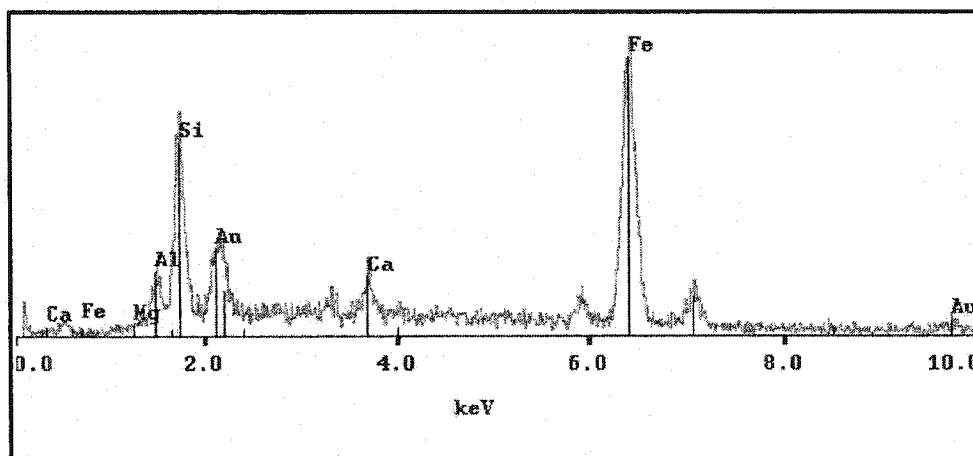
Figure A-28. X-ray diffraction pattern showing the presence of Fe-smectite (sample 4, lower Scollard Formation, Griffith's Farm locality).
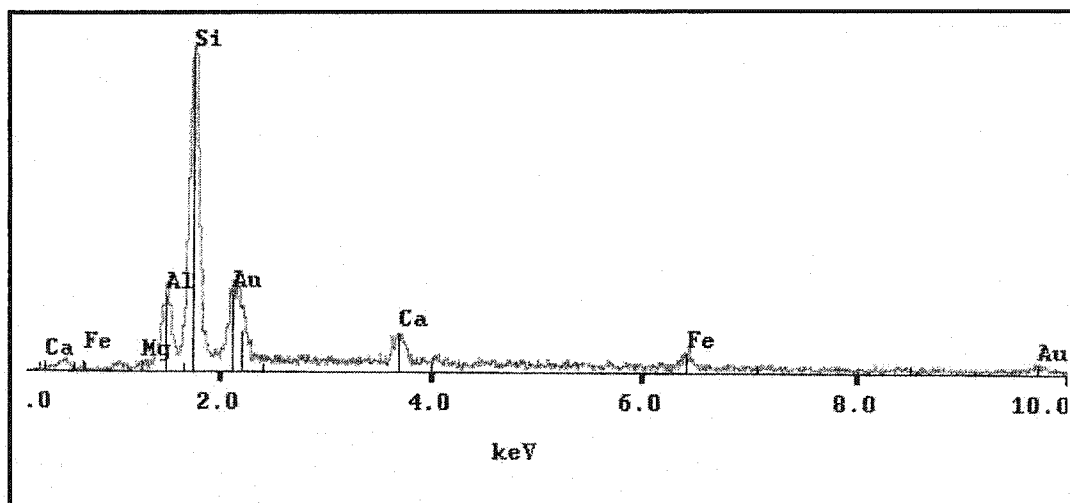
Figure A-29. X-ray diffraction pattern showing the presence of smectite (sample 3, lower Scollard Formation, Griffith's Farm locality).

168
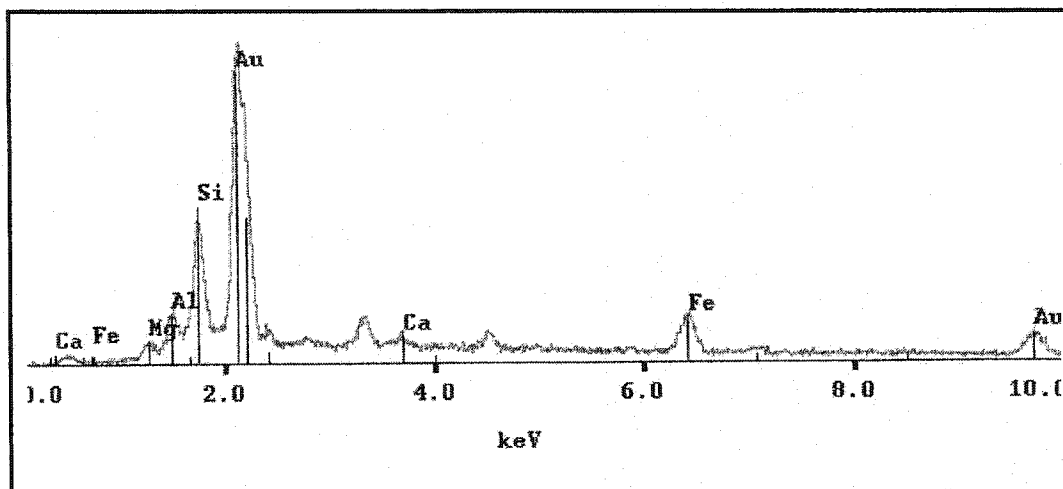
Figure A-30. X-ray diffraction pattern showing the presence of smectite (sample5 , lower Scollard Formation, Griffith's Farm locality).
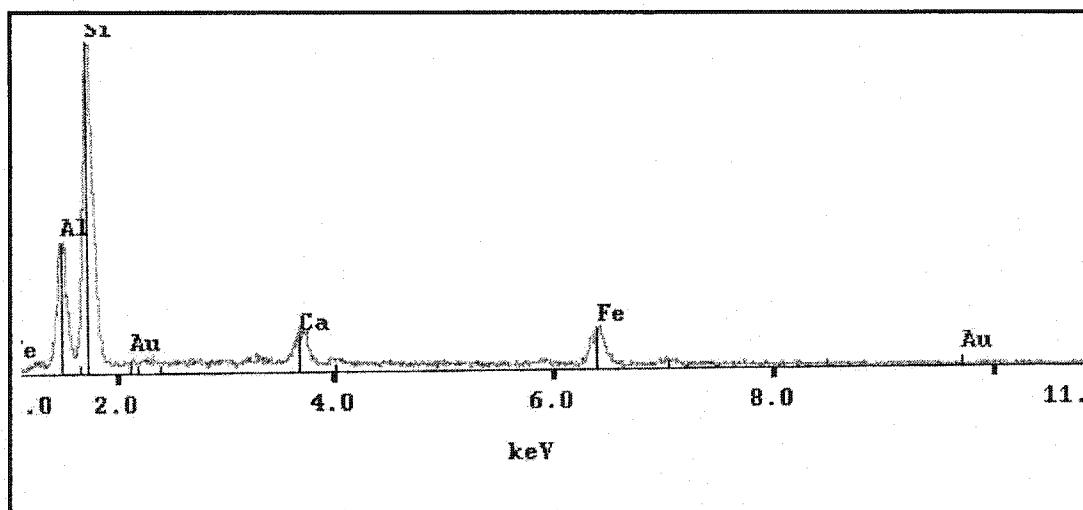
Figure A-31. X-ray diffraction pattern showing the presence of smectite (sample 6 , lower Scollard Formation, Griffith's Farm locality).

169
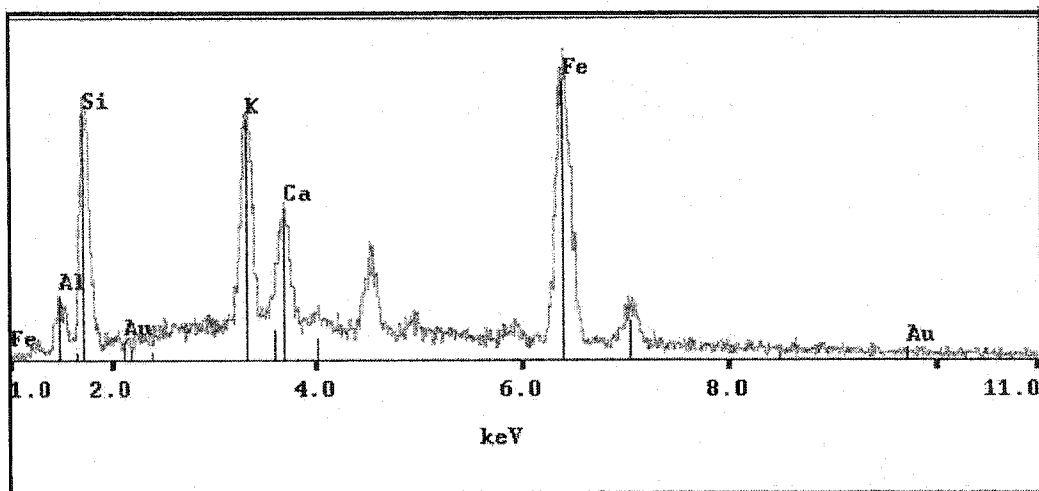
Figure A-32. X-ray diffraction pattern showing the presence of illite (sample 2 , lower Scollard Formation, Griffith's Farm locality).
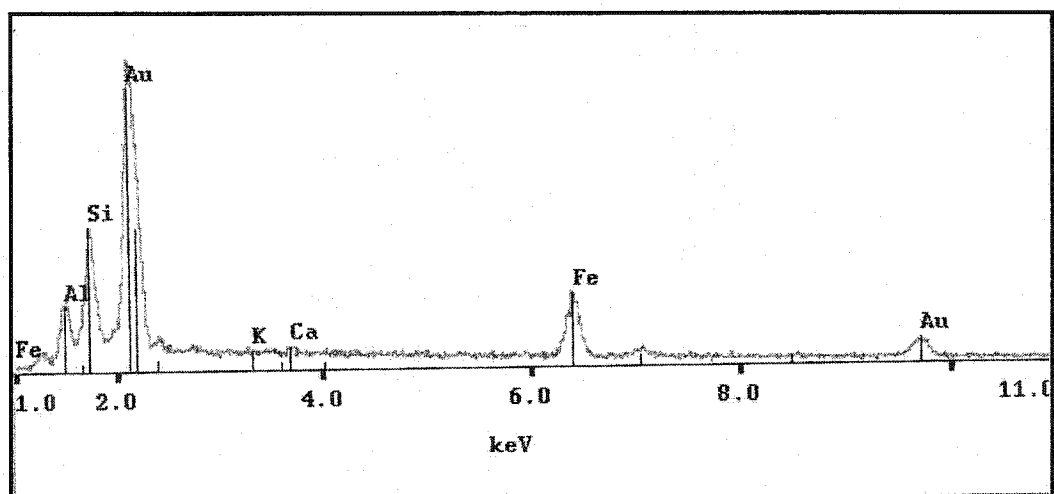
Figure A-33. X-ray diffraction pattern showing the presence of smectite (sample 3 , lower Scollard Formation, Griffith's Farm locality).
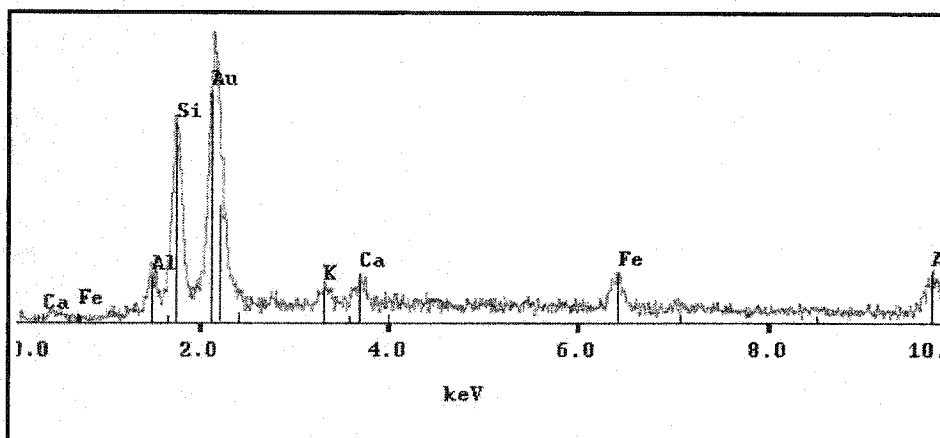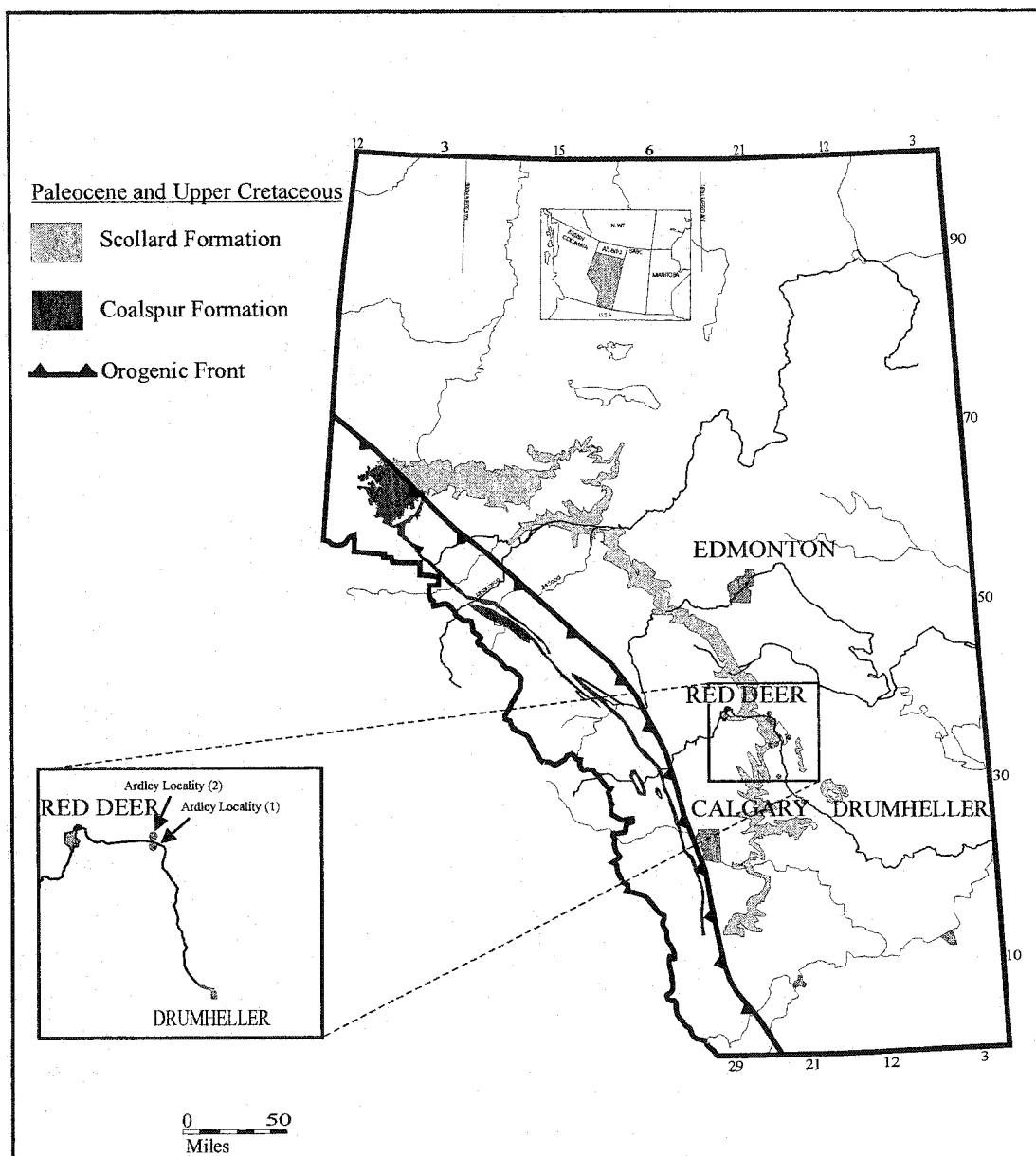
170
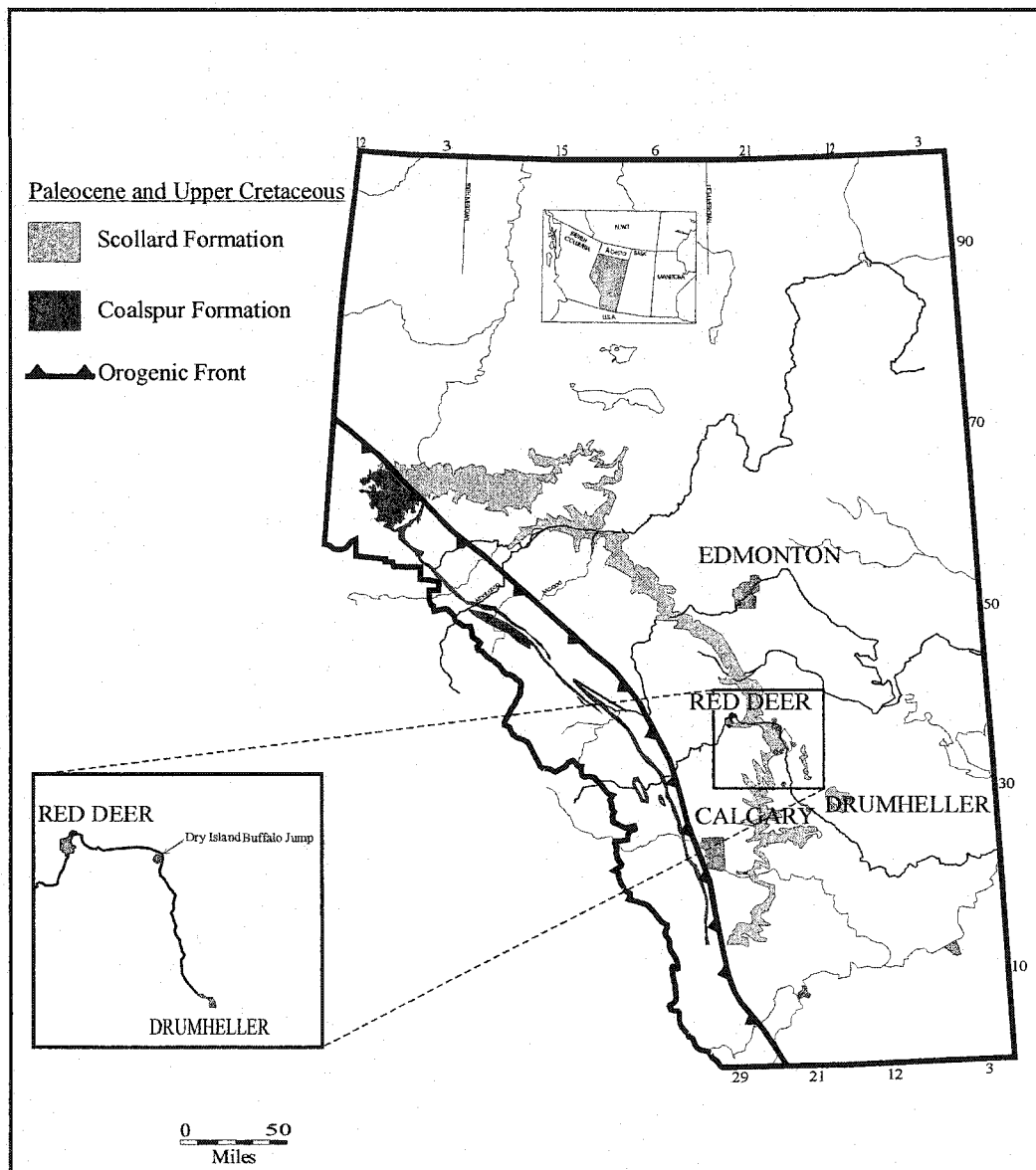
Figure 34. Outcrop distribution of the Scollard and Coalspur formations in Alberta, and the location of the studied outcrop section.
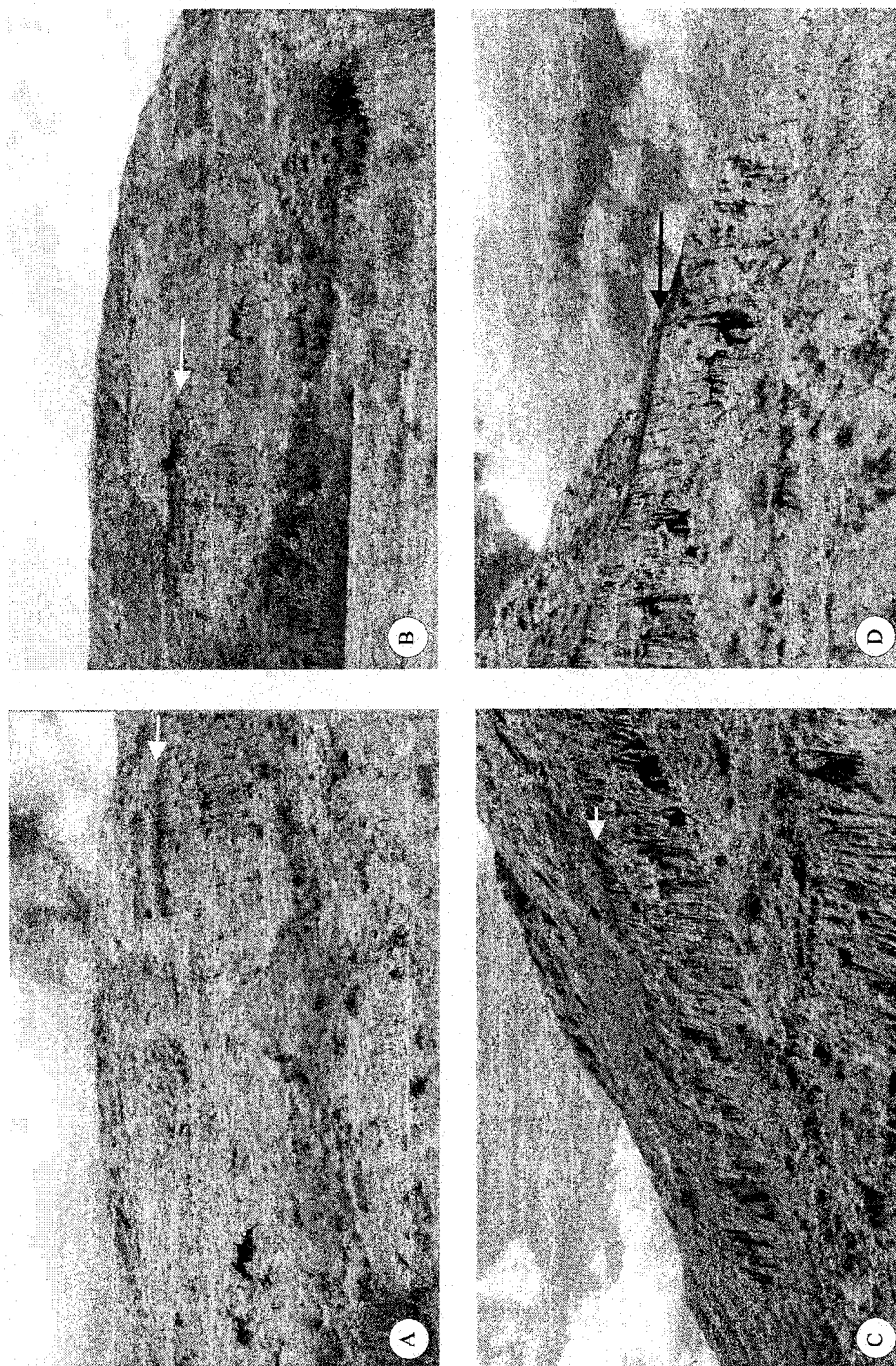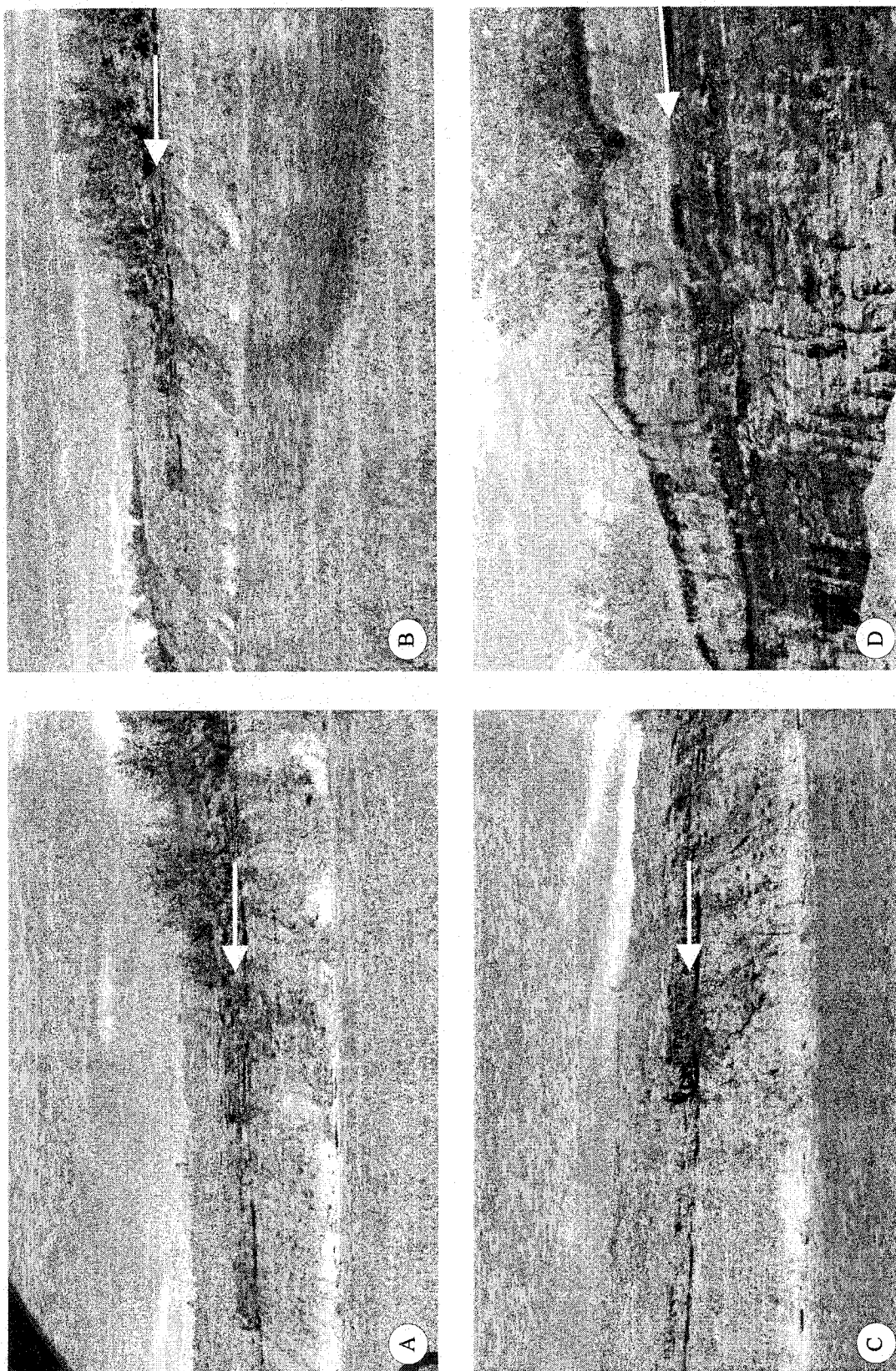
Figure A-35. Outcrop photographs of the upper Scollard Formation, Buffalo Jump Park locality showing the K-T boundary (arrows) above coal seam.

172
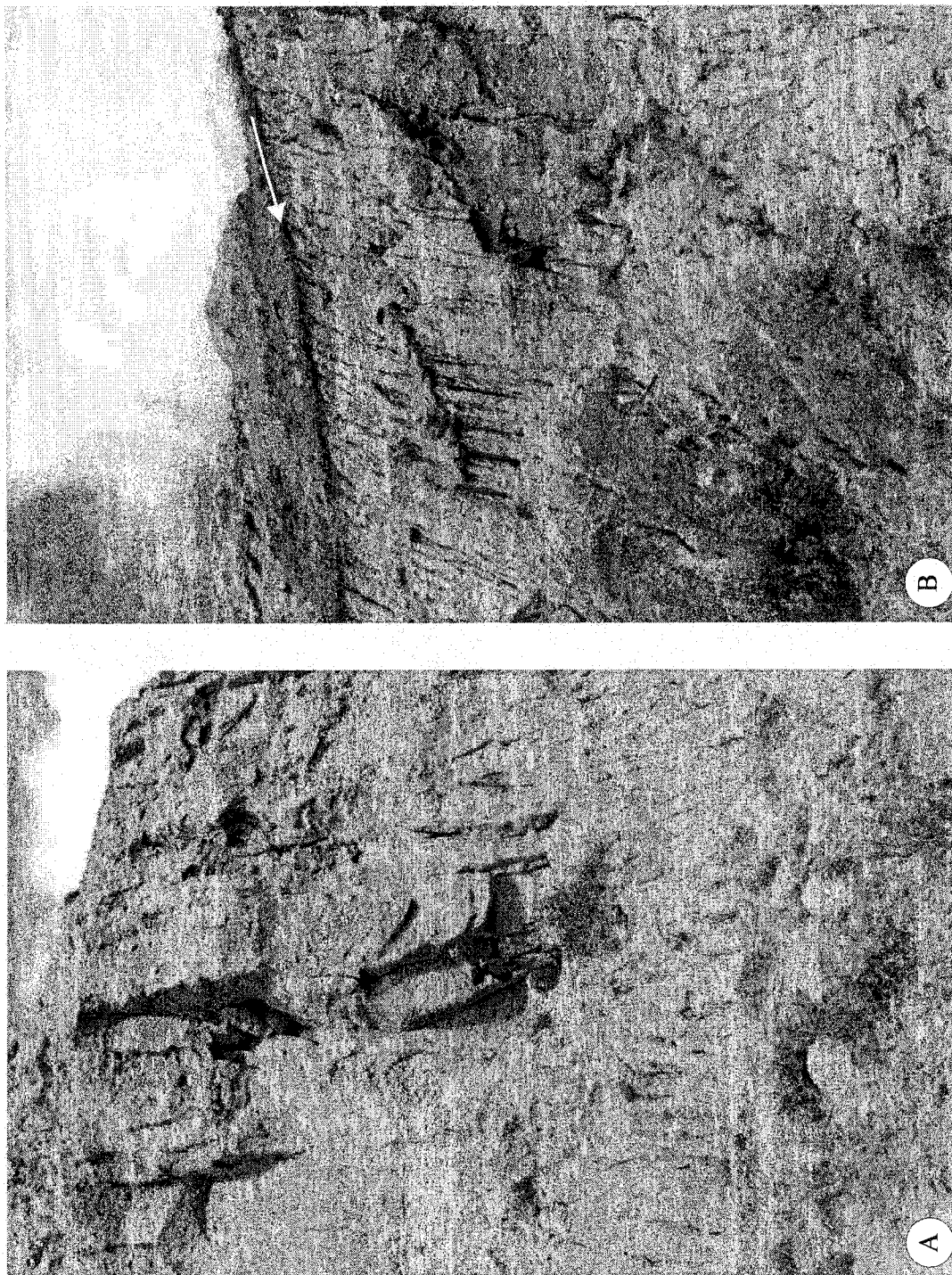
Figure A-36. Outcrop photographs of the upper Scollard Formation, Buffalo Jump Park locality: (A) outcrop photograph showing thick massive sandstone bed of meander river deposits; (B) outcrop photographs showing the K-T boundary above coal seam (arrow).
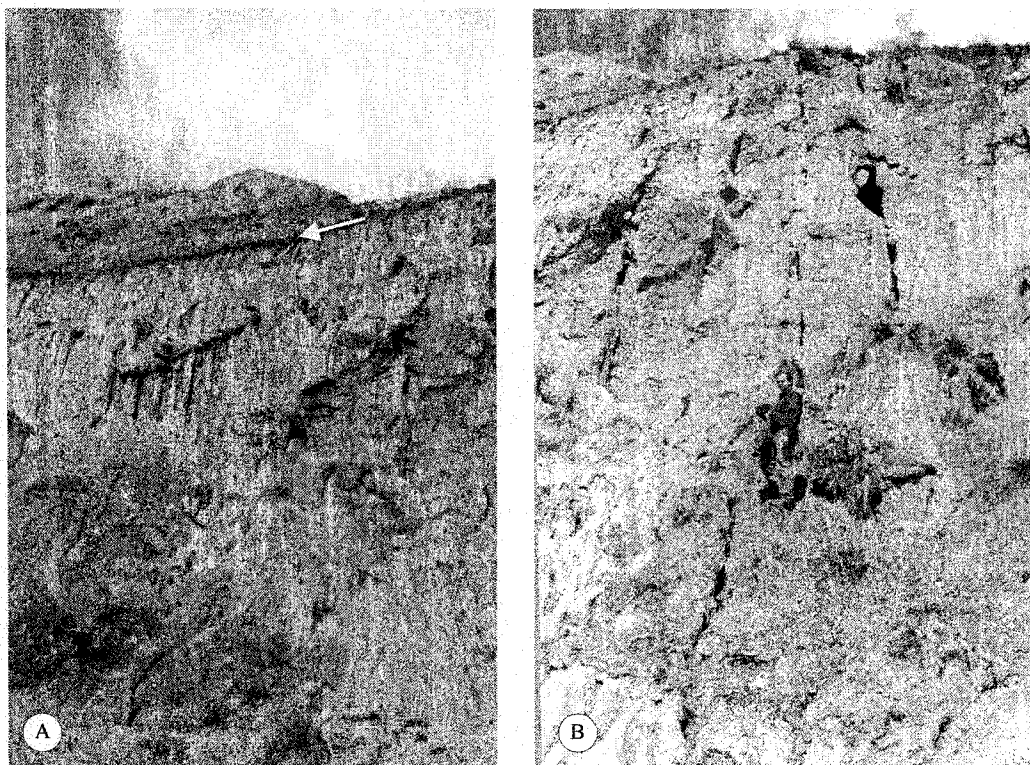
Figure A-37. Outcrop photographs of the upper Scollard Formation, Buffalo Jump Park locality: (A) outcrop photographs showing the K-T boundary above coal seam (arrow); (B) thick sandstone bed of meander river deposits.
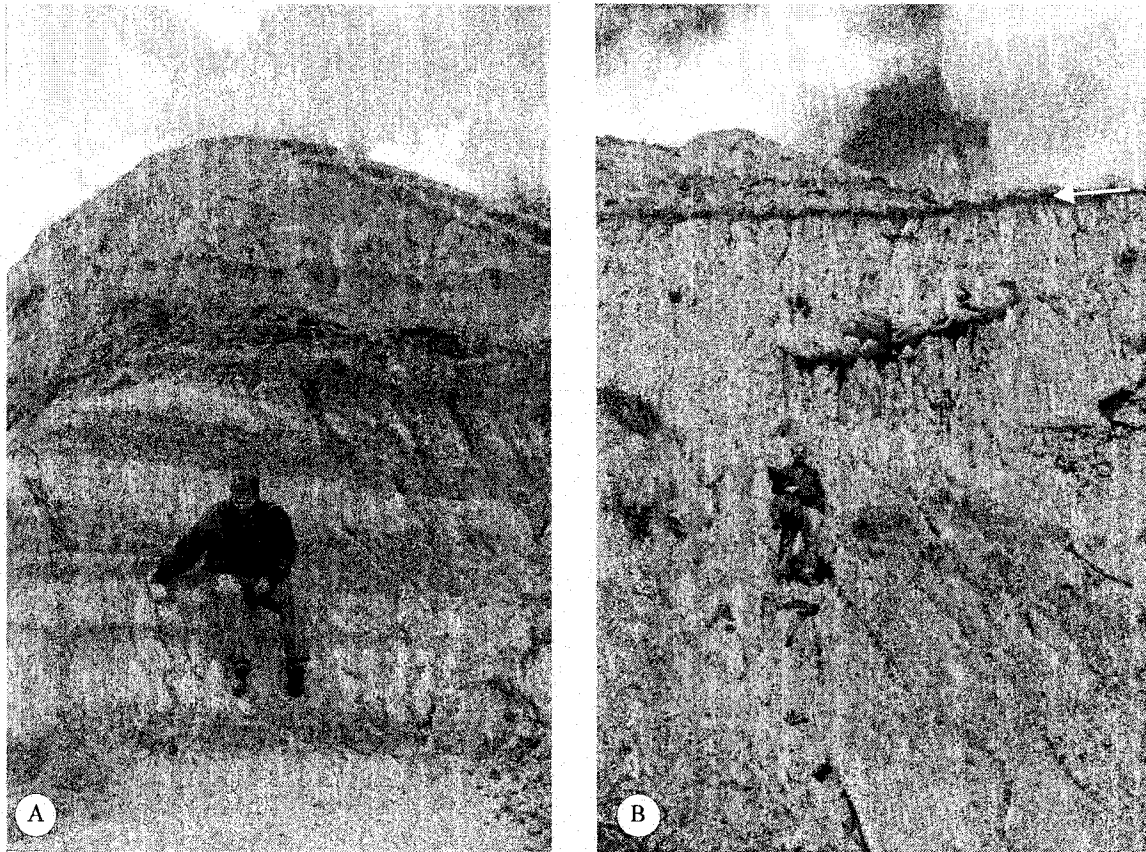
Figure A-38. Outcrop photographs of the upper Scollard Formation, Buffalo Jump Park locality: (A) floodplain deposits; (B) outcrop photographs showing the K-T boundary above coalseam (arrow).
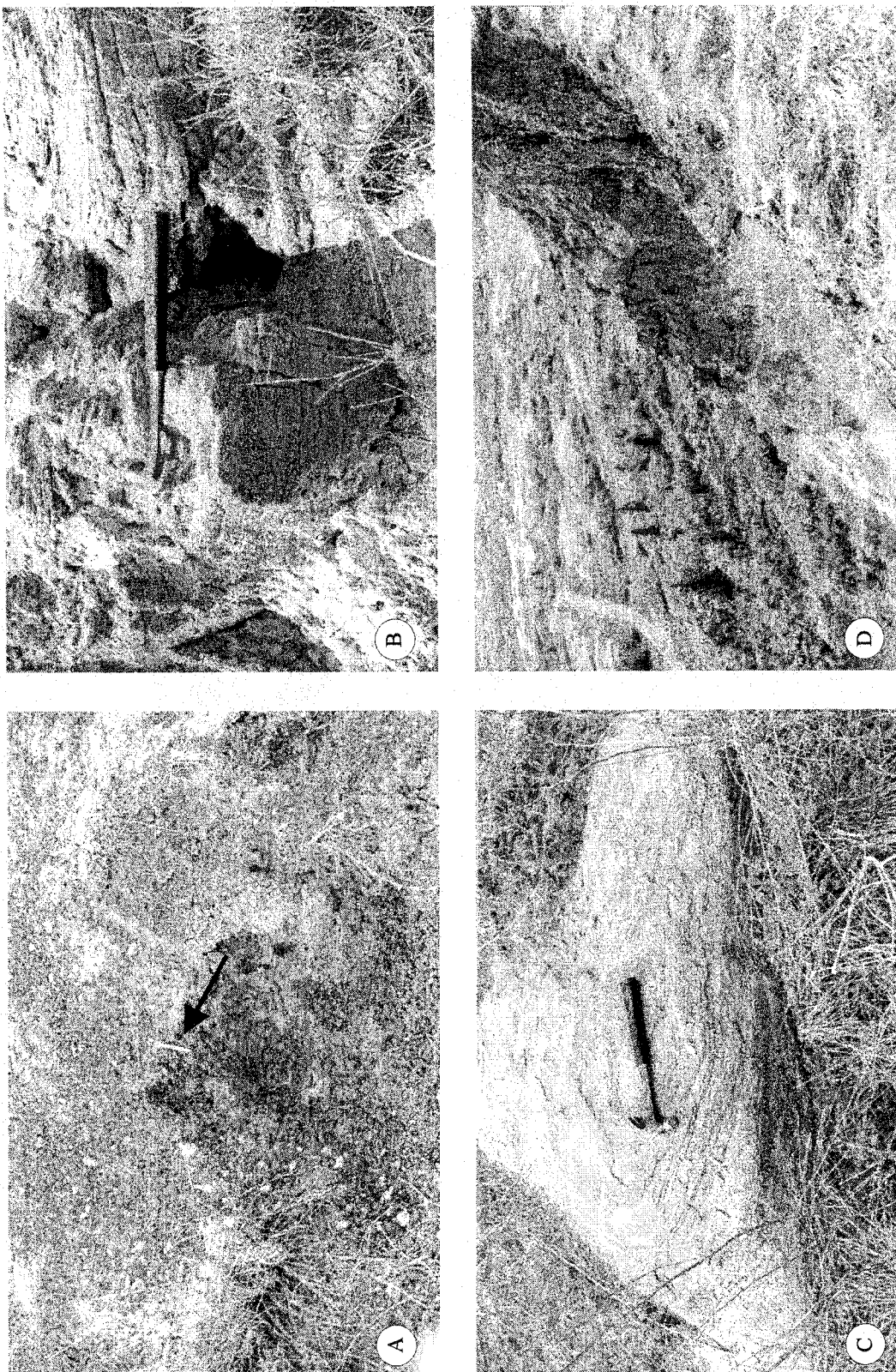
Figure A-39. Outcrop photographs of the upper Scollard Formation, Buffalo Jump Park locality: (A) outcrop photographs showing the K-T boundary above coal seam (arrow); (B) horizontal lamination of medium sand; (C) trough cross bedding; (D) outcrop photographs showing crevasse splay deposits.
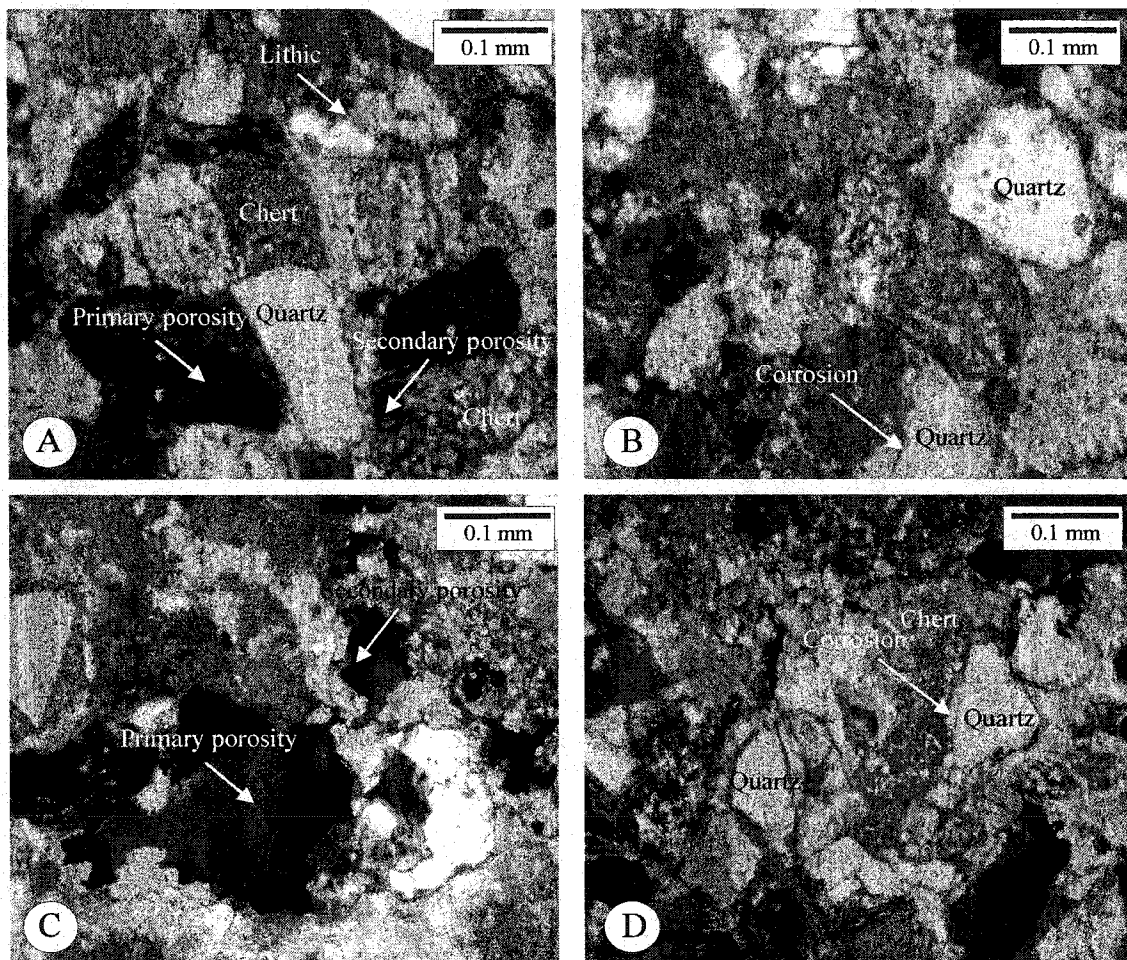
Figure A-40. Thin-section photomicrographs: (A) and (C) litharenite from the Buffalo Jump Park locality, with chert lithoclasts. Note secondary porosity (arrows) resulting from the dissolution of rock fragments, as seen under the petrographic microscope (sample T-2, upper Scollard Formation, Buffalo Jump locality); (B) and (C) litharenite from the Buffalo Jump Park locality showing corrosion of quartz grains (arrows) (sample T-2, upper Scollard Formation, Buffalo Jump locality).

177
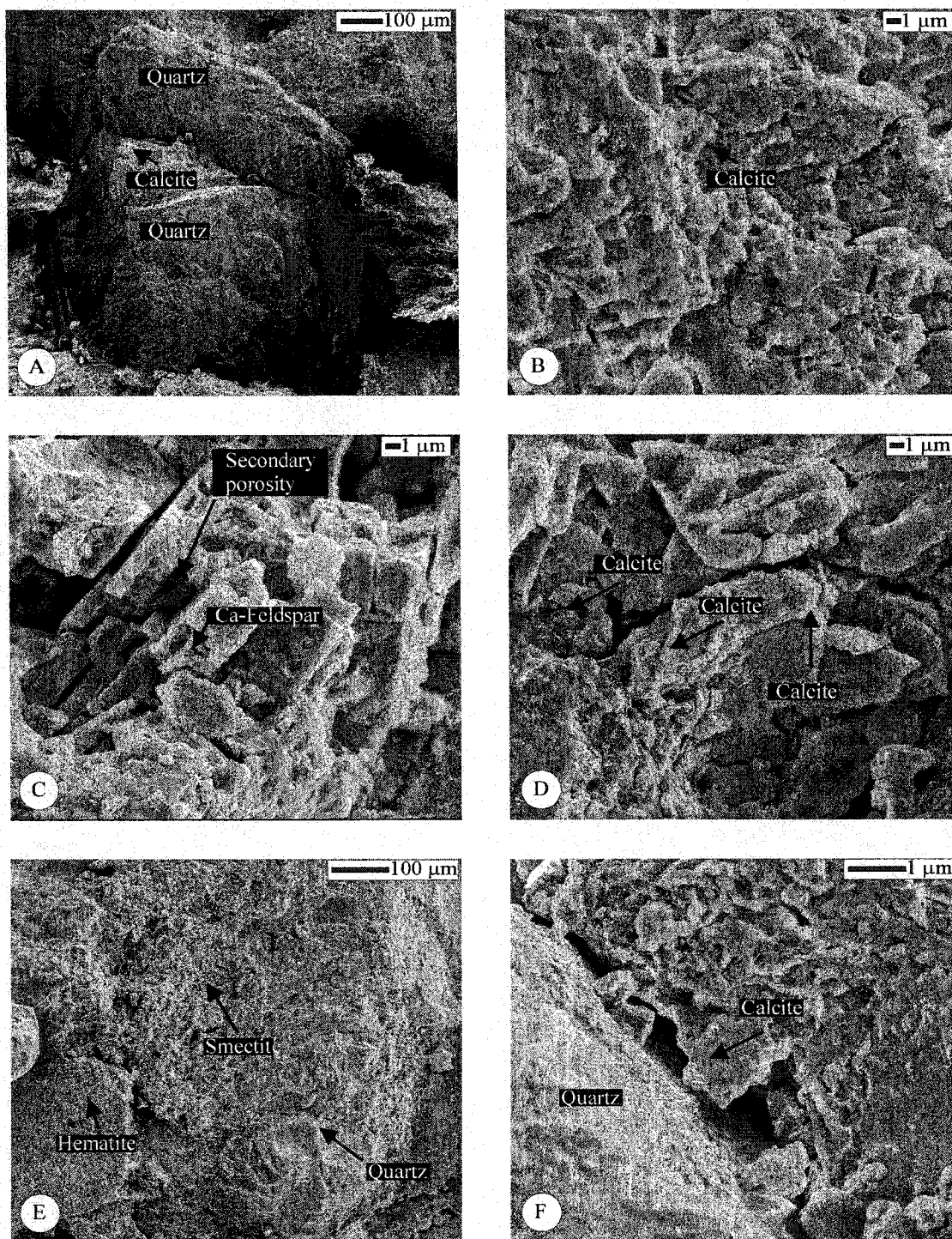
Figure A-41. Scanning electronic photomicrographs: (A) local "island" of calcite (arrow) surrounded by closely packed quartz grains; corrosion may be observed at the grain margins(sample T-2, upper Scollard Formation, Buffalo Jump locality); (B), (D) and (F) late diagenetic calcite dissolution (sample T-2, upper Scollard Formation, Buffalo Jump locality); (C) secondary (dissolution) porosity as seen under the SEM. Note the secondary leaching of the feldspar and the dissolution along the cleavage planes (sample T-1, upper Scollard Formation, Buffalo Jump Park locality); (E) smectite pore filling cement.
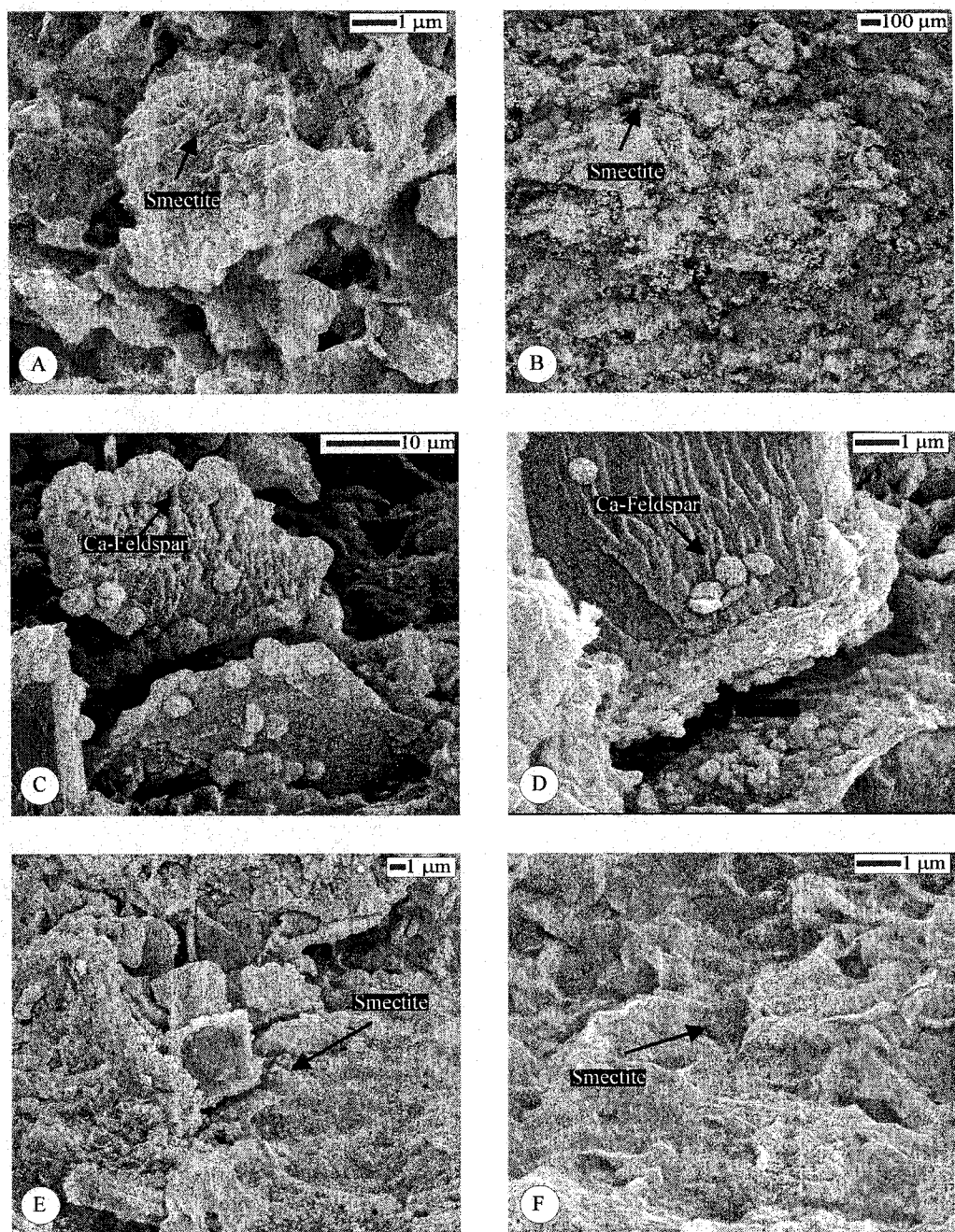
Figure A-42. Scanning electronic photomicrographs: (A), (B), (E) and (F) authigenic smectite showing highly crenulated (sample T-1, upper Scollard Formation, Buffalo Jump locality); (C), and (D) dissolution of Ca-feldspar grain as seen under the SEM (sample T-1, upper Scollard Formation, Buffalo Jump Park locality).
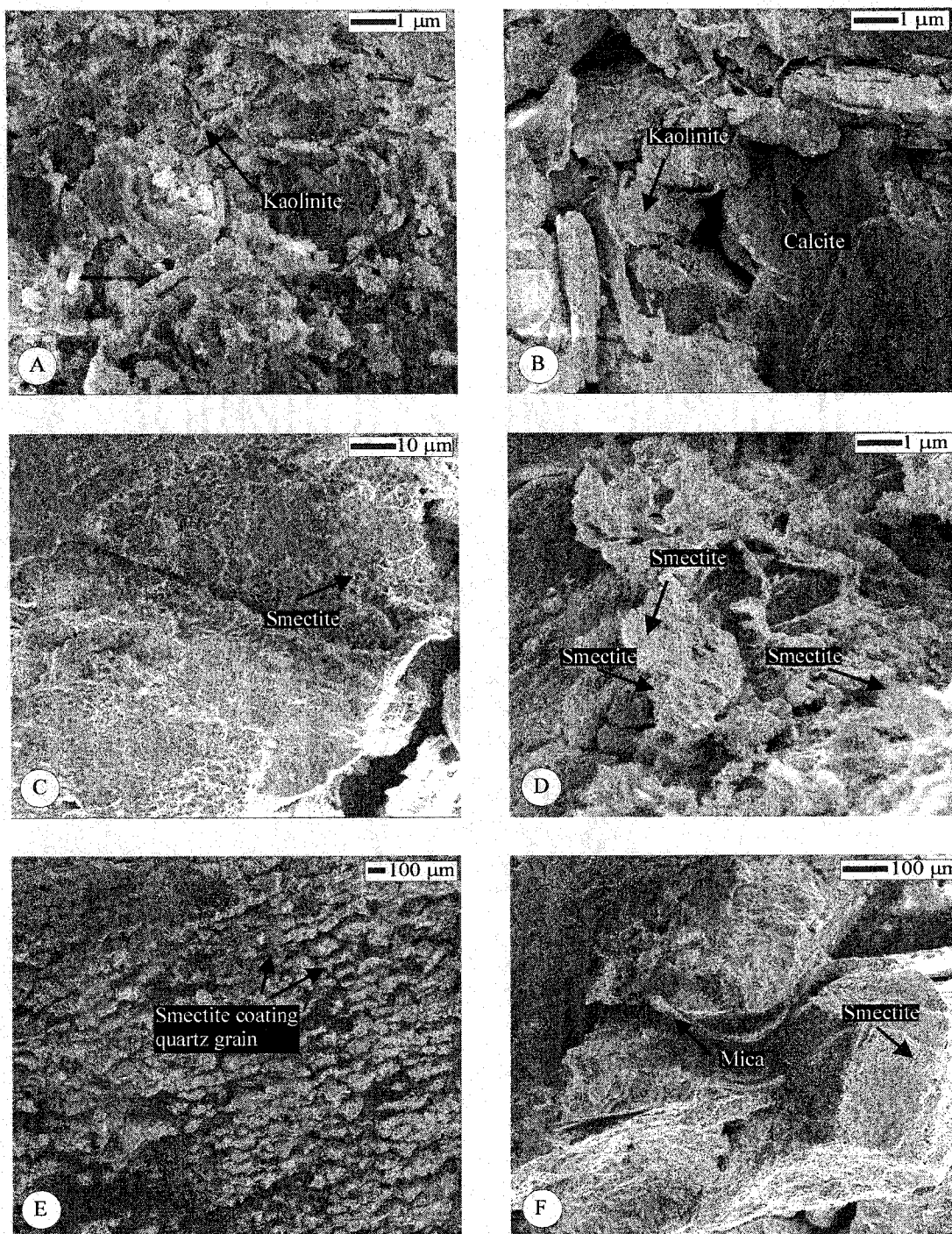
Figure A-43. Scanning electronic photomicrographs: (A), and (B) vermicular aggregates of euhedral crystals of authigenic kaolinite (sample T-1, upper Scollard Formation, Buffalo Jump locality); (C), (D), and (E) authigenic smectite coating quartz grains (sample T-2, upper Scollard Formation, Buffalo Jump Parklocality); (F) mineral deformation (mica) during the early stage of sediment compaction; this results in a decrease in primary porosity (sample T-4, upper Scollard Formation, Buffalo Jump Locality)

180
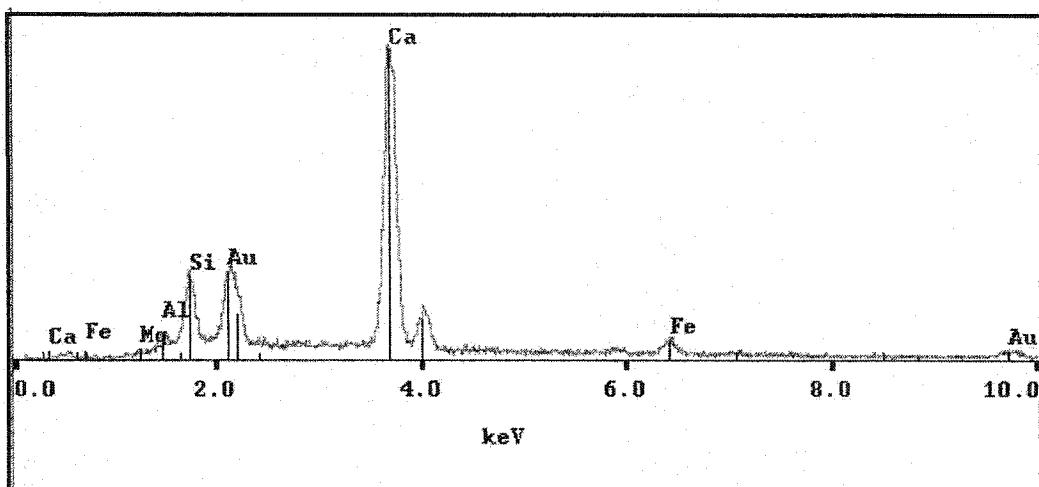
Figure A-44. X-ray diffraction pattern showing the presence of calcite (sample 2, upper Scollard Formation, Buffalo Jump Provincial Park locality).
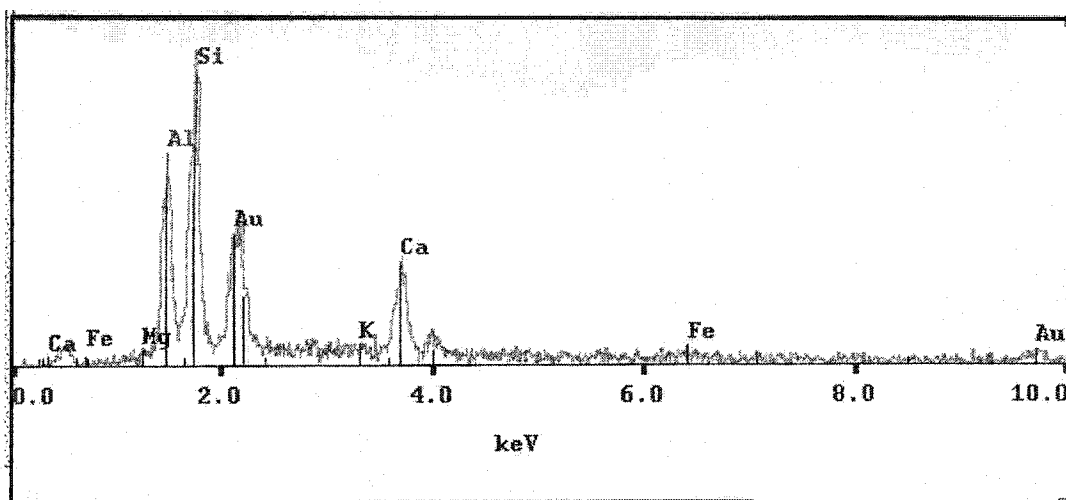
Figure A-45. X-ray diffraction pattern showing the presence of kaolinite (sample 3, upper Scollard Formation, Buffalo Jump Provincial Park locality).
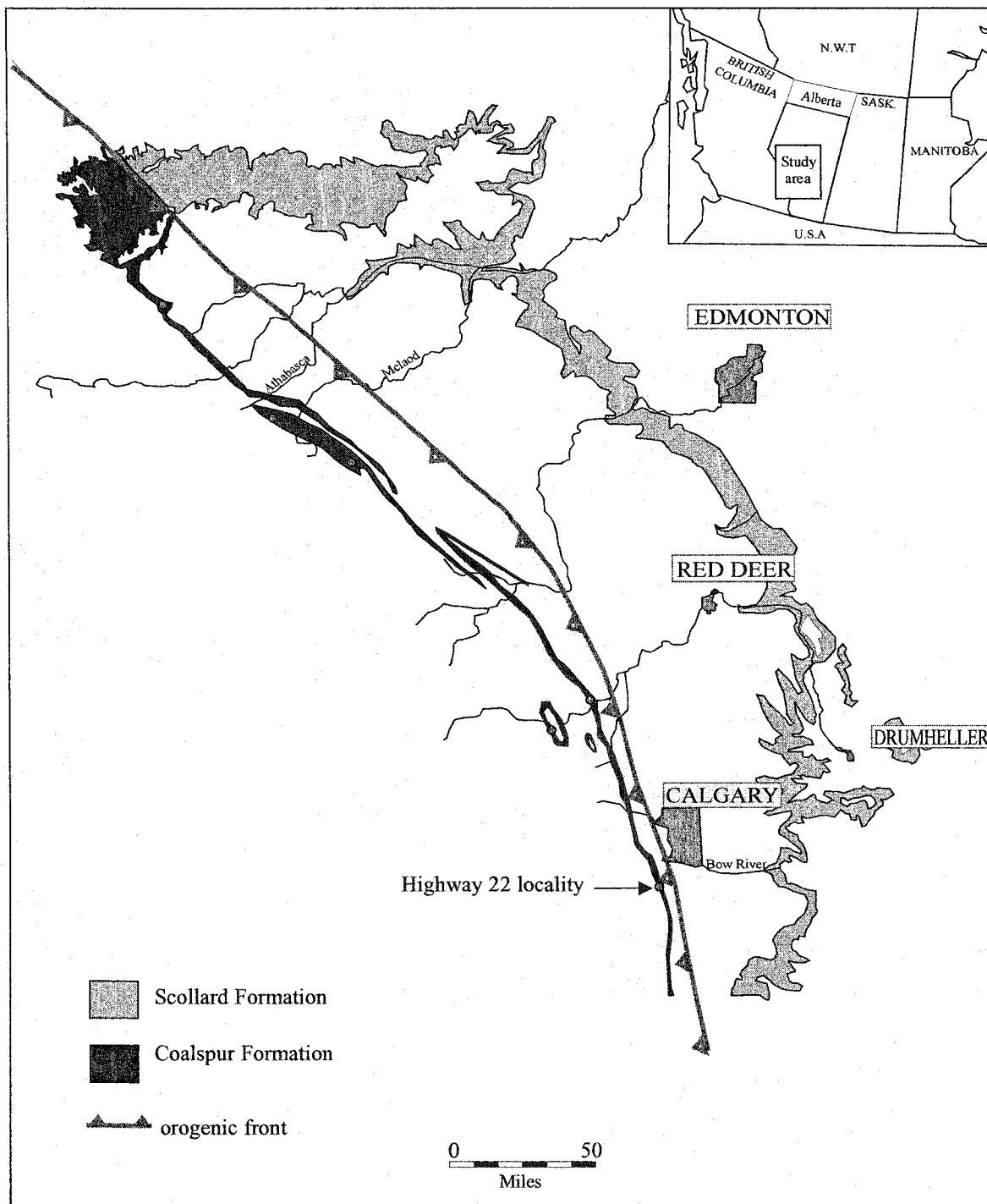
181
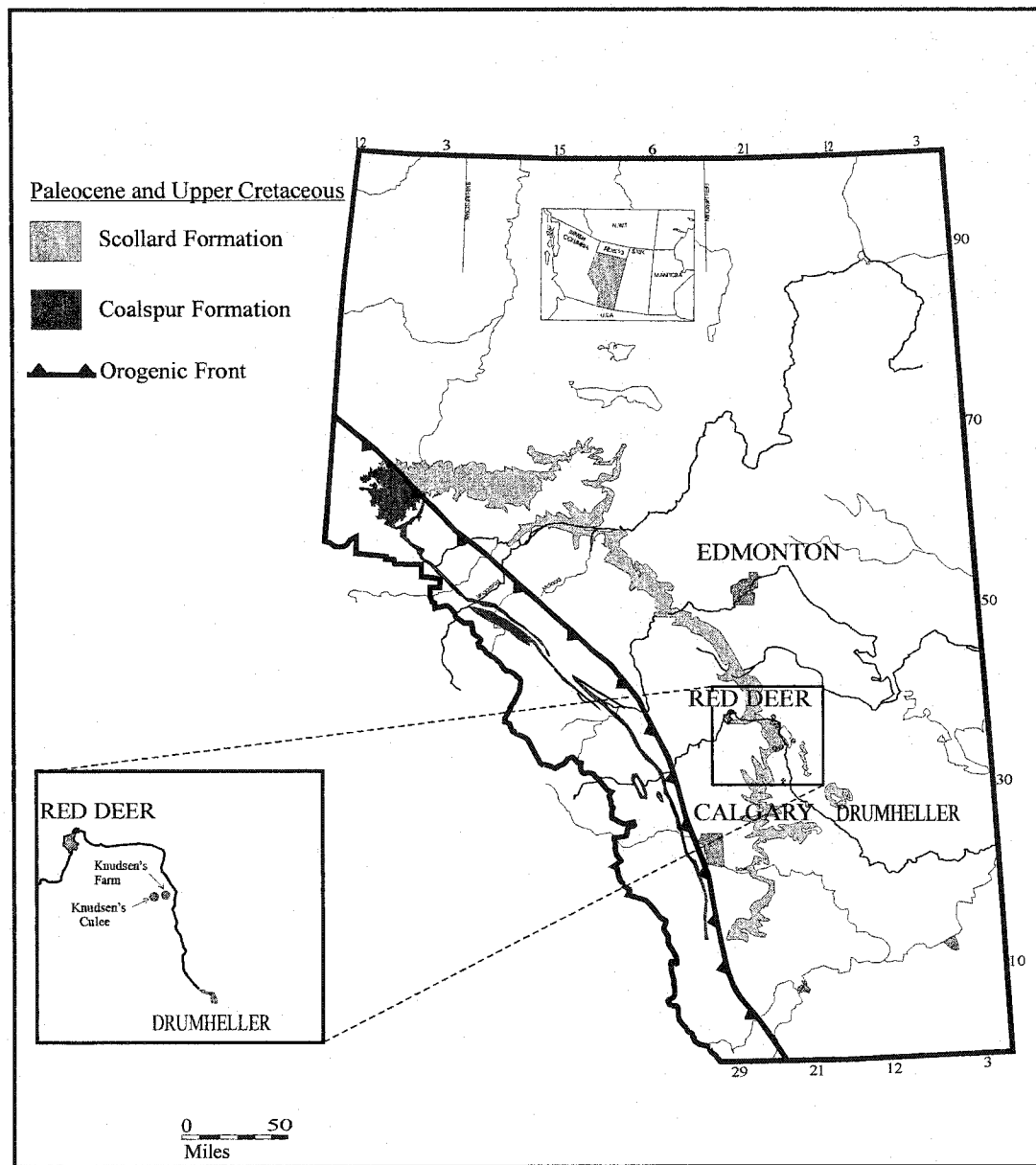
Figure 46. Outcrop distribution of the Scollard and Coalspur formations in Alberta, and the location of the studied outcrop section.
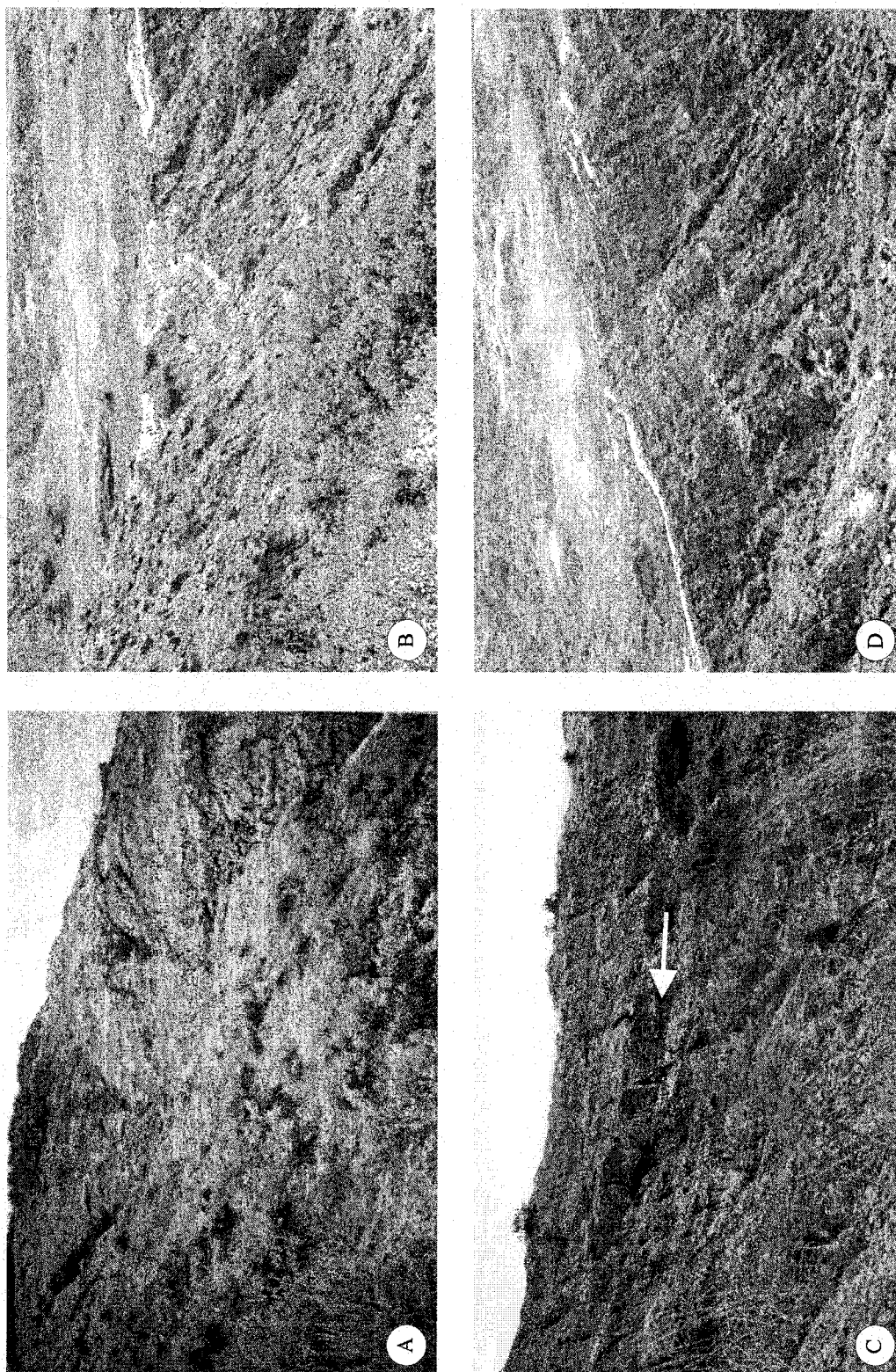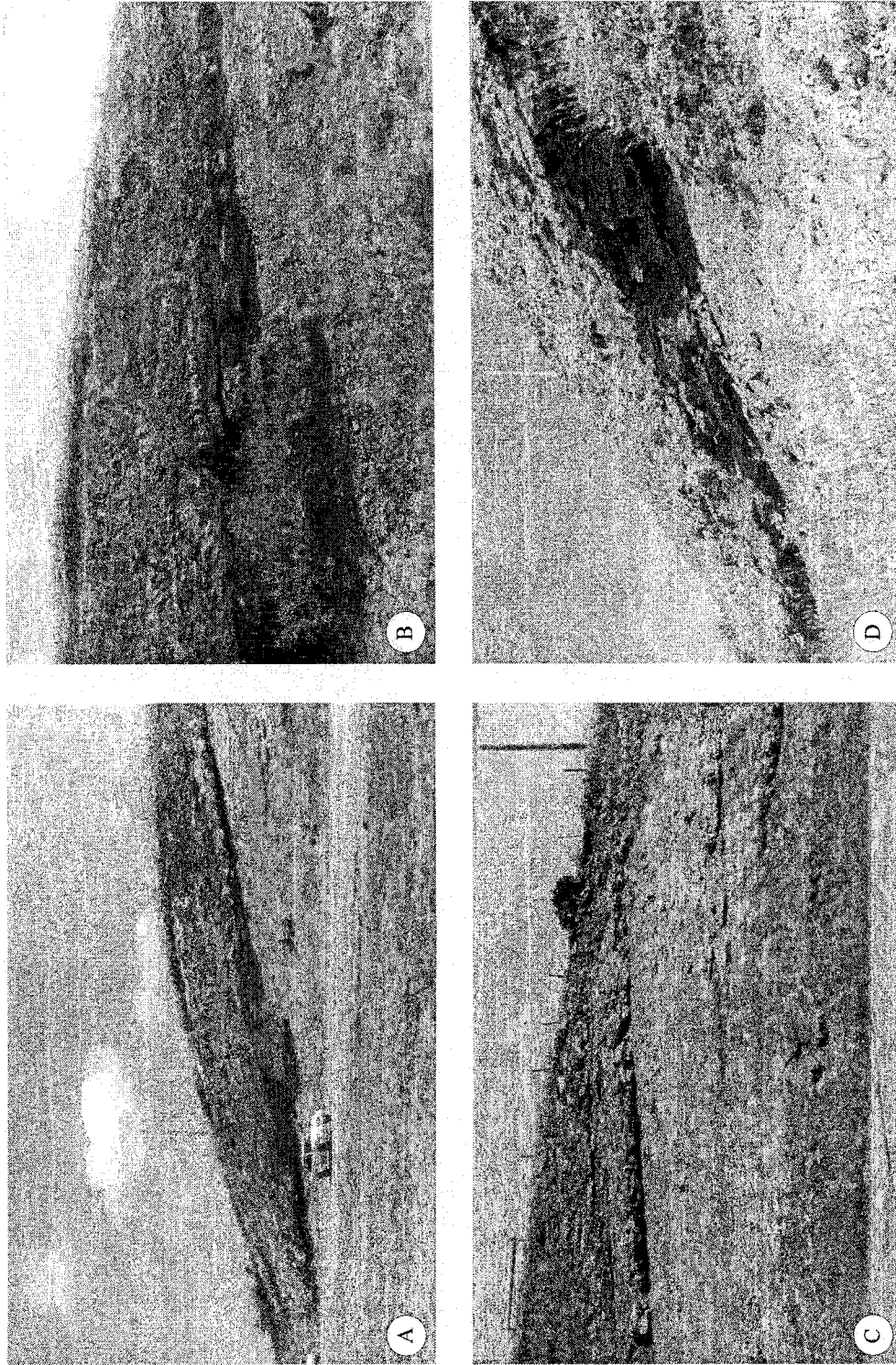
Figure A-47. Outcrop photographs of the upper Scollard Formation, Knudsen's Farm locality: (A), (B) and (D) outcrop photographs showing overbank deposits of fluvial channels; (C) sandstone bed interpreted as crevasse channel (arrow).
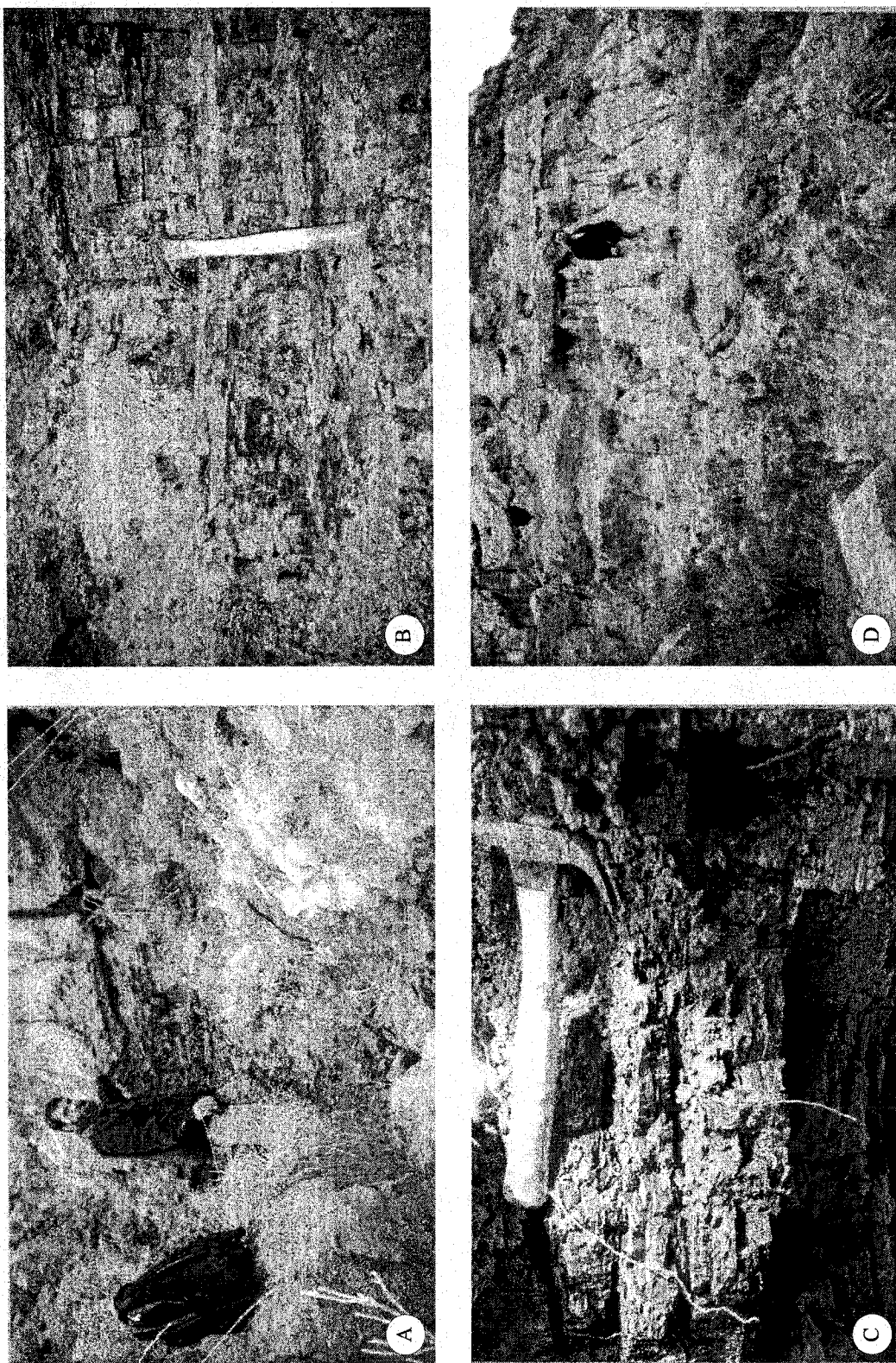
Figure A-48. Outcrop photographs of the upper Scollard Formation, Knudsen's Farm locality: (A), (B) and (C) outcrop photographs showing Ardley coal seam; (D) overbank deposits of fluvial channels.

184
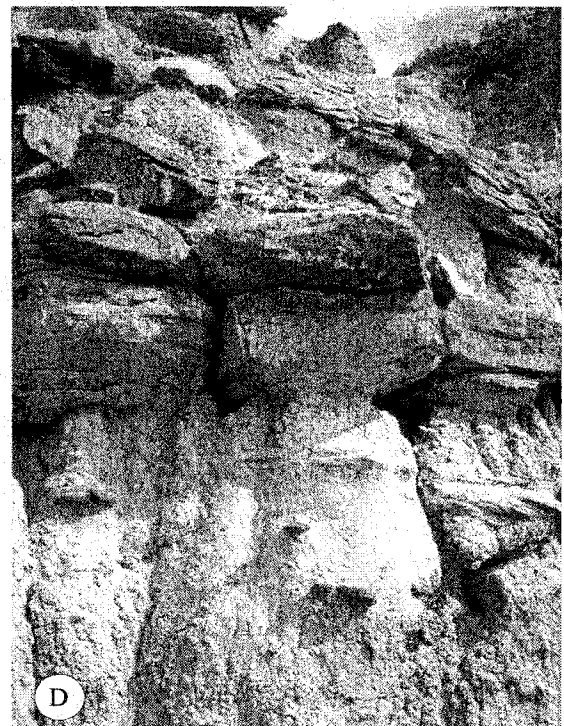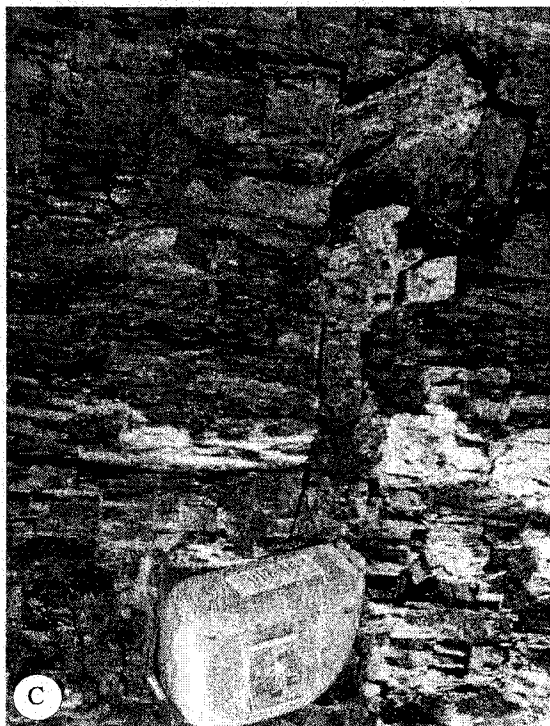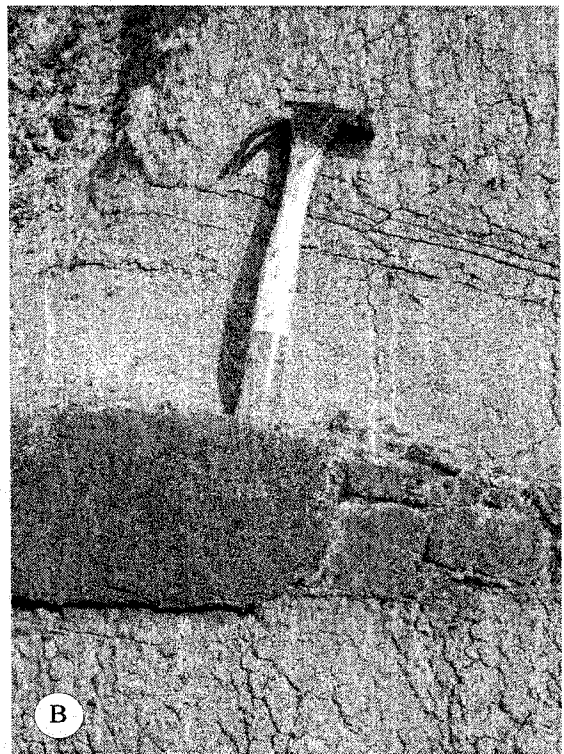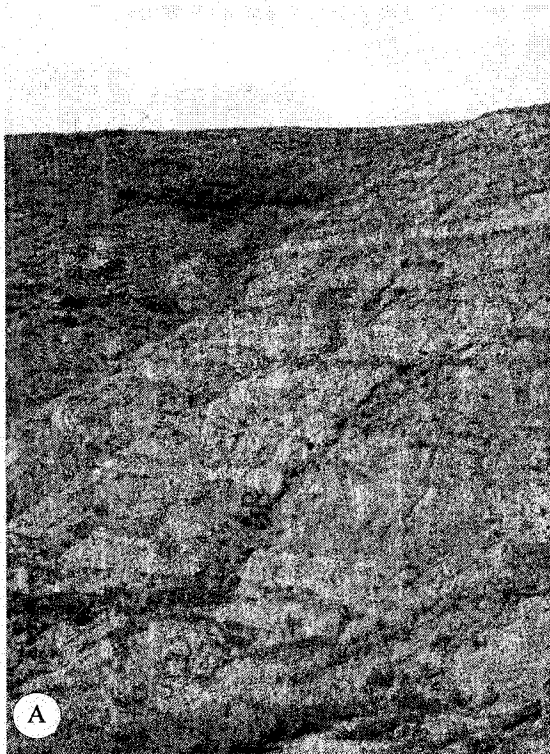
Figure A-49. Outcrop photographs of the upper Scollard Formation, Knudsen's Farm locality: (A) outcrop photographs showing overbank deposits of meander channels; (B) close-up view of sandstone bed showing planner cross bedding; (C) close-up view of Ardley coal seam; (D) crevasse splay deposits.

185

Figure A-50. Outcrop photographs of the upper Scollard Formation, Knudsen's Farm locality showing the presence of coaly bed within the upper Scollard Formation.
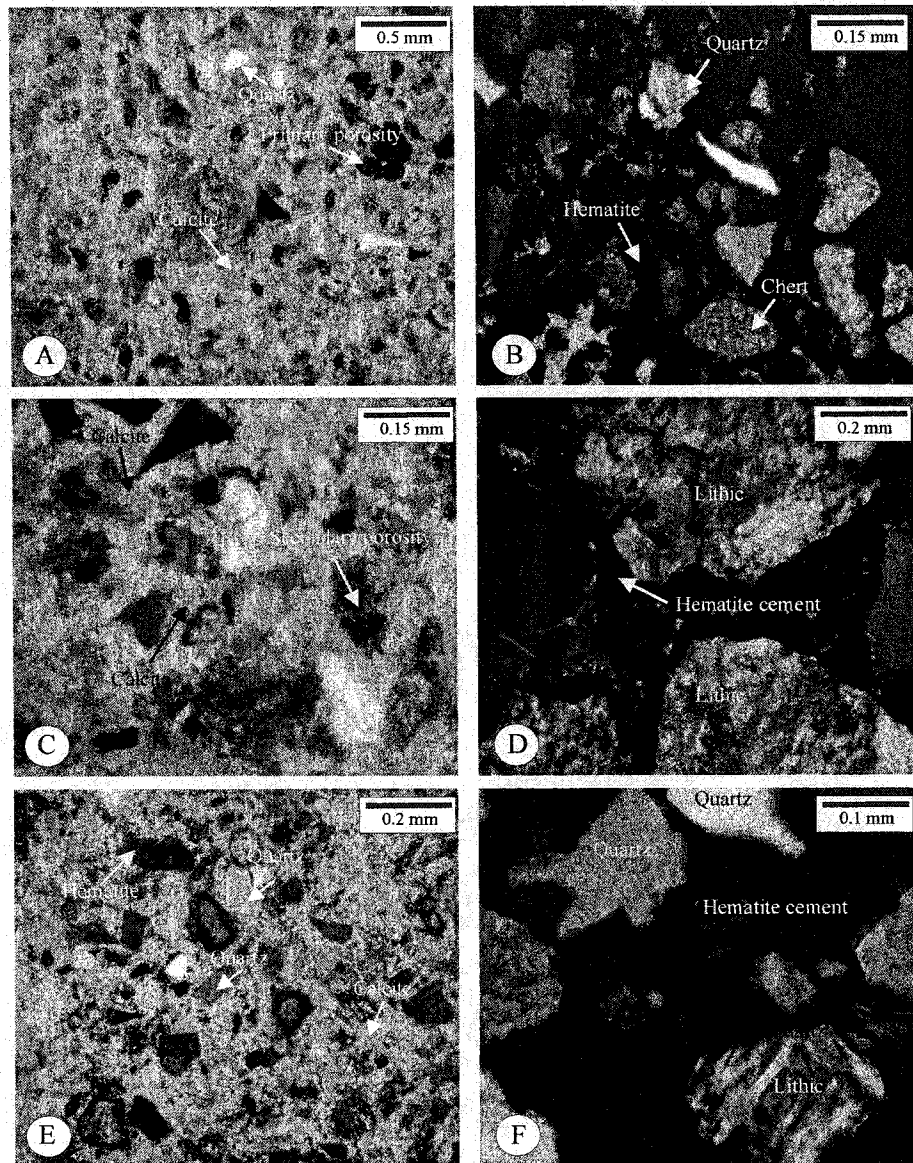
Figure A-51. Thin-section photomicrographs: (A), (C) and (E) quartz grain corroded by early poikilotopic calcite cement. Note residual primary porosity (sample K-9, upper Scollard Formation, Knudsen's Farm locality); (B), (D)and (F) litharenite from the Knudsen's Farm locality, with chert and igneous lithoclasts, cemented by hematite.
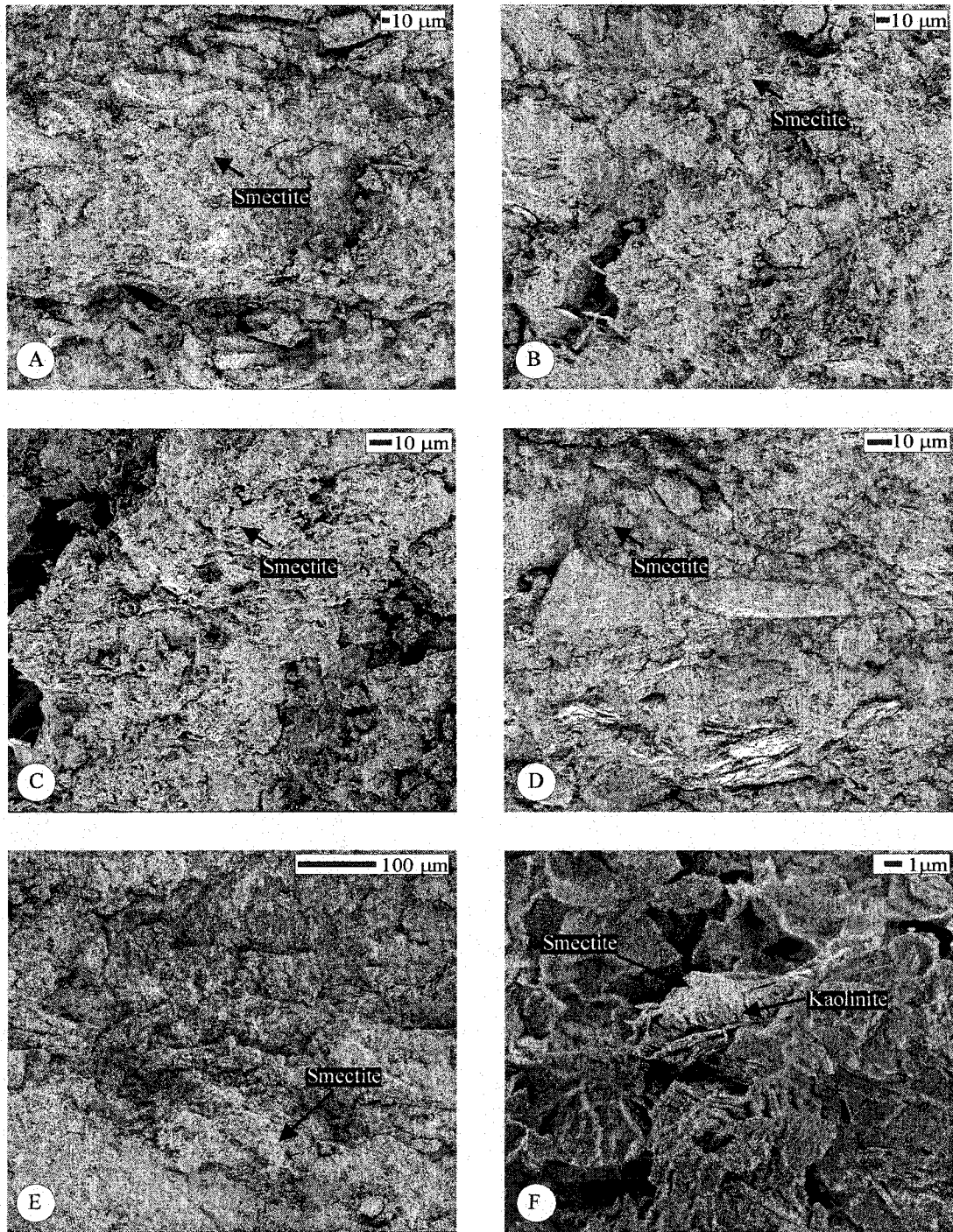
Figure A-52. Scanning electronic photomicrographs: (A), (B), (C), (D) and (E) authigenic smectite coating sandstone grains; (F) booklet shape of vermicular authigenic kaolinite covered by authigenic smectite (sample K-5, upper Scollard Formation, Knudsen's Farm locality).
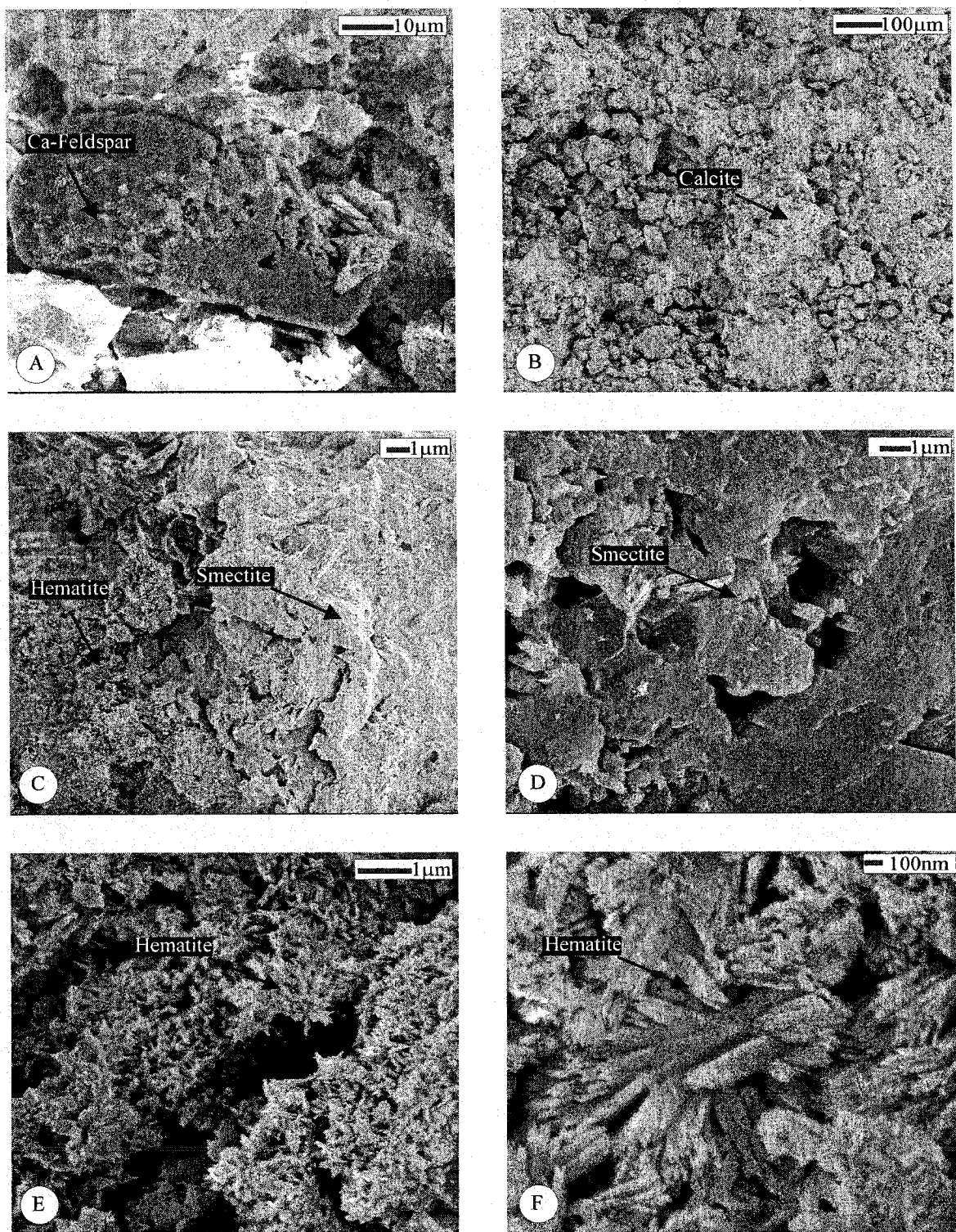
Figure A-53. Scanning electronic photomicrographs: (A) dissolution of feldspar grains followed by partial replacement with calcite (arrows) (sample K-8, upper Scollard Formation, Knudsen's Farm locality); (B) Scanning electronic photomicrographs of sandstone rock cemented by calcite(sample K-9, upper Scollard Formation, Knudsen's Farm locality); (C) non-authigenic smectite.Note late diagenetic hematite (sample K-4 , upper Scollard Formation, Knudsen's Farm locality);(E) and (F) late diagenetic needle like hematite (sample K-5, upper Scollard formation, Knudsen's Farm locality).
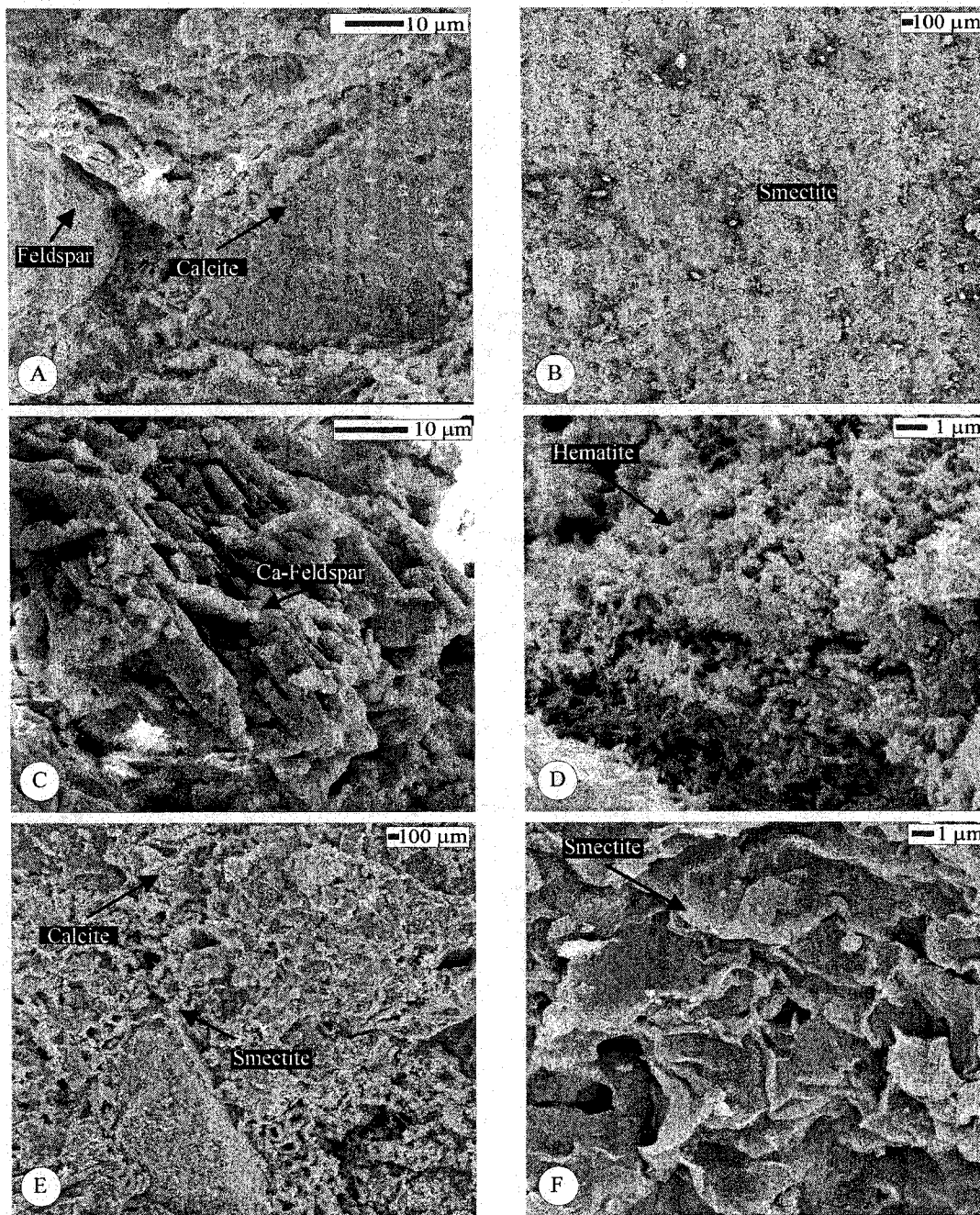
Figure A-54. Scanning electronic photomicrographs: (A) feldspar grains coated by calcite (arrows) (sample K-9, upper Scollard Formation, Knudsen's Farm locality); (B) Scanning electronic photomicrographs of sandstone sample cemented by smectite; (C) dissolution of feldspar grain (sample K-7, upper Scollard Formation, Knudsen's Farm locality); (D) late diagenetic needle like hematite (sample K-5, upper Scollard Formation, Knudsen's Farm locality); (E) non-authigenic smectite and dominate calcite cement (sample K-8, upper Scollard Formation, Knudsen's Farm locality); (F) authigenic smectite showing highly crenulated,honeycombed, and interlocking crystal shapes (sample K-9, upper Scollard Formation, Knudsen's Farm locality).
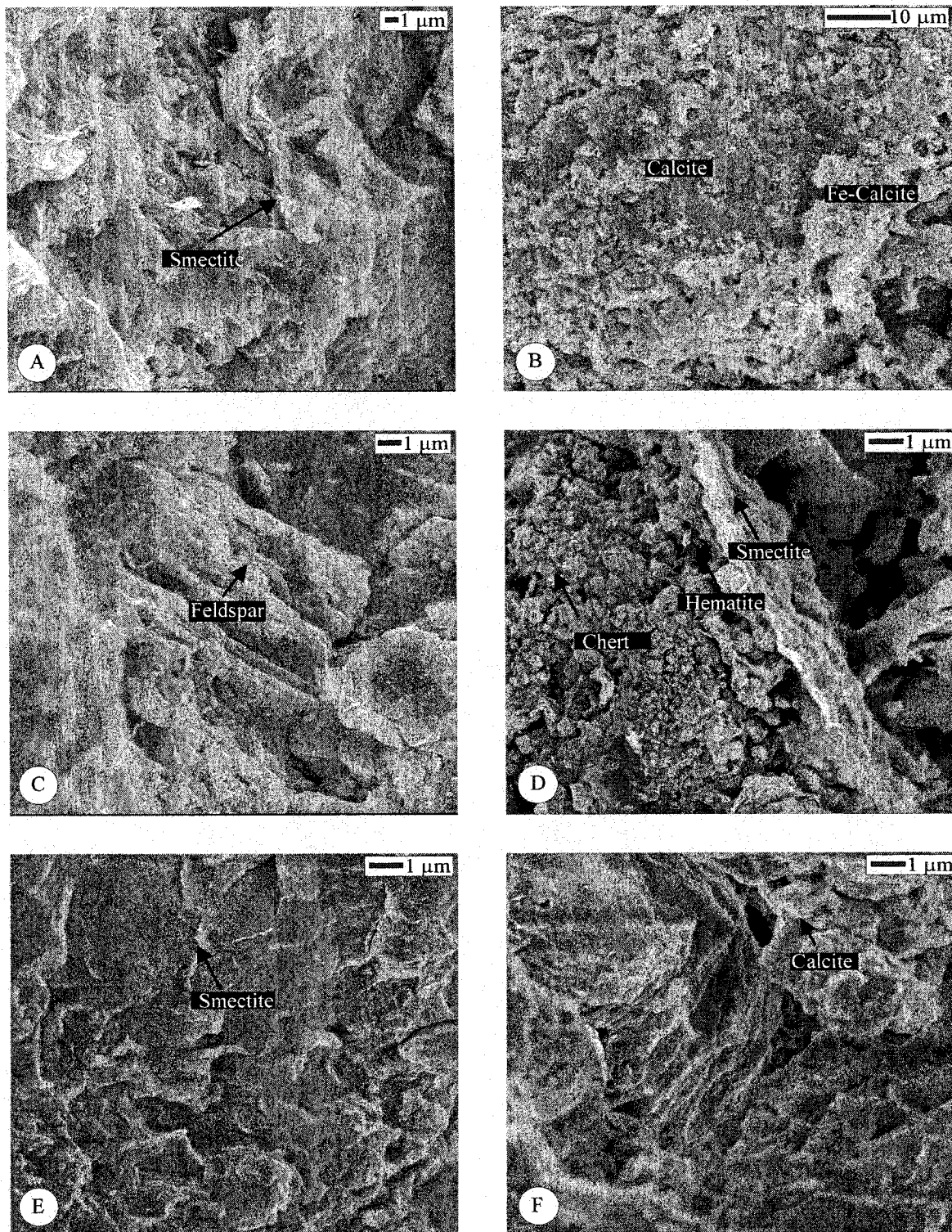
Figure A-55. Scanning electronic photomicrographs: (A) and (E) authigenic smectite showing highly crenulated, honeycombed, and interlocking crystal shapes (sample K-9, upper Scollard Formation, Knudsen's Farm locality); (B) and (F) Fe-rich calcite cement, as determined by XRD analysis (sample K-8, upper Scollard Formation, Knudsen's Farm locality); (D) chert grain coated by smectite (sample K-8, upper Scollard Formation, Knudsen's Farm locality).
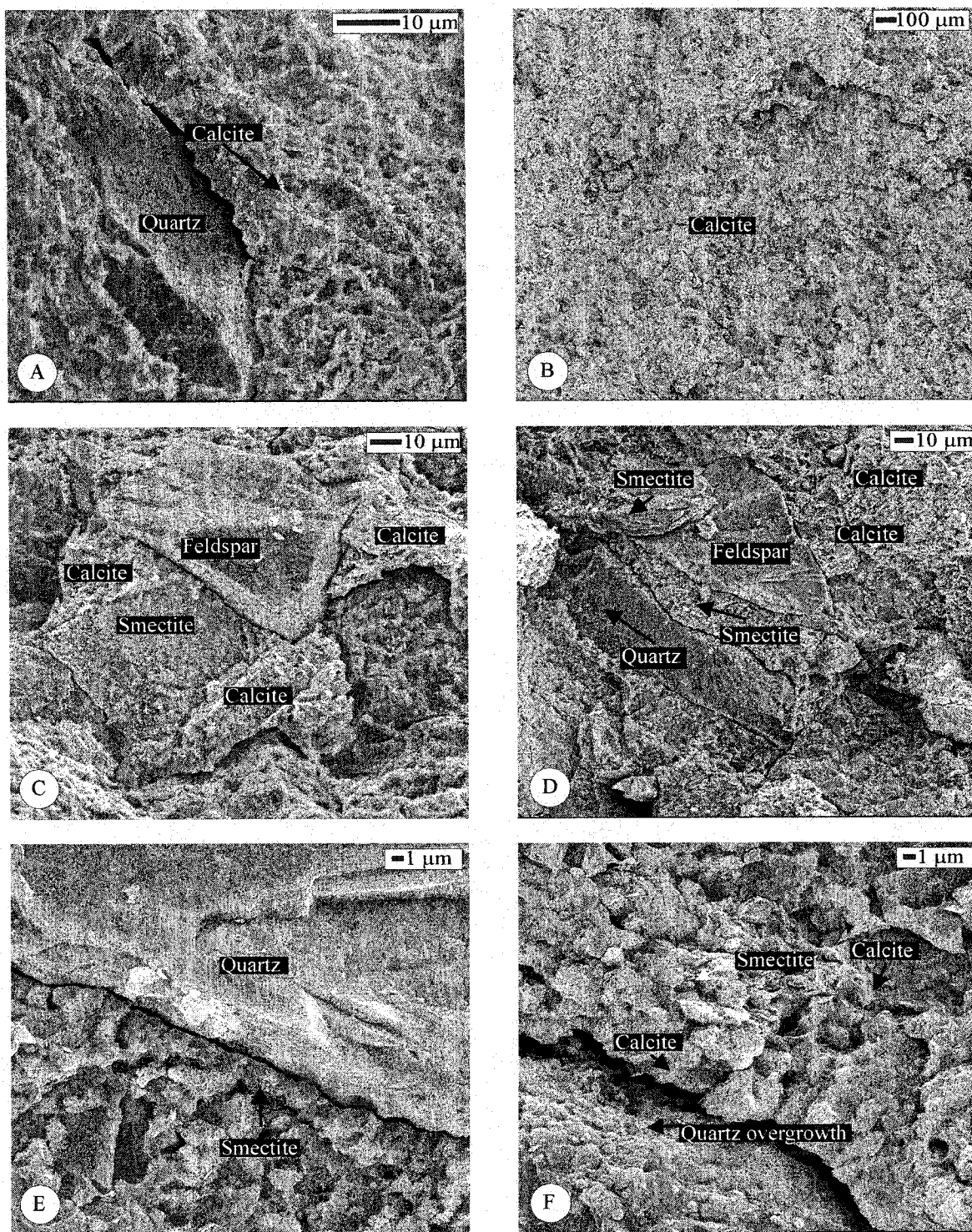
Figure A-56. Scanning electronic photomicrographs: (A) quartz grain coated by early poikilotopic calcite cement (sample K-9, upper Scollard Formation, Knudsen's Farm locality); (B) calcite cement (sample K-9, upper Scollard Formation, Knudsen's Farm locality); (C) calcite cement that invaded the clay-filled pore space and engulfed the smectite (sample K-9, upper Scollard Formation, Knudsen's Farm locality); (D) and (E) smectite pore filling cement (sample K-9, upper Scollard Formation, Knudsen's Farm locality); (F) late stage of quartz overgrowth, post-dating the precipitation of the calcite cement (sample K-7, upper Scollard Formation, Knudsen's Farm locality).

192
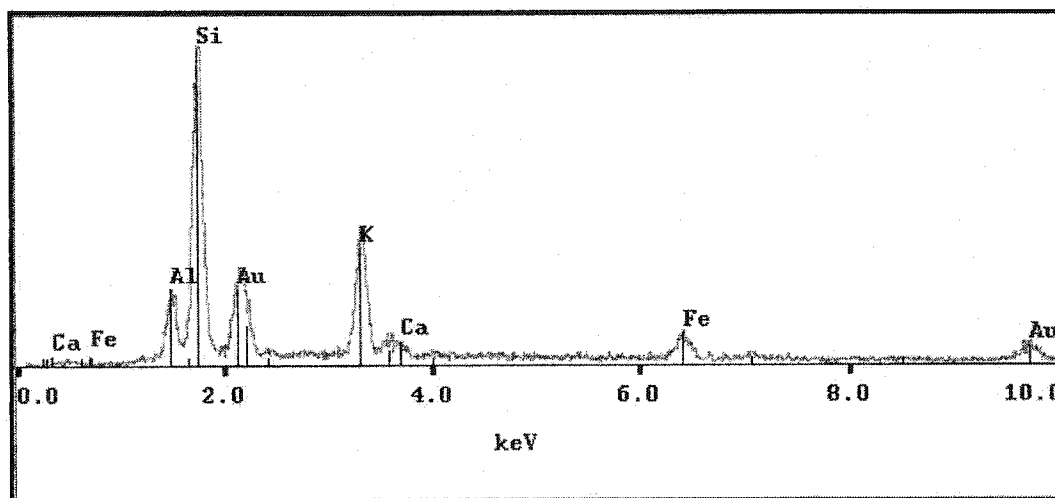
Figure A-57. X-ray diffraction pattern showing the presence of illite (sample 1, upper Scollard Formation, Knudsen's Coulee locality).
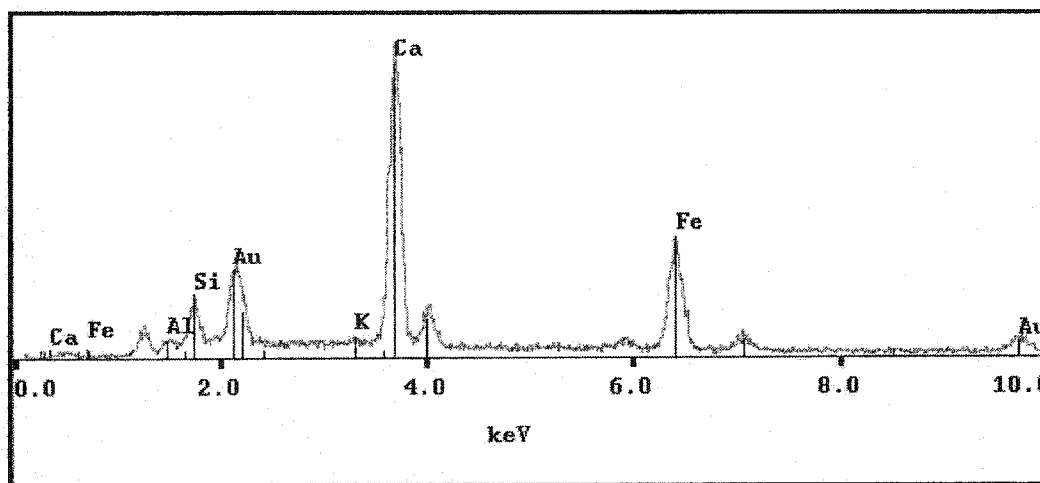
Figure A-58. X-ray diffraction pattern showing the presence of Fe-calcite cement (sample 2, upper Scollard Formation, Knudsen's Coulee locality).
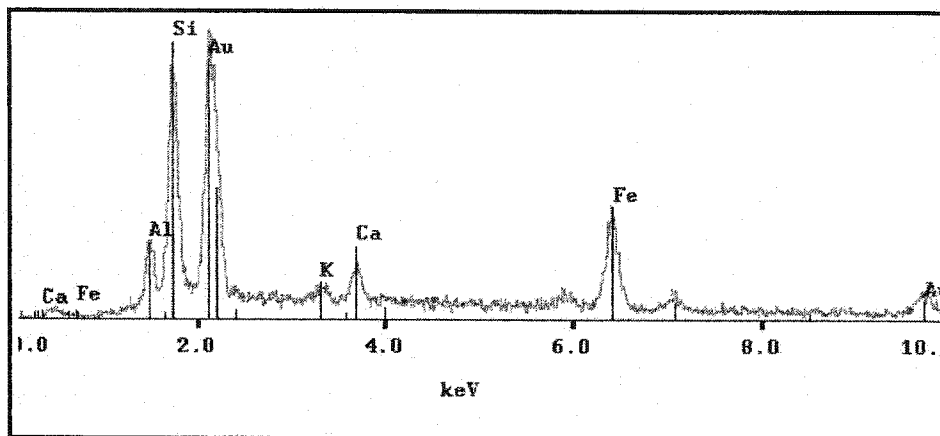
Figure A-59. X-ray diffraction pattern showing the presence of smectite (sample 9, upper Scollard Formation, Knudsen's Coulee locality).

Figure A-60. X-ray diffraction pattern showing the presence of smectite (sample 8, upper Scollard Formation, Knudsen's Coulee locality).
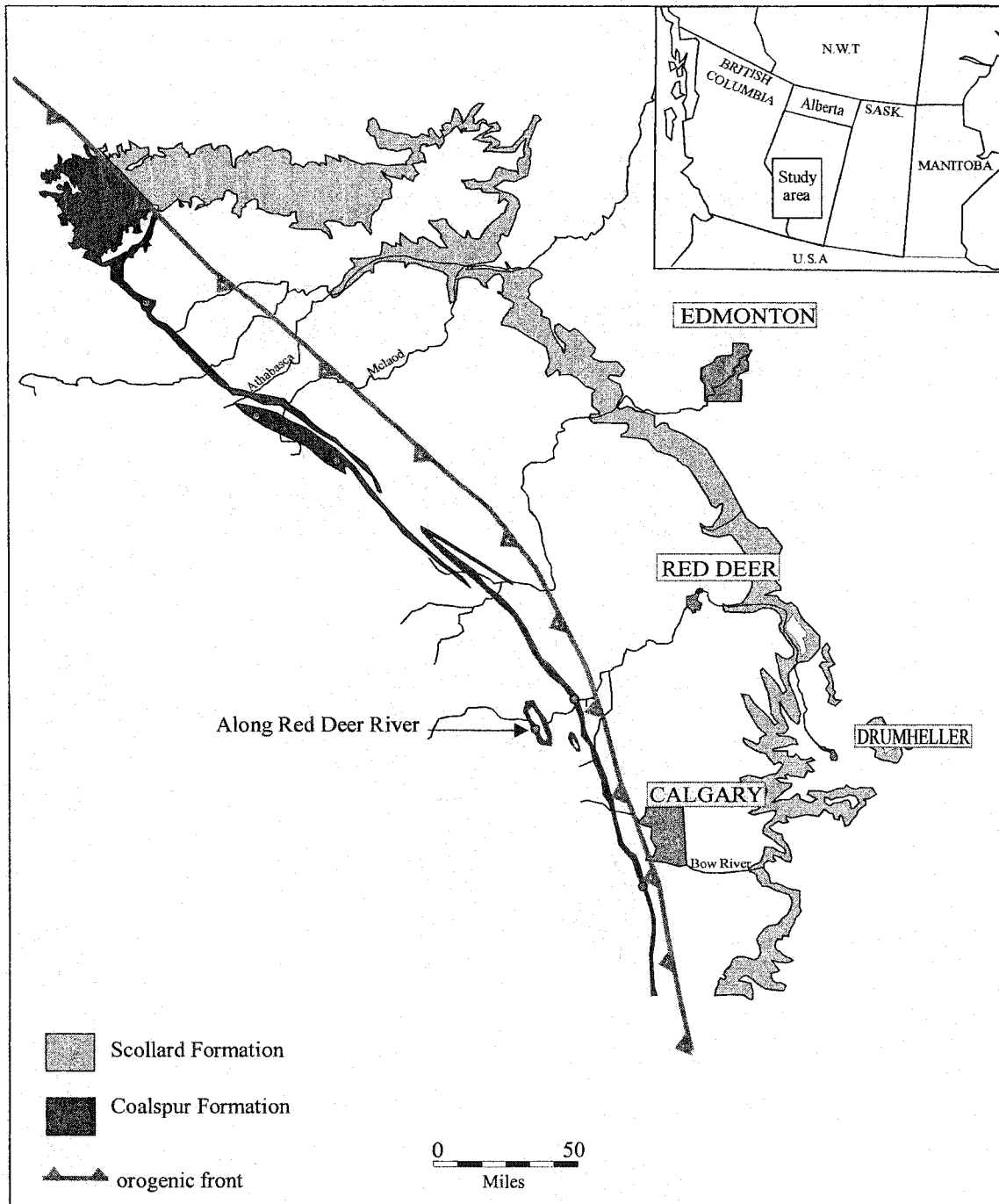
194

Figure 61. Outcrop distribution of the Scollard and Coalspur formations in Alberta, and the location of the studied outcrop section

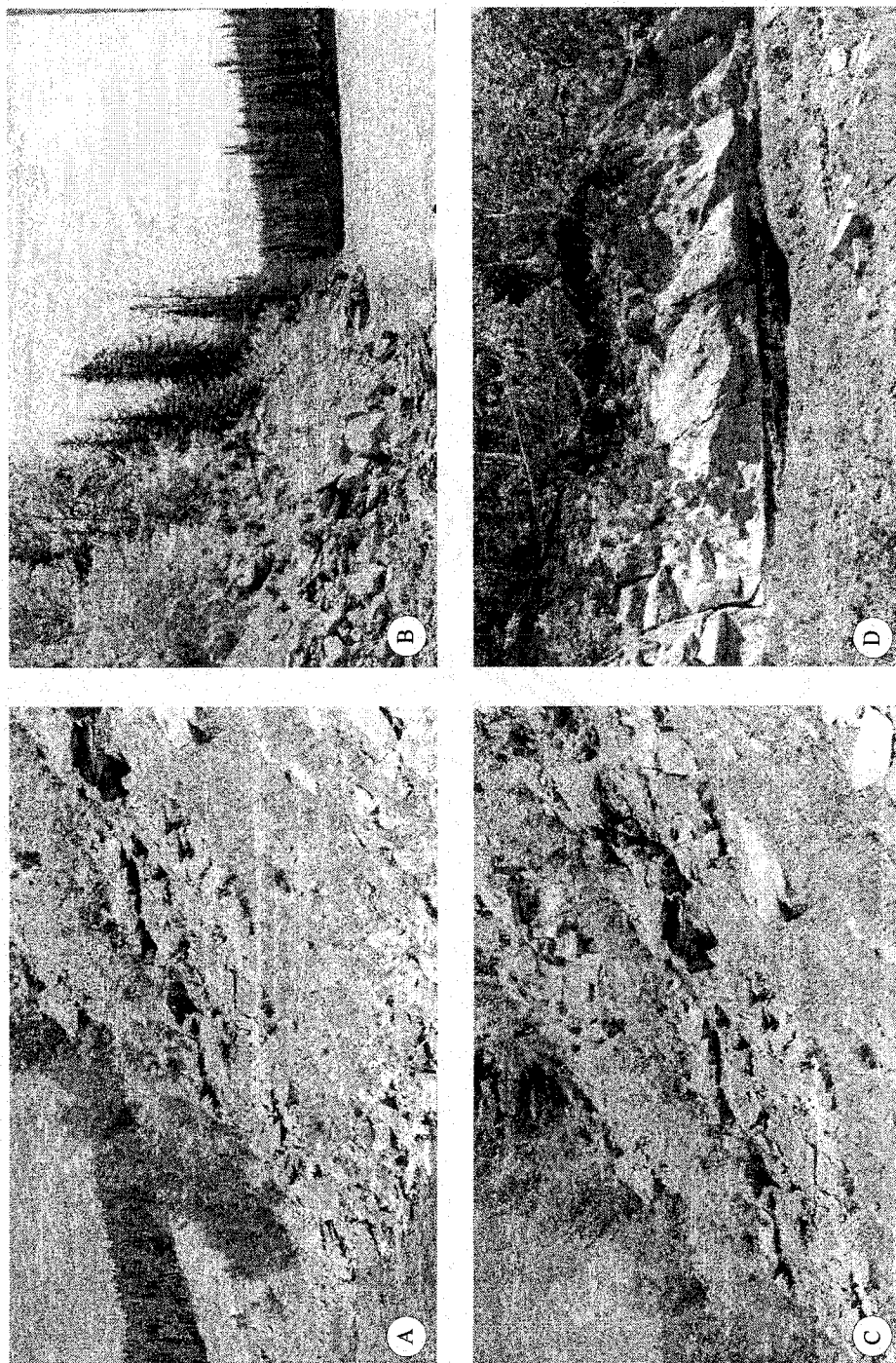Figure A-62. (A), (B) and (C)- Outcrop photographs of the upper Scollard Formation, Ardley locality showing Ardley coal zone (arrows); (D) - outcrop photograph showing the upper contact between the Scollard and Paskapoo formations (arrow).
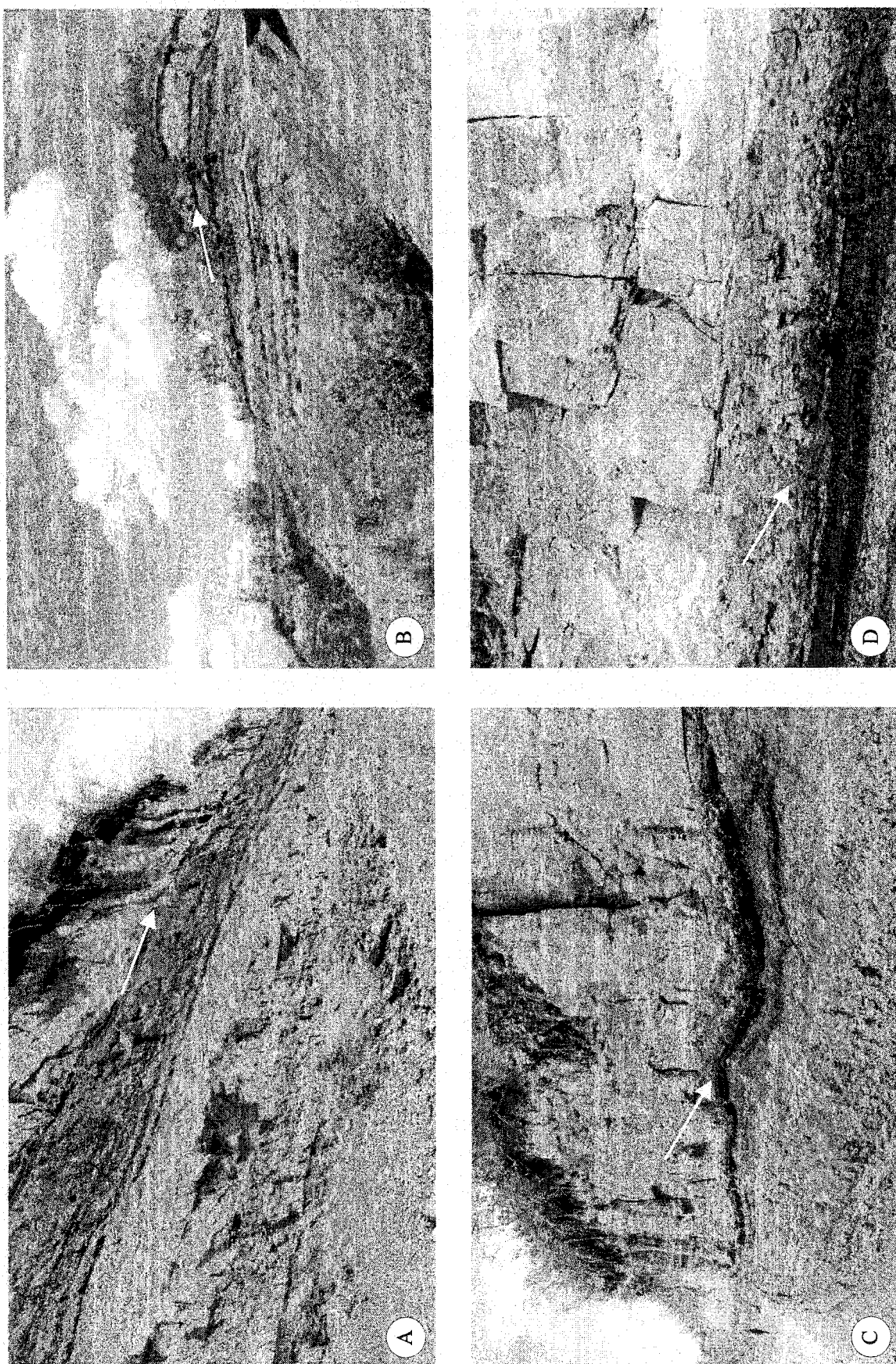
Figure A-63. Outcrop photographs of the upper Scollard Formation, Ardley locality showing the upper contact between the Scollard and Paskapoo formations (arrows).

197
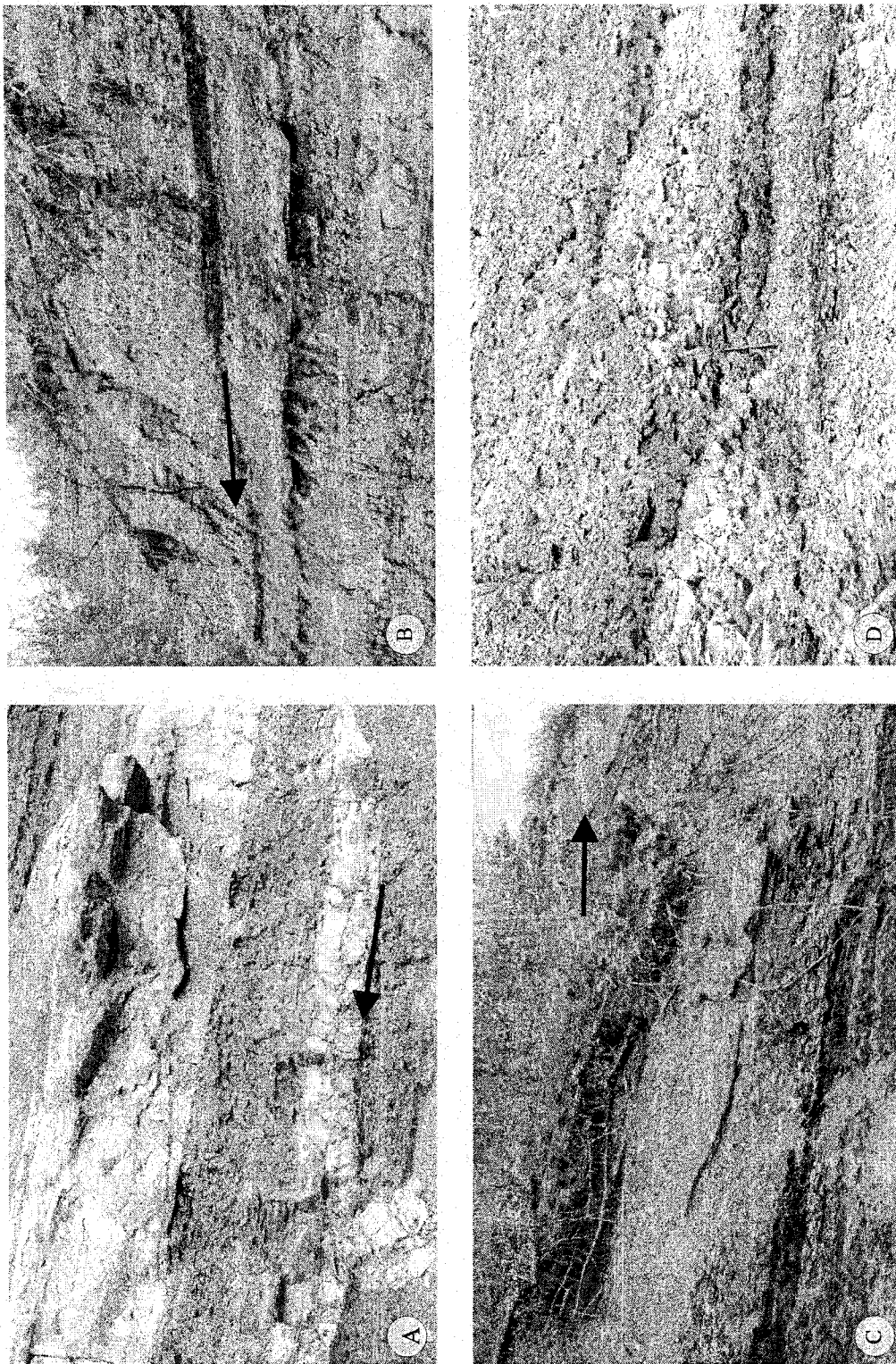
Figure A-64. Outcrop photographs of the upper Scollard Formation, Ardley locality: (A), (B) and (C) outcrop photographs showing the upper contact between the Scollard and Paskapoo formations (arrows); (D) Coal seam interbedded with siltstone beds.
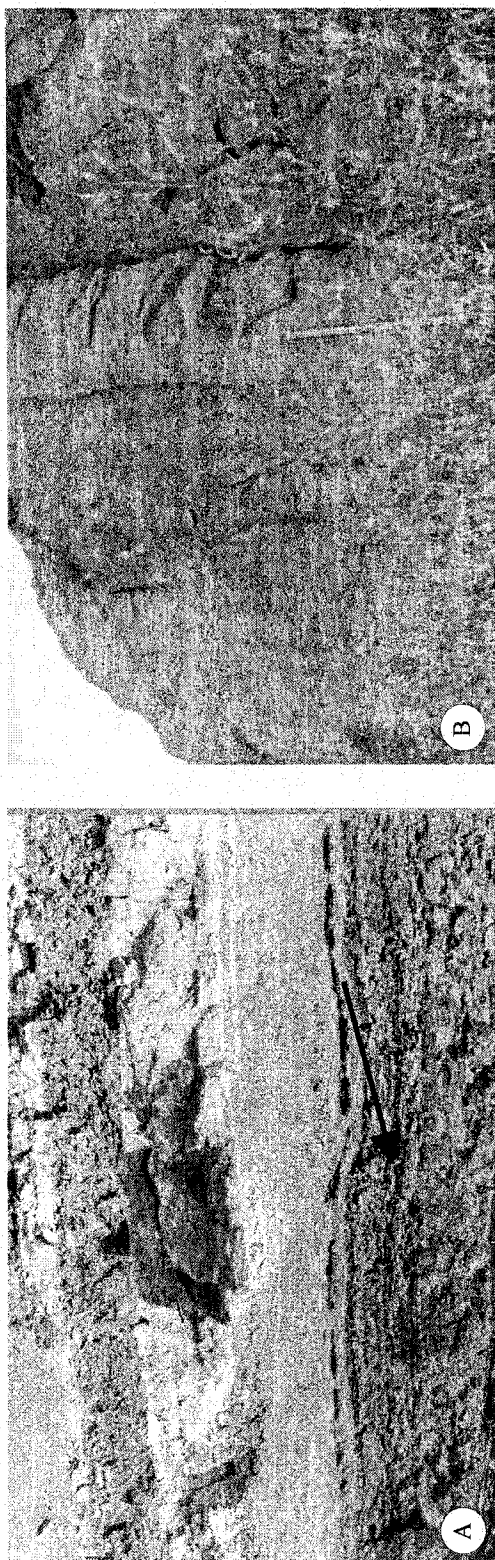
Figure A-65. Outcrop photographs of the upper Scollard Formation, Ardley locality: (A) the last coal seams in the upper Scollard formation (arrow) (B) thick sandstone bed of the Paskapoo Formation.
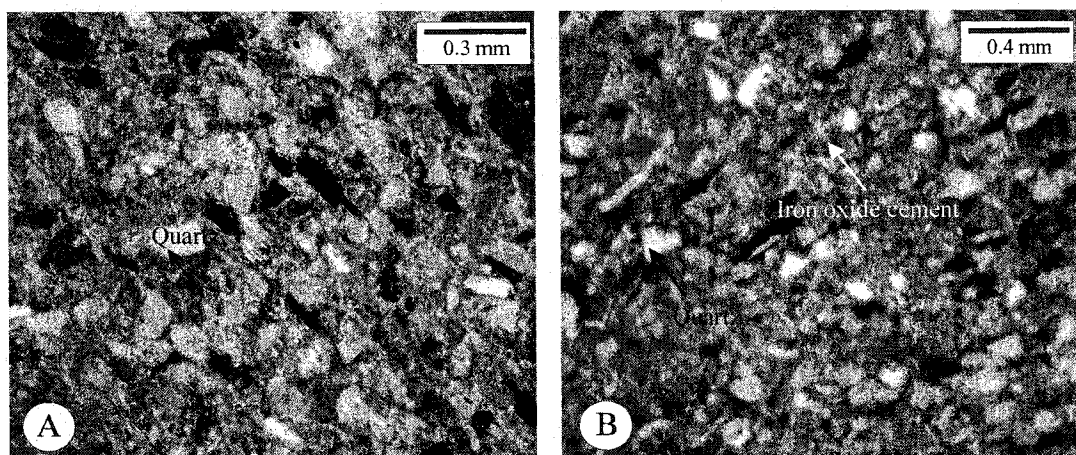
Figure A-66. Thin-section photomicrographs showing quartz arenite sandstone and iron cement (sample A-1, upper Scollard Formation, Ardley locality).
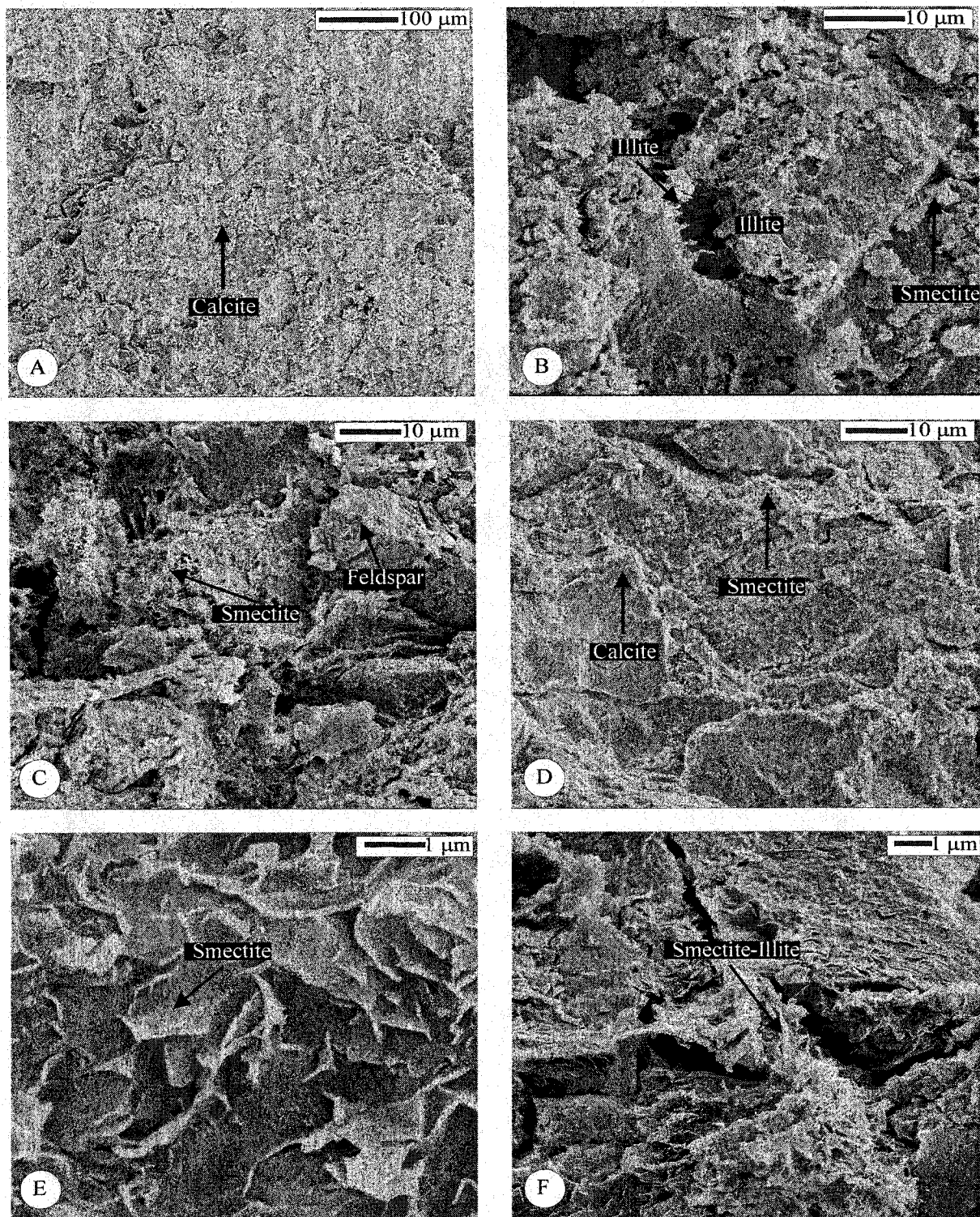
Figure A-67. Scanning electronic photomicrographs: (A) calcite cement (sample A- 2 upper Scollard Formation, Ardley locality); (B) alteration of smectite into illite (sample A-1, upper Scollard Formation, Ardley locality); © feldspar alteration to smectite (sample A-2, upper Scollard Formation, Ardley locality); (D) calcite cement that invaded the clay-filled pore space and engulfed the smectite (sample A-3, upper Scollard Formation, Ardley locality); (E)authigenic smectite pore filling cement (sample A-1, upper Scollard Formation, Ardley locality); (F) mixed layer illite-smectite (sample A-2, upper Scollard Formation, Ardley locality).

201
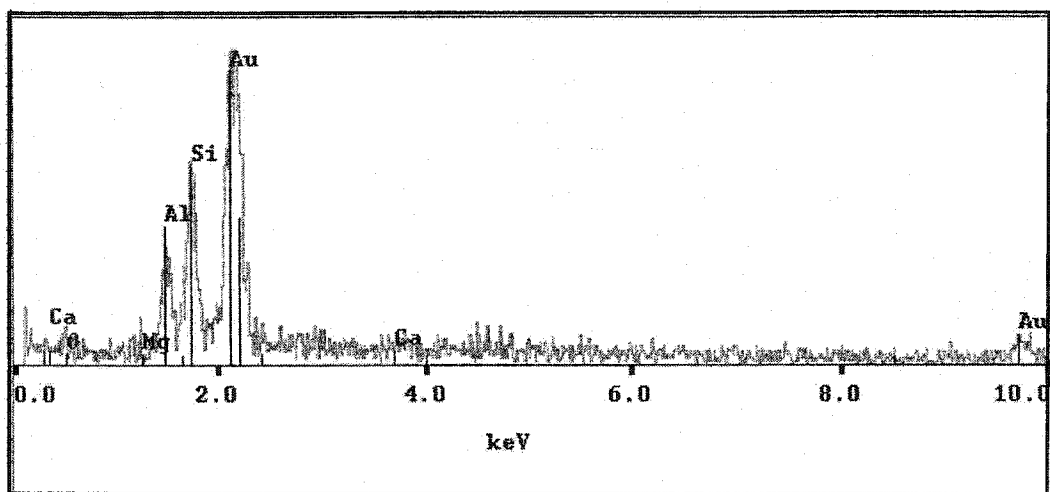
Figure 68. X-ray diffraction pattern showing the presence of kaolinite (sample A-2, upper Scollard Formation, Ardley locality)

Appendix B: outcrop photographs, thin section photographs, scanning electronic photography, and x-ray diffraction pattern from the Coalspur Formation sandstones.

Figure B-1. Outcrop distribution of the Scollard and Coalspur formations in Alberta, and the location of the studied outcrop section.

204

Figure B-2. Outcrop photographs of the Entrance Member, roadcut on highway No. 22.
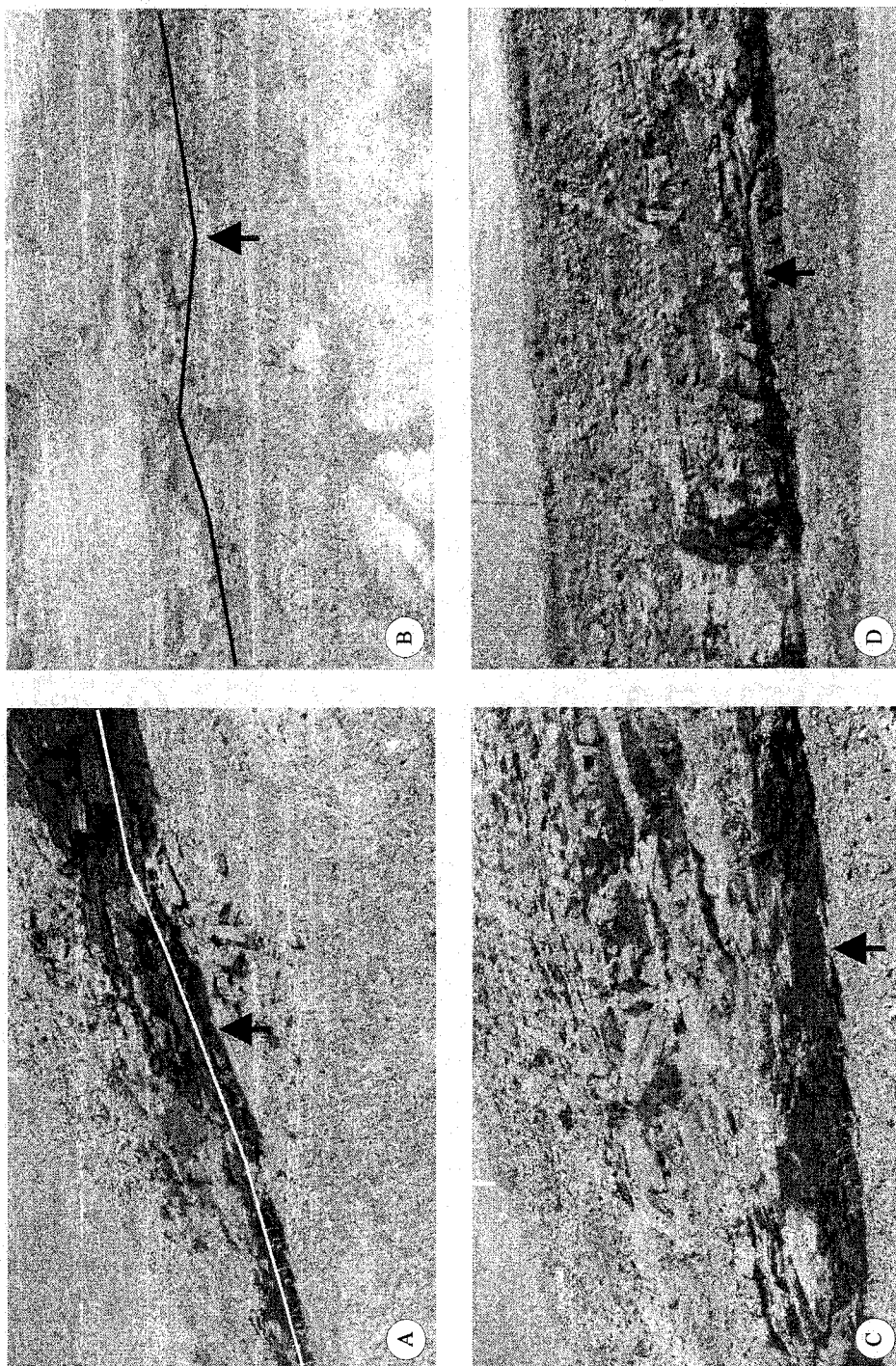
Figure B-3. Outcrop photographs of the Entrance Member, roadcut on highway No. 22: (A,B,C and D) outcrop photographs showing the upper boundary of the Belly River-Edmonton sequence (indicated by arrows) at the base of the Coalspur Formation in the roadcut on highway No. 22.
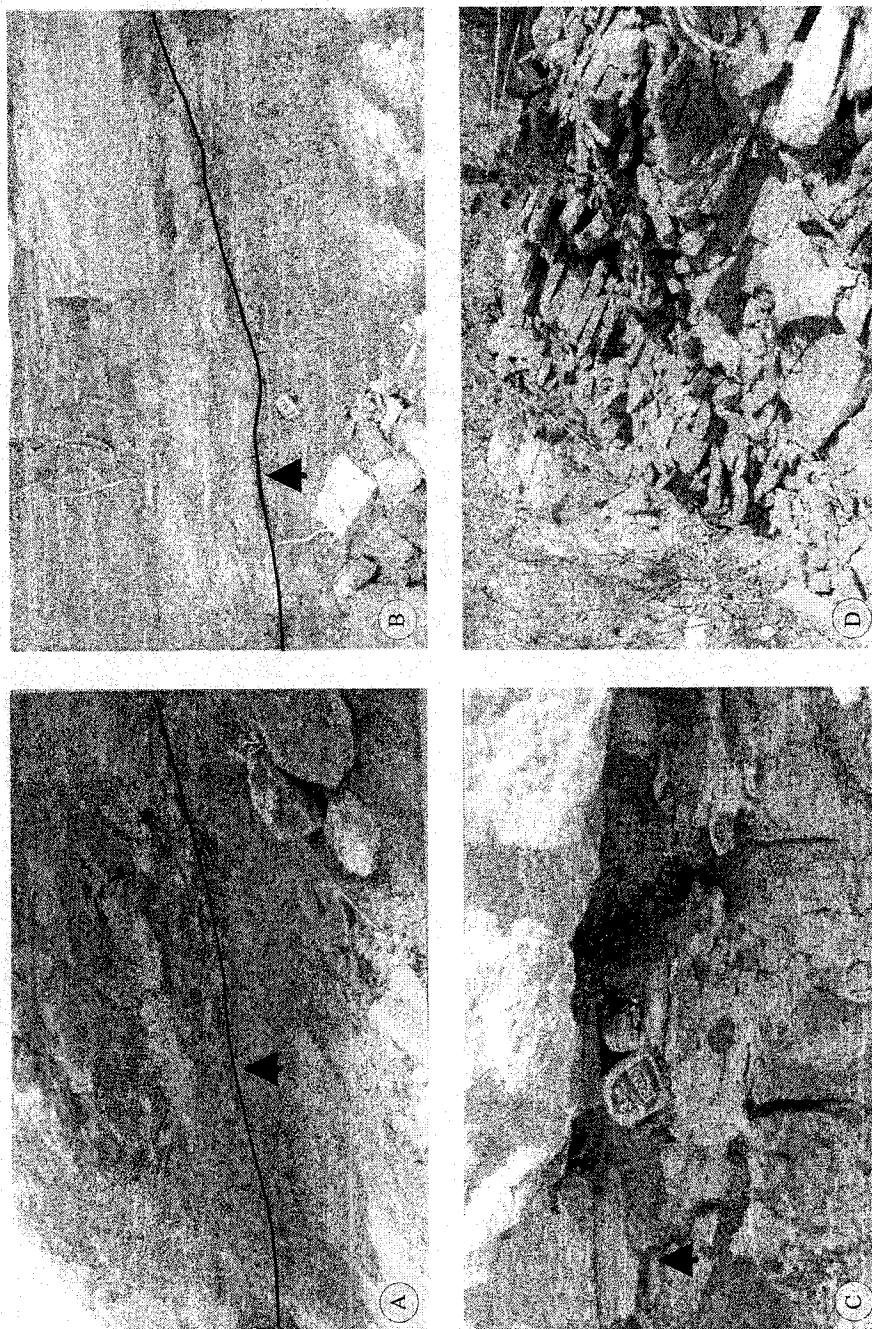
Figure B-4. Outcrop photographs of the Entrance Member, roadcut on highway No. 22: (A, B and C) close-up views showing the upper boundary of the Belly River-Edmonton sequence (indicated by arrows) at the base of the Coalspur Formation in the roadcut on highway Number 22; (D) close-up view of sandstone unit, base of the Entrance Member.
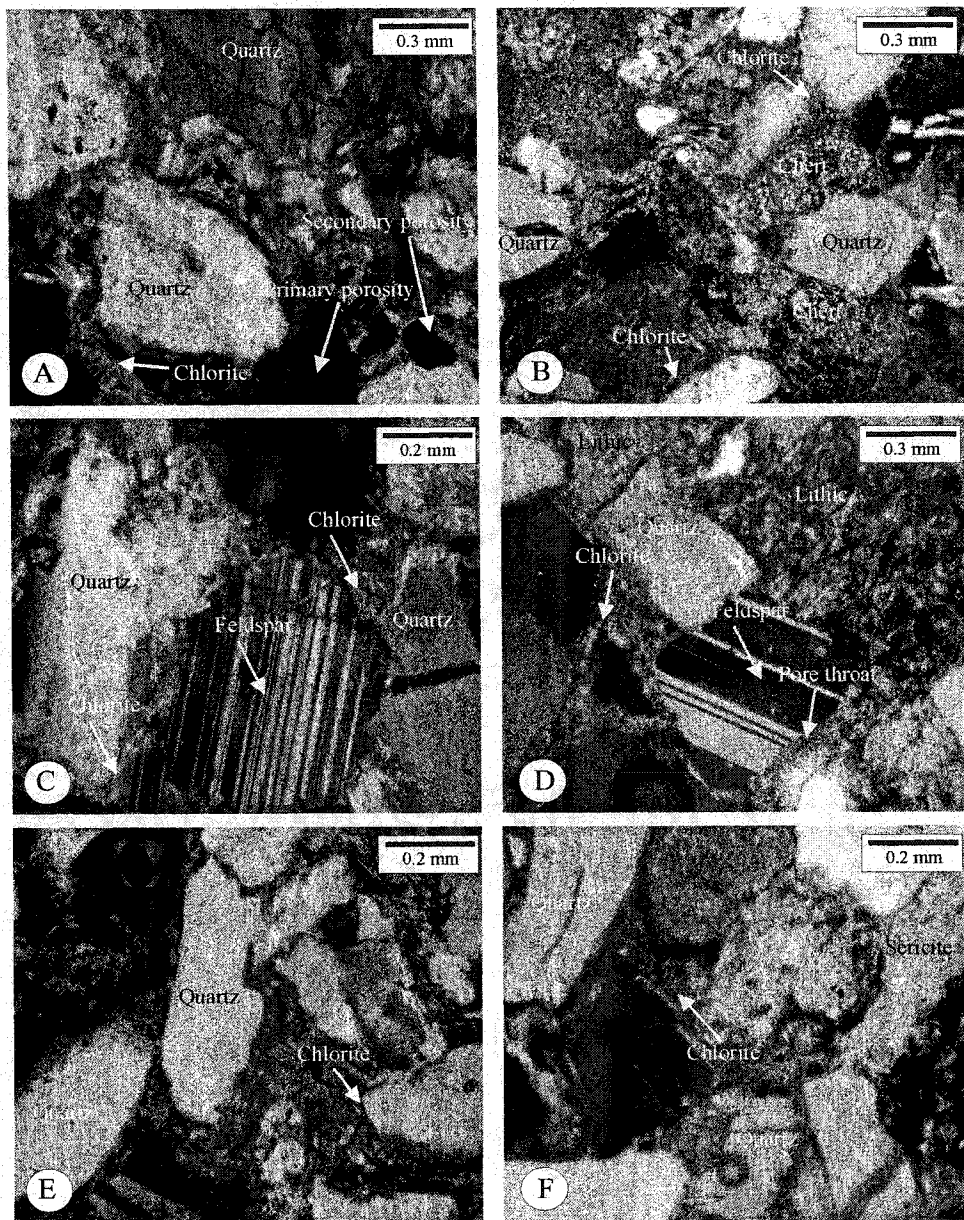
Figure B-5. Thin-section photomicrographs: (A) authigenic chlorite (arrow). Note secondary (dissolution) porosity and primary porosity (arrows) (sample 1, Entrance Member, lower Coalspur Formation, Highway 22 locality); (B) detrital grains of chert (arrows). (sample 2, Entrance Member, lower Coalspur Formation, Highway 22 locality); (C and D) detrital grains of feldspar coated by authigenic chlorite (sample 3, Entrance Member, lower Coalspur Formation, Highway 22 locality); (E and F) quartz grains coated by authigenic chlorite (sample 2, Entrance Member, lower Coalspur Formation, Highway 22 locality).

208
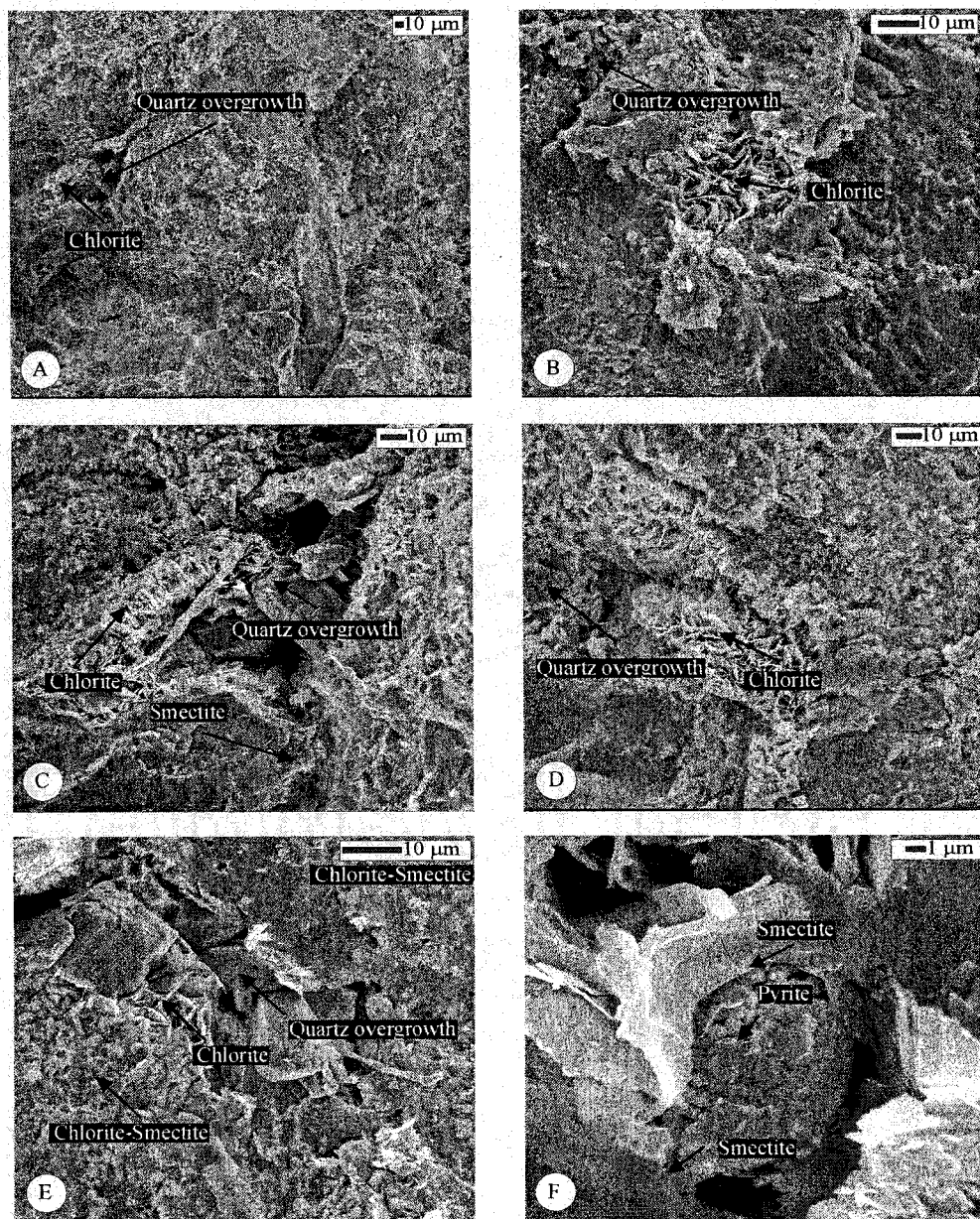
Figure B-6. Scanning electronic photomicrographs: (A, B, C, D, and E) quartz overgrowth surrounded by authigenicchlorite and smectite (sample 1, and 2, Entrance Member, lower Coalspur Formation, roadcut on highway No. 22); (F) Authigenic pyrite surrounded by authigenic smectite (arrows) (sample 1, Entrance Member, lower Coalspur Formation, roadcut on highway No.22).
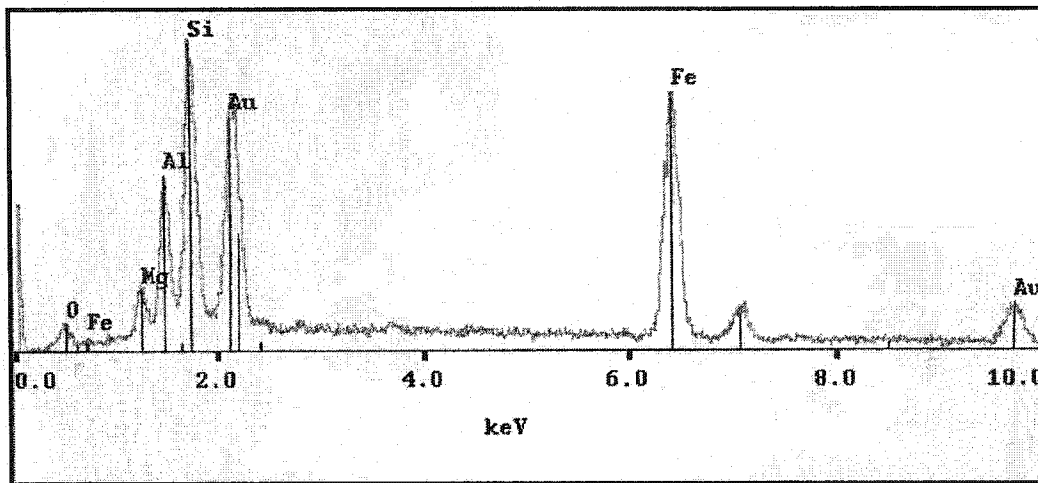
Figure B-7. X-ray diffraction pattern showing the presence of chlorite (sample 1, Entrancemember, lower Coalspur Formation, Highway 22 locality).
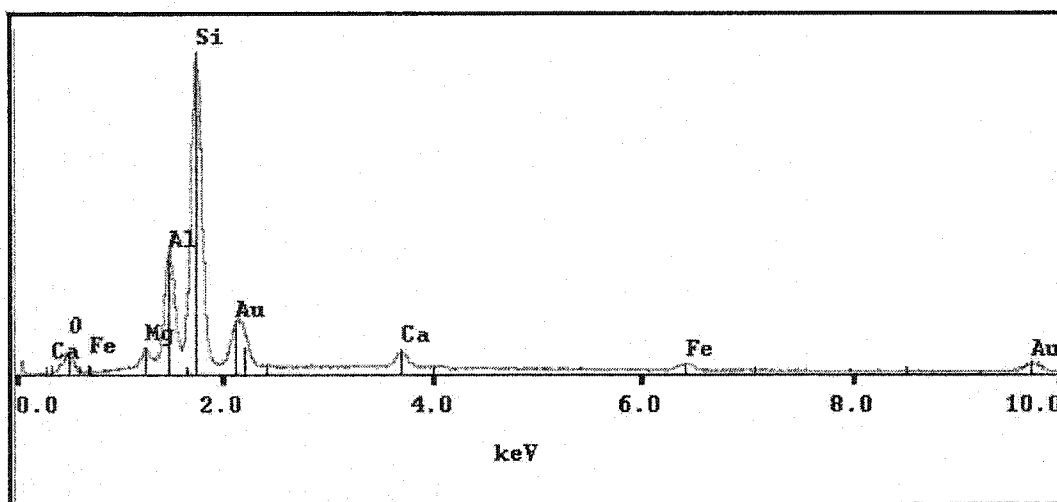
Figure B-8. X-ray diffraction pattern showing the presence of smectite (sample 2, Entrance member, lower Coalspur Formation, Highway 22 locality).
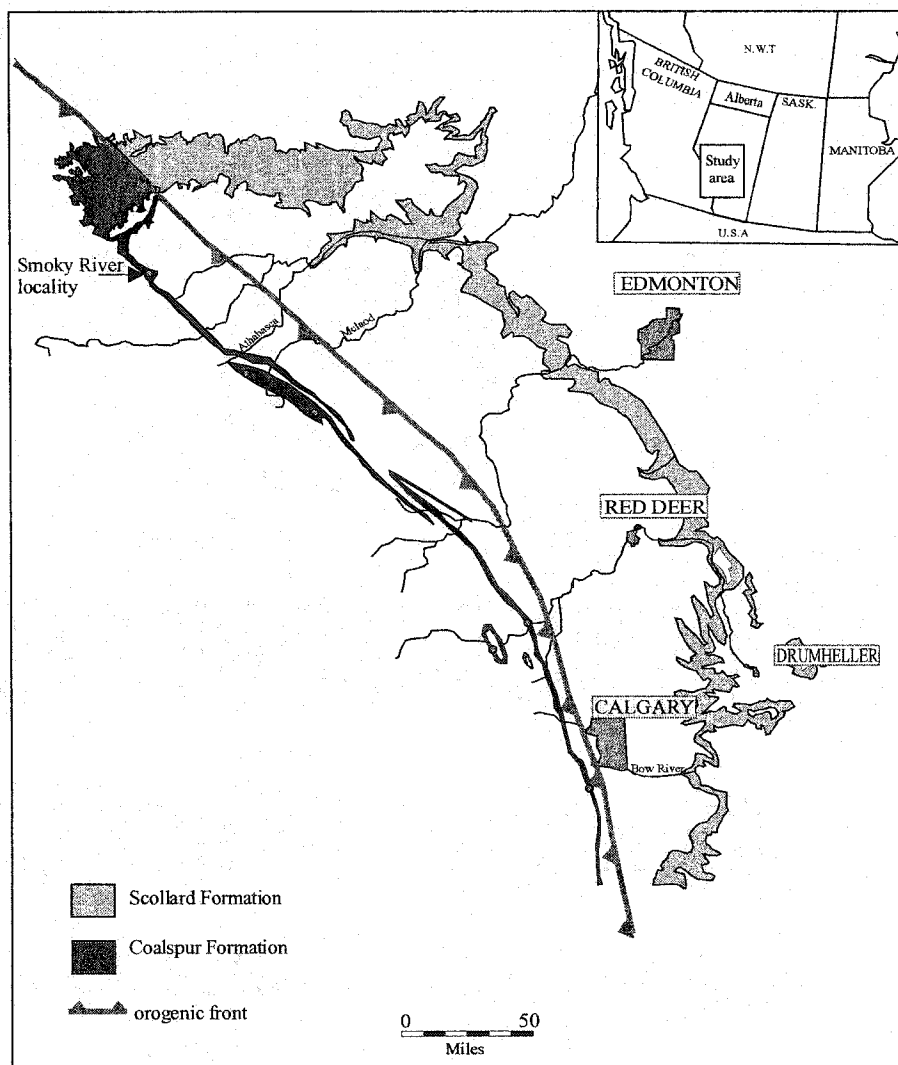
Figure B-9. Outcrop distribution of the Scollard and Coalspur formations in Alberta, and the location of the studied outcrop section, Smokey River.

211
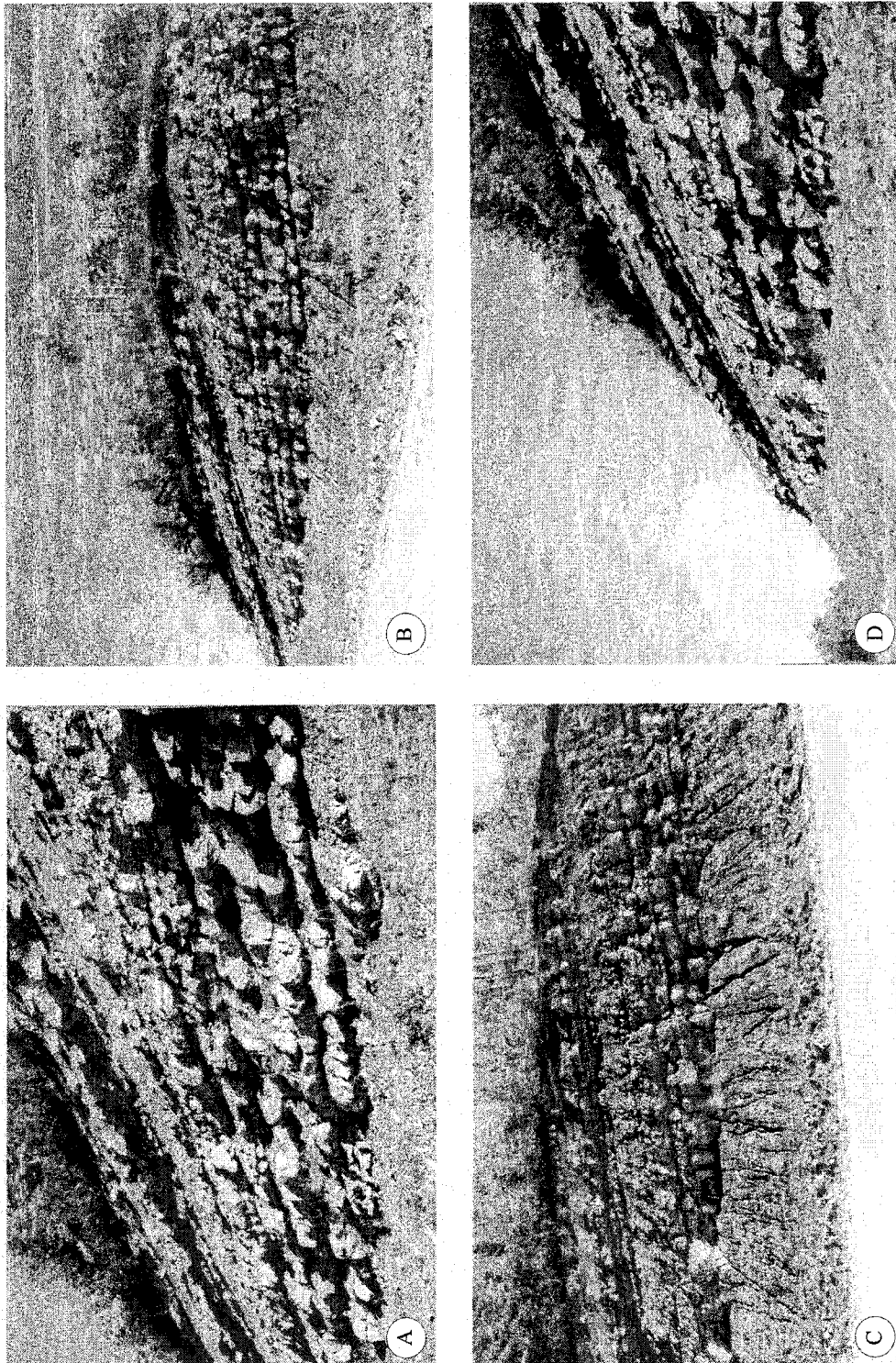
Figure B-10. Outcrop photographs of the lower Coalspur Formation, roadcut on highway 40 showing crevasse channels.

212
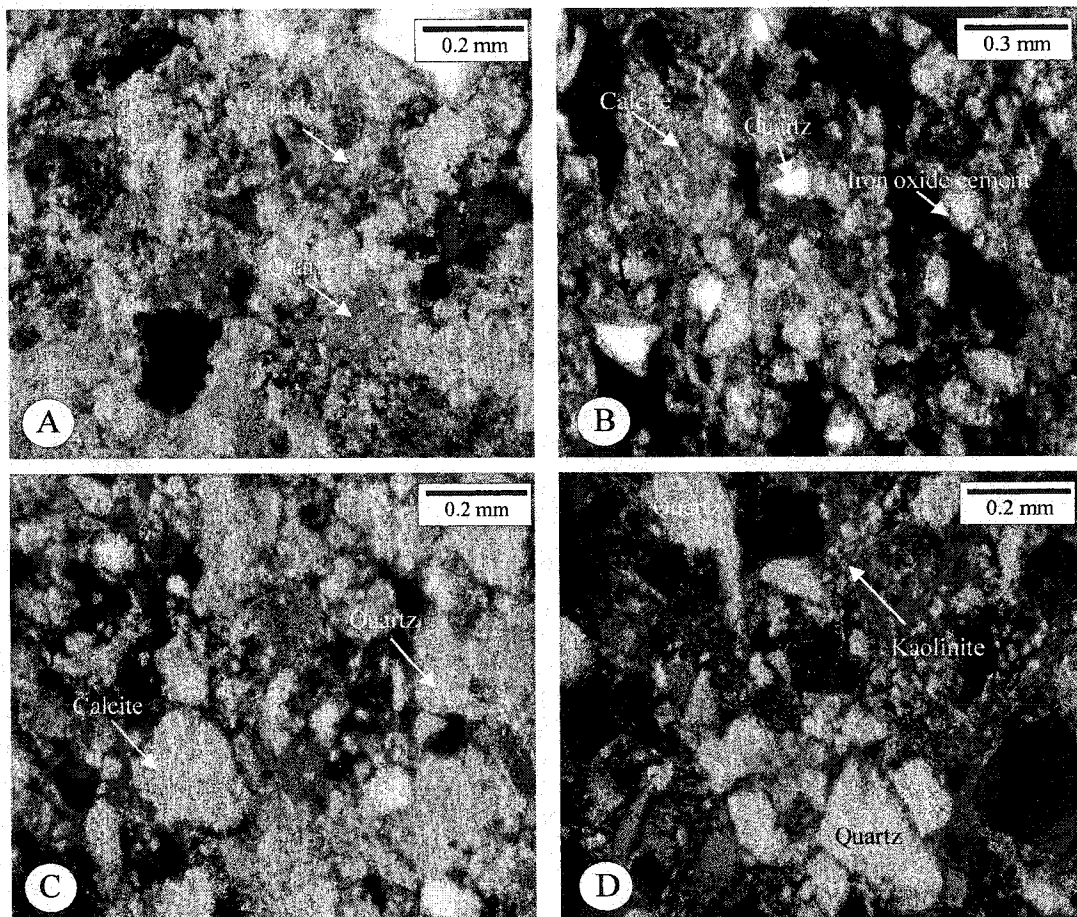
Figure B-11. Thin-section photomicrographs: (A, B, and C) early calcite cement and late Iron oxide cement (arrows)(sample 1, lower Coalspur Formation, Smokey River locality); (D) quartz grains. Note the pores between the quartz grains filled by authigenic kaolinite (arrow) (sample 2, lower Coalspur Formation, Smokey River locality).
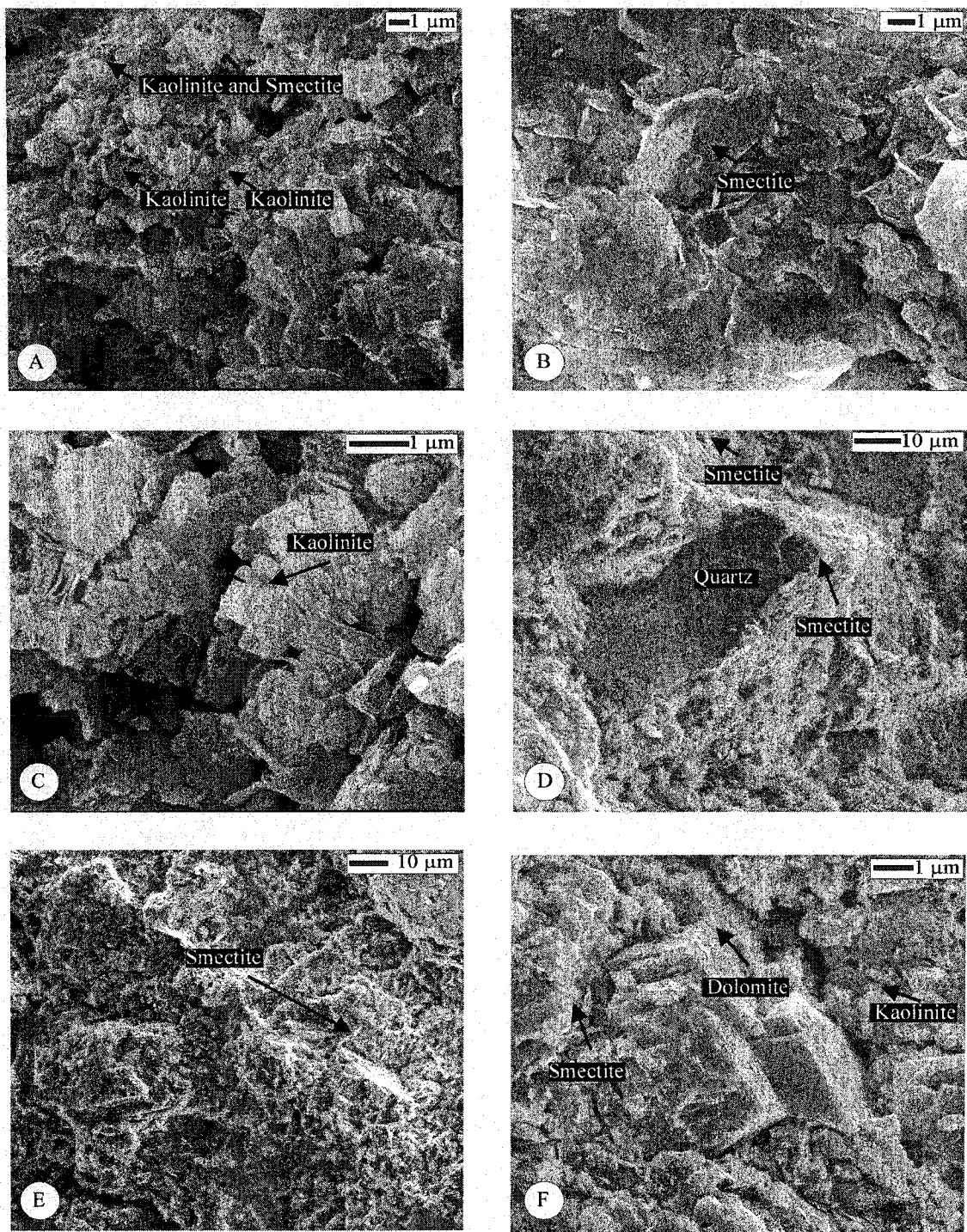
Figure B-12. Scanning electronic photomicrographs: (A) pore fills of authigenic kaolinite and smectite (sample 2, lower Coalspur Formation, the Smokey River locality); (B) authigenic smectite (sample 1, lower Coalspur Formation, Smokey River locality); (C) vermicular aggregates of euhedral crystals of authigenic kaolinite. The kaolinite booklets have consume much of the primary porosity (sample 3, lower Coalspur Formation, Smokey River locality);(D and E) quartz grain coated by authigenic smectite (sample 2, lower Coalspur Formation, Smokey River locality); (F) - dolomite grain coated by authigenic smectite (sample 4, lower Coalspur Formations, Smokey River locality).

214
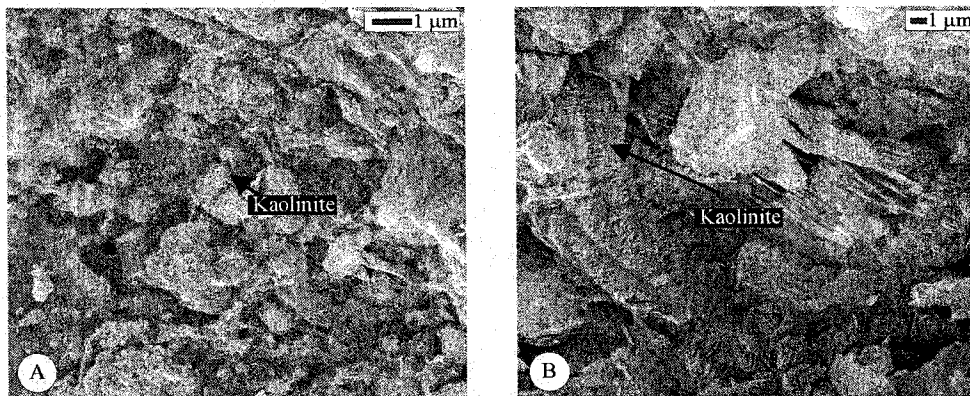
Figure B-13. Scanning electronic photomicrographs: (A) and (B) vermicular aggregates of euhedral crystals of authigenic kaolinite (sample 4, lower Coalspur Formation, Smokey River locality).
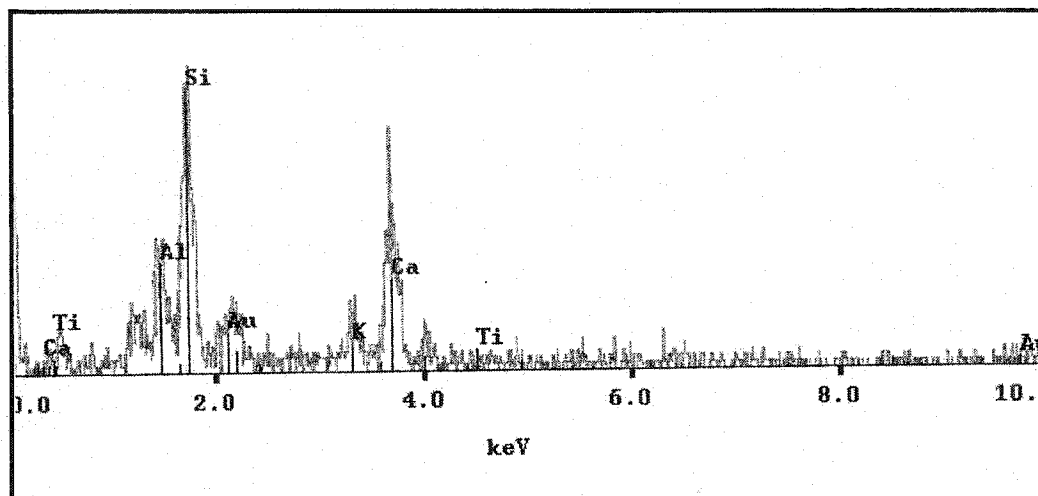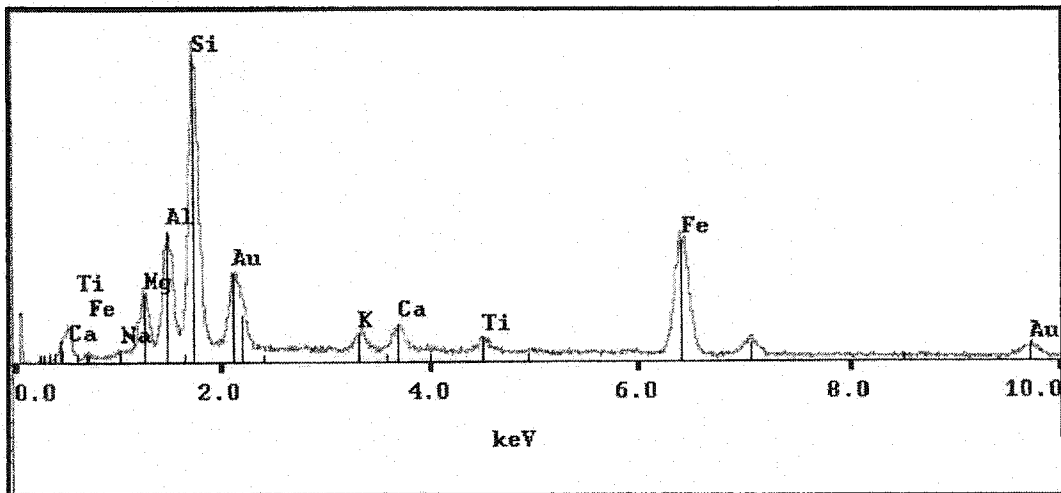
Figure B-14. X-ray diffraction pattern showing the presence of Ca- feldspar (sample 1, lower Coalspur Formation, Smokey River locality).
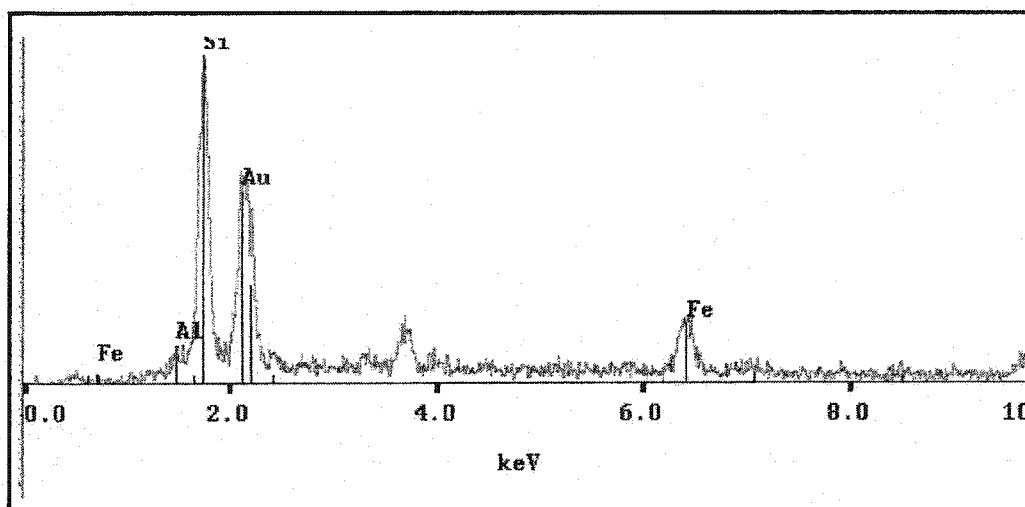
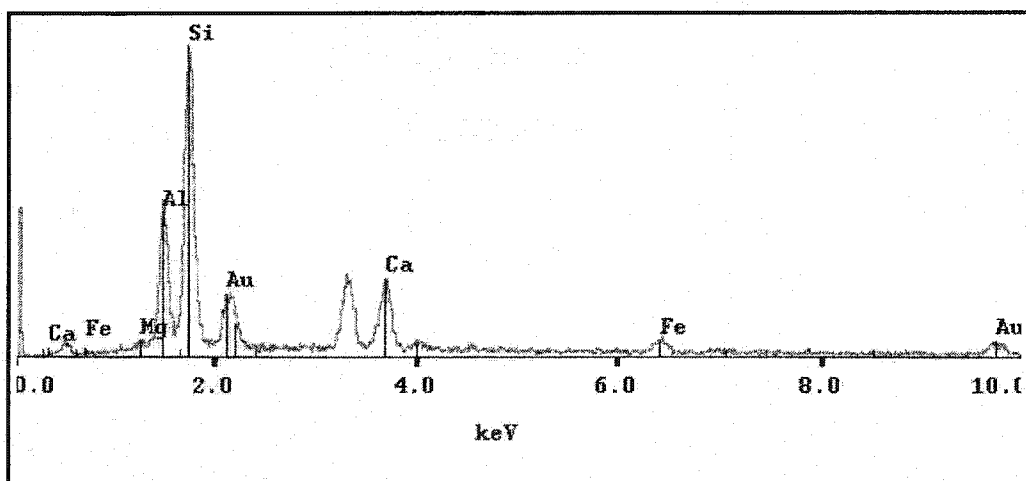Figure B-15. X-ray diffraction pattern showing the presence of smectite (sample 1, lower Coalspur Formation, Smokey River locality)
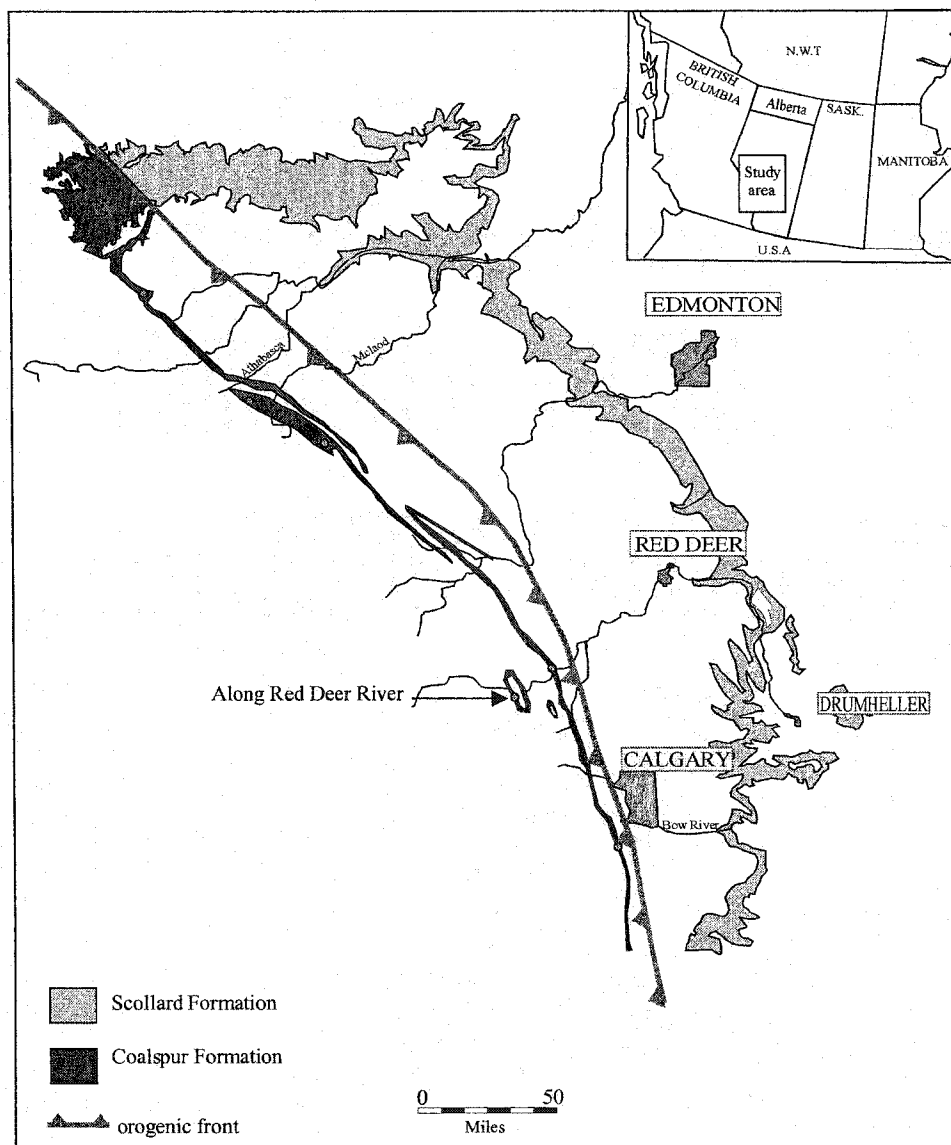
Figure B-16. Outcrop distribution of the Scollard and Coalspur formations in Alberta, and the location of the studied outcrop section, Along Red Deer River..
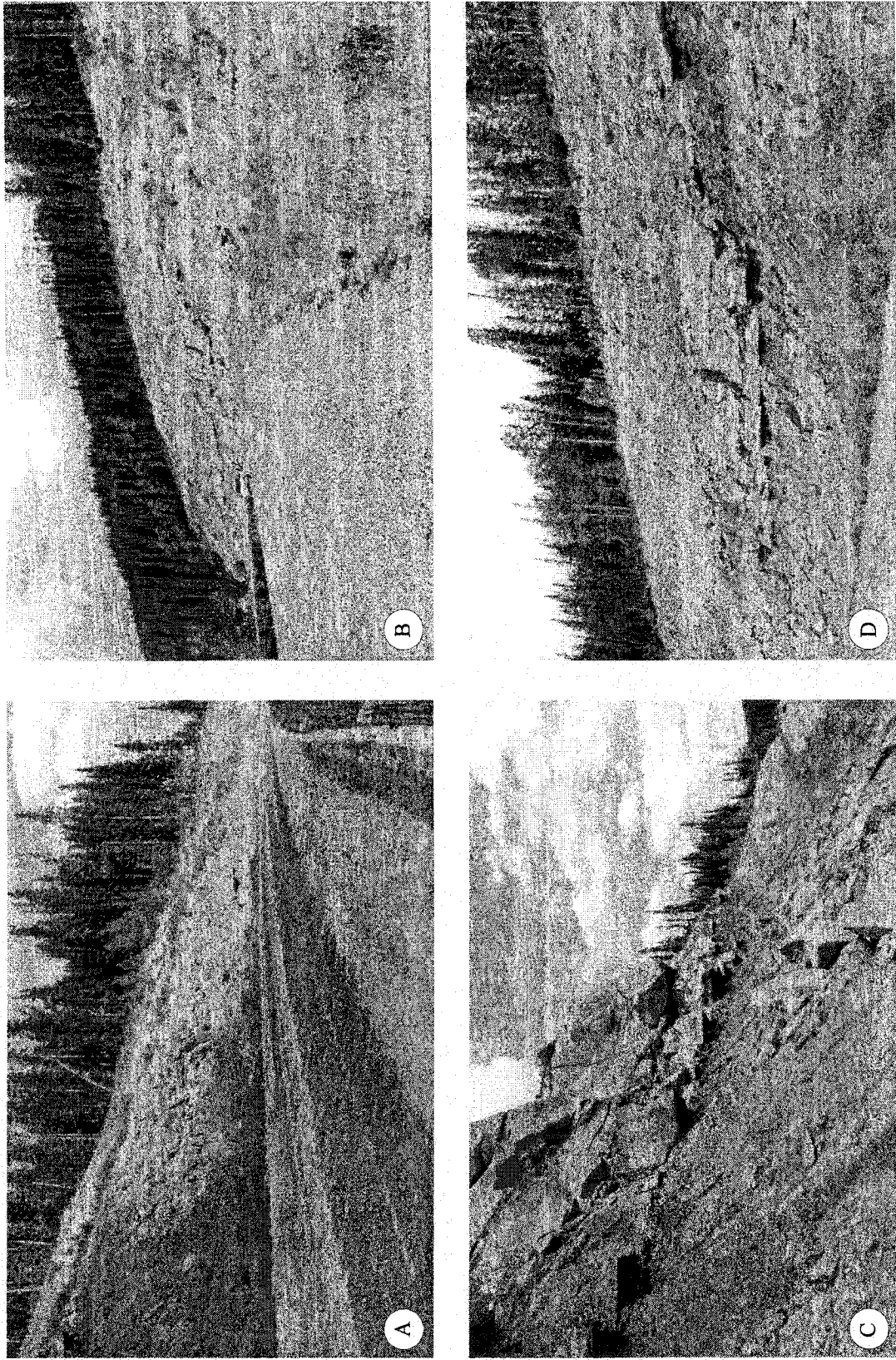
Figure B-17. Outcrop photographs of the upper Coalspur Formation, Red Deer River: (A, B and C) outcrop photographs showing distributary mouth-bar/distributary channel successions; (D) distributary channel.
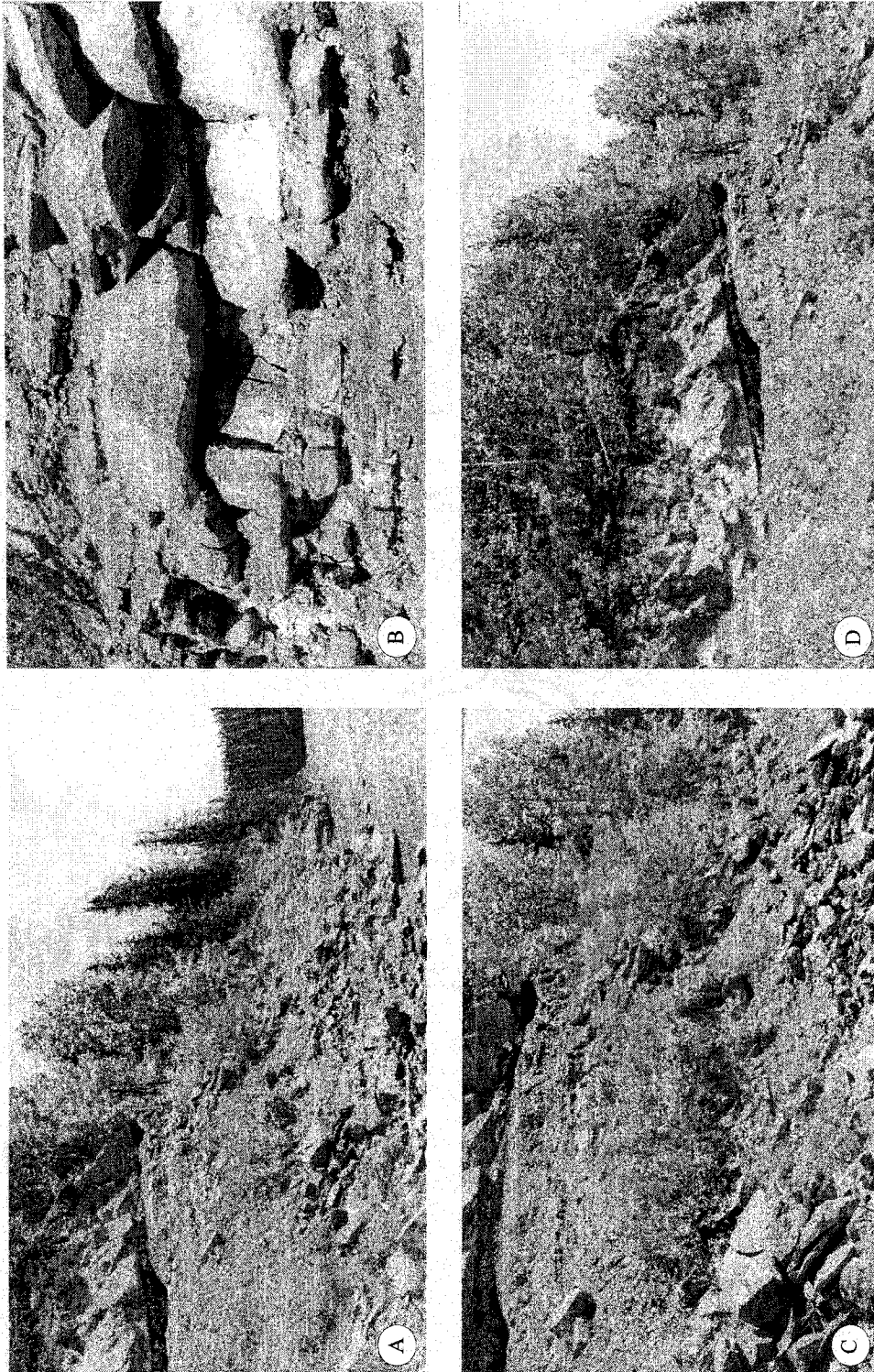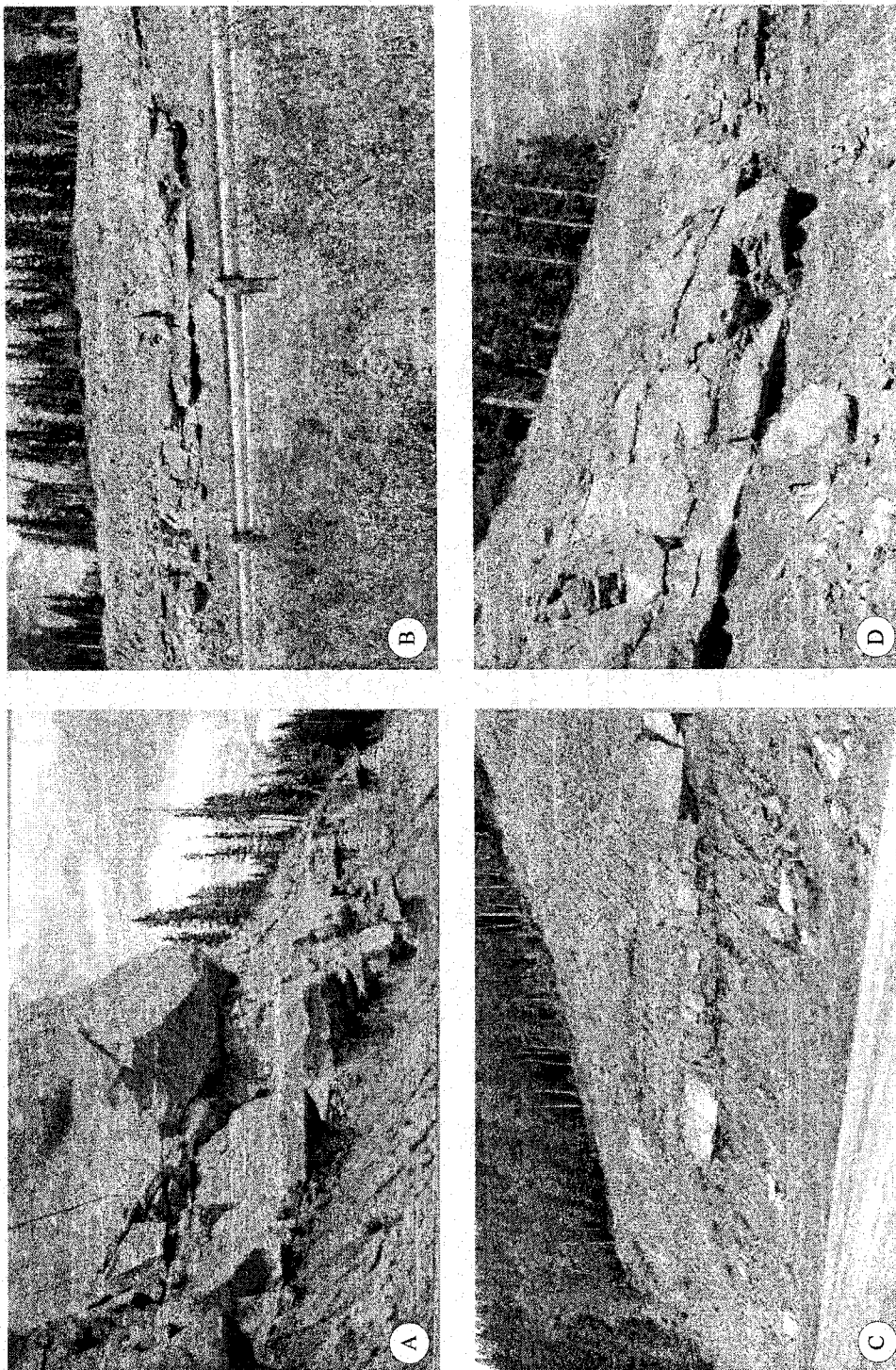
Figure B-18. Outcrop photographs of the upper Coalspur Formation, Red Deer River locality: (A, C and D) outcrop photographs showing lacustrine mudstone interbedded with distributary mouth-bar/distributary channel successions; (D) close-up view of the distributary channel.
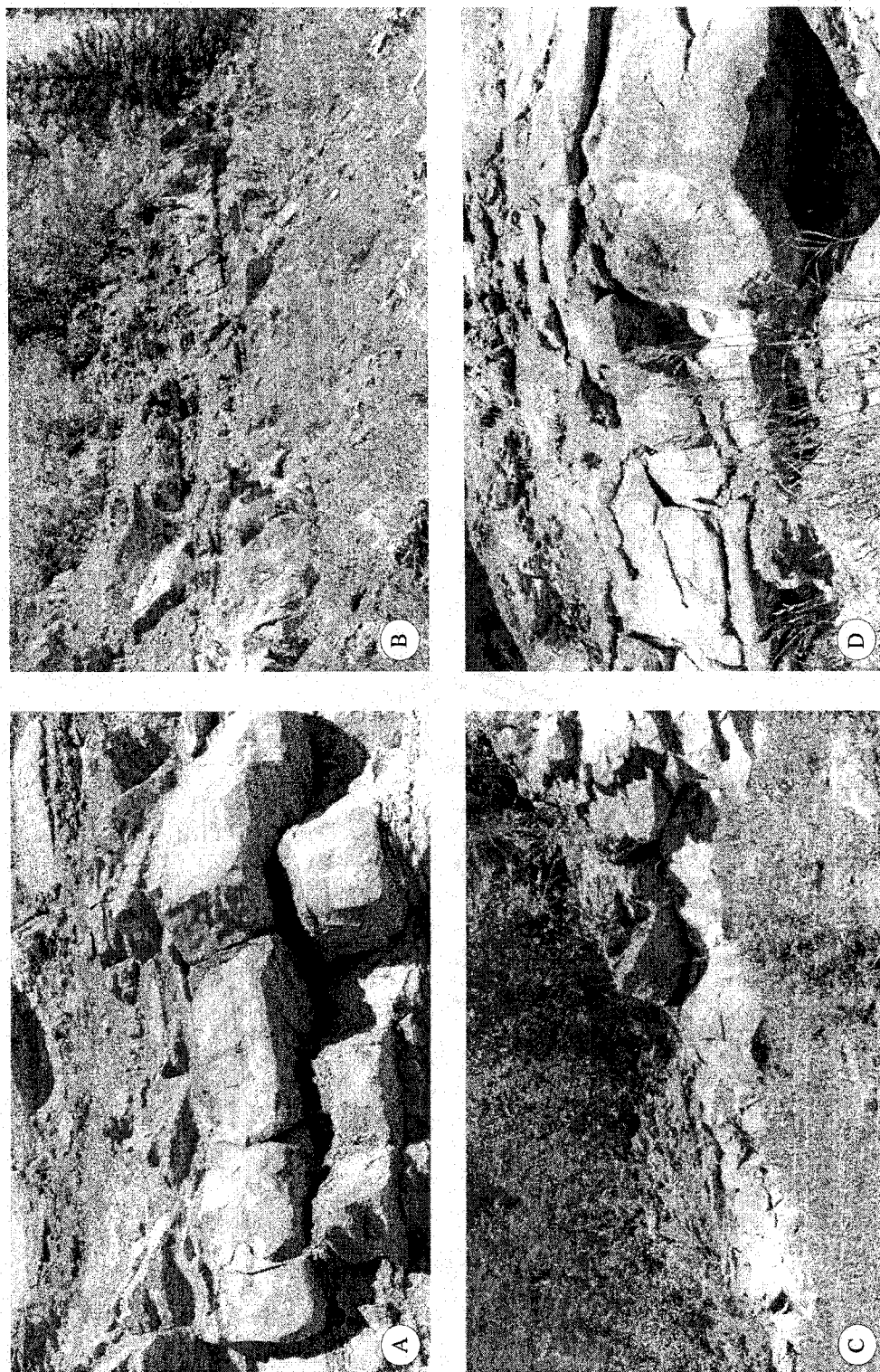
Figure B-19. Outcrop photographs of the upper Coalspur Formation, Red Deer River locality: (A) outcrop photograph showing sandstone units of distributary-channel in the upper part of the Coalspur Formation; (B, C, and D) lacustrine mudstone associated distributary channel successions.

220
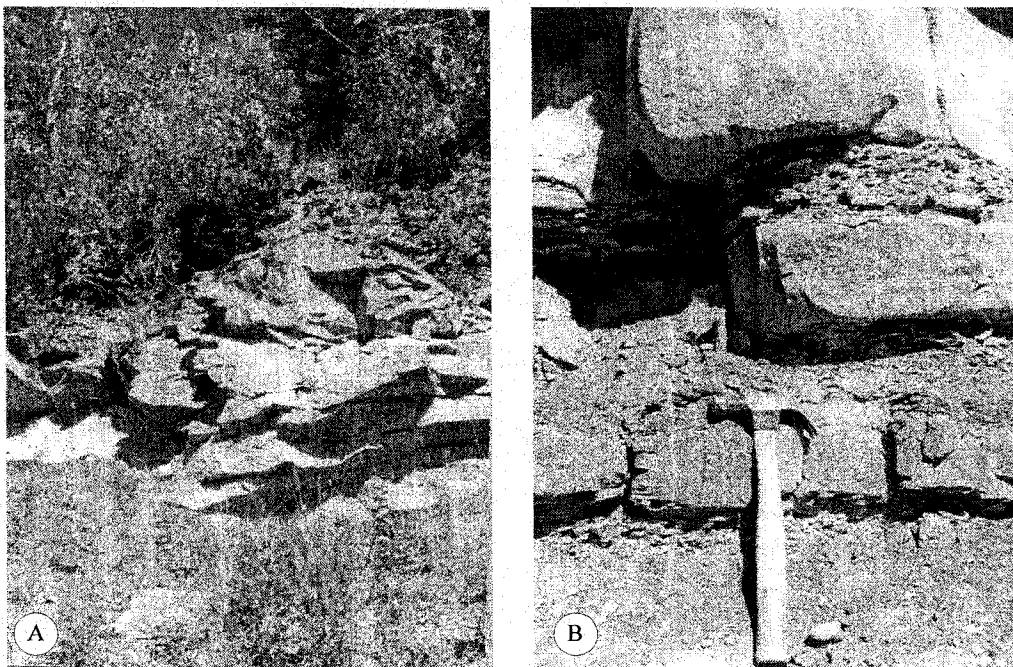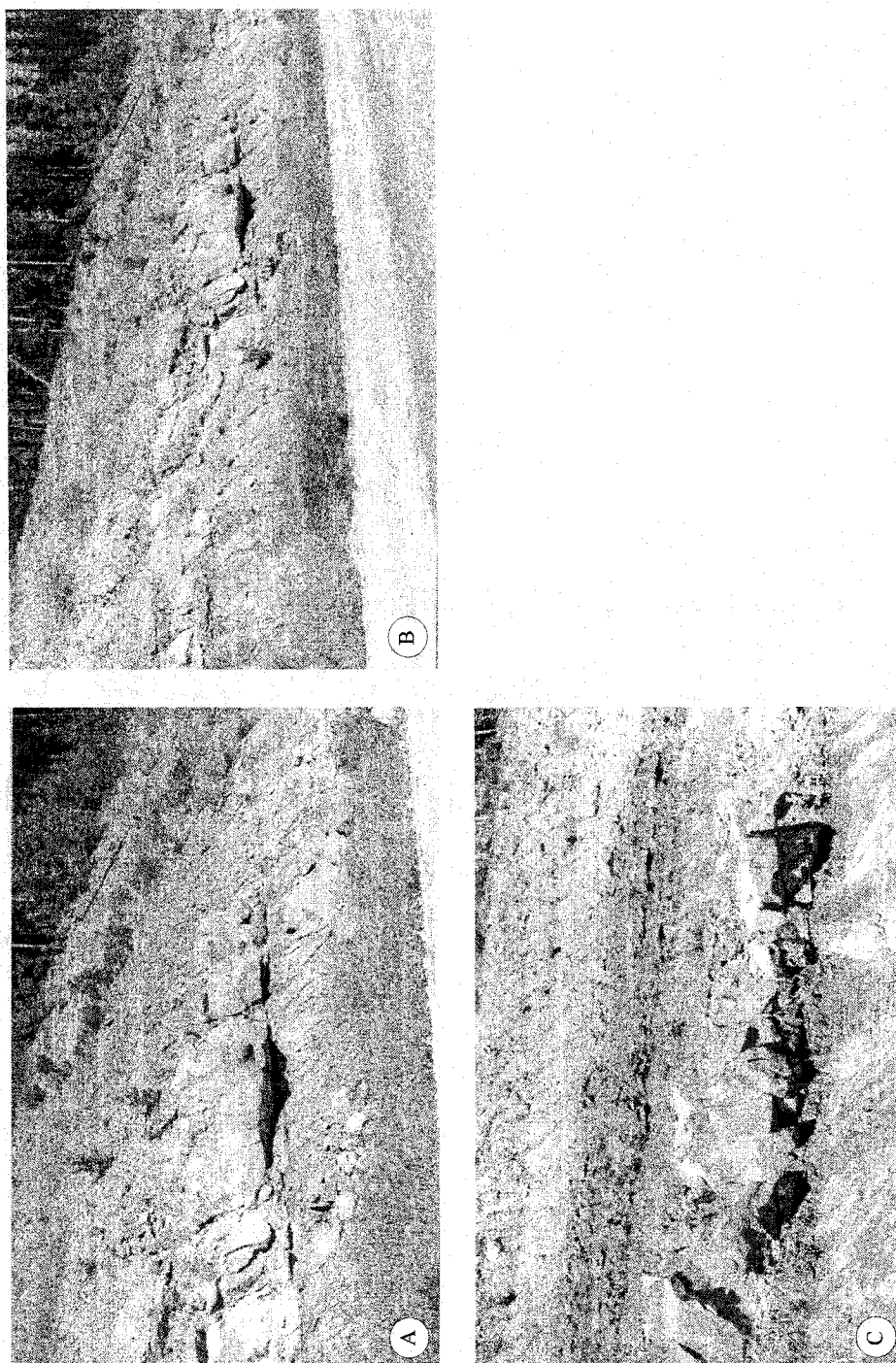
Figure B-20. Outcrop photographs of the upper Coalspur Formation, Red Deer River locality: (A) distributary channel; (B)close-up view of the sandstone lacustrine mudstone associated with distributary channel.
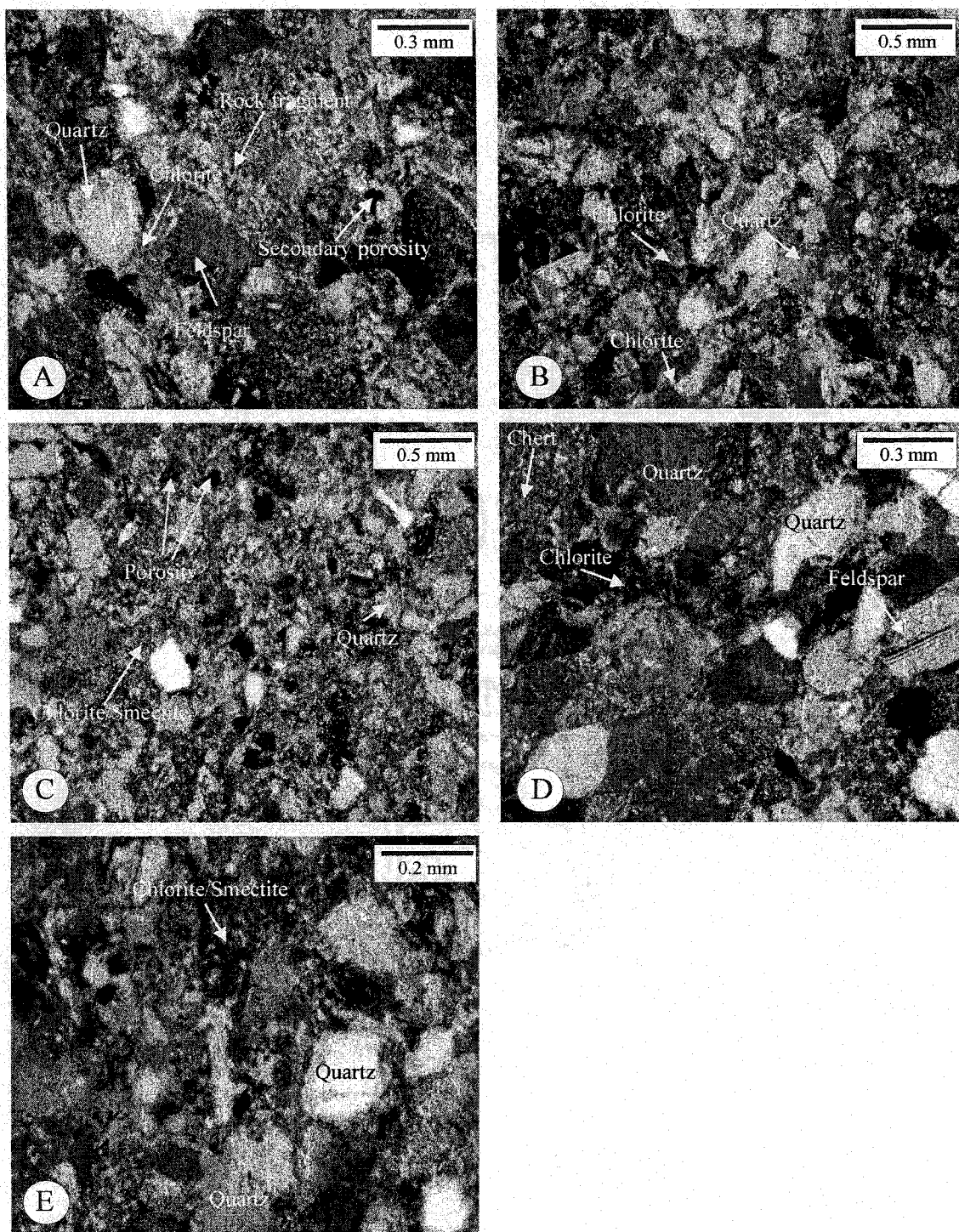
Figure B-21. Thin-section photomicrographs: (A, B and D) detrital feldspar grains, lithic, quartz and authigenic chlorite. Note secondary porosity (arrow) (sample 1, upper Coalspur Formation, Red Deer River locality); (C and E) chlorite/smectite and quartz grains (sample 2, upper Coalspur Formation, Red Deer River locality).
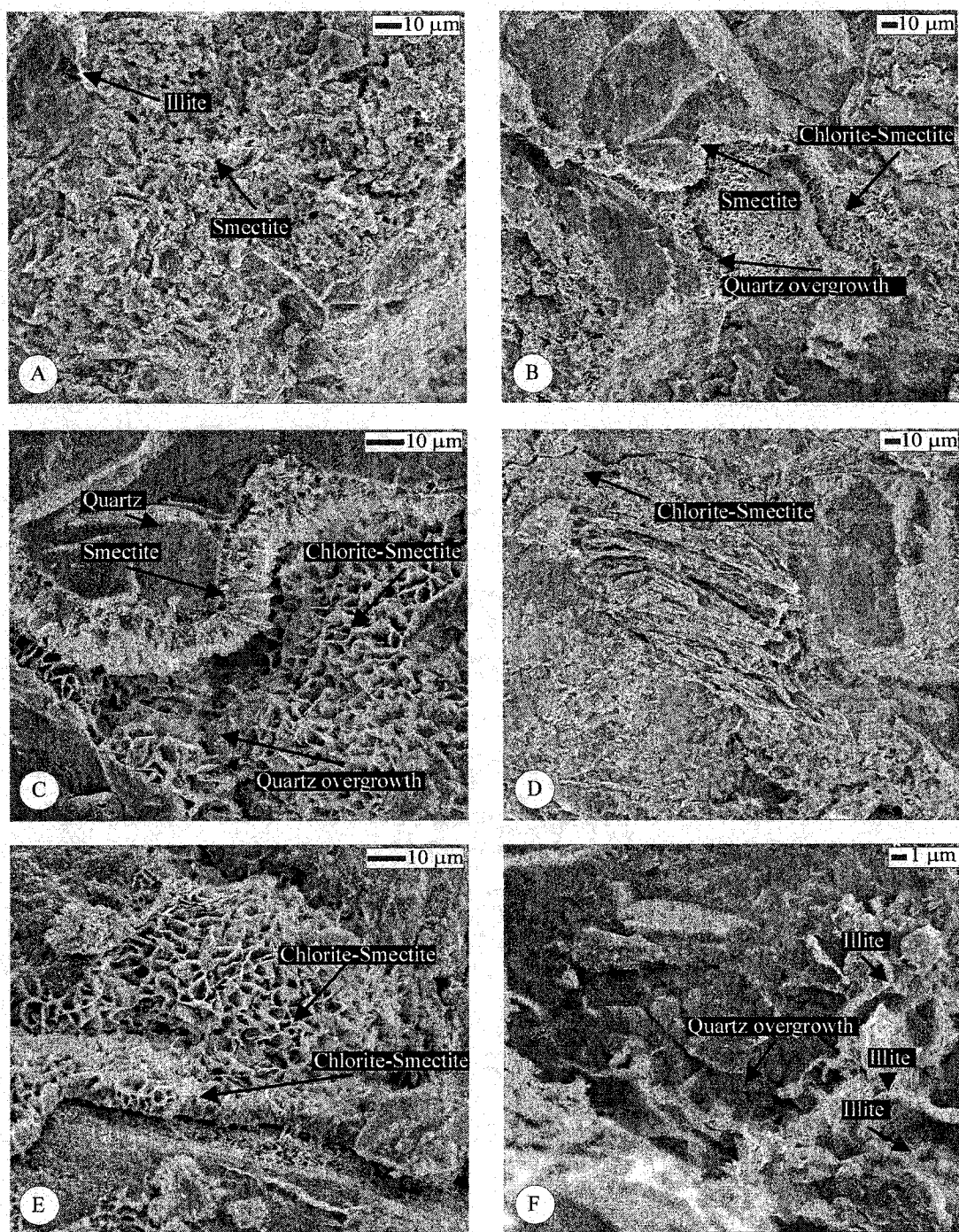
Figure B-22. Scanning electronic photomicrographs: (A) illite and smectite pore fills (sample 4,upper CoalspurFormation, Red Deer River locality); (B, C, D and E) smectite and chlorite/smectite (arrows). Note authigenic smectite and chlorite smectite are perpendicular to grain surfaces; (sample 3, upper Coalspur Formation, Red Deer River locality); (F) euhedral crystals of authigenic quartz surrounded by authigenic illite (sample 6, upper Coalspur Formation, Red Deer River locality).
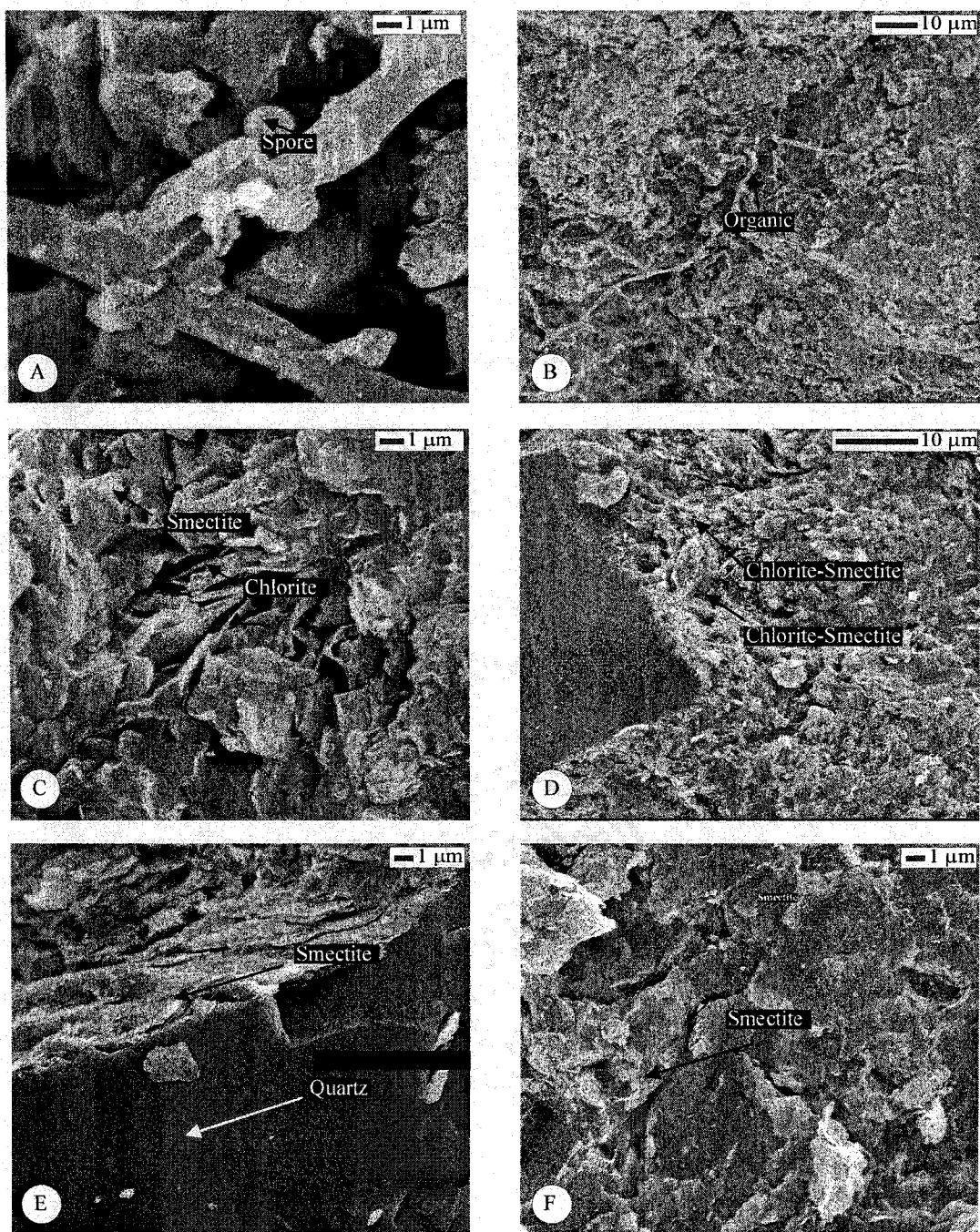
Figure B-23. Scanning electronic photomicrographs: (A and B) spore and organic matter within
the upper Coalspur sandstones (sample 7, upper Coalspur Formation, Red Deer River locality);
(C and D) grain coating smectite and authigenic smectite/chlorite (arrows); (E) quartz grain coated
by authigenic smectite (sample3, upper Coalspur Formation, Red Deer River locality); (F) grain
coating and pore fills smectite (arrows) (sample 3, upper Coalspur Formation, Red Deer locality).
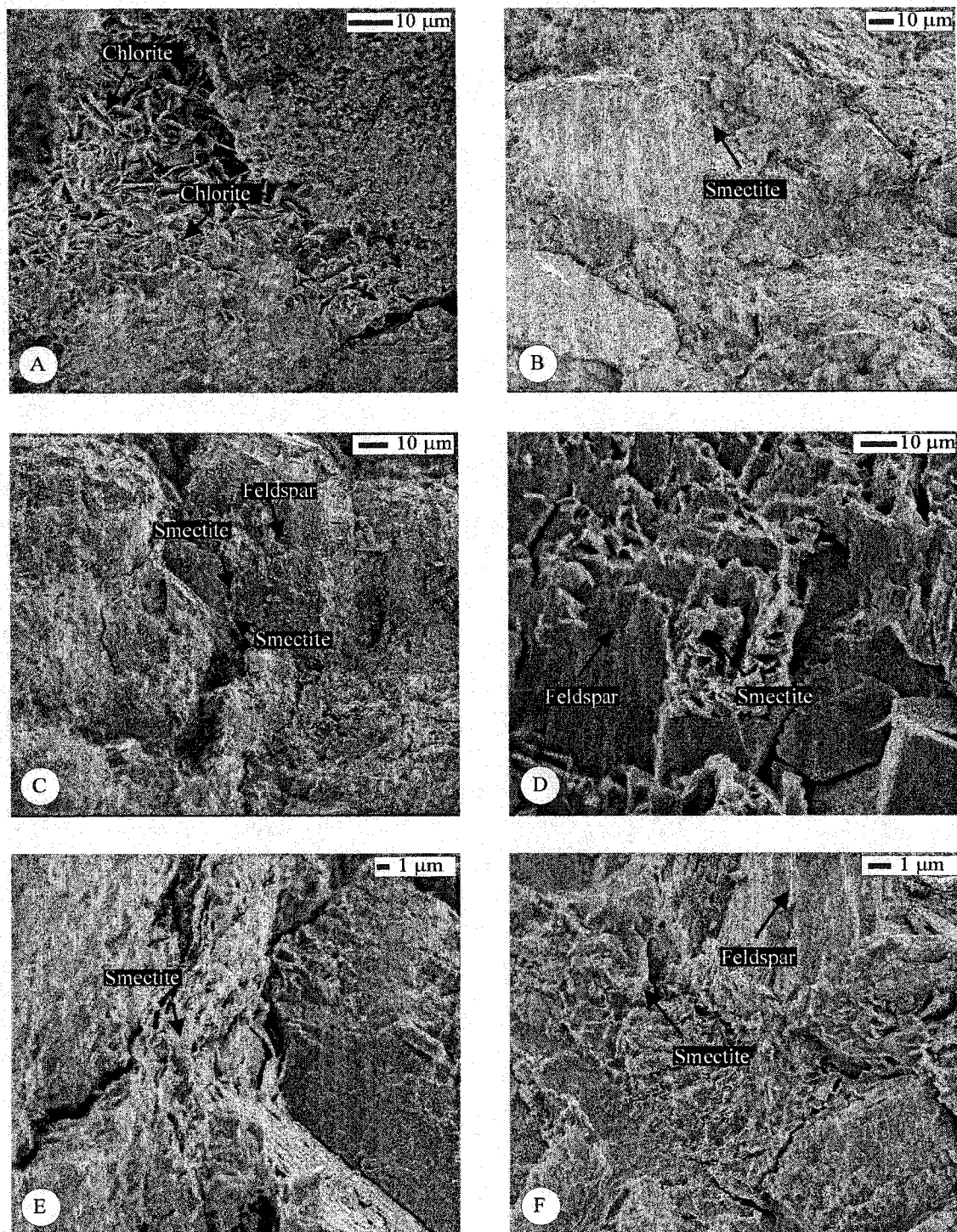
224
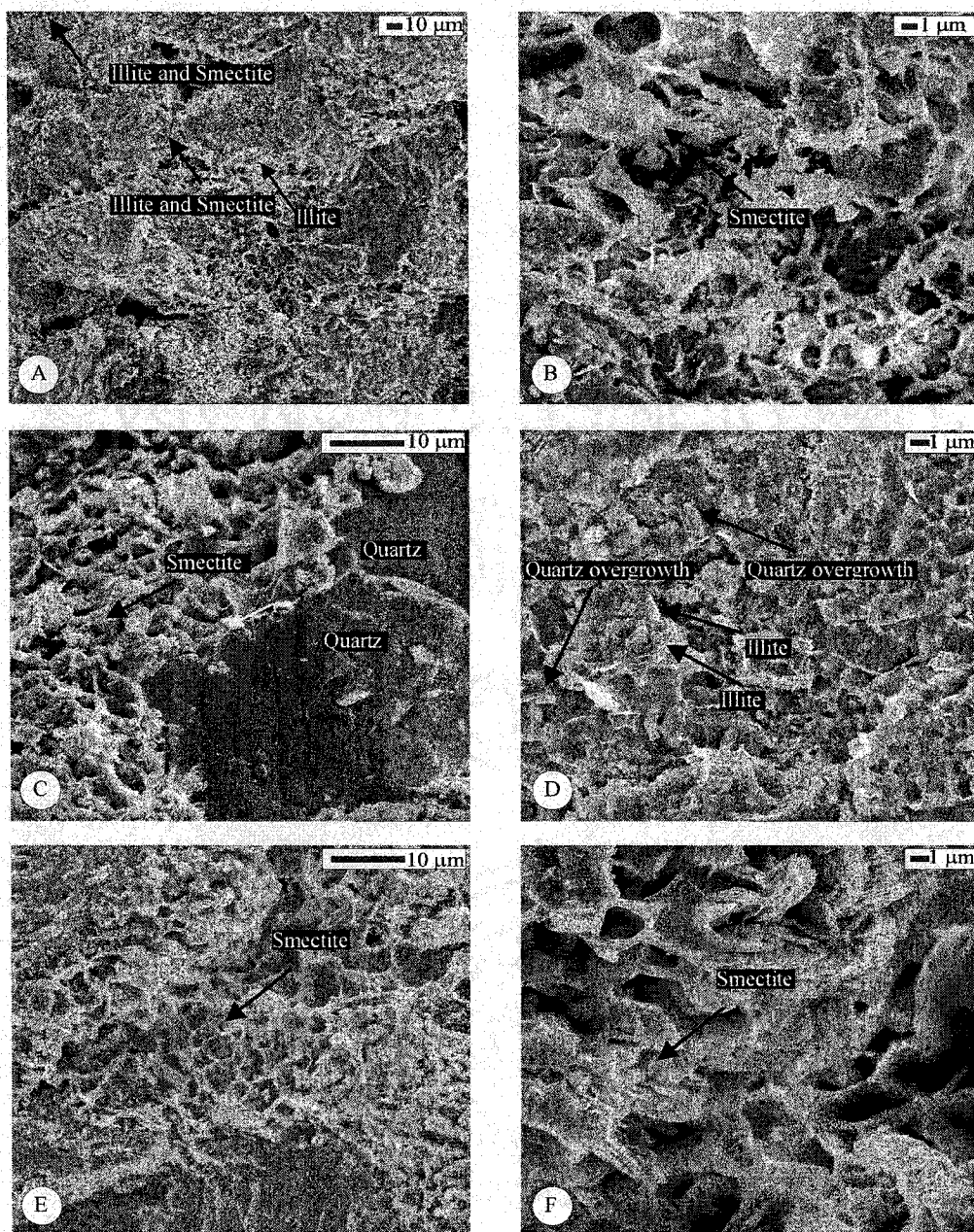
Figure B-24. Scanning electronic photomicrographs: (A and B) smectite and illite within the upper Coalspur sandstones (sample 6, upper Coalspur Formation, Red Deer River locality); (C and E) quartz grain coated by smectite; (sample 3, upper Coalspur Formation, Red Deer River locality); (D) quartz overgrowth surrounded by authigenic illite (arrows) (sample 6, upper Coalspur Formation, Red Deer River locality); (F) authigenic smectite (arrow) (sample 3, upper Coalspur Formation, Red Deer River locality).

225
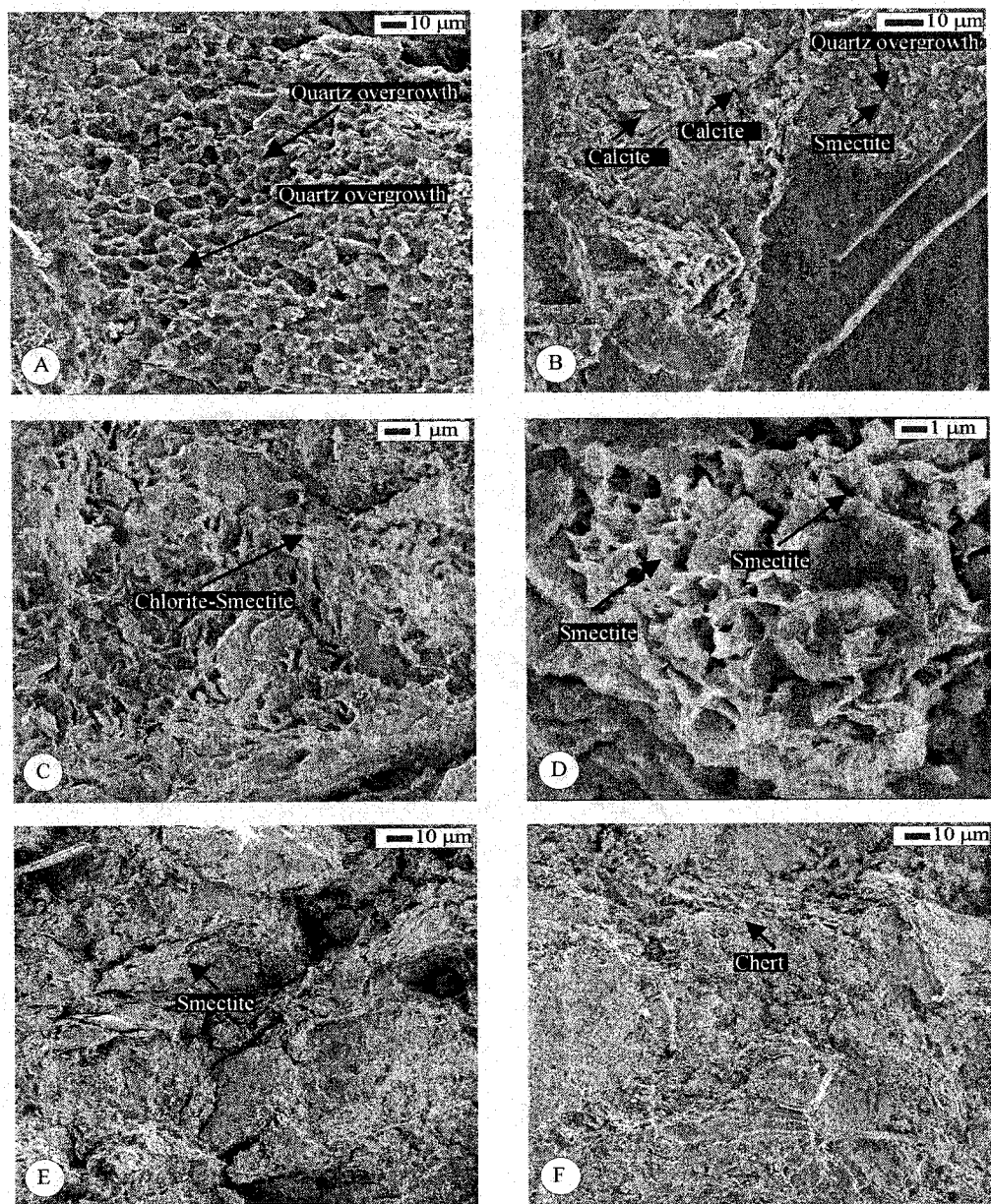
Figure B-25. Scanning electronic photomicrographs: (A) quartz overgrowth within the upper Coalspur sandstones(sample 6, upper Coalspur Formation, Red Deer River locality); (B) smectite, calcite and quartz overgrowth. Note authigenic smectite interfering with the process of quartz overgrowth; (C) authigenic smectite/chlorite (sample 2, upper Coalspur Formation, Red Deer River locality); (D and E) authigenic smectite (arrows) (sample 3, upper Coalspur Formation, Red Deer River locality); (F) chert cement within the upper Coalspur sandstones (sample 2, upper Coalspur Formation, Red Deer River locality).

226
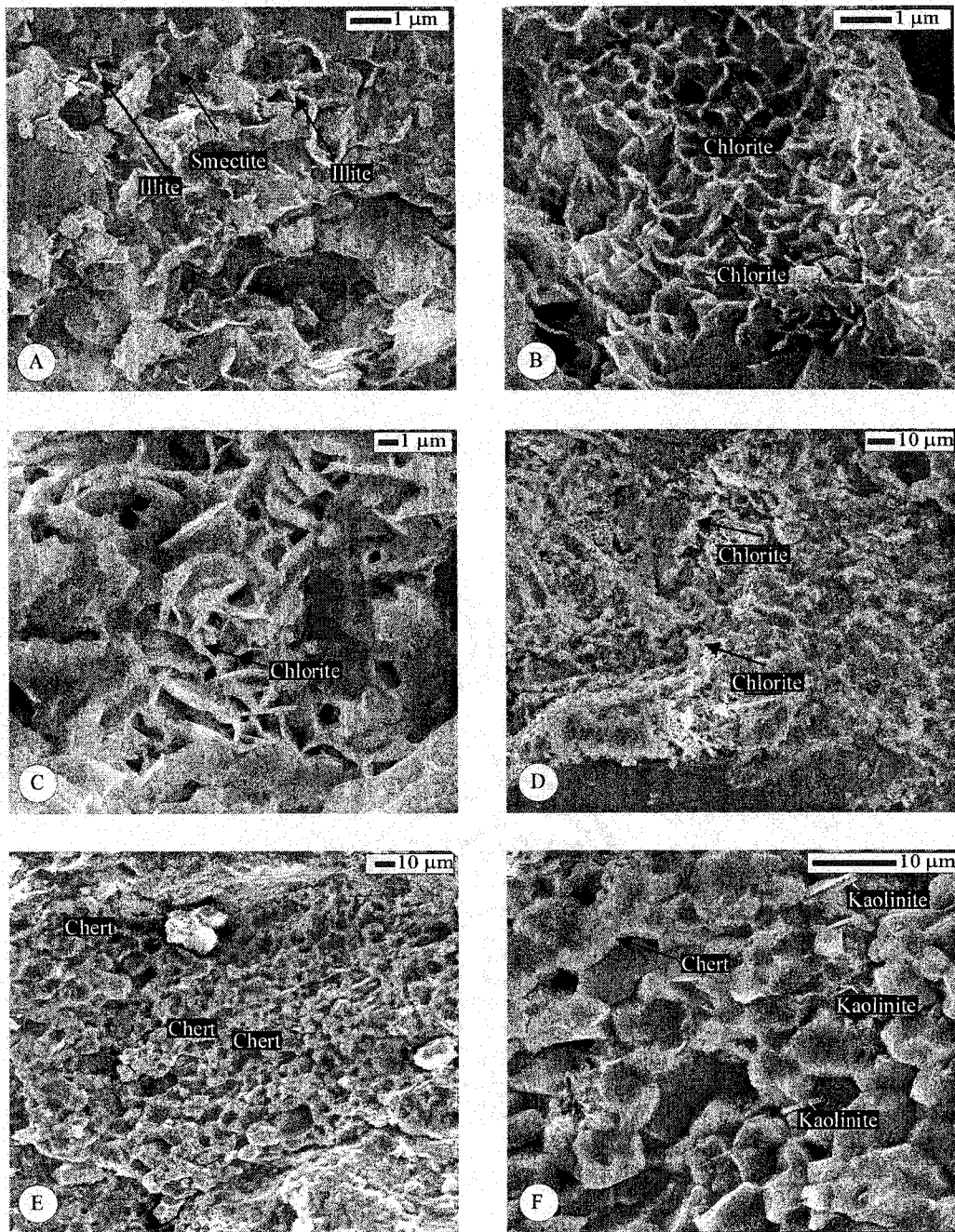
Figure B-26. Scanning electronic photomicrographs: (A) illite and smectite pore fills (sample 4, upper Coalspur Formation, Red Deer River locality); (B, C and D) authigenic chlorite. Note the Microscopic recovery efficiency (microporosity) in chlorite (sample 2, upper Coalspur Formation, Red Deer River locality); (E and F) chert cement (sample 3, upper Coalspur Formation, Red Deer River locality).
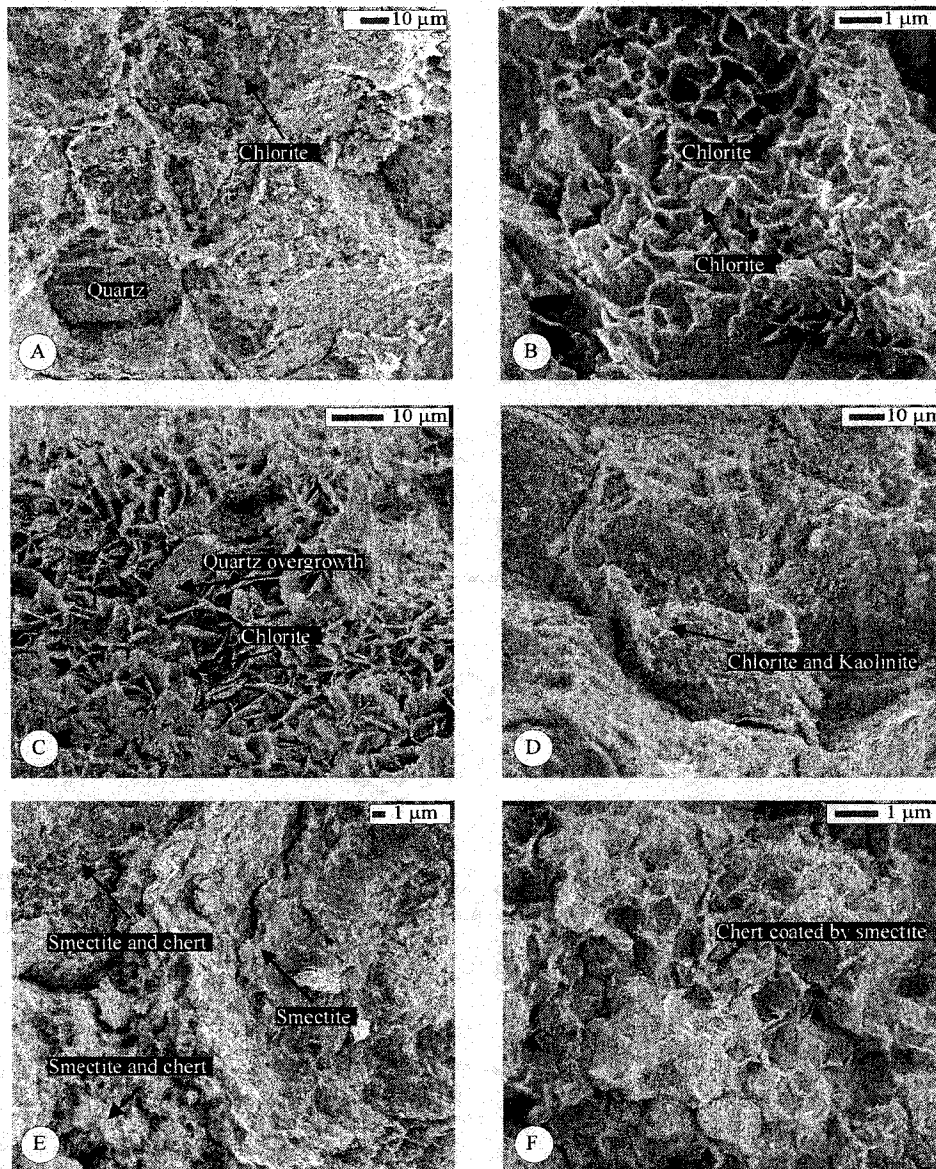
Figure B-27. Scanning electronic photomicrographs: (A and B) authigenic chlorite within the upper Coalspur sandstones (sample 2, upper Coalspur Formation, Red Deer River locality); (C) chlorite interfering with the process of quartz overgrowth (sample 2, upper Coalspur Formation, Red Deer River locality); (D) authigenic chlorite and kaolinite filled the pore space between quartz grains (sample 1, upper Coalspur Formation, Red Deer River locality);(E and F) chert cement coated by authigenic smectite (sample 3, upper Coalspur Formation, Red Deer River locality).

228

Figure B-28. X-ray diffraction pattern showing the presence of chlorite (sample 3, upper Coalspur Formation, Red Deer River locality).

Figure B-29. X-ray diffraction pattern showing the presence of smectite (sample 5, upper Coalspur Formation, Red Deer River locality).
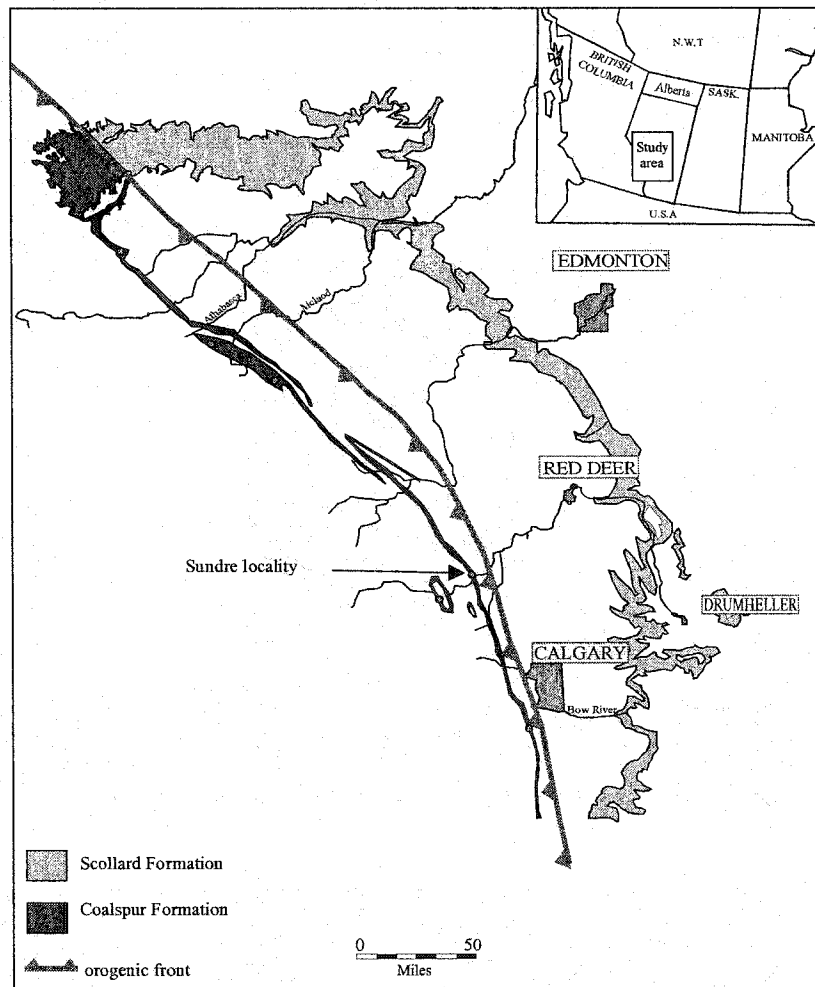
229

Figure B-30. Outcrop distribution of the Scollard and Coalspur formations in Alberta, and the location of the studied outcrop section, along the Red Deer River.

Figure B-31. Outcrop photographs of the upper Coalspur Formation, roadcut, Red Deer River locality: (A), (B), (C), and D) outcrop photographs showing distributary mouth-bar.

231

Figure B-32. Outcrop photographs of the upper Coulspur Formation, roadcut, Red Deer River locality: (A, B, C, and D) outcrop photographs showing distributary mouth-bar/distributary channel successions.
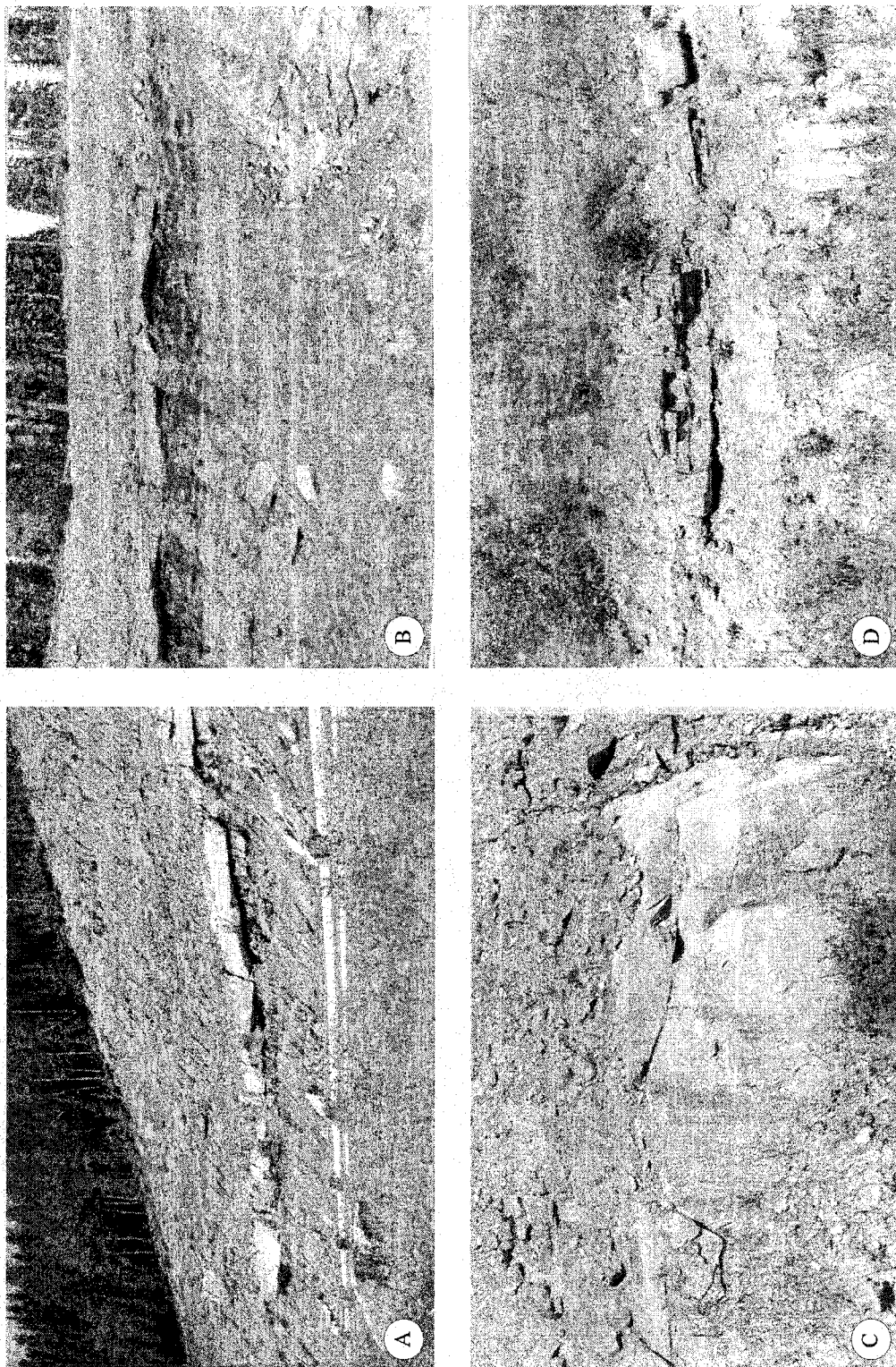
Figure B-33. Outcrop photographs of the upper Coalspur Formation, roadcut, Red Deer River locality showing distributary channel interbedded with lacustrine mudstones.

233

Figure B-34. Outcrop photographs of the upper Coalspur Formation, roadcut, Red Deer River locality: (A), (B), and (C) view of distributary channels interbedded with lacustrine mudstones..
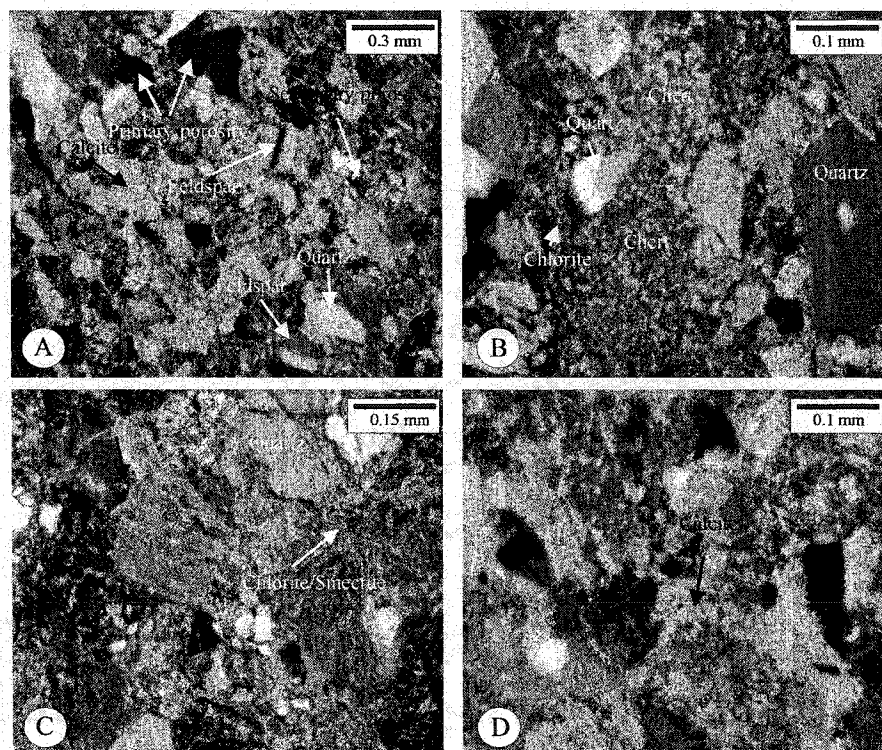
Figure B-35. Thin-section photomicrographs: (A) detrital feldspar grains, quartz, calcite cement and authigenic chlorite. Note residual primary porosity (arrows) (sample 10, upper Coalspur Formation, roadcut, Red Deer River locality); (B) quartz and chert grains (arrows) (sample 11, upper Coalspur Formation, roadcut, Red Deer Riverlocality); (C) chlorite/smectite and quartz grains (arrows) (sample 11, upper Coalspur Formation, roadcut, Red Deer River locality); (D)calcite cement (arrow) (sample 12, upper Coalspur Formation, roadcut, Red Deer River locality).

Figure B-36. Scanning electronic photomicrographs: (A) authigenic chlorite within the upper Coalspur sandstones (sample 2, upper Coalspur Formation, roadcut, Red Deer River locality); (B, C, D, E, and F) feldspar alteration into smectite (sample 12, upper Coalspur Formation, roadcut, Red Deer River locality).
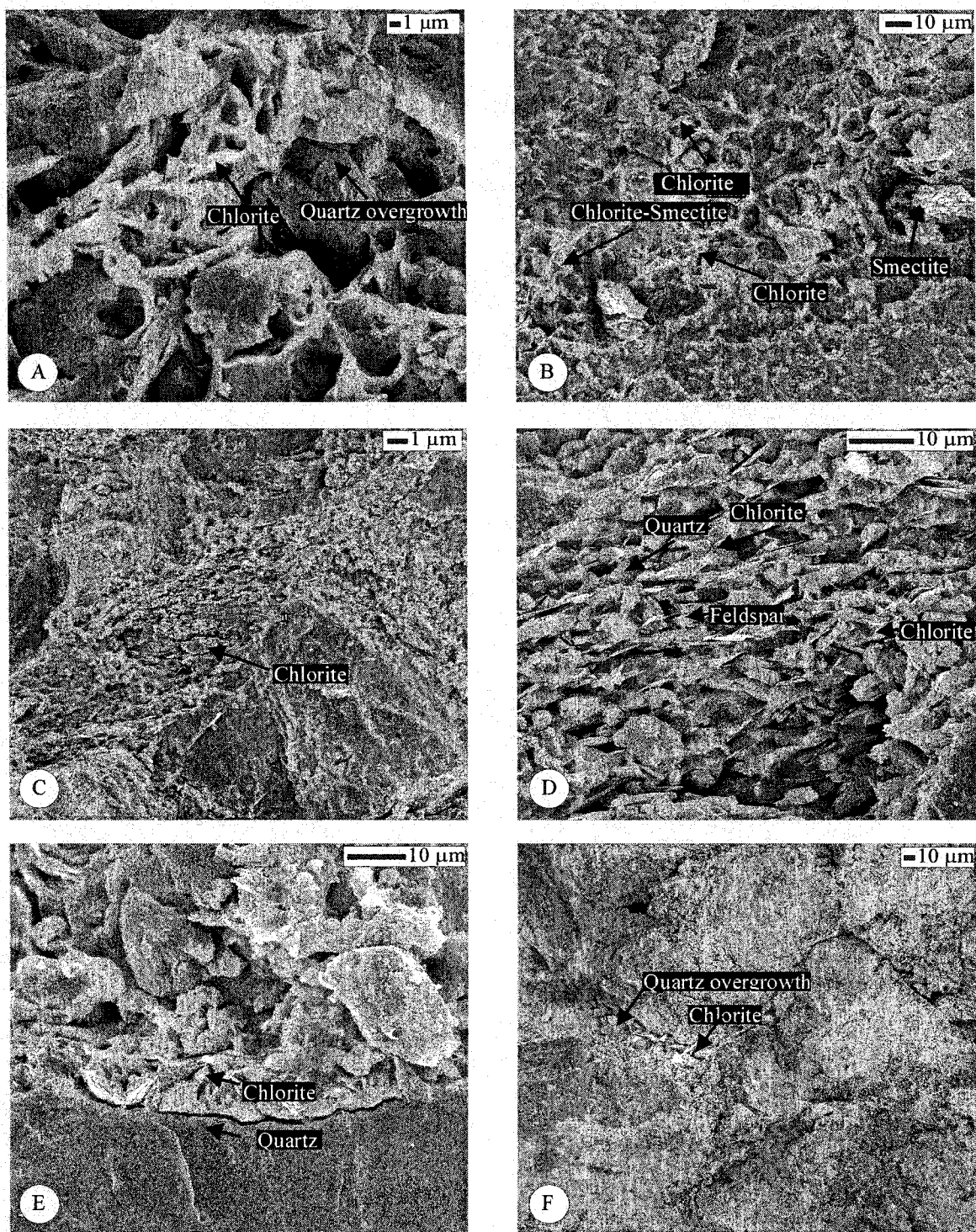
Figure B-37. Scanning electronic photomicrographs: (A, B and C) authigenic chlorite, chlorite/smectite within the upper Coalspur sandstones (sample 12, upper Coalspur Formation, roadcut, Red Deer River locality); (D) chlorite interfering with the process of quartz overgrowth (sample 11, upper Coalspur Formation, roadcut, Red Deer River locality); (E) quartz grains coated by authigenic chlorite (sample 11, upper Coalspur Formation, roadcut, Red Deer River locality); (F) chlorite interfering with the process of quartz overgrowth (sample 12, upper Coalspur Formation, roadcut, Red Deer locality).
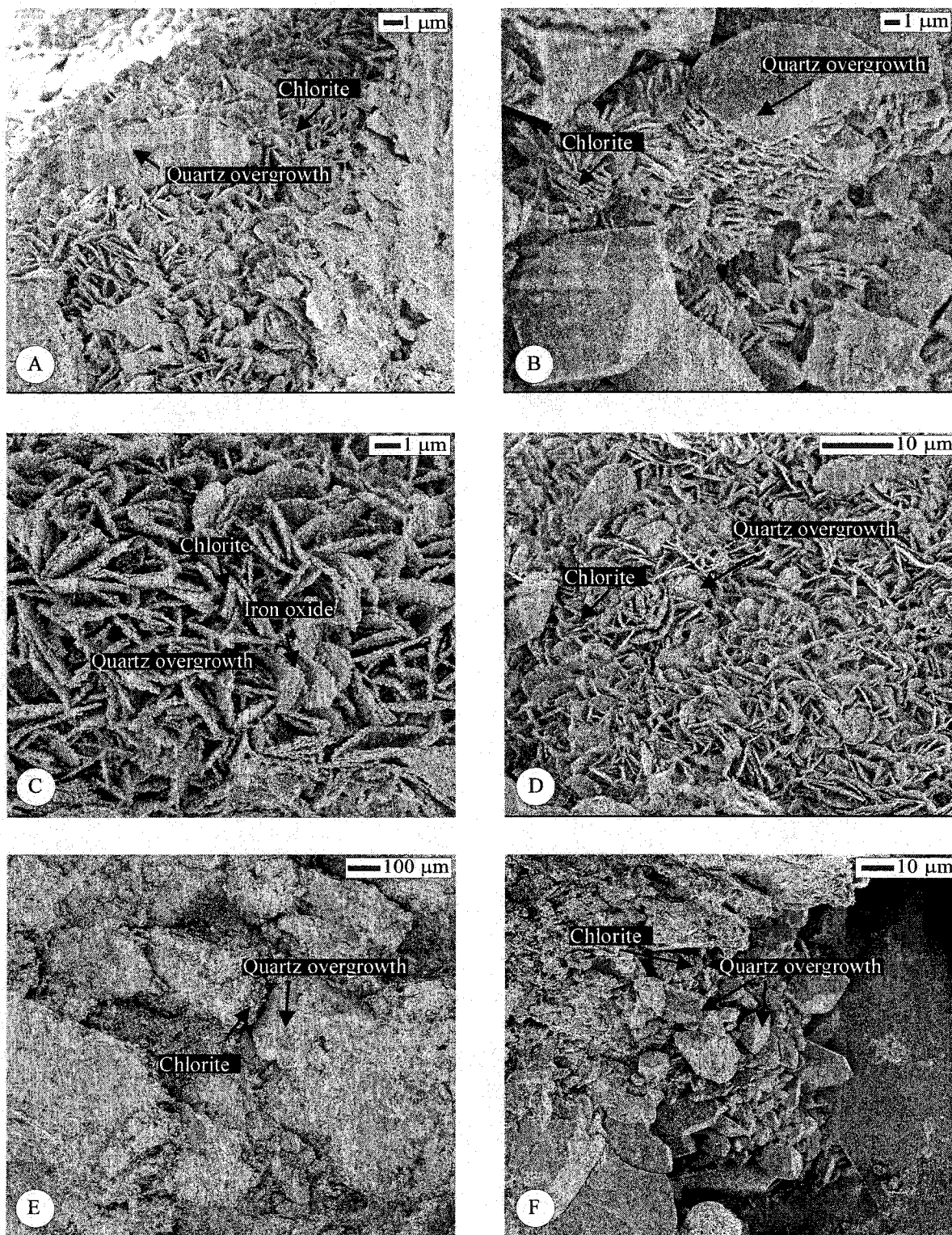
Figure B-38. Scanning electronic photomicrographs: (A, B, C, D, E and F) chlorite interfering with the process of quartz overgrowth (sample 10, upper Coalspur Formation, roadcut, Red Deer River locality
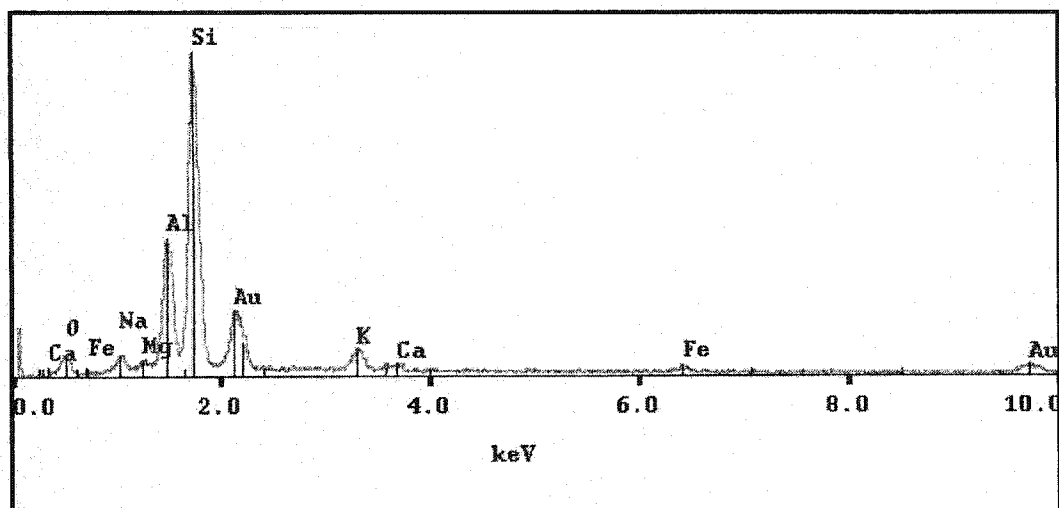
Figure B-39. X-ray diffraction pattern showing the presence of smectite (sample 10, upper Coalspur Formation, roadcut along Red Deer River).
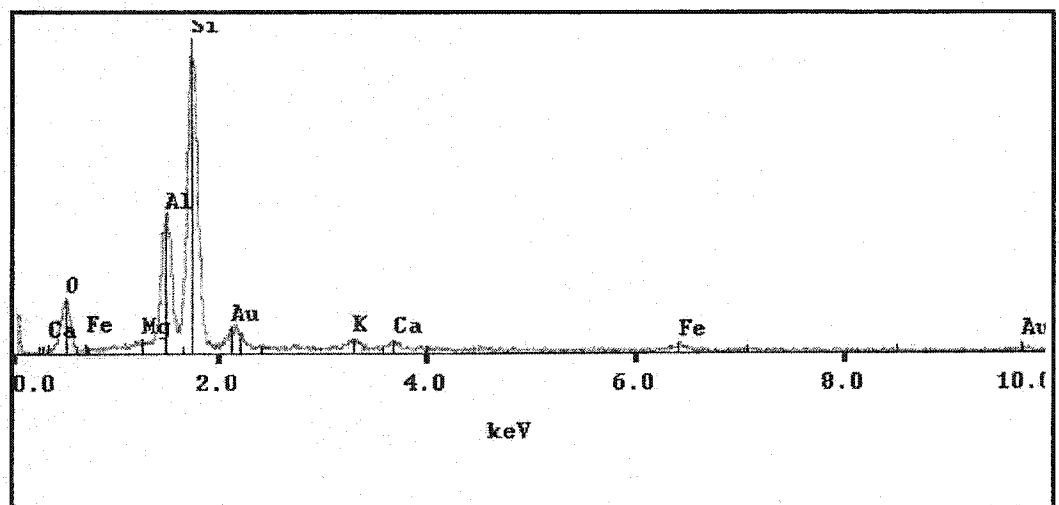
Figure B-40. X-ray diffraction pattern showing the presence of smectite (sample 11, upper Coalspur Formation, roadcut along Red Deer River).

239

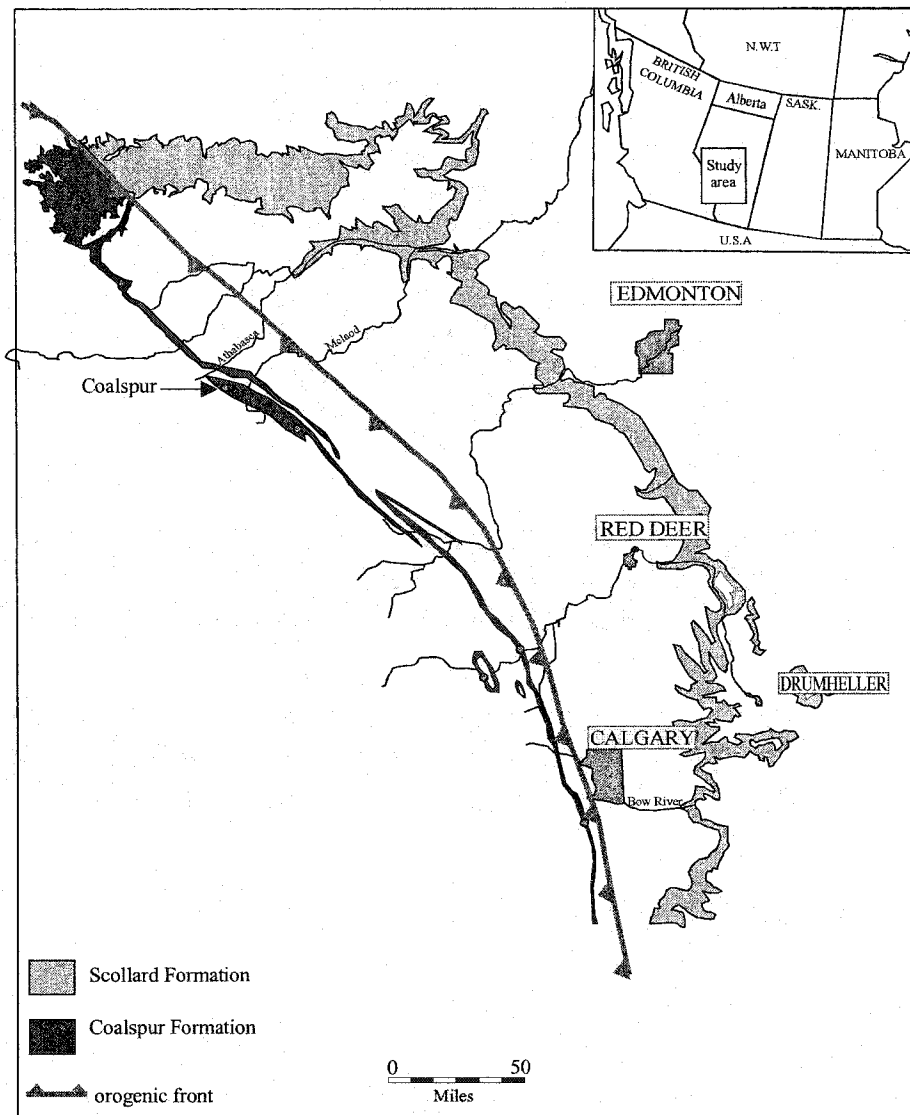Figure B-41.Outcrop distribution of the Scollard and Coalspur formations in Alberta, and the location of the studied outcrop section, Sundre locality.
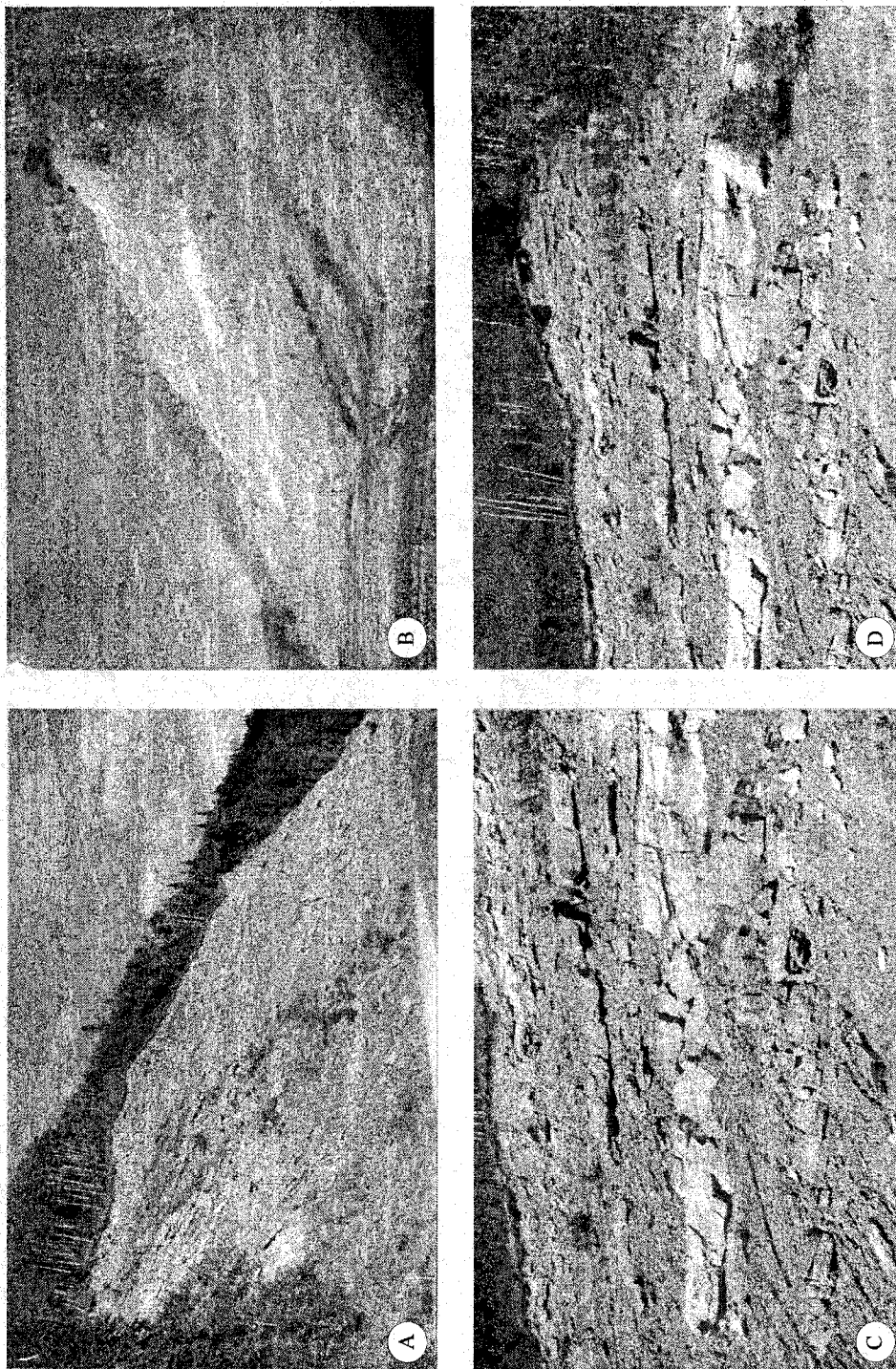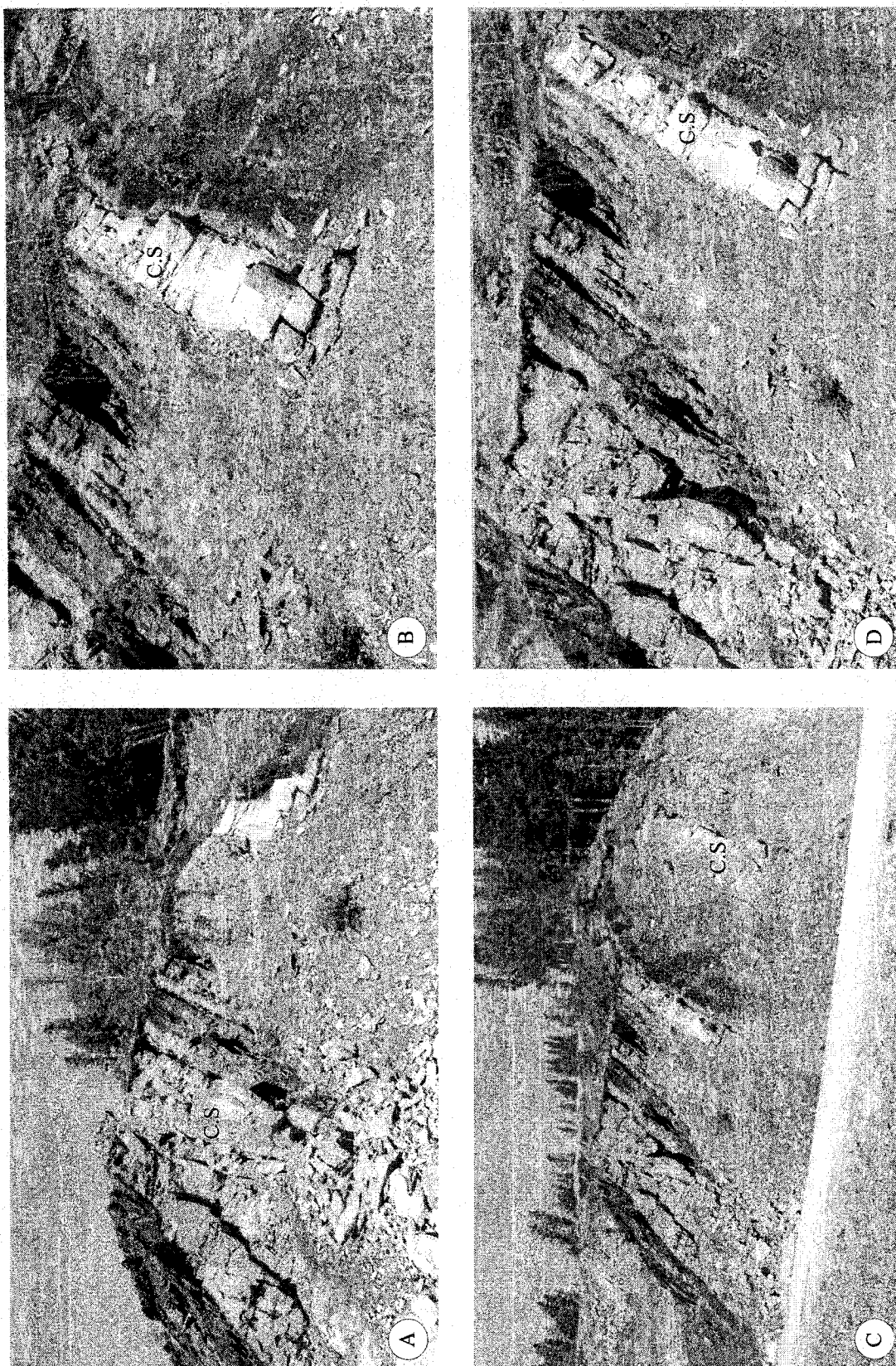
Figure B-42. Outcrop photographs of the upper Coalspur Formation, Sundre locality: (A and B) outcrop photograph showing a fluvial-lacustrine successions with lacustrine mudestones interbedded with distributary mouth-bar/distributary channel sands; (C and D) close-up views of the middle part of the section.

241
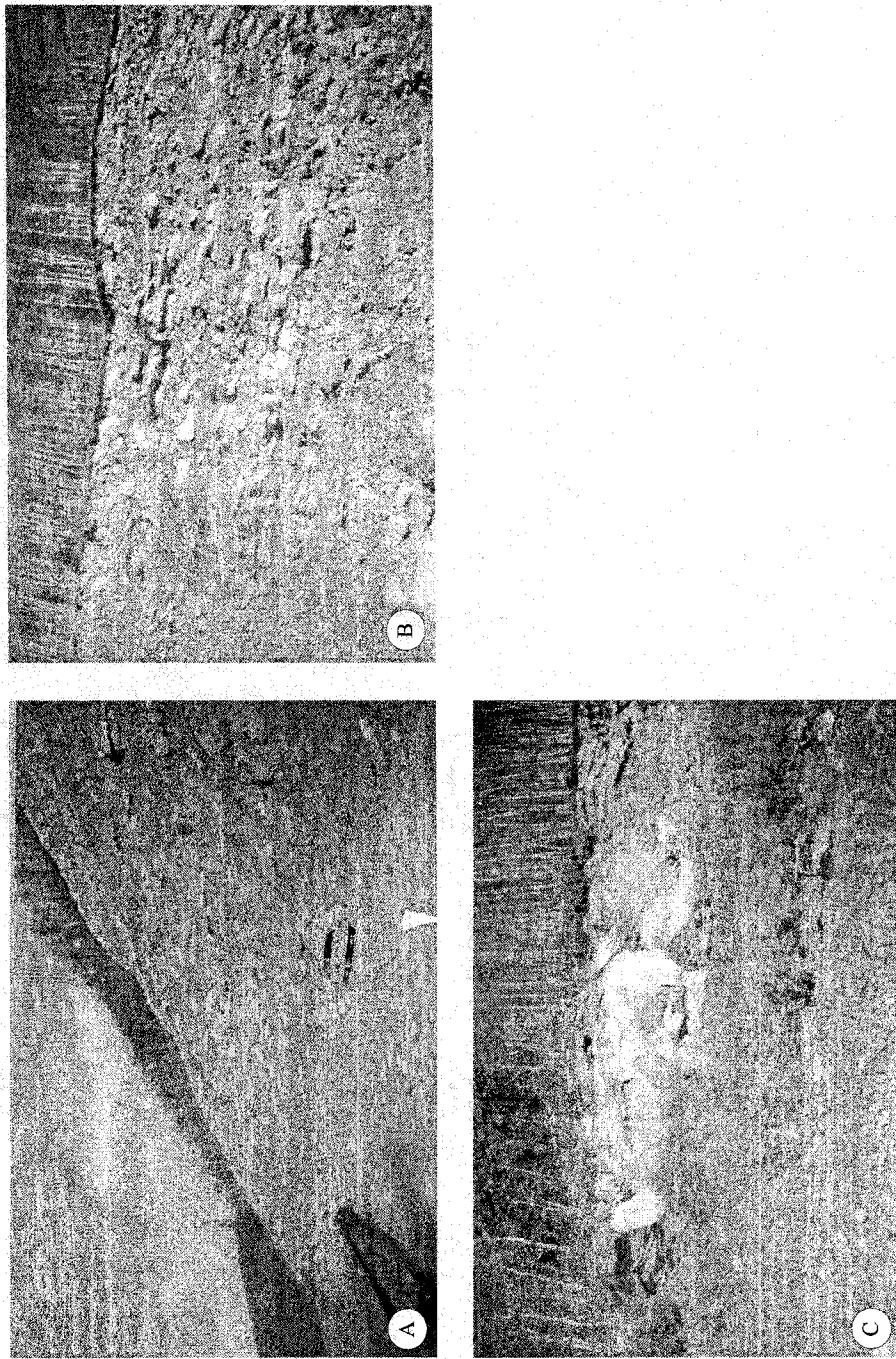
Figure B-43. Outcrop photographs of the upper Coalspur Formation, Sundre locality: (A and B) outcrop photograph showing a fluvial-lacustrine successions with floodplain/lacustrine mudstones interbedded with distributary mouth-bar/distributary channel sands; (C) close-up views of distributary channel.
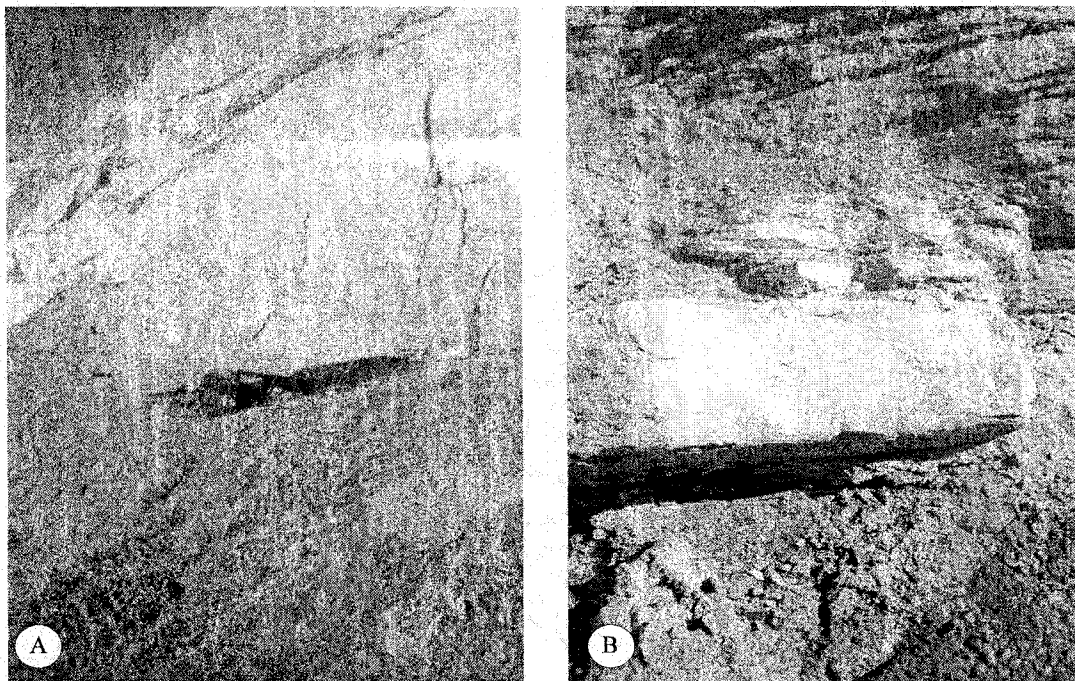
Figure B-44, a. Outcrop photographs of the upper Coalspur Formation, Sundre locality: (A and B) close-up views of sandstone unite of distributary channel.

243
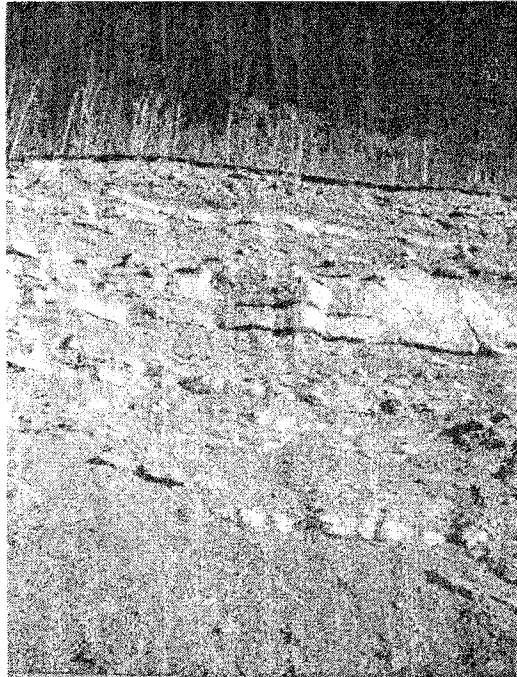
Figure B-44, b. Outcrop photographs of the upper Coalspur Formation, Sundre locality: a fluvial-lacustrine successions with floodplain/lacustrine mudestones interbedded with distributary mouth-bar/distributary channel sands.

244

Figure B-45. Thin-section photomicrographs: (A, B, C, D and F) quartz grains surrounded early calcite cement (arrows). Note secondary and residual primary porosity (sample 1, upper Coalspur Formation, Sundre locality);(F) quartz grains. Note packing of quartz grains and residue primary porosity (arrow) (sample 2, upper Coalspur Formation, Sundre locality).
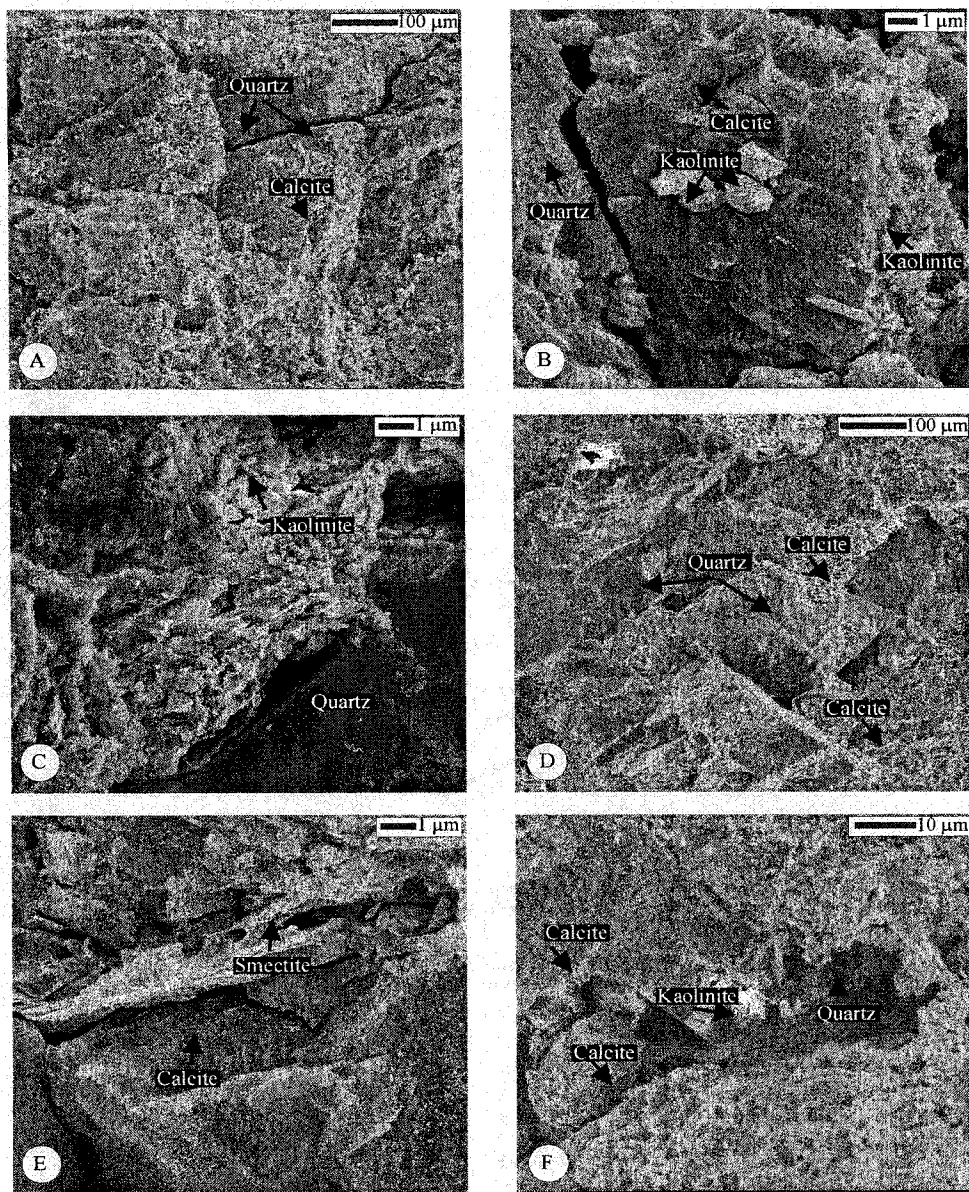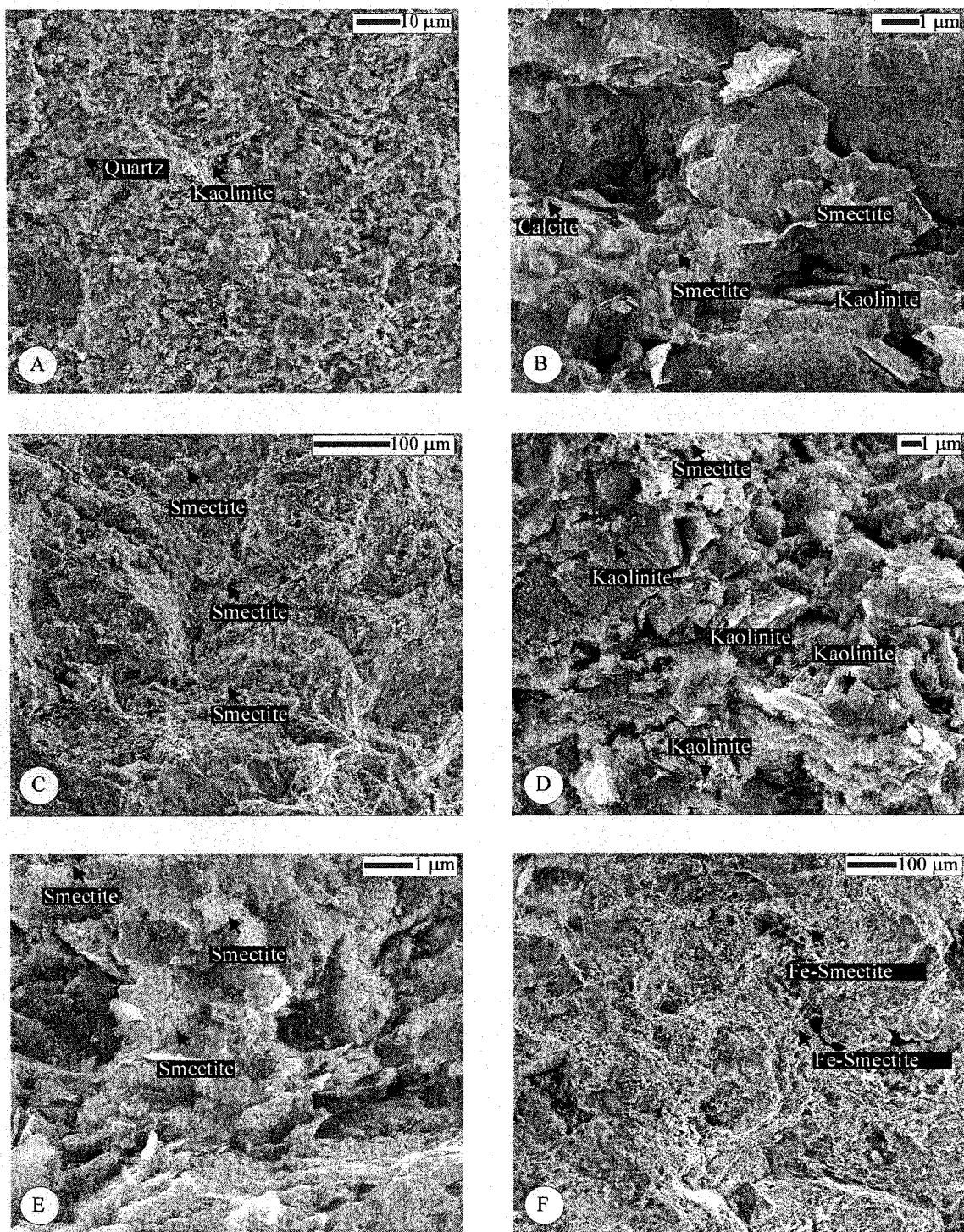
Figure B-46. Scanning electronic photomicrographs: (A) calcite cement, and quartz grains; (sample 2, upper Coalspur Formation, Sundre locality); (B) blocky calcite (arrow) surrounded quartz grains. Note the poor growth of authigenic kaolinite ; (sample 3, upper Coalspur Formation, Sundre locality); (C) vermicularaggregates of euhedral crystals of authigenic kaolinite;(sample 1, upper Coalspur Formation, Sundre locality); (E) blocky calcite cement (arrow) surrounded by quartz grains (sample 1, upper Coalspur Formation, Sundrelocality (E) blocky calcite cement (arrow) surrounded by smectite (sample 5, upper Coalspur Formation, Sundre locality; (F) quartz grain surrounded by early poikilotopic calcite cement (sample 3, upper Coalspur Formation, Formation, Sundre locality).
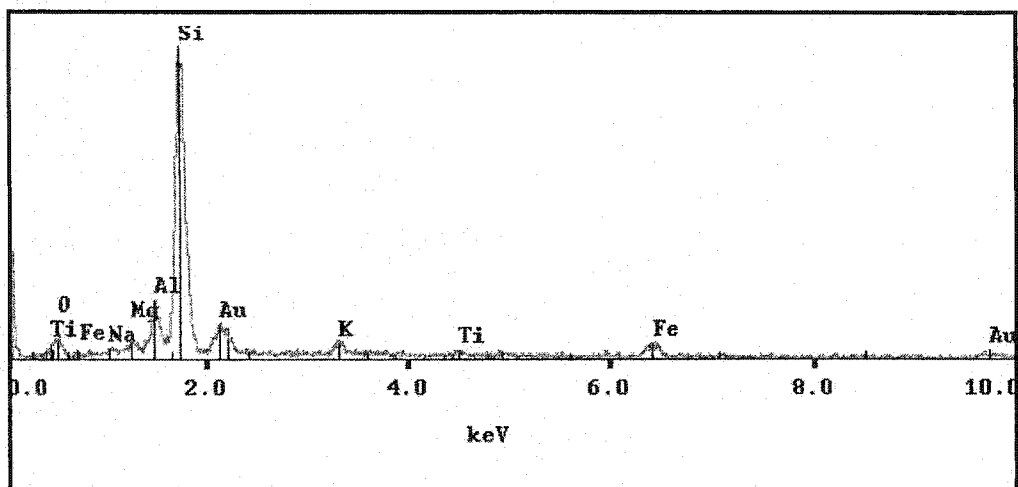
Figure B-47 X-ray diffraction pattern showing the presence of quartz (sample 2, upper Coalspur Formation, Sundre locality).
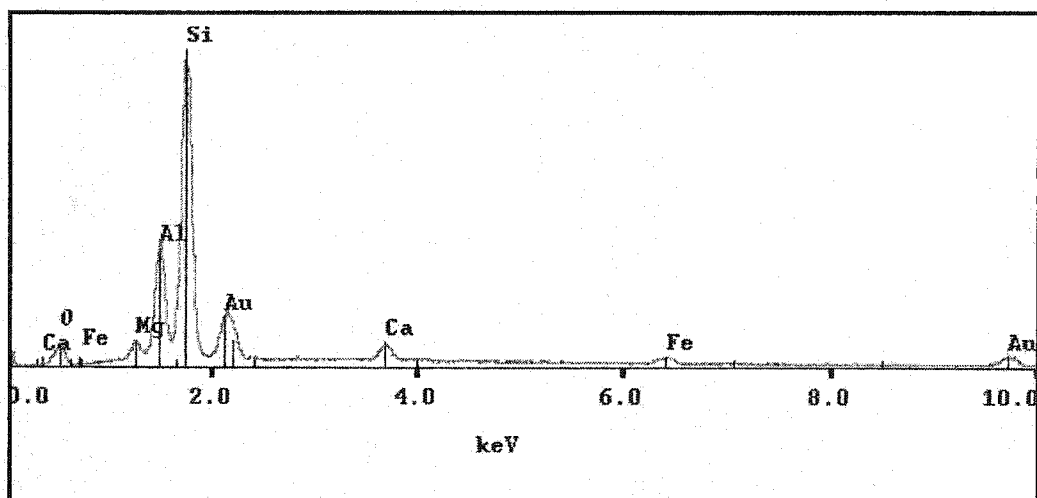
Figure B-48. X-ray diffraction pattern showing the presence of smectite (sample 3, upper Coalspur Formation, Sundre locality).

247

Figure B-49. Outcrop distribution of the Scollard and Coalspur formations
in Alberta, and the location of the studied outcrop section, Coalspur locality.

Figure B-50. Outcrop photographs of the upper Coalspur Formation, Coal Valley locality: (A and C) outcrop photographs showing coal seam interbedded with sandstone beds of splay origin (C.S.); (B and D) close-up views sandstone beds and coal swam associated very fine grained sediments.
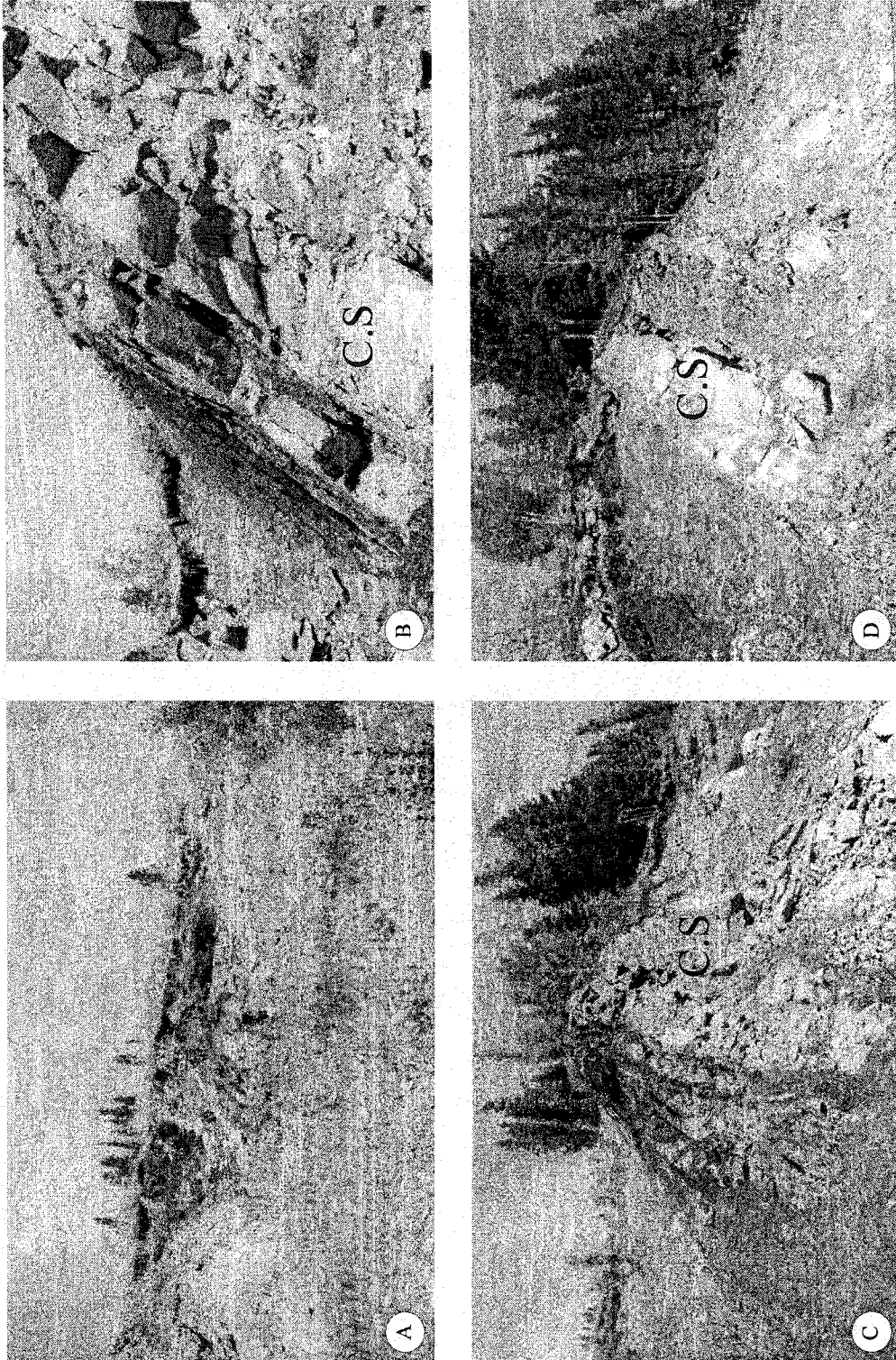
Figure B-51. Outcrop photographs of the upper Coalspur Formation, Coal Valey locality: (A) outcrop photographs showing coal seam interbedded with sandstone beds of splay origin; (B, C and D) close-up views sandstone beds of splay origin are present within the coal and associated very fine grained sediments.
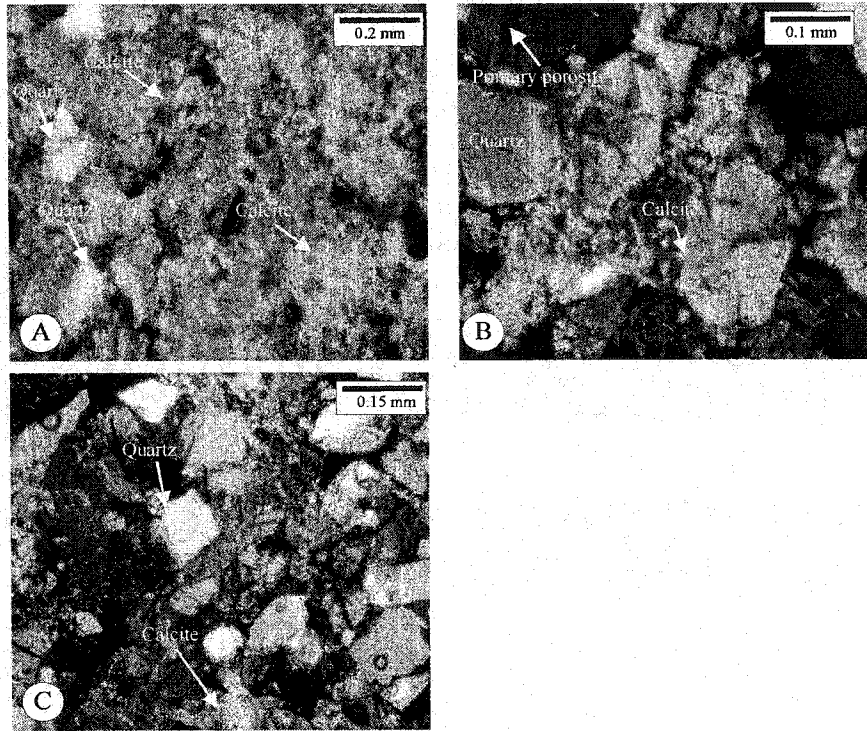
Figure B-52. Thin-section photomicrographs: (A) poikilotopic calcite cement (arrows) and monocrystalline quartz (sample 1, upper Coalspur Formation, Coalspur locality); (B) monocrystalline and calcite cement. Note primary porosity (arrow) (sample 2, upper Coalspur Formation, Coalspur locality); (C) poikilotopic calcite cement (arrow) and monocrystalline quartz (sample 2, upper Coalspur Formation, Coalspur locality).

Figure B-53. Scanning electronic photomicrographs: (A) pore fills kaolinite and quartz grains (sample 1, upper Coalspur Formation, Coalspur locality); (B) authigenic smectite and early calcite cement. Note the poor development of kaolinite (sample 2, upper Coalspur Formation, Caolspur locality); (C and E) pore fills smectite (sample 2, upper Coalspur Formation, Coalspur locality); (D) vermicular aggregates of euhedral crystals of authigenic kaolinite. The kaolinite booklets have no preferred orientation, and consume much of the primary porosity. (sample 1, upper Coalspur Formation, Coalspur locality); (F) - Fe-rich smectite, as determined by XRD analysis (sample 2, upper Coalspur Formation, Coalspur locality).
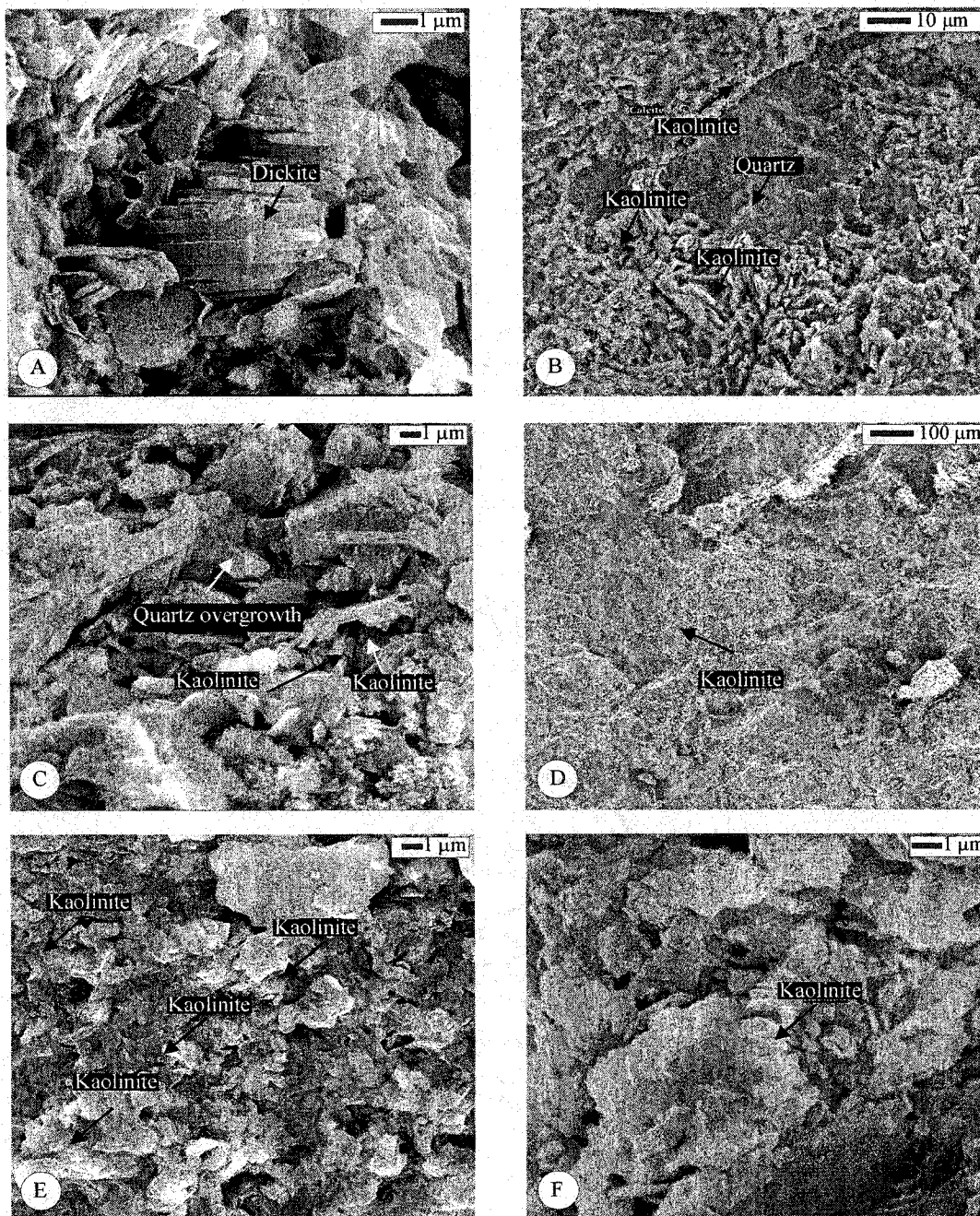
Figure B-54. Scanning electronic photomicrographs: (A) authigenic dickite within the upper Coalspur Formation (sample 4, upper Coalspur Formation, Coalspur locality); (B) quartz grain surrounded by authigenic kaolinite (sample 3, upper Coalspur Formation, Caolspur locality); (C) kaolinite interfering with the process of quartz overgrowth (sample 5, upper Coalspur Formation, Coalspur locality); (D, E, and F) aggregates of kaolinite Crystals (sample 5, upper Coalspur Formation, Coalspur locality).
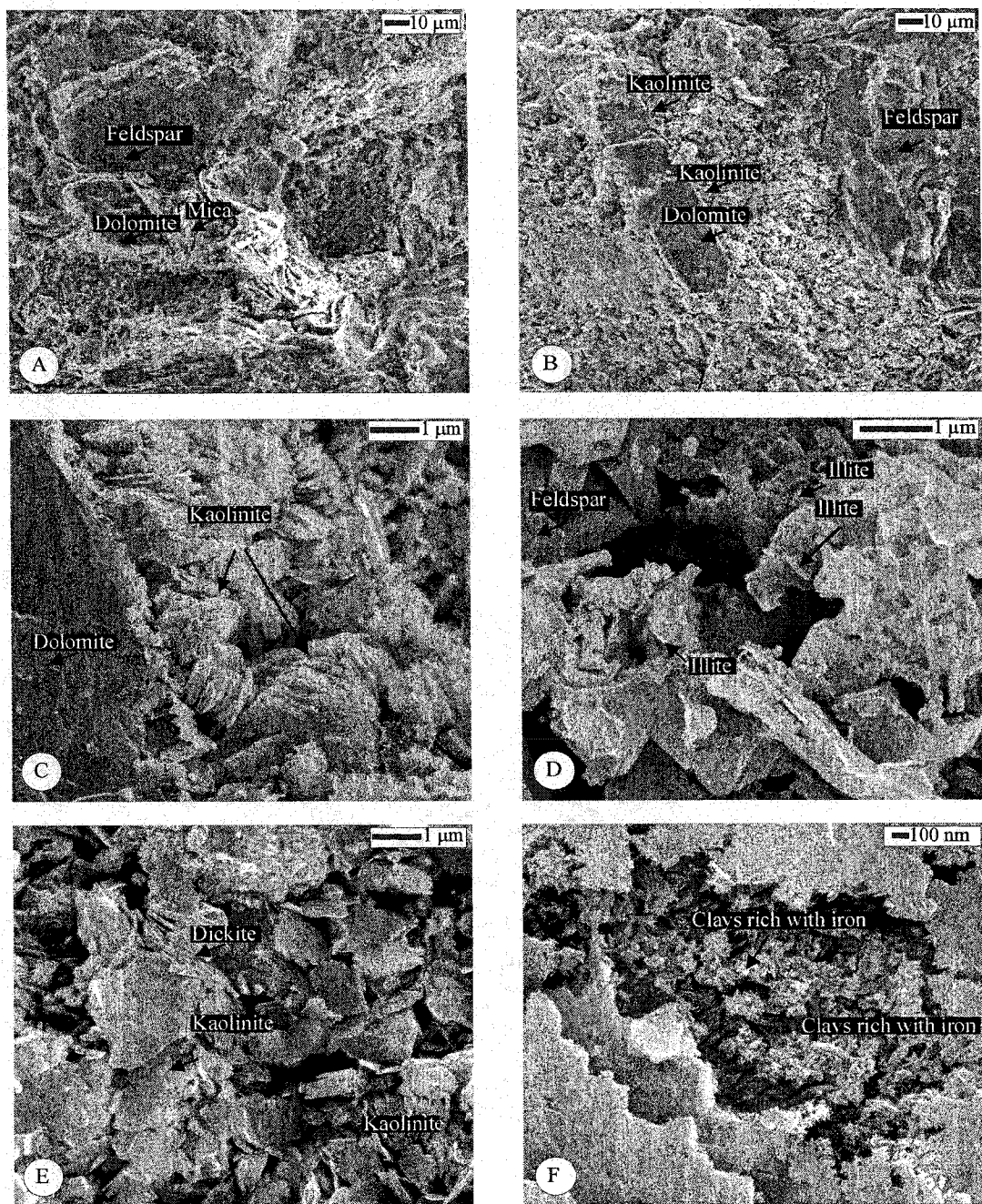
Figure B-55. Scanning electronic photomicrographs: (A) detrital grains of feldspar, mica and dolomite (sample 4, upper Coalspur Formation, Coalspur locality); (B and C) Dolomite grain surrounded by authigenic kaolinite (sample 5, upper Coalspur Formation, Caolspur locality); (D) feldspar alteration into illite (sample 4, upper Coalspur Formation, Coalspur locality); (E) aggregates of kaolinite and dickite within the upper Coalspur sandstones (sample 4, upper Coalspur Formation, Coalspur locality); (F) clays rich minerals and with iron deposits (sample 5, upper Coalspur Formation, Coalspur locality).
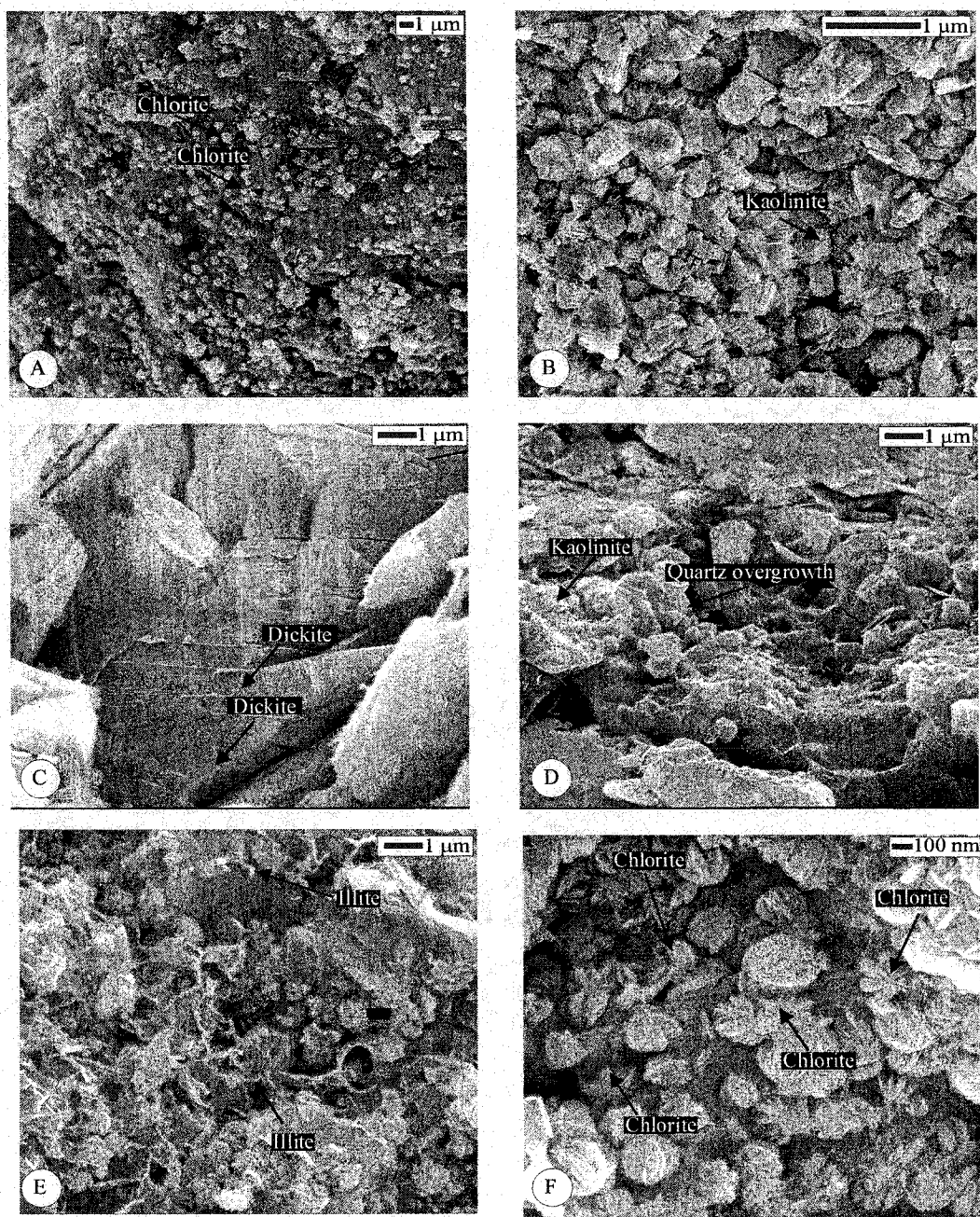
Figure B-56. Scanning electronic photomicrographs: (A and F) early diagenetic chlorite (sample 5,upper Coalspur Formation, Coalspur locality); (B) vermicular aggregates of euhedral crystals of authigenic kaolinite (sample 2, upper Coalspur Formation, Caolspur locality); (C) blocky shape of dickite crystals (sample 4, upper Coalspur Formation, Caolspur locality); (D) kaolinite interfering with the process of quartz overgrowth (sample 3, upper Coalspur Formation, Coalspur locality); (E) illite within the upper Coalspur sandstones (sample 4, upper Coalspur Formation, Coalspur locality).
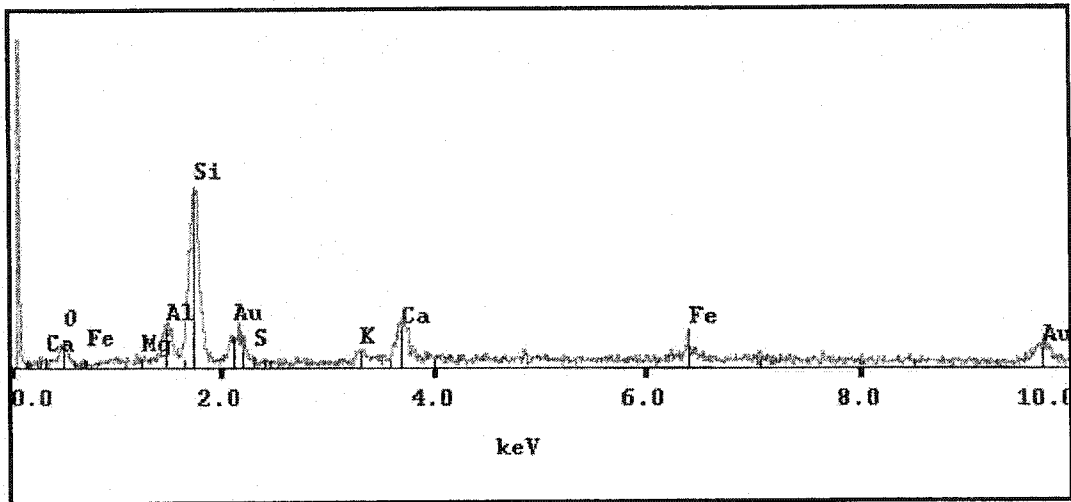
Figure B-57. X-ray diffraction pattern showing the presence of Fe-smectite (sample 1, upperCoalspur Formation, Coalspur locality).
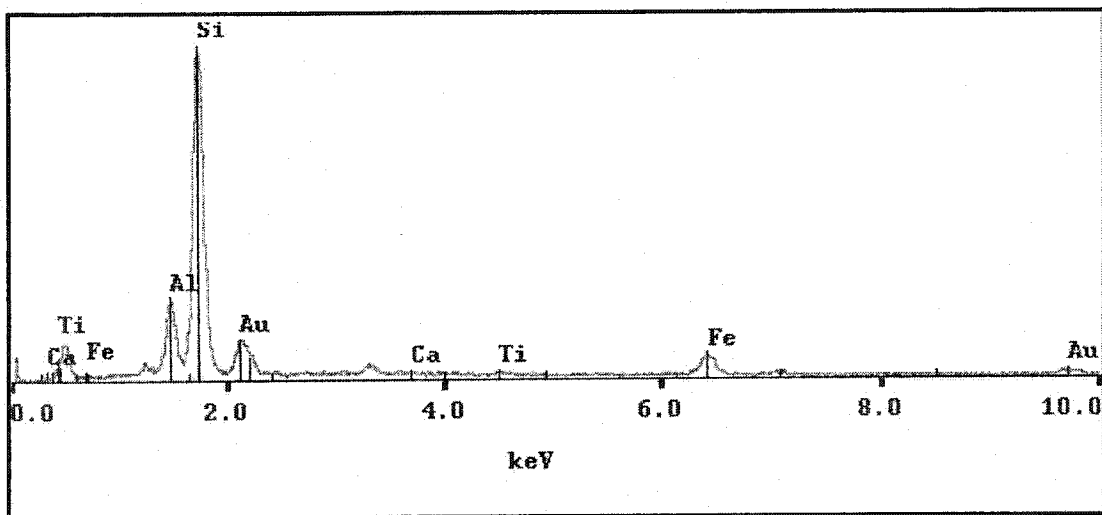
Figure B-58. X-ray diffraction pattern showing the presence of Fe-smectite (sample 2, upperCoalspur Formation, Coalspur locality).
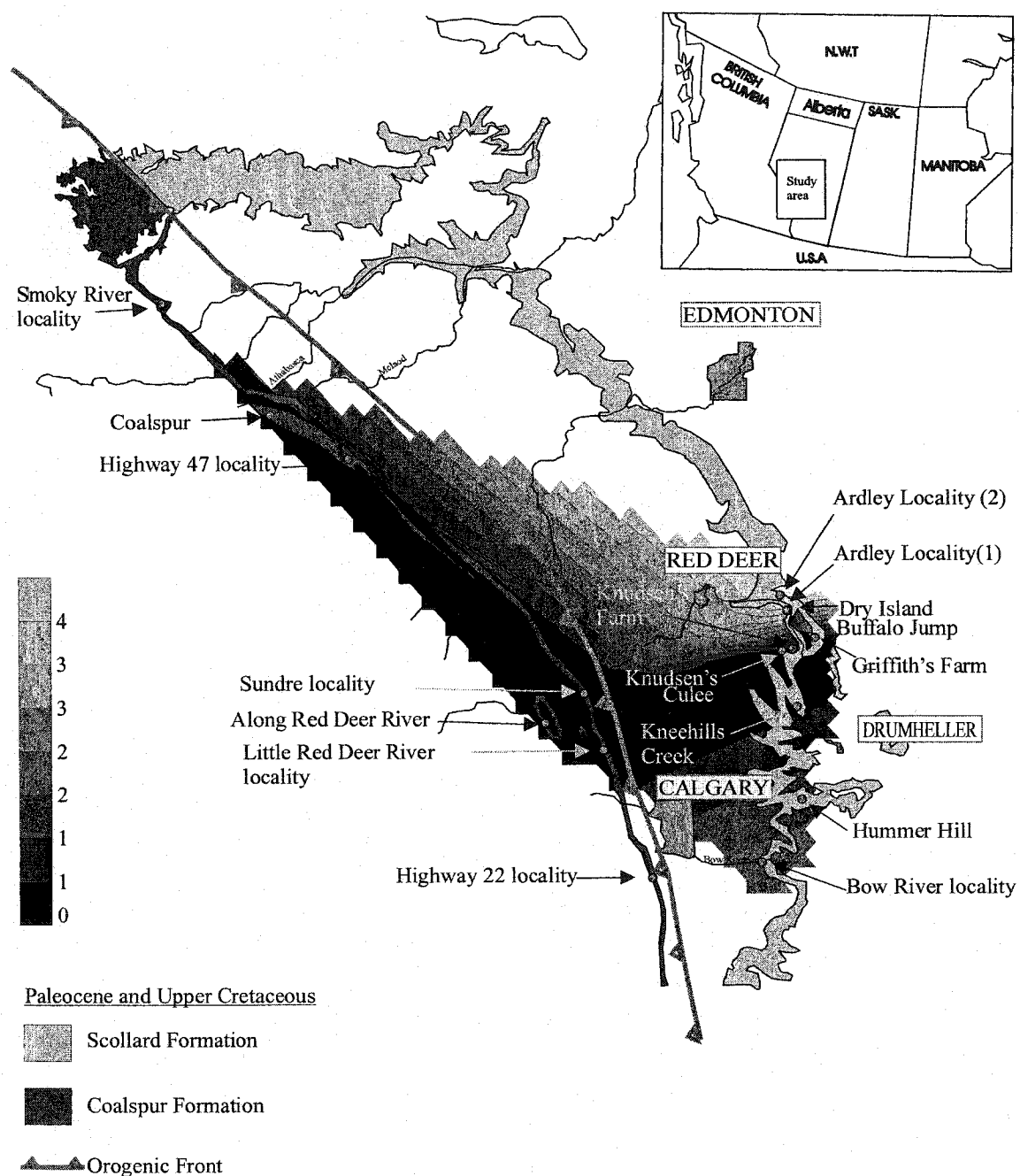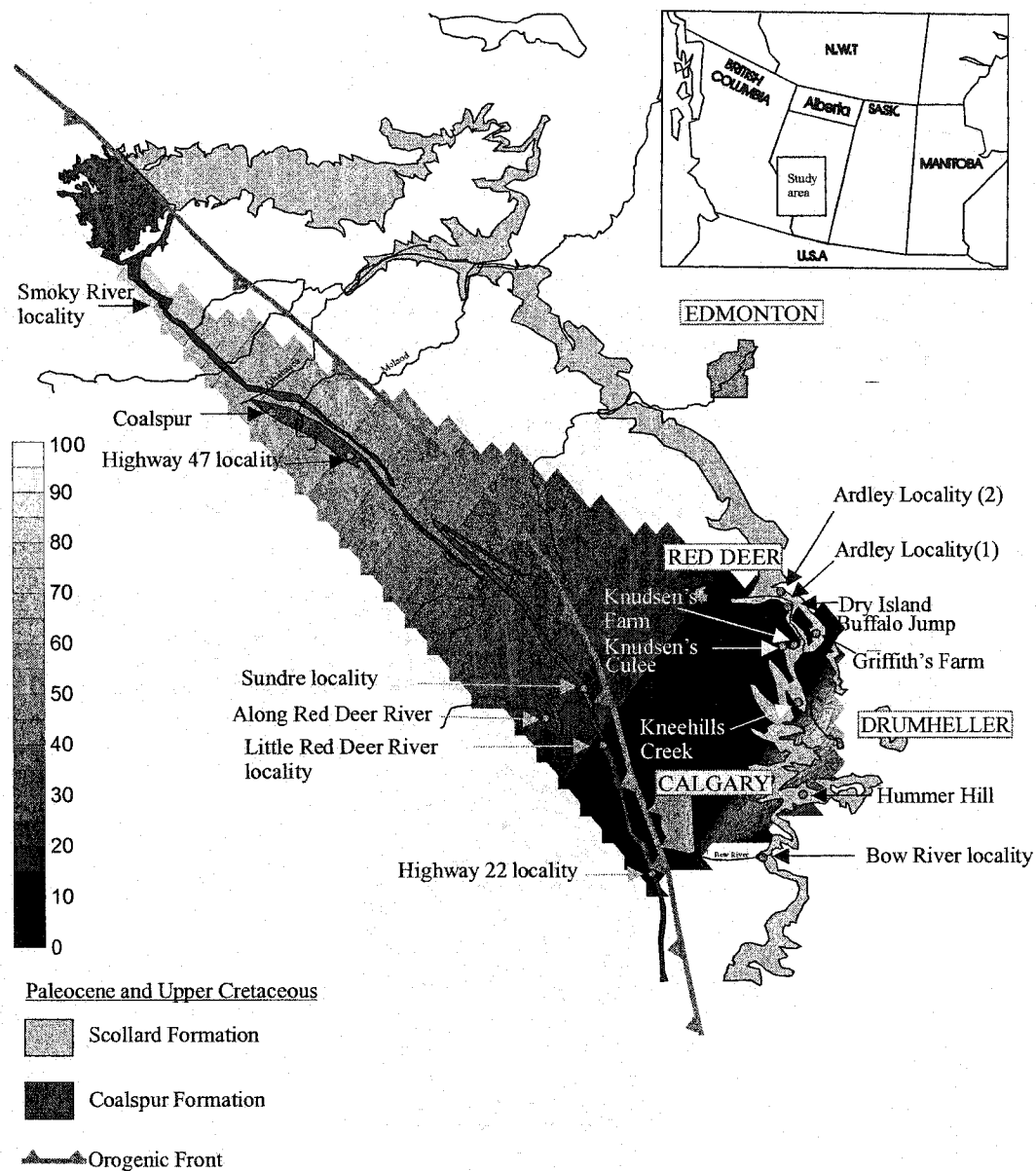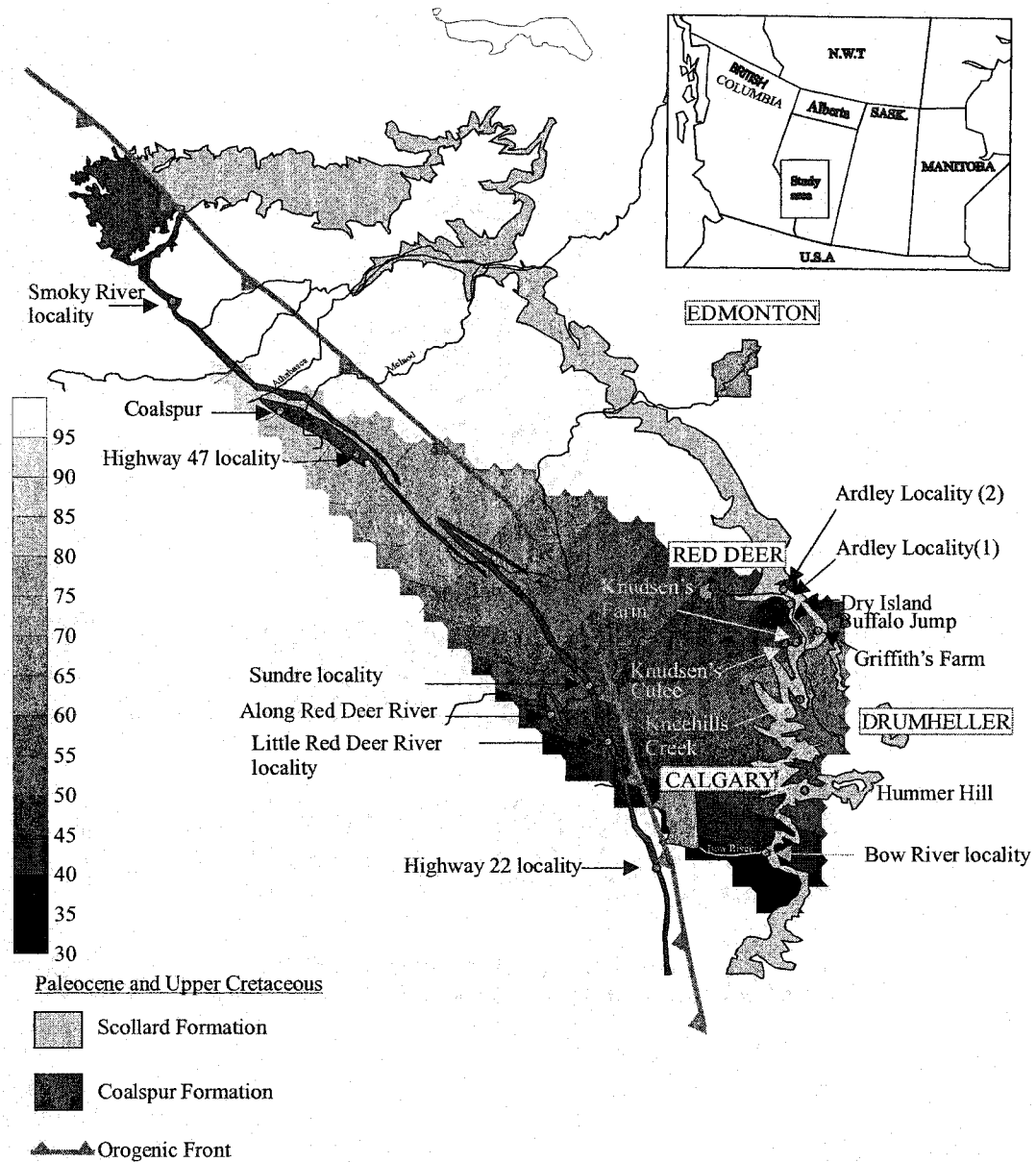
Appendix C
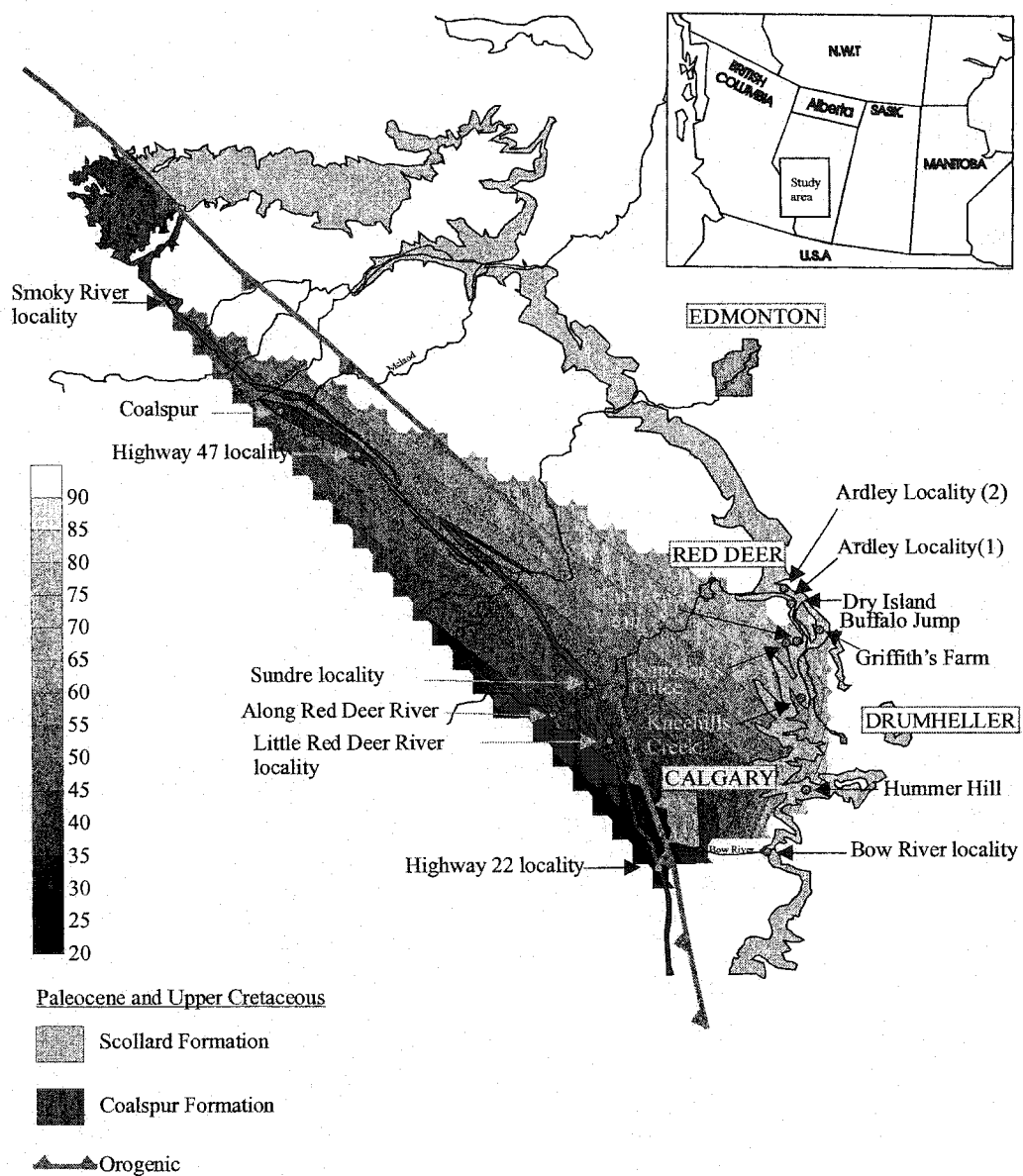
Figure C-1. Contour map showing the distribution of authigenic smectite in the lower Scollard and Coalspur sandstones, west central Alberta.
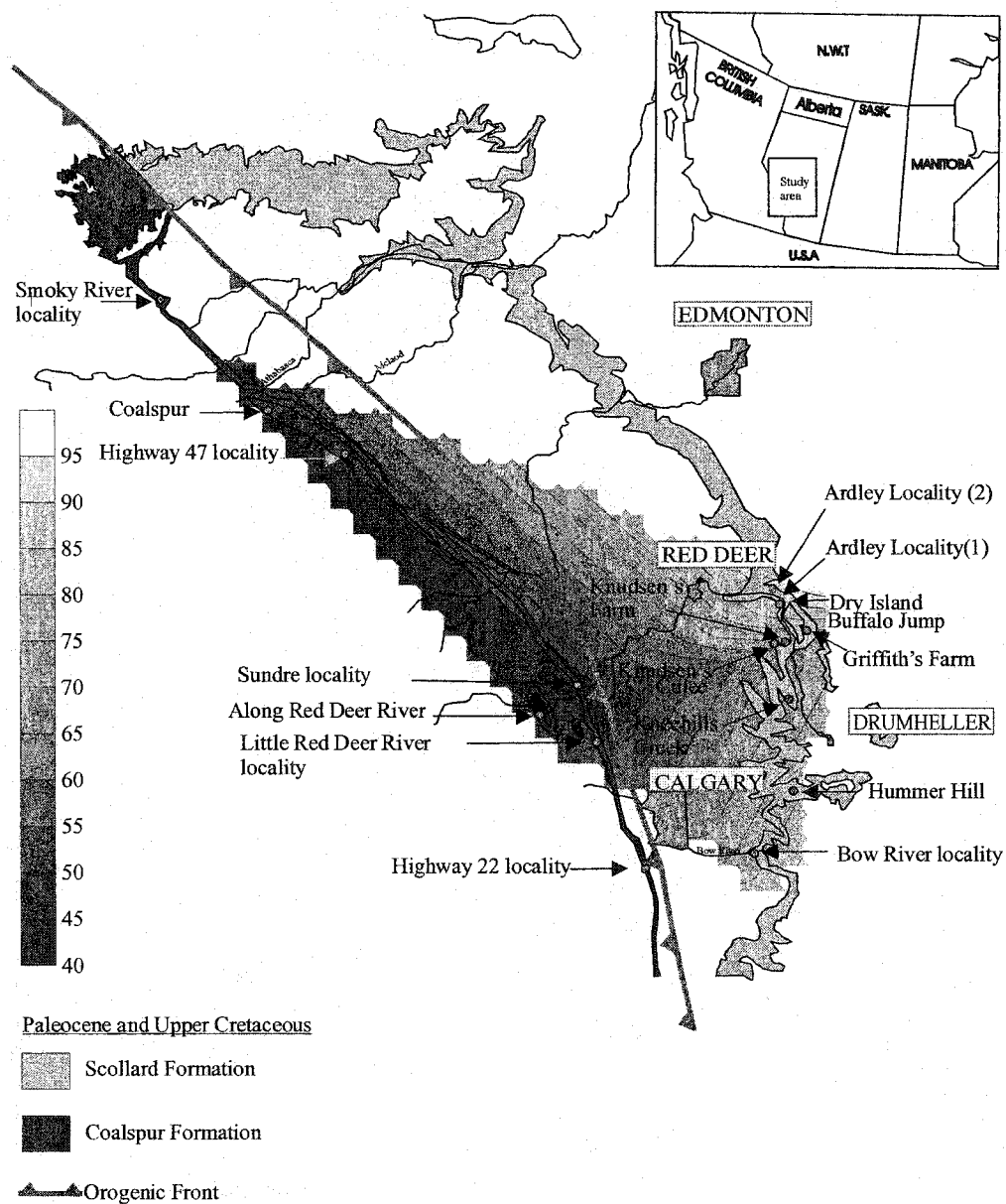
Figure C-2. Contour map showing the distribution of authigenic smectite
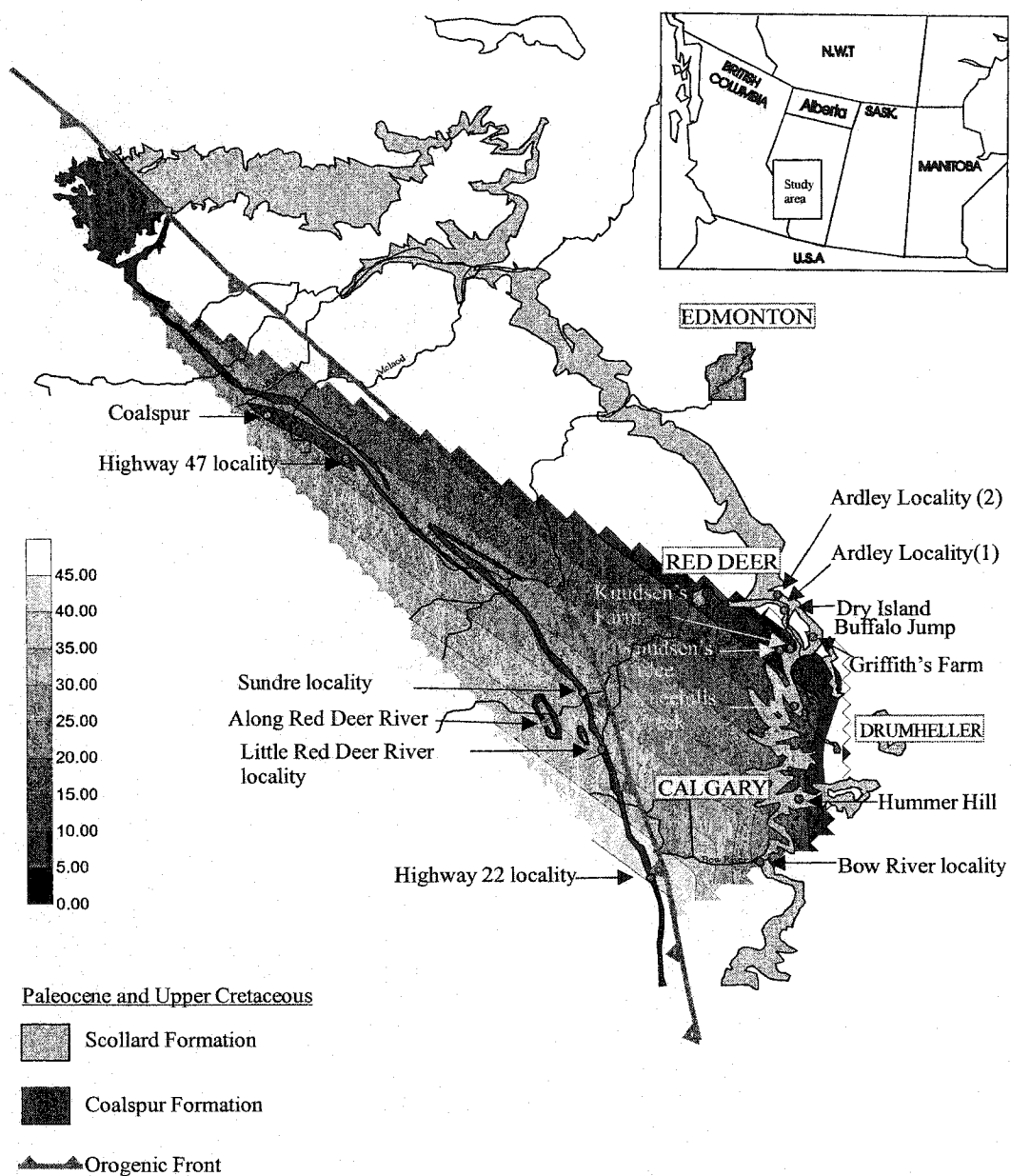in the upper Scollard and Coalspur sandstones, west central Alberta.
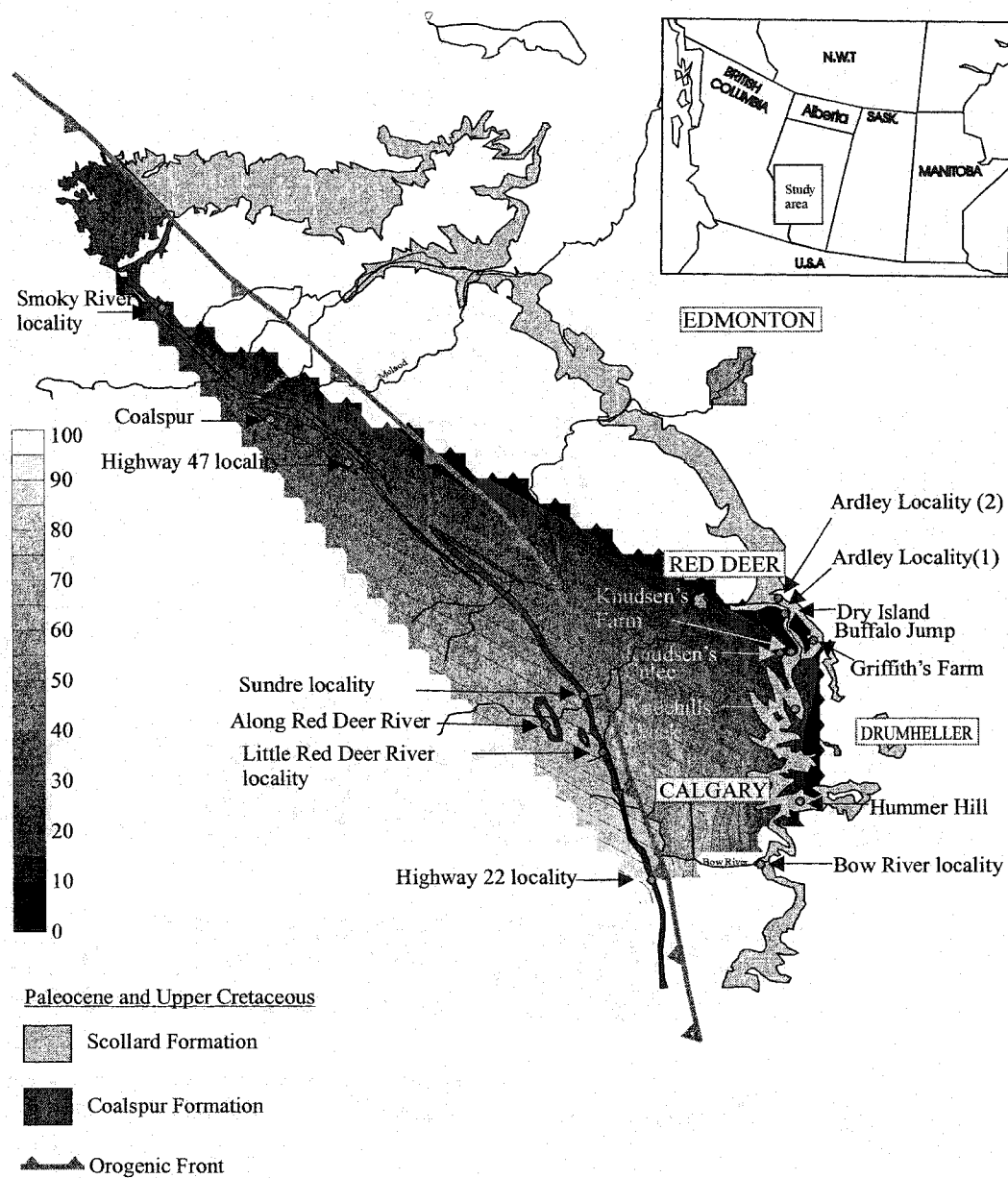
Figure C-3. Contour map showing the distribution of authigenic chlorite in the lower Scollard and Coalspur sandstones, west central Alberta.
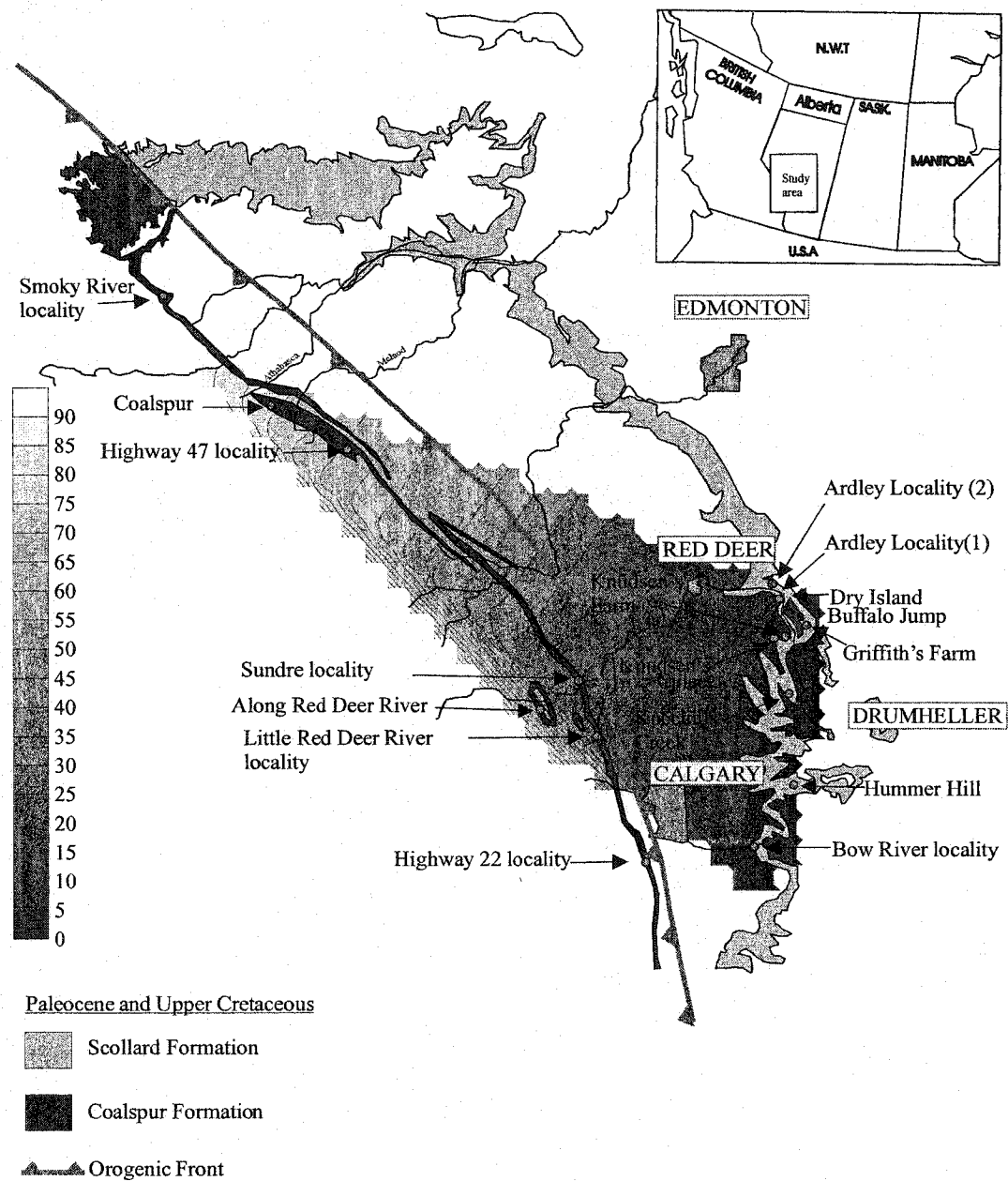
Figure C-4. Contour map showing the distribution of authigenic chlorite in the upper Scollard and Coalspur sandstones, west central Alberta.
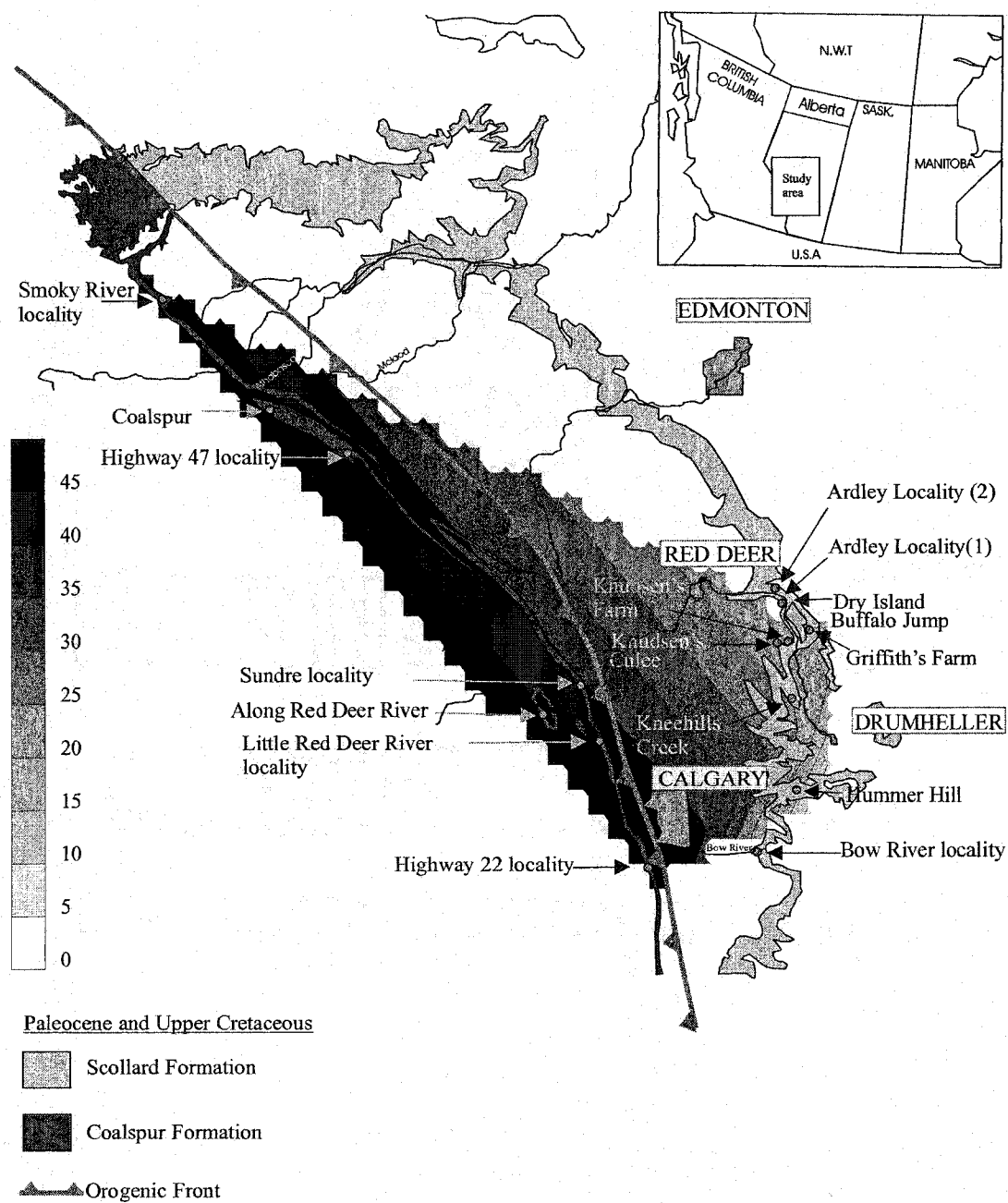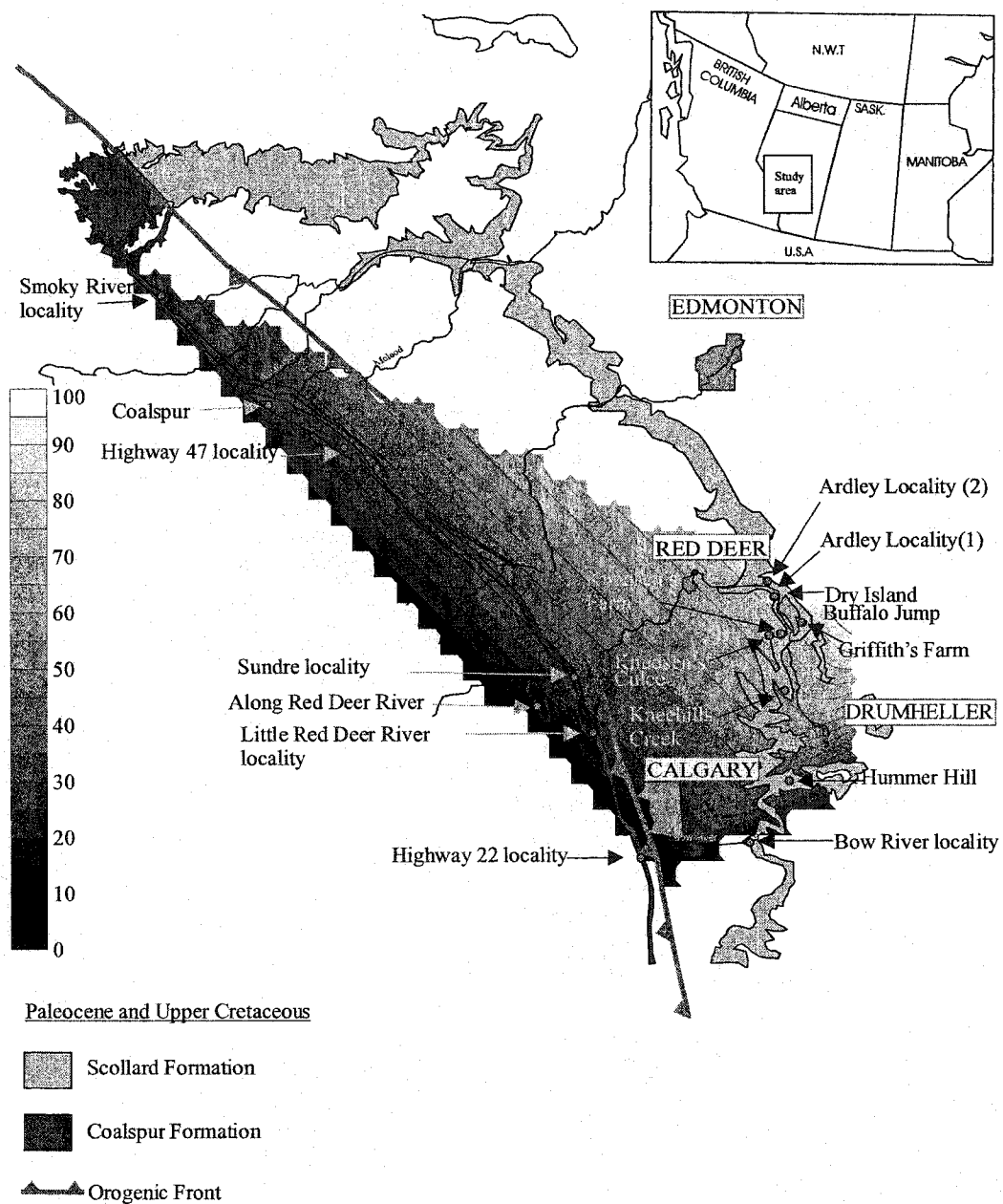
Figure C-5. Contour map showing the distribution of authigenic illite
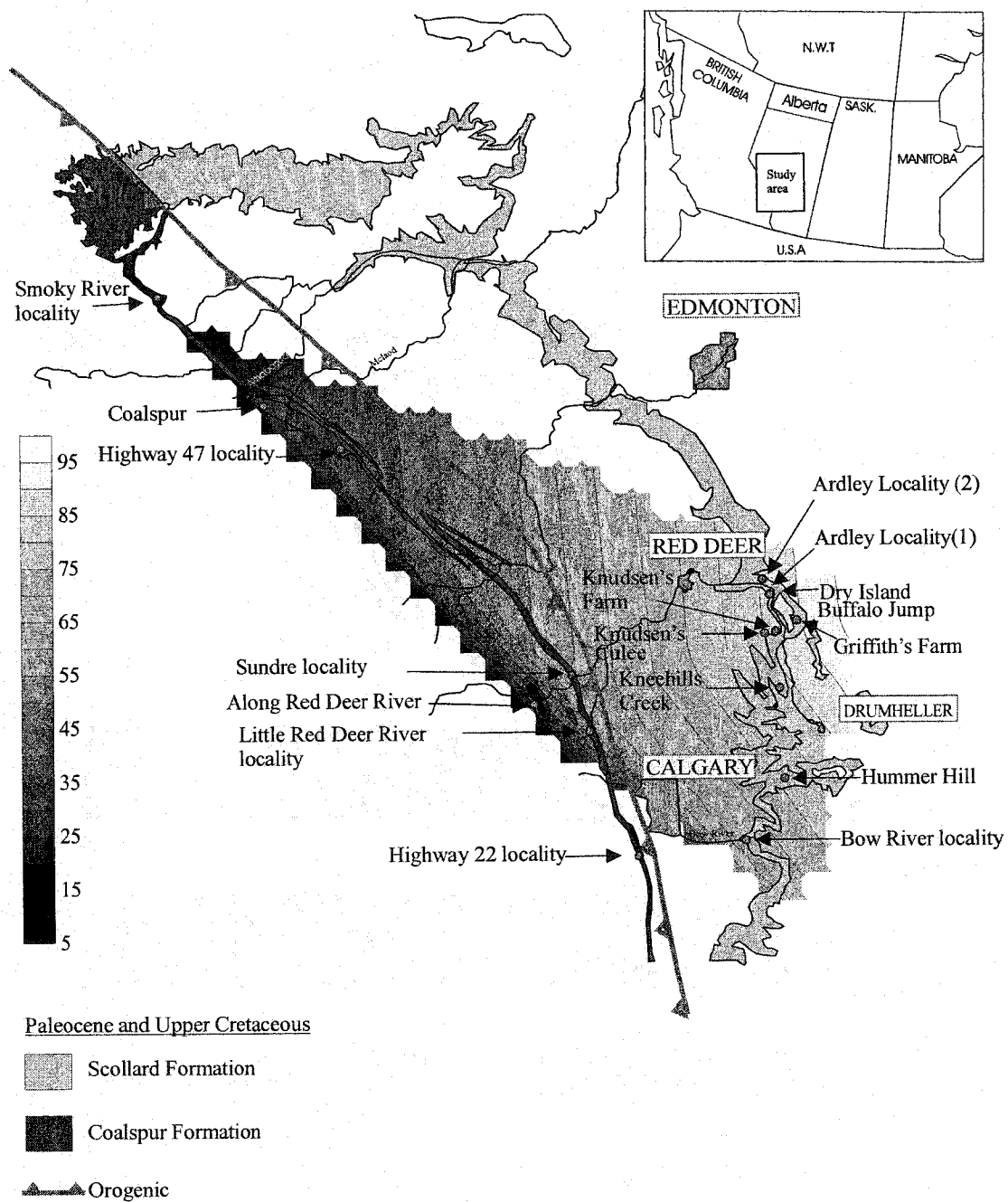in the lower Scollard and Coalspur sandstones, west central Alberta.

Figure C-6. Contour map showing the distribution of authigenic illite in the upper Scollard and Coalspur sandstones, west central Alberta.
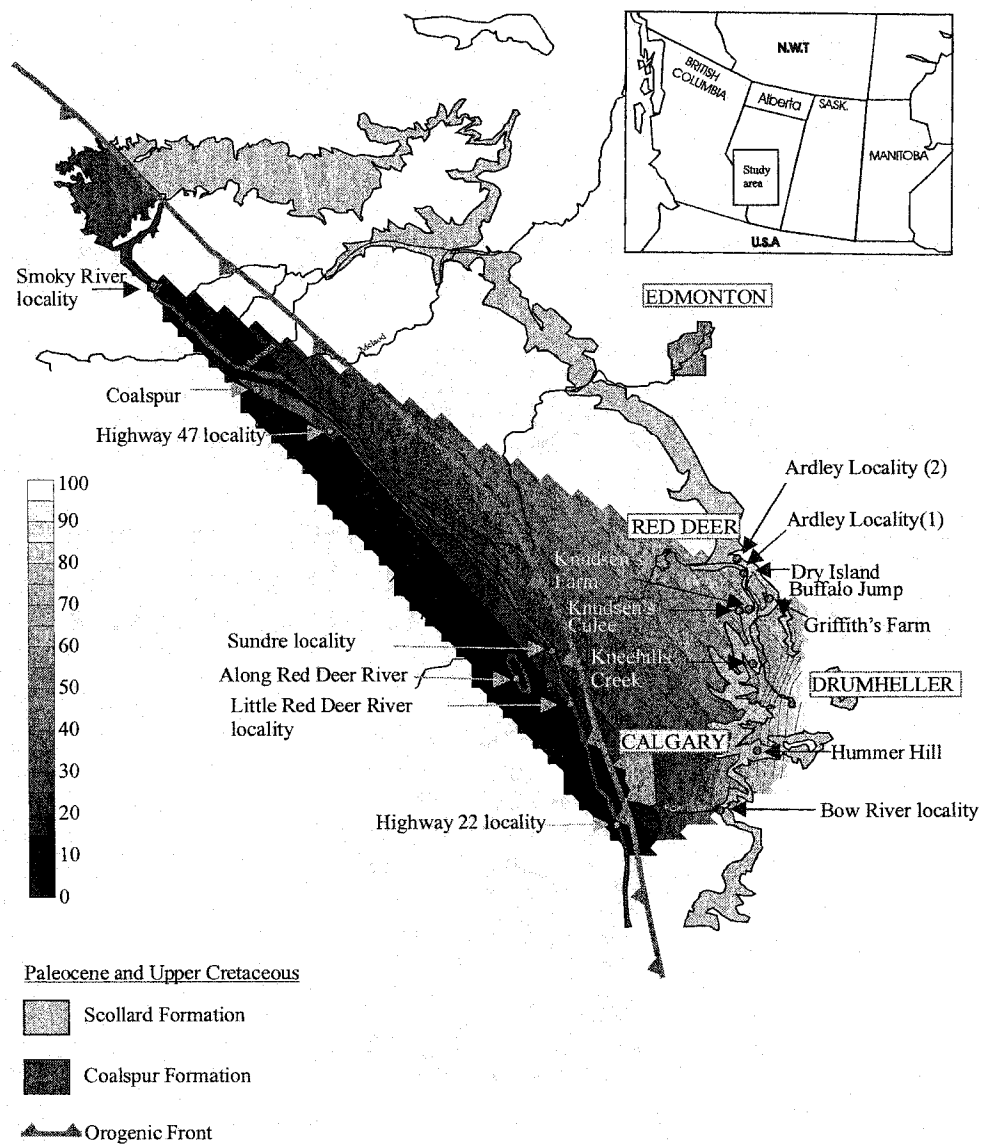
Figure C-7. Contour map showing the distribution of authigenic kaolinite in the lower Scollard and Coalspur sandstones, west central Alberta.

Figure C-8. Contour map showing the distribution of authigenic kaolinite in the upper Scollard and Coalspur sandstones, west central Alberta.

Figure C-9. Contour map showing the distribution of authigenic chlorite/smectite in the Scollard and Coalspur sandstones, west central Alberta.

266

Figure C-10. Contour map showing the distribution of calcite cement in the lower Scollard and Coalspur sandstones, west central Alberta.

Figure C-11. Contour map showing the distribution of calcite cement in the upper Scollard and Coalspur sandstones, west central Alberta.
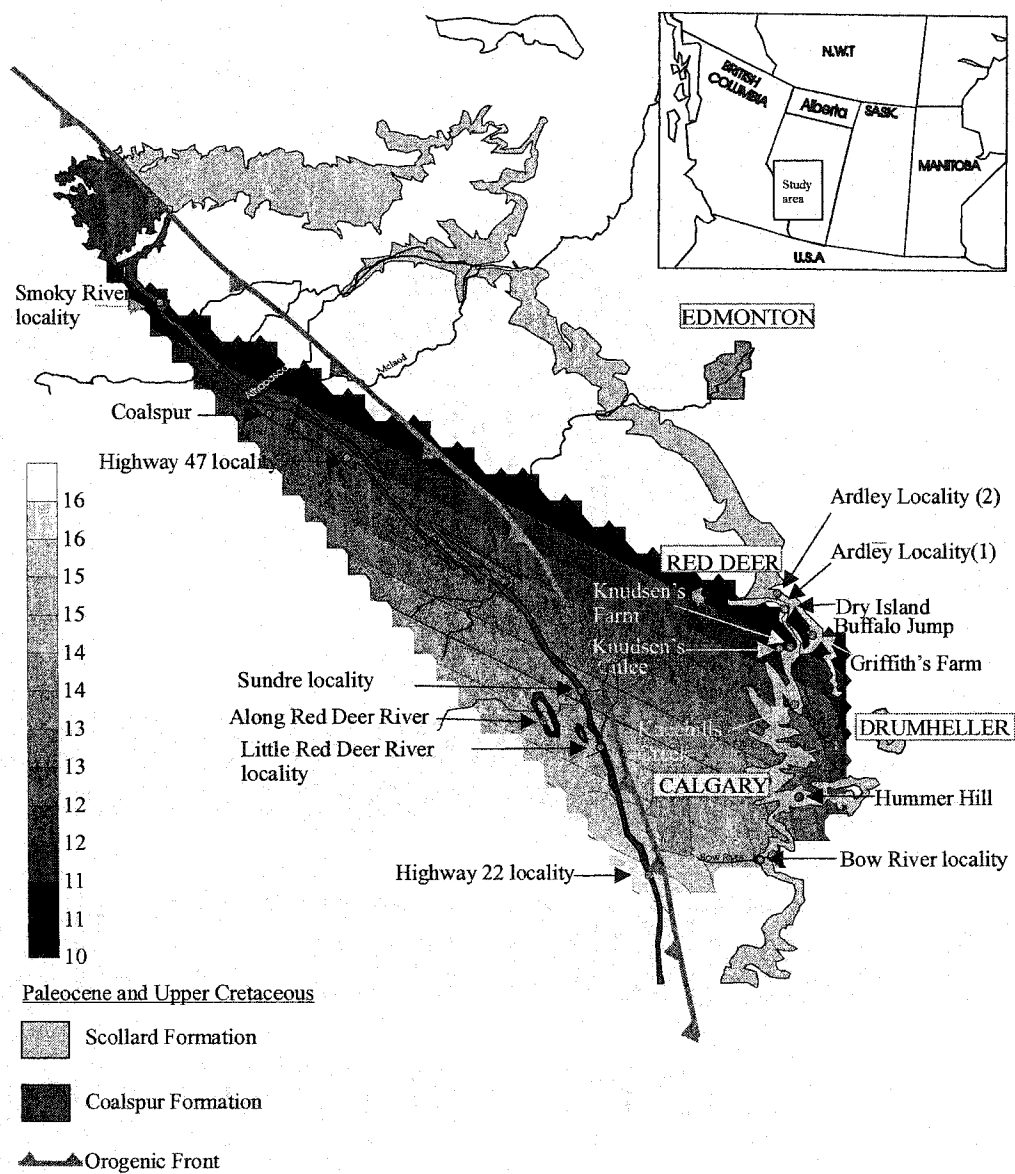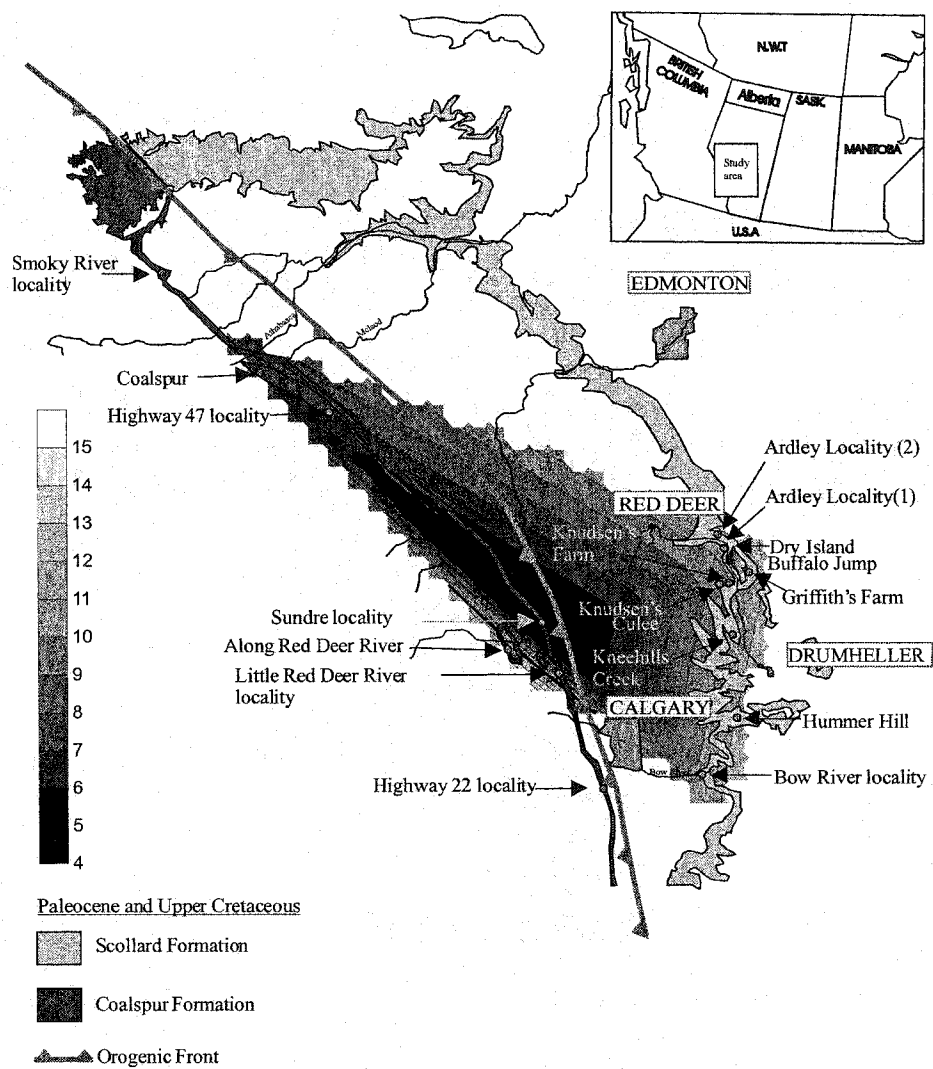
Figure C-12. Contour map showing the distribution of hematite cement in the Scollard and Coalspur sandstones, west central Alberta.

Figure C-13. Contour map showing the distribution of feldspar grains in the lower Scollard and Coalspur sandstones, west central Alberta.

Figure C-14. Contour map showing the distribution of feldspar grains in the upper Scollard and Coalspur sandstones, west central Alberta.
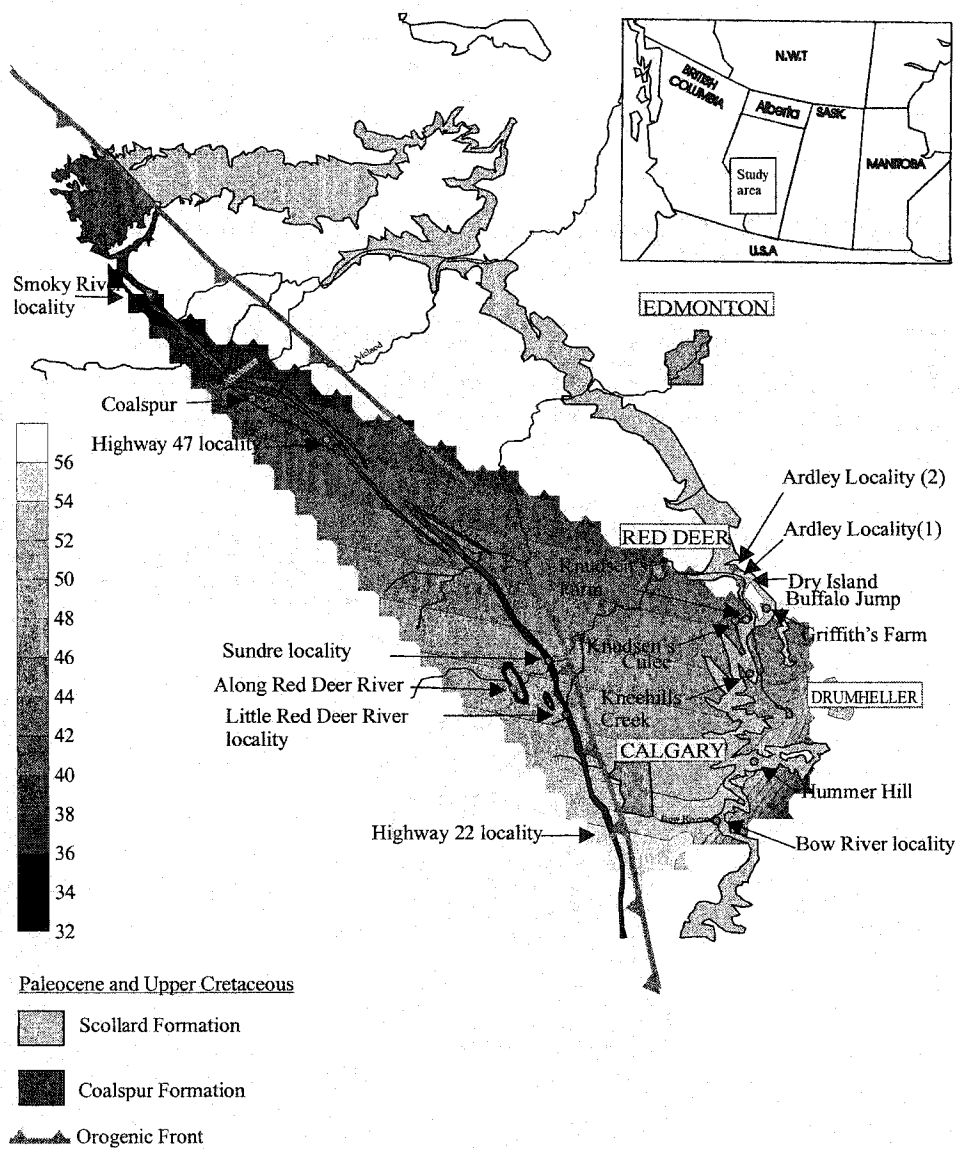
Figure C-15. Contour map showing the distribution of lithic grains in the lower
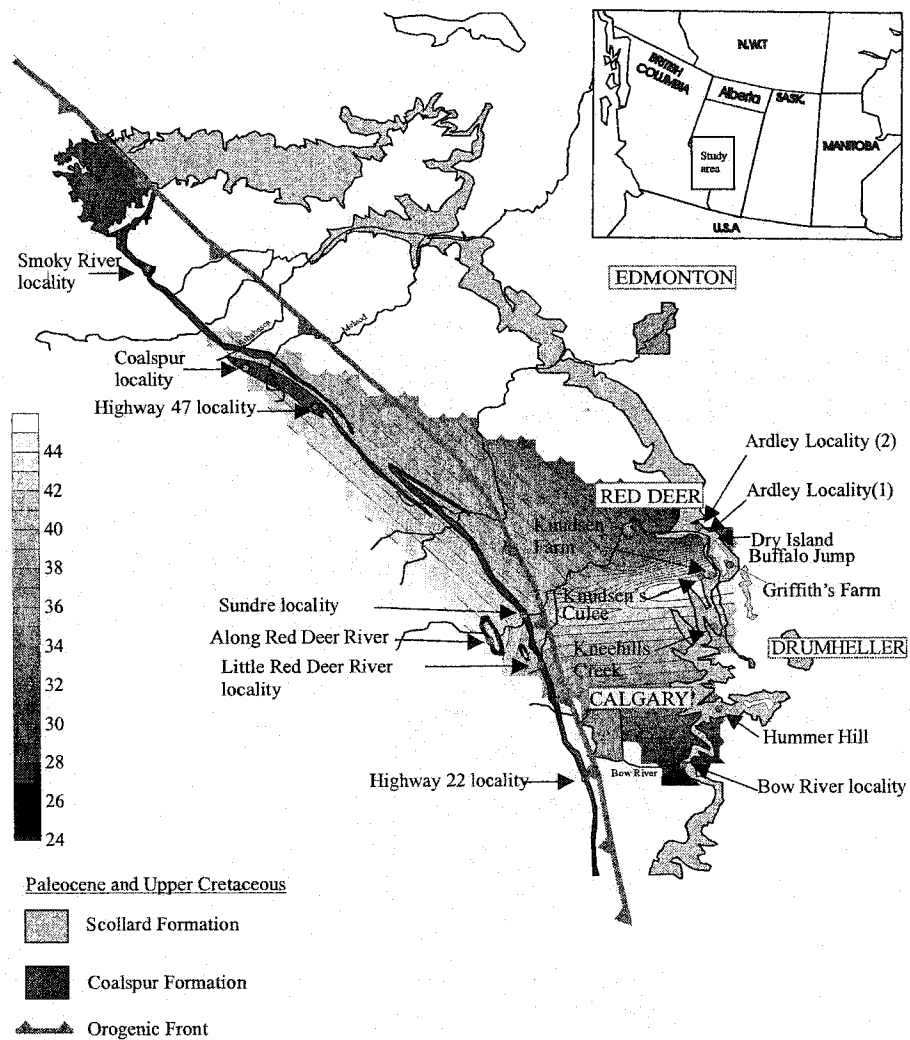Scollard and Coalspur sandstones, west central Alberta.

Figure C-16. Contour map showing the distribution of lithic grains in the upper
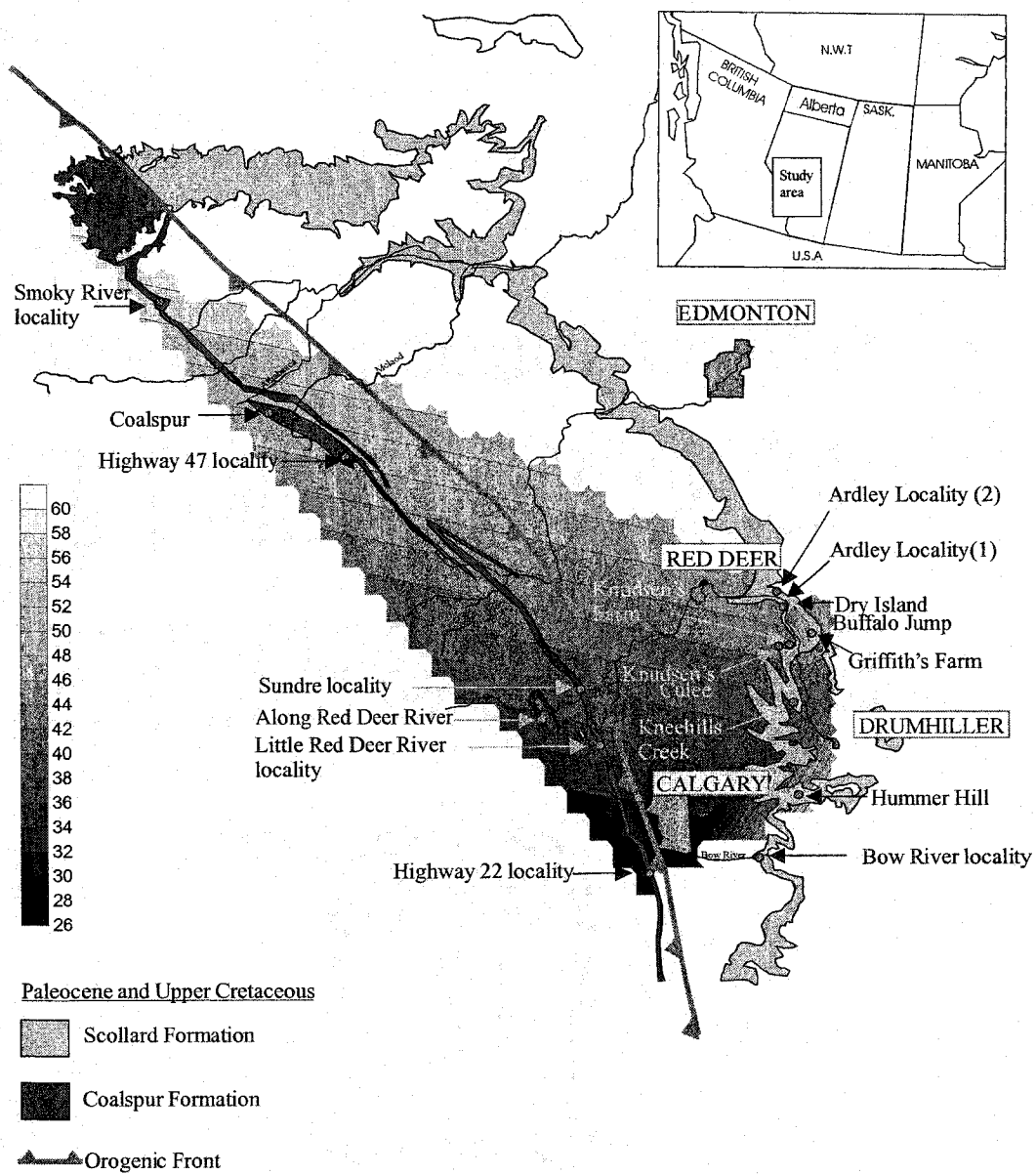Scollard and Coalspur sandstones, west central Alberta.

Figure C-17. Contour map showing the distribution of quartz grains in the lower Scollard and Coalspur sandstones, west central Alberta.
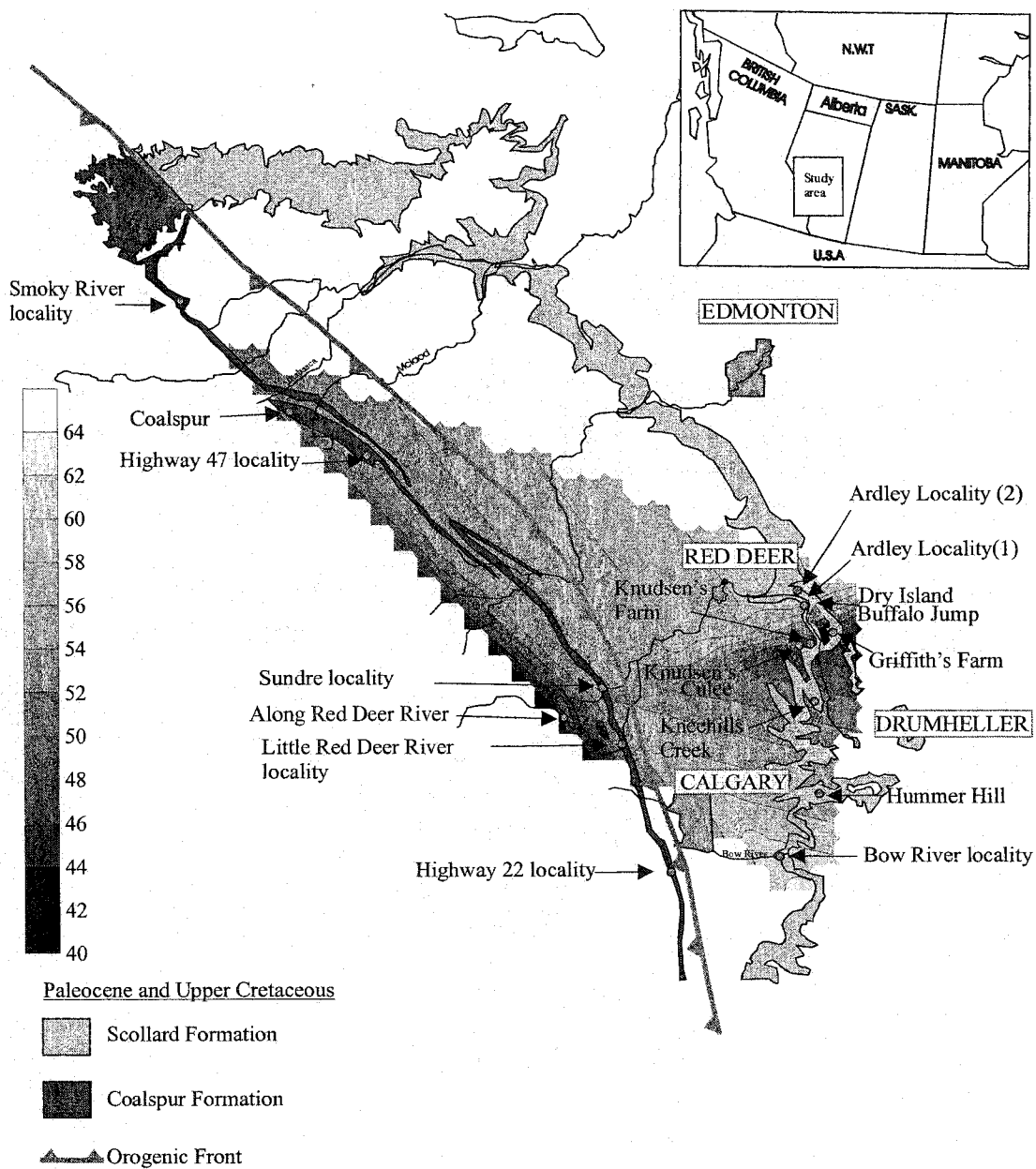
Figure C-18. Contour map showing the distribution of quartz grains in the upper Scollard and Coalspur sandstones, west central Alberta.